

***Chronic active lesions in multiple sclerosis:
novel MRI markers***

Dr Alberto Calvi

A thesis submitted to University College London
for the degree of Doctor of Philosophy

December 2022

Declaration

I, Alberto Calvi, confirm that the work presented in this thesis is my own. Where information has been derived from other sources, I confirm that this has been indicated in the thesis. Part of this work has been based on clinical trial data. Therefore, this work consists of post-hoc and retrospective analyses, including imaging and clinical data that were previously collected. Here is attached all the relevant information on the trial and cohorts employed.

MS-SMART trial – The MS-SMART trial Team at Queen Square MS centre (QSMSC), University College London (UCL) included myself and Dr Floriana De Angelis, Dr Domenico Plantone, Dr Anisha Doshi, Dr Nevin John, Dr Thomas Williams (Clinical Research Fellows) and Tiggy Beyene, Vanessa Bassan, Nicola Stuart, Laura Brockway, Alvin Zapata (Research Nurses) who performed trial visits and assisted the MRI imaging and the collection of other markers for blood, CSF and optical coherence tomography sub-studies. Since the beginning of my PhD work, I carried out, as the principal dedicated research fellow the analysis of the advanced MRI sub-study for the development of novel markers. As far as my role was concerned, I performed the following: conducting trial assessments including the assistance for MRI scans for the follow-up visits at 48 and 96 weeks; taking and processing blood and urine from most of the patients for the biomarker analysis and conducting OCTs; performing quality checks for all the MRI measures collected in the trial from the UCL site (including T2 lesion at baseline and all follow-up time-points; new T2 and enlarging lesions, new persisting T1 black holes; percentage brain volume change); optimising and processing the slowly expanding lesions (SELS) algorithm. The statistical analysis was conducted by myself under the supervision of Dr Carmen Tur. The MS-SMART trial was designed by the UK Multiple Sclerosis Society Clinical Trials Network and led by Professor Jeremy Chataway as the Chief investigator of the study. The trial co-applicants, sites and Investigators are detailed in the paper from Chataway et al. “Efficacy of three neuroprotective drugs in secondary progressive multiple sclerosis (MS-SMART): a phase 2b, multiarm, double-blind, randomised placebo-controlled trial”, *The Lancet Neurology* 2020 – DOI: 10.1016/S1474-4422(19)30485-5.

ECTRIMS-MAGNIMS – Observational cohort from the University of Siena and University of Milan multiple sclerosis centres (Italy). I performed a post-hoc analysis of the retrospective longitudinal MRI studies that were conducted in two separate Italian MS centres, as part of a collaboration between the European Committee for Treatment and Research in MS (ECTRIMS)

and the Magnetic Resonance Imaging in MS (MAGNIMS) during my fellowship. For this project, I conducted the data transfer agreement to obtain MRI scans and clinical data from the University of Milan, 'IRCCS Ospedale Maggiore Polclinico Fondazione Ca' Granda' (as a new centre previously not involved in the MAGNIMS initiative) and I promoted the ethical committee approval of the project. I conducted the MRI lesion and brain segmentation (for a subset of the cohort), followed by the SEL image analysis for the whole cohort. Several colleagues and researchers of the units have conducted the clinical assessments and data analysis phases at the MS centres of the University of Siena (Prof. N. De Stefano, Dr R. Cortese, Dr M. Battaglini) and the University of Milan (Prof. E. Scarpini, Dr M. De Riz, A. Pietroboni, Dr T. Carandini, Dr D. Galimberti).

MAGNIMS – Observational cohort from the Section of Neuroradiology, Department of Radiology, Hospital Universitari Vall d'Hebron (HUVH), Universitat Autònoma de Barcelona, Barcelona (Spain). For this project, I conducted the data transfer agreement and the visual analysis of the SWI scans with Dr Margareta Clarke during a pilot analysis (1st July – 5th July 2019) within the Neuroradiology Unit at HUVH. Then, I carried on the further image analysis at QSMSC, Institute of Neurology, London (UK) where I was supported by Dr Ferran Prados for the pipeline's implementation. The statistical analysis was supported by Dr C. Tur. Clinicians from the Neurology-Neuroimmunology Department, Multiple Sclerosis Centre of Catalonia (CEMCAT) of HUVH took part in the clinical assessments and collection of the data (Dr J. Sastre-Garriga, Ms. Marta Rodríguez Barranco) and the image analysis was supported by the research of the neuroradiology (Prof. A. Rovira, Dr D. Pareto, Mr M Alberich).

INFORMS trial – the steering committee of the trial was made of an international multicentre panel, as reported in the paper from Lublin F. et al. (Lancet. 2016), doi: 10.1016/S0140-6736(15)01314-8), 'Oral fingolimod in primary progressive multiple sclerosis (INFORMS): a phase 3, randomised, double-blind, placebo-controlled trial.'

The Queen Square MS Centre UCL Institute of Neurology London (supported by the UK MS Society and the UCL-UCLH joint Biomedical Research Centre) was the leading MRI analysis centre. Members of the central MRI analysis team were the following: David G MacManus, Tarek A Yousry, Claudia A M Wheeler-Kingshott, Özgür Yaldizli, Jon Stutters, Catherine M Dalton, Virginia Santana, Almudena Garcia-Gomez, Carolina Crespo, David H Miller.

I conducted a post-hoc retrospective analysis of the combined MRI and clinical data as part of the Oxford Big Data Initiative (BDI), after the application of a re-analysis proposal to the Progressive MS Alliance (Dr D. Arnold). The image analysis has been conducted at QSMSC and was supported by Dr Ferran Prados, Zoe Mendelsohn and Dr Weaam Hamed.

Abstract

The heterogeneity of multiple sclerosis (MS) clinical spectrum is in part explained by the differential distribution and accumulation of distinct demyelinating lesion types. At their onset, new lesions are recognised in early MS, while in the late disease stages the chronic active lesions predominate and are associated with disability progression. Pathologically, those lesions are characterised by activated iron-enriched macrophages-microglia at the border promoting radial expansion, and severe neuro-axonal loss in the core. Despite the availability of magnetic resonance imaging (MRI) markers for chronic inflammatory activity, their contribution to MS prognostication of disability progression is still unknown.

In this work, the initial focus was on the pathobiology and radiological correlations, which was realised as a literature review on the topic of imaging chronic active lesions in MS. Then, a novel technique based on deformation field computation to detect slowly expanding lesions (SELs) was implemented. Firstly, the association between SELs and other MRI markers for MS inflammatory activity and neurodegeneration was analysed in a secondary-progressive MS trial to establish their impact on disability. Then, the work was extended to relapse-onset MS, including a combined analysis of SELs and persisting black holes (PBHs), as a surrogate of structural tissue damage using hypointensity on T1-weighted scans. In a further analysis, SELs and paramagnetic rim lesions (PRLs) at susceptibility imaging, as an alternative marker of chronic active lesions, were investigated in an early relapse-onset MS cohort. Finally, an evaluation of the volumetric evolution of the newly developed lesions, and including the evaluation of treatment effects, was conducted on a primary-progressive MS trial.

The clinical impact of all the imaging markers assessed was combined with physical and cognitive data, to assess the evolution of MS disability. Overall, this work has provided an overview of the currently available imaging markers to evaluate chronic inflammatory activity in MS.

Impact Statement

In this thesis work, I addressed the research question of developing MRI biomarkers signalling disability progression in MS. I co-developed and applied techniques to evaluate the chronic active lesions, using volumetric longitudinal imaging and other quantitative MRI measures evaluating structural damage and susceptibility paramagnetic depositions. As a major result, I have shown the practical application of those markers and the clinical relevance to physical and cognitive disability scores in MS. Moreover, I demonstrated their relation to other MS-specific radiological measures, and I explored the dynamic evolution at MRI following the trajectories of expansion of newly developed lesions from their formation.

The work presented in this thesis is associated with publications in peer-reviewed journals, and I presented my results in oral presentations at national and international conferences including the European Committee for Treatment and Research in MS (ECTRIMS) in 2018 and 2021, the Guarantors of Brain and the MS frontiers UK conferences (2022). Those accomplishments have already had an impact on the academic world interested in the discovery of MS biomarkers: in the last year, commentaries in the field have been published and several citations derived from this project (Weber C et al. 2021, Wood H. et al. 2022, Rodriguez-Mogeda C. et al. 2022, Collongues N. et al. 2022). Moreover, the novel techniques employed in this project open the doors to future research in the application of multimodal analysis of markers for chronic inflammatory activity.

The translation of the pipelines implemented in this work has facilitated engagement across the research department, including seminars and meetings between clinical research fellows and visiting international MS researchers. This work was the basis for a post-doctoral application I applied for, which was successfully awarded by ECTRIMS in March 2022. In the future fellowship, I will move forward as an independent post-doctoral researcher and focus on the integration of imaging metrics and biological markers of chronic activity to predict disability outcomes and treatment responses in MS.

This work could provide additional future benefits outside the academia in the clinical setting and for pharmaceutical progress. In the short term, clinical trials could benefit from the application of the techniques developed in this work. For example, some of the pipelines have already started to be employed at UCL and will be extended to the collaborative centres. Furthermore, some of those techniques can now be evaluated for inclusion in future guidelines to assess chronic active lesions in MS monitoring.

In the medium term, this work has paved the way for further application of multiple volumetric and quantitative MRI techniques and foresees an expansion of combinations of imaging modalities. This could stimulate the information technology industry and the development of more advanced scanners. There has been recently an exponential increase in research employing artificial intelligence and the contribution of this thesis is at the outset of the automatization of imaging markers. This field of research will employ those techniques to promote the definition of accurate biomarkers for the optimisation of strategies to detect the pathogenetic mechanisms in MS.

In the longer term, the goal of this work will consist of providing sensitive tools for prognostication of disability progression and for treatment efficacy evaluation. Finally, the biomarkers that will be developed could be employed by pharmaceutical companies to ultimately develop new treatments to halt disability progression.

Acknowledgements

I would like to thank all the people with MS who volunteered their time and dedication to take part in the studies carried out as part of this thesis, particularly those who travelled long distances and those living with major disabilities. They gave me every day the motivation to carry on with this research.

The work I have undertaken was possible thanks to an international collaborative framework facilitating the exchange of ideas and data, through the Magnetic Resonance Imaging in Multiple Sclerosis (MAGNIMS), a consortium that has made a significant contribution to defining the role of MRI in diagnosis and monitoring treatments in MS. I am grateful to the ECTRIMS, Guarantors of Brain and UK MS society for supporting my research work throughout the years and for giving me the possibility to carry on the PhD at UCL. By applying for their fellowship proposals, I learned how to develop the skills to foster an independent career in MS clinical research.

Thank you to my primary supervisor, Prof. Frederik Barkhof, my mentor who supported me in all situations, helped me to build upon my skills, establish my confidence and reflect on my actions to reach the maturity of an independent researcher. I was privileged to have a variegated team of subsidiary supervisors who all committed to my development as a scientist. Dr Declan Chard taught me how to develop critical thinking and always reminded me to translate it into rationality. A special greeting to Dr Ferran Prados who accompanied me in the discovery of the exciting world of computational sciences and to Dr Carmen Tur for the sensible guidance in the statistical analyses.

I am thankful for the support of the UCL team, Prof. Jeremy Chataway, Prof. Claudia Wheeler-Kingshott, Prof. Olga Ciccarelli, Prof. Ahmed Toosy, Prof. David Miller and Prof. Alan Thompson who gave me inspiration for a career in the academic environment and strongly supported me in the continuation of my work at QSMSC.

Thank you to friends and colleagues at QSMSC as they all made my PhD journey a possibility of constructive exchange: Dr Marcello Moccia, Dr Floriana De Angelis, Dr Sara Collorone, Dr Rosanna Cortese, Dr Alessia Bianchi, Dr Nevin John, Dr Anisha Doshi, Dr Thomas Williams, Dr Michael Foster, Dr Lukas Haider, Dr Sarah Wright, who were always available and supportive. The Nursing team who created an enjoyable work environment: Vanessa Bassan, Tiggy Beyenne, Alvin Zapata, Laura Cecconi, Mariana Agiu, Sarah Pullinger, Megan Wynne, Ana Herrera-Jimenez, Staci Conway. All the Research Associates, Iwona Pisarek, Patrizia Pajak, Sarah Alexander. Thank you to the administrative team Charlotte Burt, Tina Holmes, Judith Jolleys and Marie Braisher. Thank you to the engineers, scientists, radiographers, physicists, and the to the NMR trial unit team: Jon Stutters, David Mac Manus, Philippa Bartlett, Jonathan Steel, Carolina Crespo, Almudena Garcia-Gomez, Marios Yannakas, Francesco Grussu, Marco Battiston, Antonio Ricciardi.

Thanks to my clinical supervisors who helped me over those years to grow up my skills in a different medical system as a conscientious neurologist: Dr Anand Trip, Dr Sara Simeoni, Dr Afraim Salek-Haddadi, Dr Apehka Shah.

I thank all my friends in Milan and in London, and those who made me discover the beauty of life and enjoy the years of PhD all over Europe. Thanks to Matteo, Teresa, Martina, Andrea, Alessandro, Barbara, Lucia, Anna, Riccardo, Leonardo, Vittorio, Eleonora, Davide, Fabio for being close to me over those years and to Leonidas for his love and disposition to cultivate a life path.

My profound greetings are to my family. To my father Luigi and to my sister Caterina who made me always reflect on improving my qualities and my professional growth and to my mother Enrica, who was a continuous inspiration for life and beyond, and an example of willpower and positivity.

Publications associated with this thesis

Calvi A, Haider L, Prados F, Tur C, Chard DT, Barkhof F. “In vivo imaging of chronic active lesions in multiple sclerosis.” *Mult Scler*. 2020 Sep 23. doi: 10.1177/1352458520958589.

Calvi A, Prados F, Tur C, Chard DT, Stutters J, De Angelis F, John N, Williams T, Doshi A, Samson RS, MacManus D, Gandini Wheeler-Kingshott CA, Ciccarelli O, Chataway J, Barkhof F, on behalf of the MS SMART Investigators. “Association of Slowly Expanding Lesions on MRI With Disability in People with Secondary Progressive Multiple Sclerosis”. *Neurology*. 2022 Apr 26;98(17): e1783-e1793. Epub 2022 Mar 11. PMID: 35277438. doi:10.1212/WNL.0000000000200144.

Calvi A, Tur C, Chard DT, Stutters J, Ciccarelli O, Cortese R, Battaglini M, Pietroboni A, De Riz M, Galimberti D, Scarpini E, De Stefano N, Prados F, Barkhof F. “Slowly expanding lesions relate to persisting black-holes and clinical outcomes in relapse-onset multiple sclerosis.” *Neuroimage Clin*. 2022 May 16; 35: 103048. PMID: 35598462. doi: 10.1016/j.nicl.2022.103048.

Calvi A, Clarke MA, Prados F, Chard DT, Ciccarelli O, Alberich M, Pareto D, Barranco MR, Sastre-Garriga J, Tur C, Rovira A, Barkhof F. “Relationship between paramagnetic rim lesions and slowly expanding lesions in multiple sclerosis”. *Mult Scler*. 2022 Dec 14;13524585221141964. doi: 10.1177/13524585221141964.

Calvi A, Mendelsohn Z, Ahmed W, Chard DT, Tur C, Stutters J, MacManus D, Kanber B, Gandini Wheeler-Kingshott CA, Barkhof F, Prados F, “Treatment-induced reduction of incident lesions evolving into chronic active lesions in primary-progressive MS”. Under submission to *Journal of Neurology, Neurosurgery, and Psychiatry*.

Other publications during the period of completion of the PhD

Kanber B, Nachev P, Barkhof F, **Calvi A**, et al. “High-dimensional detection of imaging response to treatment in multiple sclerosis.” *NPJ Digit Med*. 2019 Jul 16; 2:66 doi: 10.1038/s41746-019-0127-8. eCollection 2019.

Collorone S, Cawley N, Grussu F, Prados F, Tona F, **Calvi A**, et al. “Reduced neurite density in the brain and cervical spinal cord in relapsing-remitting multiple sclerosis: A NODDI study.” *Mult Scler*. 2019 Nov 4. doi: 10.1177/1352458519885107.

Tur C, Grussu F, De Angelis F, Prados F, Kanber B, **Calvi A**, et al. “Spatial patterns of brain lesions assessed through covariance estimations of lesional voxels in multiple Sclerosis: The SPACE-MS technique.” *Neuroimage Clin*. 2021 Dec 2; 33:102904. doi: 10.1016/j.nicl.2021.102904. Online ahead of print. PMID: 34875458

List of abbreviations

ABH: acute black hole

ADEM: acute disseminated encephalomyelitis

APC: antigen-presenting cell

BBB: blood-brain barrier

BH: black hole

BICAMS: brief international assessment of cognition for MS

BPF: brain parenchymal fraction

BRNB: Rao brief repeatable neuropsychological battery

ARR: annualized relapse rate

CEL: contrast-enhancing lesions

CDA: confirmed disability accumulation

CDP: confirmed disability progression

CDMS: clinically-definite MS

CGM: cortical grey matter

CI: confidence interval

CIS: clinically isolated syndrome

CL: cortical lesions

CNS: central nervous system

CSF: cerebrospinal fluid

DBM: deformation-based morphometry

DCE: dynamic contrast enhancement

DMT: disease-modifying treatments

DIT: dissemination in time

DIR: double inversion recovery

DIS: dissemination in space

DGM: deep grey matter

DMT: disease modifying therapy

EAE: experimental autoimmune encephalomyelitis

EBV: Epstein-Barr Virus

EDSS: expanded disability status scale

fMRI: functional magnetic resonance imaging

FID: free induction decay

GMM: Gaussian mixture model
GIF: geodesical information flows
GM: grey matter
FLAIR: fluid attenuated inversion recovery
FS: Kurtzke functional system
GBCA: gadolinium-based contrast agents
GRE: gradient-echo
HLA: Human Leukocyte Antigen
IFN: interferon
LME: leptomeningeal enhancement
LPM: lesion probability map
MACFIMS: minimal assessment of cognitive function in MS
MAGNIMS: Magnetic Resonance Imaging in MS
MBP: myelin basic proteins
MHC: major histocompatibility complex
MOG: myelin oligodendrocyte glycoprotein
MOGAD: myelin oligodendrocyte glycoprotein antibody disease
MP-RAGE: magnetization-prepared rapid acquisition with gradient echo sequences
MRI: magnetic resonance imaging
MRS: magnetic resonance spectroscopy
MS: multiple sclerosis
MSFC: multiple sclerosis functional composite
MTR: magnetization transfer ratio
NAWM: normal-appearing white matter
NBV: normalised brain volume
NHPT: nine-hole peg test
NMI: normalised mutual information
NMOSD: neuromyelitis optica spectrum disorders
NO: nitric oxide
OCT: optical coherence tomography
PASAT: paced auditory serial addition test
PBH: persisting black hole
PBVC: percent brain volume change
PD: proton density

PET: positron emission tomography
PIRA: progression independent of relapsing activity
PLP: proteolipid-protein
POMS: paediatric onset multiple sclerosis
PPMS: primary progressive multiple sclerosis
PRL: paramagnetic rim lesion
PROM: patient-reported outcome measures
PSIR: phase-sensitive inversion recovery
QSM: quantitative susceptibility mapping
RAW: relapse-associated worsening
RF: radiofrequency
RIS: radiologically isolated syndrome
ROI: region of interest
ROS: reactive oxygen species
RRMS: relapsing-remitting multiple sclerosis
SD: standard deviation
SDMT: symbol digit modalities test
SEL: slowly expanding/evolving lesion
SLCVA: Sloan low-contrast visual acuity
SPMS: secondary progressive MS
SWI: susceptibility-weighted imaging
TBM: tensor-based morphometry
TE: echo time
TNF: tumour necrosis factor
TR: repetition time
T1: longitudinal relaxation
T2: transverse relaxation
T25FW: timed 25-foot walk
VEP: visual evoked potential
VGM: voxel-guided morphometry
WM: white matter

Table of Contents

1	Introduction to Multiple Sclerosis	22
1.1	Introduction	22
1.2	Epidemiology and comorbidities	22
1.3	Clinical features and MS phenotypes.....	24
1.4	Clinical and patient-reported outcome measures	28
1.5	Aetiology.....	31
1.6	Pathogenesis.....	35
1.7	Neuropathology.....	39
1.8	Chronic active (smouldering, or slowly expanding) lesions	43
1.9	Diagnosis of multiple sclerosis	45
1.10	Therapy	48
1.11	Rationale for thesis.....	52
2	Imaging chronic active lesions in MS.....	54
2.1	Magnetic resonance imaging markers in MS.....	54
2.2	Imaging lesions in MS with conventional MRI	55
2.2.1	Spatial localisation of MS lesions	57
2.2.2	Contrast-enhancing lesions (CELs)	58
2.3	Imaging tissues beyond white matter lesions in MS	61
2.3.1	Grey matter damage: cortical lesions and GM atrophy	61
2.3.2	Leptomeningeal enhancement.....	63
2.3.3	Global brain and spinal cord atrophy	63
2.3.4	Connectivity MRI metrics.....	65
2.3.5	MR spectroscopy.....	65
2.3.6	Diffusion-weighted imaging (DWI).....	67
2.3.7	Positron emission tomography (PET)	68
2.4	MRI markers for chronic lesions in MS.....	70
2.4.1	T1 hypointensity and the black holes.....	70

2.4.2	Persisting black holes (PBHs).....	72
2.5	Quantitative and volumetric MRI measures	74
2.5.1	Magnetization transfer ratio (MTR).....	74
2.5.2	Volumetric MRI basics: segmentation and registration.....	76
2.5.3	Deformation-based analysis	78
2.5.4	Susceptibility MRI	79
2.6	Markers for chronic active lesions	81
2.6.1	Paramagnetic rim lesions at susceptibility MRI	81
2.6.2	Slowly expanding lesions (SELs) at volumetric MRI	85
2.6.3	Conclusions on the current MRI markers for progression in MS	89
3	Characterising the slowly expanding lesions in secondary-progressive MS	91
3.1	Introduction and aim of the study	91
3.2	Pilot analysis	91
3.2.1	The SEL detection algorithm	92
3.2.2	Methods and Results of the pilot study	95
3.3	Extension to the SEL study population.....	98
3.3.1	Methods.....	100
3.3.1.1	Data collection & clinical assessments	100
3.3.1.2	MRI acquisitions	101
3.3.1.3	T2 lesion segmentation, SEL detection and tissue segmentation	101
3.3.1.4	Structural analysis of MTR within lesion types.....	102
3.3.1.5	Statistical analysis	103
3.3.2	Results.....	105
3.3.2.1	Clinical-demographic and conventional MRI metrics	105
3.3.2.2	Descriptive analysis of SEL-derived metrics.....	107
3.3.2.3	Association between SEL and conventional MRI metrics.....	109
3.3.2.4	MTR analysis within SEL-derived lesion types	110
3.3.2.5	Associations between SELs, demographic and clinical features .	111
3.3.2.6	SELs and clinical disability outcomes	111
3.3.3	Discussion	117

4	Slowly Expanding Lesions and Persisting Black Holes	122
4.1	Background and objectives	122
4.2	Material and methods	124
4.2.1	Participants and MRI acquisitions	124
4.2.2	Clinical assessments	125
4.2.3	T2 lesion, tissue segmentation and SEL detection	125
4.2.4	T1 ratios and MTR within lesion types	126
4.2.5	PBH detection	126
4.2.6	Statistical analysis	127
4.3	Results	129
4.3.1	Cohort demographics and clinical features	129
4.3.2	Descriptive analysis of MRI metrics	130
4.3.3	High, intermediate and low SEL count clusters	132
4.3.4	Associations between T1-black holes, PBHs and SELs	134
4.3.5	Associations between SELs and brain volumes	134
4.3.6	T1 intensity ratio and MTR within SELs	135
4.3.7	SEL associations to disability and risk of progression	137
4.4	Discussion	138
5	Relationship between Paramagnetic Rim Lesions and Slowly Expanding Lesions.....	143
5.1	Introduction	143
5.2	Materials and methods	145
5.2.1	Participants, MRI acquisitions and clinical assessments	145
5.2.2	Lesion and brain segmentation, SEL detection	146
5.2.3	PRL detection on SWI	146
5.2.4	Lesions and categories according to SELs and PRLs	147
5.2.5	Statistical analysis	147
5.3	Results	149
5.3.1	Cohort demographics and clinical features	149
5.3.2	Patient categories according to SELs and PRLs	150
5.3.3	SELs and PRLs correspondence and radiological descriptive analysis	150

5.3.4	SELs and PRL in treated versus non-treated, and in short versus long time intervals	153
5.3.5	Association analysis of SELs, PRLs and radiological measures	155
5.3.6	Radiological and clinical measures by patient groups according to SEL & PRLs.....	155
5.3.7	SELs and PRLs relationship to demographics	157
5.3.8	EDSS progression in relation to SELs and PRLs	157
5.4	Discussion	159
6	Evolution patterns of the new lesions in primary-progressive MS	162
6.1	Introduction and aim of the study	162
6.2	Definition of the cohort.....	164
6.3	Methods.....	165
6.3.1	Data collection, trial information, clinical assessments	165
6.3.2	MRI acquisitions	166
6.3.3	MRI analysis: new lesions and tissue segmentation	166
6.3.4	MRI volumetric deformation analysis	167
6.3.5	Statistical analysis	168
6.4	Results	168
6.4.1	Clinical-demographic characteristics	168
6.4.2	MRI characteristics	169
6.4.3	Descriptive analysis of new lesions and SELs, lesion level.....	171
6.4.4	Descriptive analysis of the Jacobians.....	172
6.4.5	Descriptive analysis of SELs at the patient level.....	173
6.4.6	Association between Jacobians and SELs with MRI metrics	174
6.4.7	Cross-sectional and longitudinal associations between Jacobian and SELs with clinical measures	175
6.4.8	Conventional MRI measures and treatment effect.....	176
6.4.9	Jacobian, SELs and treatment effect	177
6.5	Discussion	178
7	Discussion, conclusion, and future directions.....	184

7.1	Thesis overview	184
7.2	Clinical relevance and future directions.....	187
7.2.1	Insights on the pathogenetic mechanisms within chronic active lesions 188	
7.2.2	Contribution of the thesis	189
7.2.3	Commentary from recent literature	191
7.2.4	Future directions	192
7.3	Final considerations	194
	Bibliography	196

List of Tables

Table 1-1. Pathological features of chronic active lesions	44
Table 2-1. SEL detection algorithm steps and subtypes of SEL lesions obtained	87
Table 2-2 Features and limitations of markers for progression in multiple sclerosis	90
Table 3-1. Pilot analysis: lesion counts and volumes by type with preliminary and optimized SEL algorithm	96
Table 3-2. MRI acquisition parameters	101
Table 3-3. Demographic, clinical, and radiological characteristics of the patients whose scans contributed to the SEL study	106
Table 3-4. SEL-derived metrics at the patient level (n= 345)	107
Table 3-5. SEL-derived metrics at the patient level by treatment allocation arm. .	109
Table 3-6. Magnetization Transfer Ratio (MTR) at baseline and 96 weeks follow-up, and MTR changes over time in the different lesion types.	110
Table 3-7. Multiple linear/logistic regressions between SEL-associated log-volumes and clinical scores.	113
Table 3-8. Association between SEL-derived volumes and clinical outcomes over time using mixed-effects regression models	115
Table 3-9. Multiple linear regression using a multiple imputation model	117
Table 4-1. MRI acquisition parameters	125
Table 4-2. Clinical-demographic and radiological characteristics of the patients enrolled in the study.	130
Table 4-3. Lesion counts and volumes, by SEL types, total BH and PBH at the patient level	131
Table 4-4. Clinical demographics and radiological characteristics by high, intermediate and low SEL count clusters	133
Table 4-5. Distribution of black holes counts divided by the SEL-derived categories	134
Table 4-6. Cross-sectional and longitudinal T1 intensity ratio within lesion types	135
Table 4-7. Cross-sectional MTR at baseline and last follow-up within lesion types	137
Table 5-1. Clinical-demographic characteristics of the patients enrolled in the study.	149

Table 5-2. Patient categories according to presence or absence of SELs and PRLs	150
Table 5-3. Radiological measures: counts and volumes and brain-derived measures	152
Table 5-4. SEL- and PRL-derived metrics at baseline at the patient level in the treated and non-treated population	154
Table 5-5. SEL- and PRL-derived metrics at the patient level in the short- and long-time range interval sub-cohorts	155
Table 5-6. Clinical-demographic and radiological characteristics in groups according to the presence of SEL and PRLs	156
Table 5-7. Association between the SEL-PRL measures and categories with EDSS over time using mixed-effects regression models	158
Table 6-1. Demographic and clinical characteristics	169
Table 6-2. MRI measures in the active and inactive PPMS cohort	170
Table 6-3. Descriptive analysis of the SEL-derived lesion types and volumes	171
Table 6-4. Jacobian expansion in the SEL-derived categories	172
Table 6-5. Patient-level descriptive analysis of the new lesions and the SEL categories	174
Table 6-6. Correlation Matrix showing the correlation coefficients (Spearman) between all the MRI radiological measures included in the study	175
Table 6-7. Mixed-effect regression models to investigate association between clinical scores and Jacobians and SEL volumes	176
Table 6-8. MRI measures in treated and non-treated patients of the active PPMS sub-cohort	177
Table 6-9. Differences in SEL-derived measures between the treated and non-treated	178

List of Figures

Figure 1-1. Prevalence of Multiple Sclerosis by country (2020).	23
Figure 1-2. Descriptors of disease activity in relapsing MS phenotypes.	27
Figure 1-3. Descriptors of disease activity in progressive MS phenotypes.	27
Figure 1-4. Risk factors and modifiers for disease course in MS.	32
Figure 1-5. Mechanisms of axonal damage in the final pathways contributing to neurodegeneration.	39
Figure 1-6. MS lesion classification.	42
Figure 1-7. Distribution of types of lesions in pathology depending on disease duration.	45
Figure 1-8. Disease-modifying treatments for multiple sclerosis, mechanisms of action.	49
Figure 2-1. Imaging targets for the pathogenetic mechanisms involved in MS.	54
Figure 2-2. Typical supratentorial and infratentorial MS lesions at T2-weighted or FLAIR.	55
Figure 2-3. Typical spinal cord lesions in MS.	58
Figure 2-4. Examples of brain typical contrast-enhancing lesions (CELs) in MS.	59
Figure 2-5. Example of cortical lesion in MS.	62
Figure 2-6. Example of lesion in active and chronic stage at axial views of FLAIR (a), gadolinium T1-weighted (b) and [¹¹ C]PK11195 PET (c).	69
Figure 2-7. Example of black holes (BHs).	71
Figure 2-8. Example of MTR map (on right - b) and the corresponding T2-weighted scan (on the left - a).	75
Figure 2-9. Example of paramagnetic rim lesions in the periventricular white matter.	82
Figure 2-10. Example of a nascent lesion developing a paramagnetic rim over a follow-up on a 7T FLAIR-SWI.	85
Figure 3-1. Lesion segmentation, deformation field map and Jacobian heat map. (figure re-adapted from Elliott C. et al., MSJ, 2018)	92
Figure 3-2. Classification of lesions according to the SEL detection algorithm.	93
Figure 3-3. Constancy and concentricity of expansion	94
Figure 3-4. Regression line of the candidate SEL volume and total white matter lesion (WML) volume, and 95% CI in the grey area.	97

Figure 3-5. Example of outliers discarded from the SEL analysis.....	99
Figure 3-6. Flowchart showing the enrolment of subjects into the SEL extension study.	100
Figure 3-7. Direct Acyclic Graphs (DAGs) showing the relationship between the variables included in the statistical models.....	104
Figure 3-8. Lesion probability map (LPM).....	108
Figure 3-9. Example of patient with high number of SELs.	110
Figure 3-10. Regression line, drawn using R, showing the relationship between EDSS change from baseline to week 96 and baseline definite SEL volume (ml).	112
Figure 4-1. Patient clusters according to SEL counts. The yellow vertical bars indicate the cut-offs defined by the Gaussian mixture model on the distribution of the possible SEL counts. The first cut-off is set at n=2 SELs, the second cut-off at n=10 SELs.	128
Figure 4-2. Example of patient with SEL and PBH.....	132
Figure 4-3. T1 change over time within SEL-derived lesion metrics.	136
Figure 5-1. Stacked bar plot of PRL and SEL counts.	151
Figure 5-2. Example of a PRL+ at baseline and the correspondence to a SEL.	153
Figure 6-1. Flowchart showing the enrolment of subjects into the SEL study.	164
Figure 6-2. Bar plot showing the distribution of the new lesions (year 1) by type.	171
Figure 6-3. Jacobian expansion in the SEL-derived lesion types	173
Figure 6-4. Example of a new lesion corresponding to a SEL.....	174

1 Introduction to Multiple Sclerosis

1.1 Introduction

Multiple sclerosis (MS) is a complex demyelinating disease characterized by varying degrees of inflammation and neurodegeneration occurring within the whole tissues of the central nervous system (CNS). MS has an impact on neuroinflammatory diseases and a rising prevalence trend due to the young age of onset, chronic course and improvements in treatment management (Browne *et al.*, 2014). The “Sclérose en plaques” was recognised as a condition by Jean-Martin Charcot who first analysed the clinical and pathological features in 1868, together with the illustrations of Carswell and Cruveilhier in view of previous case presentations and reports from the literature (Compston, 1988).

1.2 Epidemiology and comorbidities

The estimated number of people with MS is 2.8 million people worldwide in 2020 with an increasing trend in the past 7 years (Walton *et al.*, 2020). This equates to 1 in 3,000 people in the world living with MS and a global prevalence of ~36 per 100,000 (<https://www.atlasofms.org/map/spain/epidemiology/number-of-people-with-ms>, 2020). In the UK, 130,000 people are affected by MS with a prevalence of 196 per 100,000 people) and every week around 100 more people are diagnosed with this condition (<https://www.mssociety.org.uk/what-we-do/our-work/our-evidence/ms-in-the-uk>, 2018).

There is a considerable variation in the prevalence between countries according to latitude, with the highest prevalence reaching figures around 1 in every 300 (Germany, Italy – San Marino, Denmark, USA) with lower numbers in Africa, South-East Asia and Western Pacific regions (Walton *et al.*, 2020) (**Figure 1-1**). The higher incidence and prevalence with increasing latitude (latitudinal gradient) mainly in Europe and North America have been linked to either genetic and environmental MS-related risk factors (Koch-Henriksen and Sørensen, 2010). The globally increased prevalence can

be attributed in part to population growth, improvements in the diagnosis, treatment and supporting measures. In addition, there has been an increased reporting of MS with the establishment of clinical registers (Browne *et al.*, 2014).

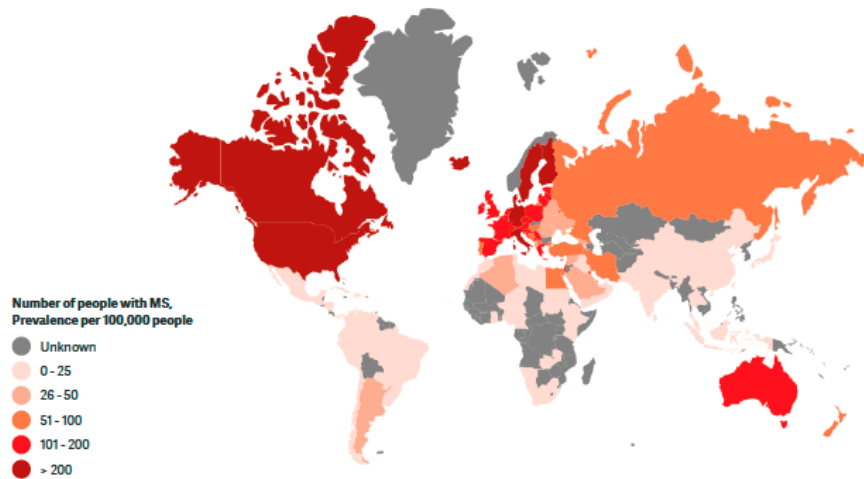


Figure 1-1. Prevalence of Multiple Sclerosis by country (2020).

MSIF <http://www.msif.org> [MS Atlas, WHO & MSIF]

MS is at least twice as common among women than men, with regional differences as the female-to-male ratio is considerably higher in some regions, such as 3 or 4 to 1 (examples include Egypt, Iran, the Palestinian Authority and Sudan), and in some countries, this gender skew has been increasing in the last decades (Alonso and Hernán, 2008). MS is usually diagnosed in early adulthood, with an average age of onset of 32 (Koch-Henriksen and Sørensen, 2010). People with MS are living with this neurological disease for many decades, with significant impact on their social and economic wellbeing. A fraction between 3 and 10% are diagnosed under the age of eighteen, and they are defined as paediatric onset multiple sclerosis (POMS) (Langille, Rutatangwa and Francisco, 2019).

In epidemiological studies, the most frequently studied comorbidities of MS are psychiatric and other autoimmune (thyroid disease and psoriasis) disorders, cancer, lung disease and epilepsy. Based on meta-analysis, the five most frequent comorbidities are depression, anxiety, hypertension, hyperlipidaemia and chronic lung

disease (Marrie *et al.*, 2015). MS co-morbidities have been associated with diagnostic delays, disability progression, and worsened quality of life (Marrie *et al.*, 2015), including a higher risk of mortality. The main direct cause of death in the majority of patients is MS-related, with a 7-year shorter (Lunde *et al.*, 2017) life expectancy and almost threefold higher mortality compared to the general population. However, a rise in the survival rate has been observed in the last decades.

1.3 Clinical features and MS phenotypes

Clinically, MS has heterogeneous presentations and clinical courses but can be considered as a single disease within a disease spectrum extending from relapsing to progressive phenotypes in keeping with the diagnostic criteria (Lublin *et al.*, 2014). Symptoms and signs of MS are extremely variable as they result from injury in any part of the central nervous system (CNS), corresponding to the presence of demyelinating lesions and leading to variable clinical manifestations such as visual disturbances and diplopia, sensory complaints, motor deficits, vertigo and balance problems.

Typical presentations are unilateral optic neuritis, focal supratentorial syndrome, focal brainstem or cerebellar syndrome, partial myelopathy. Most of the patients experience fatigue in daily life activities, especially the ones requiring more physical effort. Furthermore, some patients describe stereotypical recurring brief symptoms, representing discharges originating along demyelinated axons, such as trigeminal neuralgia and other paroxysmal symptoms (Compston and Coles, 2008). MS detrimentally affects various aspects of cognitive functioning in particular attention, information processing speed, episodic and working memory, verbal fluency, visuospatial analysis and executive function (Rocca *et al.*, 2015). Cognitive decline often emerges early in the disease, but impairment is more prevalent and may impact with higher severity with advanced disease (Chiaravalloti and DeLuca, 2008).

From the consensus of the US National Multiple Sclerosis Society Advisory Committee on Clinical Trials in Multiple Sclerosis, four clinical subtypes of MS were

defined (Lublin FD, 1996): clinically isolated syndrome (CIS), relapsing-remitting MS (RRMS), primary progressive MS (PPMS) and secondary progressive MS (SPMS).

CIS is a monophasic neurological episode with symptoms and objective findings suggestive of a focal or multifocal demyelinating event, requiring further investigations to exclude mimics (Lublin *et al.*, 2014; Thompson *et al.*, 2017). The factors that can predict clinical development to meet the criteria of clinically-definite MS are the following: younger age, higher cerebral lesion load, asymptomatic infratentorial or spinal cord lesions, presence of gadolinium-enhancing lesions, cerebrospinal fluid (CSF) specific oligoclonal bands, abnormal visual evoked potentials (Miller, Chard and Ciccarelli, 2012) and low vitamin D levels (Ascherio *et al.*, 2014). Despite it is not being considered an MS subtype per se, the radiologically isolated syndrome (RIS) refers to incidental imaging findings nonspecific but suggestive of inflammatory demyelination in the absence of clinical signs or symptoms. RIS may raise the suspicion of MS, depending on the morphology and location of detected MRI lesions, with highly suggestive imaging changes carrying a higher risk of future MS clinical symptoms (Okuda *et al.*, 2009).

RRMS is the most frequent phenotype, characterized by relapses followed by a variable degree of recovery and interspersed with periods of clinical inactivity. Relapses are acute or subacute episodes of neurological deficit lasting for at least 24 hours, in the absence of fever or infection, reaching a plateau that can last up to several weeks, followed by partial or complete recovery. The disease course for RRMS is mainly linked to the frequency of relapses usually within 6 or 12 months, but the accumulation of disability is also influenced by clinical-demographic factors (i.e. sex, age at disease onset, disease duration and course from diagnosis, pregnancy) (Jokubaitis *et al.*, 2016), radiological factors and exposure to treatments.

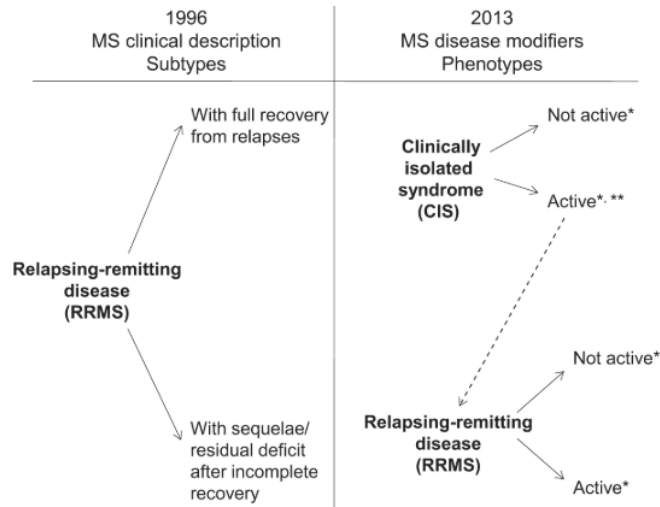
Secondary-progressive disease course (SPMS) is marked by a steadily increasing disability such as impaired ambulation, sphincter dysfunction and cognitive decline with or without superimposed relapses (Lorscheider *et al.*, 2016). In most clinical contexts, SPMS is diagnosed retrospectively by a history of gradual worsening after an initial relapsing disease course. The susceptibility to progression used to be more than half of the RRMS patients before the treatment era (Tremlett, Zhao and

Devonshire, 2009), while it has now reduced since the systematic use of treatments and it could be estimated between 15% and 30% of patients after 10 years of diagnosis (Leray *et al.*, 2010; Cree *et al.*, 2016).

Primary progressive multiple sclerosis (PPMS) constitutes about 5 to 15% of patients from the onset, and it is characterised by the absence of clear-cut attacks. PPMS patients experience a continuous and steady worsening of neurologic functions from diagnosis. Clinical-demographic factors are different, such as later age at onset (mean age 40 years), male predominance, prevalence of motor/sphincter symptoms (Langer-Gould *et al.*, 2006). The disability develops faster and this is also related to reduced availability of treatments compared to RRMS (Miller and Leary, 2007). Several clinical, imaging and genetic data are currently suggesting that PPMS is a part of the spectrum of progressive MS phenotypes and that any differences are relative rather than absolute (Lassmann, Brück and Lucchinetti, 2007).

In 2013, Lublin *et al.* revised the standardized descriptions in regards to the pattern and course of MS, including consideration of disease activity and disease progression (Lublin *et al.*, 2014) (**Figure 1-2, Figure 1-3**). The concept of disease activity is based on either clinical relapse rate or MRI evidence of contrast-enhancing lesions and/or new or unequivocally enlarging T2 lesions. Disease progression is a process of confirmed accumulation of disability, defined by a clinical worsening that persists over a specific number of months (usually 3 or 6 in clinical trials), independent of relapse activity. Patients with progressive MS are further classified based on whether the disease is clinically progressing or not progressing. Disease progression is defined as an objective increase in neurological disability, confirmed after 6-12 months.

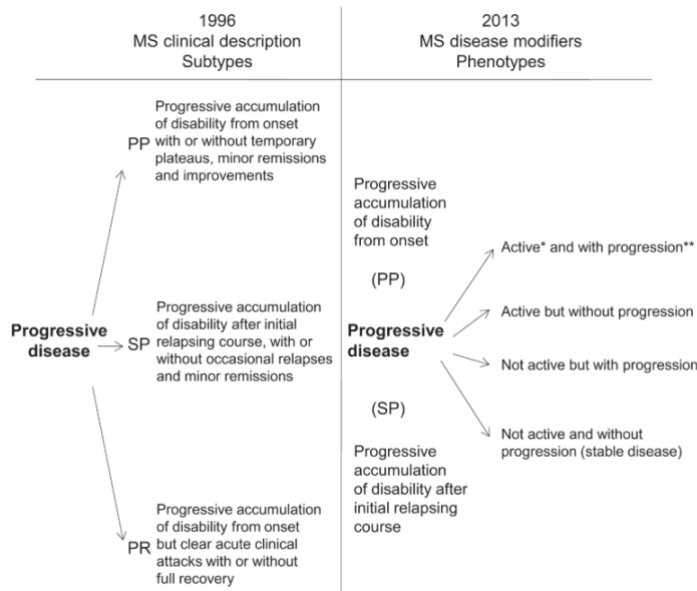
Figure 1 The 1996 vs 2013 multiple sclerosis phenotype descriptions for relapsing disease



*Activity determined by clinical relapses and/or MRI activity (contrast-enhancing lesions; new or unequivocally enlarging T2 lesions assessed at least annually); if assessments are not available, activity is "indeterminate." **CIS, if subsequently clinically active and fulfilling current multiple sclerosis (MS) diagnostic criteria, becomes relapsing-remitting MS (RRMS).

Figure 1-2. Descriptors of disease activity in relapsing MS phenotypes. (From Lublin et al. 2014, Neurology)

Figure 2 The 1996 vs 2013 multiple sclerosis phenotype descriptions for progressive disease



*Activity determined by clinical relapses assessed at least annually and/or MRI activity (contrast-enhancing lesions; new and unequivocally enlarging T2 lesions). **Progression measured by clinical evaluation, assessed at least annually. If assessments are not available, activity and progression are "indeterminate." MS = multiple sclerosis; PP = primary progressive; PR = progressive relapsing; SP = secondary progressive.

Figure 1-3. Descriptors of disease activity in progressive MS phenotypes. (From Lublin et al. 2014, Neurology)

1.4 Clinical and patient-reported outcome measures

Clinical impairment in MS can be measured through specific measures, which are generally used as primary outcomes in phase III trials. Those measures have been classified as follows: measures of clinical relapses, measures of disability progression and patient-reported outcome measures (PROMs).

Relapse-based outcomes measures are relevant for relapse-onset MS, and they include the number of relapses or considered as a binary phenomenon (proportion or number of patients with, versus those without relapse), the time to first relapse while on treatment (a common metric in CIS trials, indicating conversion to clinically definite MS), and composite outcome measures. The annualized relapse rate (ARR), the most widely used outcome measure, is defined as the number of relapses per patient-year during treatment. Due to some lack of specificity of the ARR on the severity of relapses, another version is considering only severe relapses that require intravenous steroid treatment and/or hospitalization or that result in a high level of disability. As secondary trial endpoints, the percentage of relapse-free patients and the percentage of patients with one or more relapses have been used as further clinical metrics, which are strongly dependent on the study duration.

Regarding the clinical measures relevant for progressive MS phenotypes, they include the following: metrics that quantify progression as a continuous phenomenon; metrics that consider progression as a binary phenomenon, such as the proportion of patients with or without confirmed disability progression (CDP); metrics that quantify the confirmed improvement in disability as a binary phenomenon; metrics that quantify the time to CDP; and composite outcome measures (Tur *et al.*, 2018). Currently, as a result of the inclusion of several MS-specific measures assessing either the physical (upper/lower limb) and the cognitive functions as described below, the composite worsening in all those measures has generally been referred to as confirmed disability accumulation (CDA) (Kappos *et al.*, 2020).

In the research trial context, and more often in clinics, the Expanded Disability Status Scale (EDSS) and Kurtzke Functional System (FS) are the most widely used clinical measures to assess the disease severity and monitor treatment effects (Kurtzke, 1983).

Based on a neurological examination, the EDSS is an ordinal nonlinear scale that quantifies disability throughout eight FS - pyramidal, cerebellar, brainstem, sensory, bowel and bladder, visual, cerebral (mental) and other functions - and allows to assign an FS Score in each of these. The results of the ratings from each FS are combined with the measured walking distance and independence with activities of daily living, and a final score from 0 to 10 is given with higher scores indicating a more severe disability. EDSS steps 1.0 to 4.5 refer to people with MS who are able to walk without any aid, while EDSS steps 5.0 to 7.5 are defined by the progressive impairment to walking, and values ranging from 7.5 to 9.5 describe a high dependence for the wheelchair use. There are some limitations of the EDSS: it is weighted towards the pyramidal FS and the score is mainly driven by impairment in ambulation whilst being less sensitive towards other functions (i.e. cognitive, bladder, upper limbs) (Amato and Ponziani, 2016); there is a high inter and intra-observer variability; a reduced sensitivity to change in EDSS could link to an apparent lack of effect in some phase II clinical trials (Cohen *et al.*, 2012). CDP is usually related to worsening of EDSS that persists for either 3 months or 6 months, and it is confirmed when the change in EDSS score increases by 1.5 points when the starting EDSS is 0, by 1.0 point for starting EDSS scores lower or equal than 5.5 and by 0.5 points for starting EDSS scores greater than 5.5.

The National MS Society's Clinical Outcomes Assessment Task Force recommended an alternative outcome measure for clinical trials to overcome the limitations of EDSS, the MS functional composite (MSFC) (Rudick *et al.*, 1997; Fischer *et al.*, 1999). This is a composite score characterised by three components: timed 25-foot walk (T25FW) assessing walking speed, Nine-hole peg test (NHPT) assessing arm function, paced auditory serial addition test - 3 seconds (PASAT) (Cutter *et al.*, 1999; Fischer *et al.*, 1999) assessing auditory information processing speed for the cognitive sphere. The three components of the MSFC are reported as Z-scores, which are standardised by comparing the patient's performance to a reference population and a total negative score is related to neurologic deterioration (Uitdehaag *et al.*, 2002). The three Z-scores are partially independent and differ in the direction of change (deterioration indicated by higher scores on the 9HPT and T25FW vs lower scores on the PASAT) and units of measurement (time versus number of correct answers). The choice of the reference population (the pooled dataset used to develop the MSFC, the entry scores from

patients enrolled in a particular study, or healthy controls) can influence the weighting of individual components and comparisons can be difficult (Polman and Rudick, 2010). There are some limitations, such as practice effects or fatigue in completing PASAT, the lack of the reporting of some domains (such as a score assessing the visual function) and the difficulty in interpreting of the composite scale.

Therefore, other scales have been validated as alternative cognitive assessments, e.g. the symbol digit modalities test (SDMT), which has a high sensitivity for the assessment of information processing speed, as a fast low-cost and efficient test to use in the routine clinical practice (Parmenter *et al.*, 2007). In addition, the Rao brief repeatable neuropsychological battery (BRNB) (Rao, 1990), the minimal assessment of cognitive function in MS (MACFIMS) (Grossi *et al.*, 2020), and the Brief International Assessment of Cognition for MS (BICAMS) (Corfield and Langdon, 2018) have been all successfully used in trials. For the visual function, a widespread test is the Sloan low-contrast visual acuity (SLCVA) chart.

Recently, new clinical measures have been introduced to better specify the events occurring over the MS course. For example, in a recent trial relapse-associated worsening (RAW) was defined as a neurological event confined within 90 days after a relapse (Kappos *et al.*, 2020). RAW is usually separate from the progression independent of relapse (PIRA), which occurs without any recorded relapse within a defined time interval. Those new definitions for MS-related clinical events reflect that there is a single disease continuum with an underlying progressive disease course and a highly variable superimposed accumulation of disability resulting from relapses with incomplete recovery.

Patient-reported outcome measures (PROMs) have been also introduced in the clinical trials in order to assess broadly multidimensional domains from the patient perspective in the form of questionnaires, including health distress, sexual function, overall quality of life, cognitive function, energy, pain, walking, sleep quality, fatigue, and social function. Some of them include the MS quality-of-life questionnaire, the functional assessment of MS, and the MS impact scale, which are assessing both physical and psychological impact of the disease (Hobart *et al.*, 2001). However, other PROMs have been designed to focus on a single function, such as ambulation, depression or fatigue

(MS walking scale-12, Beck depression inventory and modified fatigue impact scale) (Cohen *et al.*, 2012).

Despite the importance of this definition and all the clinical measures described so far, there are still several limitations in the definition of disability progression. Those measures (i.e. CDP or CDA) are a construct of the trial setting and they do not always depict the overall complexity of disease progression occurring in MS. Another fact to take into consideration is the summation of the ageing effects and the comorbidities (described in the next paragraph), which are all contributing to a faster deterioration (Marrie *et al.*, 2015). Overall, a future need is to favour the analysis of MS progression, due to the high complexity level, and to include the multiple functions that are affected over the disease course and their impact on the daily routine.

1.5 Aetiology

The aetiology of MS is largely unknown, but it is widely recognized that it has multifactorial causation, involving both genetic, endogenous and environmental risk factors (Compston and Coles, 2008). There is a complex interaction between those risk factors, acting together in a likely autoimmune mechanism, leading ultimately to demyelination and neuroaxonal loss (**Figure 1-4**).

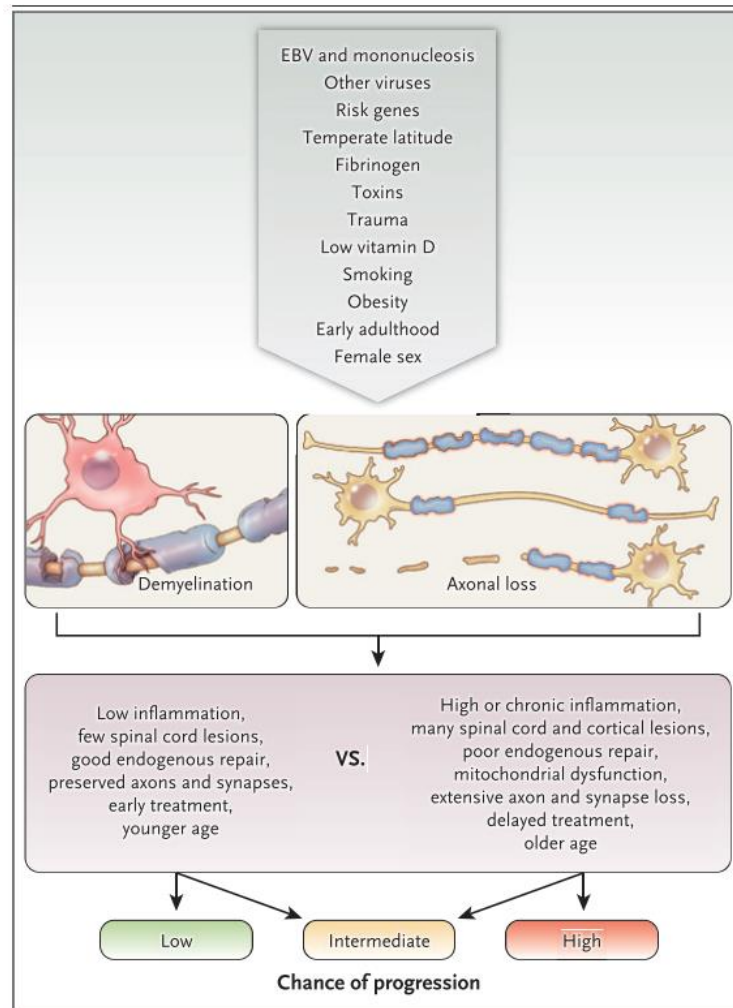


Figure 1-4. Risk factors and modifiers for disease course in MS.
(adapted from Reich D et al., NEJM 2018)

Epidemiological studies have shown a definite role of environmental factors in determining the disease risk for MS. Amongst those factors the latitude gradient, Epstein-Barr Virus (EBV) infections, low vitamin D levels, dysregulated microbiota, obesity, smoking and pollution have provided some evidence for their contribution to higher risk in MS (Ascherio and Munger, 2007; Belbasis *et al.*, 2015; Laura *et al.*, 2016). From a recent systematic review and meta-analyses on 44 risk factors, the authors included infections and vaccinations, comorbid diseases, surgeries, traumatic events and accidents, exposure to toxic environmental agents, and biochemical biomarkers (Belbasis *et al.*, 2015). Only three of these risk factors were supported by evidence with strong epidemiological credibility: evidence of EBV (infectious mononucleosis), low vitamin D levels and smoking.

The latitude gradient was the first described example of how the environment affects the risk of MS. Kurtzke et al. divided areas into high, medium and low risk, according to the latitude: higher prevalence of MS is seen with increasing distance north or south of the equator (Kurtzke, 1975). Interestingly, the risk of MS is modified depending on the birthplace and early life living location. Migration in childhood (considered for people aged < 15 years) from low prevalence to high prevalence parts of the world is associated with an increased risk of developing MS compared with the population of origin (Kurtzke, 2013). The latitude factor is related to additional environmental factors implicated in MS, such as the lack of sunlight exposure and a low vitamin D status, the second being directly affected by the first factor. The geographical distribution of MS suggests that reduction of duration and intensity of UV radiation is strongly correlated with a higher prevalence of disease (Tremlett *et al.*, 2008). A number of studies have found a higher MS risk as well as a poorer prognosis in subjects with low Vitamin D levels (Ascherio *et al.*, 2014).

Many bacterial and viral agents have been associated with multiple sclerosis, but EBV is the only one confirmed to have an implication in MS pathogenesis. Almost all patients (>99%) with MS are infected during adolescence with EBV (showing specific high antibody titres) compared with 94% of age-matched controls (Ascherio and Munger, 2007). EBV involvement in the pathogenesis of MS is not fully understood. MS may be influenced by deficient infection control, resulting in EBV-infected B cells accumulating in the CNS (Fernández-Menéndez *et al.*, 2016). The hygiene hypothesis proposes that low exposure to childhood infections predisposes individuals to proinflammatory immune responses to antigens that increase MS risk (Fleming and Cook, 2006), resulting in a possible protective role from certain infections.

Smoking is consistently recognized as a risk factor for the subsequent development of MS, and it is associated with faster disability progression (Hempel *et al.*, 2017). Numerous mechanisms have been proposed to explain the adverse effects of smoking on MS, including immunomodulatory effects, demyelination, increased nitric oxide and nitric oxide metabolites and disruption of the blood-brain barrier, but all remain speculative (Ascherio, Munger and Lünemann, 2012).

With regards to the genetic factors, the high degree of heritability of MS has been well established by studies describing a higher concordance rate in monozygotic compared to dizygotic twins (Hawkes and Macgregor, 2009). MS has a moderate level of heritability, with a sibling relative recurrence risk of ~ 6.3 (Hemminki *et al.*, 2008), reflecting clustering within families due to genetic factors. Over the years, genetic association studies have shown that the most impacting genetic loci associated with MS are related to the Human Leukocyte Antigen (HLA) from the major histocompatibility complex (MHC). The link to the HLA serotype DR2 has been evidenced since the 1970s and it has been consistently replicated (Jersild, Svejgaard and Fog, 1972). Carriers of the HLA DRB1*15:01 allele are about three times more likely to develop MS than non-carriers, while HLA-A*02:01 allele is considered as a protective factor (Patsopoulos *et al.*, 2013; Sawcer, Franklin and Ban, 2014).

The Genome-wide association study identified 200 autosomal susceptibility variants outside MHC, one chromosome X variant, and 32 independent associations within the extended MHC (Patsopoulos *et al.*, 2019). The genetic suggestive effects jointly plain $\sim 48\%$ of the estimated heritability for MS, of which the HLA locus accounts for 20-30% of the genetic susceptibility, and the other part is occupied by variants outside the MHC. Such variants, with minor genetic effects, include genes involved in the development, maturation and terminal differentiation of immune cells (including B, T, natural killer, and myeloid cells) that may contribute to the onset of MS. Recent studies sequencing the mitochondrial DNA (Ban *et al.*, 2008), found evidence of susceptibility loci related to MS, such as missense mutations that could lead to an excess of reactive oxygen species (ROS), and for variants in proteins involved in oxidative phosphorylation (Poursadegh Zonouzi *et al.*, 2014). Despite those new genetic variants identified, they can explain only a fraction of the heritability in MS, and the remainder is likely to be the result of undefined interactions between risk factors and risk alleles that are yet to be discovered.

Overall, those studies are implicated in MS gene networks operating in both the adaptive and innate arms of the immune system, as well as the enrichment of genes expressed in the microglia, and mutations implying energetic dysfunction (Sawcer, Franklin and Ban, 2014). The polygenic mode of MS inheritance provides the rationale for developing aggregate genetic burden scores, including all identified genome-wide

susceptibility variants, in an attempt to better predict the cumulative effects of genetic liability. For example, each multiple sclerosis-associated alleles (weighted by its effect size) can be summed and calculated for each individual, as a measure of the MS genetic burden (De Jager *et al.*, 2009).

1.6 Pathogenesis

The pathogenetic mechanisms in MS are hypothesised to represent an autoimmune process due to the evidence of an extensive primary inflammatory demyelination, as shown by local inflammatory cells attacking myelin within the MS lesions (Hemmer, Kerschensteiner and Korn, 2015; Alan J Thompson *et al.*, 2018). The replication and refinement of pathological and immunological studies over the years have shown that those features are widespread not only in the focal lesions but extend within all tissues over the whole brain and spinal cord. The disrupted interplay between adaptive and innate immunity and a pro-inflammatory environment favours chronic demyelination and neurodegeneration. It is still unknown whether the primary event is an inflammatory process or whether there is initial neurodegeneration subsequently amplifying the inflammatory reactions.

Over the years research has been centred on understanding the mechanisms involved in MS pathogenesis, which have been greatly shaped by findings from animal models such as experimental autoimmune encephalomyelitis (EAE), specific-pathogen-free-bred mouse and primates. From those studies, it appears that the pathogenic immune response in MS might be initiated in two ways. The first one, from an initial event taking place inside the CNS as a primary cyto-degenerative central process (“inside-out”) that causes neuronal damage, subsequently favouring an activation of the peripheral immune system, supported by the evidence of presence of lesions in MS in the absence of T and B-cells (Barnett and Prineas, 2004). On the other hand, the “outside-in” model (Stys *et al.*, 2012) support that the primary pathogenetic event starts in the context of a systemic response caused by a trigger, leading to an aberrant immune response. Several trigger mechanisms have been investigated (e.g. reactivity between microbial antigens and autoantigens, priming autoimmune responses by a strong inflammatory stimulus), which might account for the initiation of autoimmune

responses. Antigen-specific activation of T cells might be triggered in lymphoid tissue associated with the human gut or bronchial system. Microbiota, especially in the gut, might provide both antigenic and adjuvant signals for T-cell differentiation (Berer *et al.*, 2011).

The adaptive immune system is considered the crucial player of MS inflammation: T cells and B cells are selectively recruited by CNS-restricted specific target antigens (H Babbe *et al.*, 2000). T cells isolated from MS lesions and in the CSF were derived from clonal expansion, suggesting that antigen-specific T-cell responses greatly contribute to the disease process (H Babbe *et al.*, 2000). The epitopes of the target antigens recognized by T cells in the perivascular cuffs or in the CNS parenchyma remain unknown, however, they are supposed to be linked to myelin (Schirmer, Srivastava and Hemmer, 2014). One of the putative auto-antigen is myelin oligodendrocyte glycoprotein (MOG) that can induce EAE (Von Büdingen *et al.*, 2001).

More in detail, the generation of the adaptive immune responses involves the expansion of large numbers of specific lymphocytes from few precursors, through intermediation of antigen presenting cells (APCs). The adaptive immune response involves T cells (CD4⁺ helper and CD8⁺ cytotoxic) and B cells, and the autoimmune event is sustained by presence of auto-reactive cells among those classes. Some autoreactive T cells can derive from the escape of the removal in the thymus from the peripheral immune system, and they are attracted via cytokines/chemokines attraction due to their high avidity and state of activation to the CNS compartment (Charo and Ransohoff, 2006), crossing the blood-brain barrier (BBB) through interaction with adhesion molecules.

Once in the CNS, they are re-activated locally by APCs to start a complex immune attack directed against the myelin through recruitment of the other immune cells. However, they necessitate further triggering events to generate the autoimmune cascade. Those cells can be activated through bystander activation (Selmaj, Raine and Cross, 1991), in which non-specific inflammatory events, such as infections, stimulate an increase in cytokines and chemokine levels activating T cells against auto-antigens. An alternative pathway to sustain the cross-activation of T-cells is the molecular mimicry, driven by the similarity of antigens from self-molecules, or autoantigens.

Another mechanism is also linked to a general reduction of the tolerance of the immune system (Libbey, McCoy and Fujinami, 2007). Maintenance of peripheral immunological tolerance is dependent on CD4⁺ regulatory T cells (T-reg), and their loss leads to multiorgan autoimmunity (Josefowicz, Lu and Rudensky, 2012). Effector CD4⁺ T cells interact with the APCs and they differentiate into Th-1 and Th-2 phenotypes, and within the former class there is strong evidence for the participation of a specific subset of Th17 cells in autoimmune pathological processes (Korn *et al.*, 2009). This subset of T cells can drive tissue damage through the local upregulation and release of the interferon (IFN), the tumour necrosis factor (TNF) family, and the complement activation (Zipp and Aktas, 2006).

However, although responsible for the initial steps of the pathogenetic process, CD4⁺ T cells tend to accumulate in the venular perivascular spaces and only in the parenchyma during the second stage infiltrate (Holger Babbe *et al.*, 2000). Instead, MHC-1 restricted CD8⁺ T lymphocytes represent the major components in the lesions ranging from 60% to more than 85% of the T cells (Lassmann, Brück and Lucchinetti, 2007), mediating the tissue injury not only through an antigen-specific cytotoxic action, but also through antigen-independent mechanisms (Zipp and Aktas, 2006). On the other hand, B cells can escape the negative selection in the bone marrow or become reactive towards self-antigens to initiate autoimmune reactions (Wucherpfennig and Strominger, 1995), they closely interact with T helper cells, from which they receive signals to proliferate, producing immunoglobulins. B cells are present in lesions, meninges, and the CSF in most patients with multiple sclerosis and they are likely to be supported by cytokines and survival factors that are produced by glial cells (Henderson *et al.*, 2009).

The innate immune system, mainly consisting of phagocytic cells, has also an important role in the initiation and progression of multiple sclerosis. Macrophages/microglia promote the proinflammatory response directly or by acting as APCs and activating T/B cells. Early microglial activation contributes to the development of lesions, as it has been shown that a switch to the M1 phenotype promotes pro-inflammatory cytokines/chemokines production during the early disease phase, followed by recruitment of other immune cells with a shift to M2 phenotype favouring an anti-inflammatory environment as a recovery during the later phase

(Correale, 2014). When activated, macrophages/microglial cells could contribute to pathology through several possible mechanisms, including secretion of proinflammatory cytokines, chemokines, free radicals, and increased release of glutamate (Correale, 2014).

During the progressive phase of the disease, the contribution of the peripheral immune system decreases, and immune responses are thought to be confined to the CNS compartment. CNS pathology changes from focal to diffuse white matter injury associated with microglia activation and diffuse lymphocytic and monocytic infiltrates, and increasing cortical involvement, which is associated with lymphoid-like follicles in the meninges (Howell *et al.*, 2011). In this context diffuse tissue injury is also caused by other mechanisms, including degeneration of chronically demyelinated axons, damage or dysfunction of astrocytes (Schreiner *et al.*, 2015), and microglia activation (van Horssen *et al.*, 2012).

The resulting inflammatory reaction, which typically follows a relapsing-onset course in the initial stages of the disease, can be followed by further demyelination and tissue injury in a detrimental cycle. The propagation of the autoimmune events over time can be sustained with the following mechanisms: ‘epitope spreading’, referring to antigens released following tissue damage that can activate other clones of autoreactive cells (McMahon *et al.*, 2005); ‘cumulative autoimmunity’, involving the recruitment of new self-antigens of the axon that are subsequently exposed (Krishnamoorthy *et al.*, 2009). Macrophages/microglia also contribute to chronic mechanisms, as they secrete neuroaxonal damaging substances such as cytokines, ROS and nitric oxide (NO) (Smith and Lassmann, 2002).

The final pathways that might explain the progression of the disease are associated with chronic oxidative injury and channelopathy, with impairment of oxygen consumption and oxidative stress causing disturbed ion channel homeostasis (Halliwell, 2006). ROS and NO produced by macrophages/microglia inactivate proteins of the mitochondrial respiratory chain responsible for energy failure depletion that results in the impairment of ion channels (Waxman, 2008). In particular, this leads to sodium-potassium exchange impairment resulting in intracellular sodium accumulation, which favours membrane depolarization and promotes activation of

axon-damaging calcium-dependent enzymes (**Figure 1-5**). Concurrent hypoxia, caused by inflammatory damage of the vessels and localised oedema on the local microcirculation (Sosa and Smith, 2017), as well as by the increased energy demand on the demyelinated axons contributes to the accumulation of neurodegenerative mechanisms and loss of neuro-axonal function.

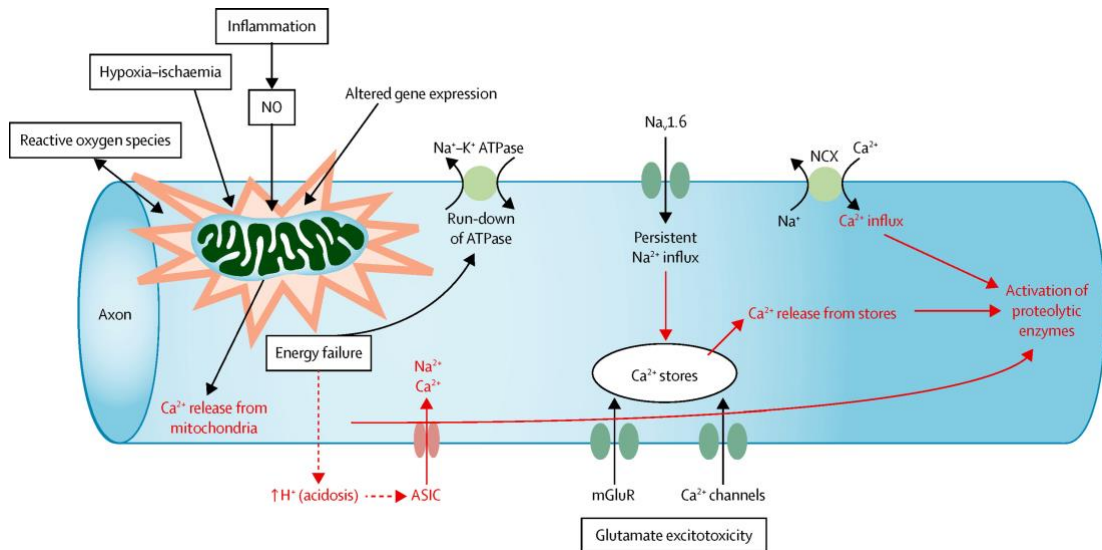


Figure 1-5. Mechanisms of axonal damage in the final pathways contributing to neurodegeneration.

(Adapted from Ciccarelli O, Lancet Neurol, 2014)

1.7 Neuropathology

The pathological findings typical of MS are the presence of inflammatory demyelinating changes, neuro-axonal loss, and gliosis, involving both the white matter (WM) and grey matter (GM) all over the CNS. The main pathological hallmark of MS is the presence of sharply demarcated focal inflammatory WM plaques, also defined as ‘lesions’ (Compston and Coles, 2008; Alan J Thompson *et al.*, 2018). Pathological examination shows characteristic perivascular inflammatory infiltrates, reflecting inflammatory activity (mainly T lymphocytes, a few B lymphocytes and activated macrophage/microglia) and neurodegenerative changes (i.e., gliosis and axonal damage) with a heterogeneous composition depending on the stage of lesion evolution. Classic MS lesions are rounded or oval, with variable extension to the periphery into the parenchyma, and they might be confluent, resulting in a wide range of dimensions

(from <1 mm to several centimetres). However, there are also diffuse inflammatory changes and axonal injury not only confined to focal lesions within those areas that are usually macroscopically normal, thus called normal-appearing white matter (NAWM) (Kutzelnigg *et al.*, 2005).

Relapse-onset early MS is characterised by presence of WM lesions with extensive BBB leakage, therefore called active. On the contrary, in chronic and progressive MS stages lesions do not show this characteristic (i.e. inactive), as they are most frequently found in longstanding disease duration (Frischer *et al.*, 2015). The progressive stage of the disease is thus characterised by a gradual expansion of WM lesions in the absence of BBB leakage, with prominent degeneration of chronically demyelinated axons as major cause of irreversible disability (Mahad, Trapp and Lassmann, 2015). Another important substrate of progressive MS is the presence of GM pathology, with a relative absence of immune cell infiltrates (Kutzelnigg *et al.*, 2005). Brain atrophy is mainly driven by GM volume loss and shows marked regional variations (more extensive involvement of hippocampus, frontal and temporal cortices as well as the cingulate gyrus (Gilmore *et al.*, 2009)). In MS, brain atrophy occurs at rates of 0.5–1.5% per year, and faster rates could be seen in the progressive phases of the disease and in the deep GM structures (Eshaghi, Prados, W. Brownlee, *et al.*, 2018). Ectopic B cell follicle-like structures close to leptomeninges in cerebral sulci have been correlated to cortical lesion formation in SPMS (Frischer *et al.*, 2009). There is increasing evidence that accumulating cortical GM pathology is present from the early stages of MS and plays an important role in the severity of both physical and cognitive disability (Calabrese, Filippi and Gallo, 2010).

Over the years several pathological classification systems for lesion types have been introduced, identifying different ‘patterns’ to suggest the aetiological mechanisms and evolution of the lesions. The term ‘acute’ has been referred to lesions found in cases of fulminant MS causing severe disability and death within 6 months, and it is not currently used for staging. The ‘Bö/Trapp’ system described lesions based on the cellularity as active (hypercellular), chronic active or mixed active-inactive (hypocellular lesion centre with a hypercellular rim) and inactive (hypocellular) (Bö *et al.*, 1994; Trapp *et al.*, 1998). The ‘Lassmann/Lucchinetti/Brück’ system added the concept of demyelinating and remyelinating activity, also including in the

classification of both the early and late phases of these processes, depending on the presence of certain myelin degradation products (Brück *et al.*, 1995; Lassmann *et al.*, 1998; Lucchinetti *et al.*, 2000). The ‘De Groot/van der Valk’ modification combined both systems and, furthermore, introduced pre-active lesion areas that may precede active lesions (Van Der Valk and De Groot, 2000). The Vienna consensus system combined the key characteristics of the presence of inflammatory cells (macrophages/microglia), as well as demyelinating changes (myelin breakdown products), resulting in up to six different lesion types. In addition to that, the classification of the GM lesions has been revised (Bø *et al.*, 2003) based on four types of cortical lesions: type I (cortical-juxtacortical), type II (entirely cortical, small and perivascular), type III (subpial, not extending beyond layers 3 and 4), type IV (extend over the entire width of the cortex).

An updated classification has been recently presented by Kuhlmann *et al.* (Kuhlmann *et al.*, 2017), which simplifies the subtypes of MS lesions in the following categories: active, mixed active-inactive, and inactive (**Figure 1-6**). Active lesions are the initial phenotype of MS lesions, which typically surround veins, with inflammation and demyelination seen concurrently over days to weeks (Alan J Thompson *et al.*, 2018). They are characterized by loss of myelin, diffuse and dense infiltration of the complete lesion area with CD68-positive cells mostly with a foamy morphology (indicating that the formation of the lesion has been in the previous days/weeks) and a lower number of T cells usually localised perivascularly, and astrogliosis (expressed by high glial fibrillary acidic protein) (Kuhlmann *et al.*, 2017).

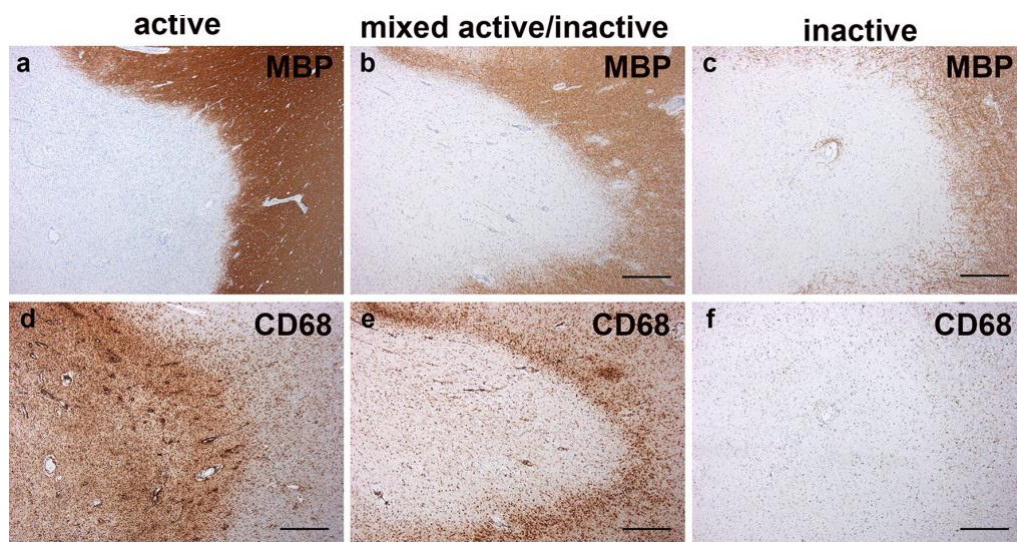


Figure 1-6. MS lesion classification.

(from Kuhlmann T. et al, *Acta Neuropathologica*, 2017)

Active lesions can be further sub-categorised into subtypes depending on the presence or absence of myelin degradation products (Lucchinetti *et al.*, 1996) in macrophages: major or minor molecular weight myelin proteins (i.e. cyclic nucleotide diphosphoesterase, MOG or myelin-associated protein) in early active and demyelinating lesions, late active and demyelinating lesions that show only major myelin proteins (i.e. myelin basic proteins - MBP or proteolipid-protein - PLP); and active post-demyelinating lesions in which the destruction of myelin has ceased and the wave of demyelination has passed. A description of the pre-active lesion has been given with reference to areas that may precede the lesion formation, as characterised by microglial clusters in close vicinity to microvessels surrounded by lymphocytic infiltrates (Singh *et al.*, 2013). It is debated whether pre-active lesions should be considered a separate type as this infiltration might be not specific.

On the other hand, the inactive (or also called silent) lesions are sharply demarcated, hypocellular, as they are almost completely depleted of oligodendrocytes and macrophages/microglia with astrocytes forming a gliotic scar. They present marked loss of axons, and some ongoing axonal damage is demonstrated by axonal swellings. Those are the dominating lesions in patients with disease duration of more than 15 years and SPMS without relapses (Frischer *et al.*, 2015).

The mixed active-inactive (or chronic active) lesions have a hypocellular lesion centre with activated macrophages/microglia limited to the rim or lesion border. The centre of the lesion is almost completely depleted of phagocytes, which are present in the rim, surrounding the lesion partially or completely, in association with hypertrophied astrocytes and moderate T cells infiltrates. The thickness of the rim of macrophages/activated microglia around such a lesion is highly variable, apparently reflecting the activity and speed of lesion evolution (Kuhlmann *et al.*, 2017).

Finally, approximately 20% of the lesions display extensive remyelination, thus it has prompted the definition of a specific lesion type, usually referred as to shadow plaques. The extent of remyelination may differ from lesion to lesion, and it is usually less frequently seen in the progressive MS phenotypes (Patrikios *et al.*, 2006).

1.8 Chronic active (smouldering, or slowly expanding) lesions

Chronic active lesions, also called smouldering or slowly expanding lesions, have been recently studied as they are the dominant lesion type in progressive MS, which might imply a higher risk for disability with their accumulation. The chronic active lesions are pathologically defined as a subset of the mixed active-inactive lesions, in which there is a narrow rim of MBP+/PLP+ macrophages/microglia in the cytoplasm reflecting ongoing demyelinating activity (Frischer *et al.*, 2009). In terms of the evolution of the lesion to the stage of chronic active, it is unclear whether the signs of demyelinating activity in the rim can contribute to a slow expansion of the lesions, whether they represent a new wave of inflammation and demyelination, or they are the last remnant of an earlier demyelinating lesion. As a hypothesised evolution mechanism it is thought that chronic active lesions represent those fractions of the active lesions failing to remyelinate (Goldschmidt *et al.*, 2009). An escape immune surveillance mechanism can perpetuate inflammation which is confirmed by the presence of ongoing demyelination localised in the rim, harbouring axonal injury (Kornek *et al.*, 2000). The most important pathological features of the chronic active lesions are shown in **Table 1-1**.

Table 1-1. Pathological features of chronic active lesions

Pathological characteristic	Description for the chronic active lesions
Cellular distribution and myelin degradation products	<ul style="list-style-type: none"> • Complete demyelination in the lesion core with sparse inflammatory infiltrates • Less prominent perivascular cuffs of mononuclear cells • Lack of early activation macrophage markers
Rim features, thickness and morphology of the macrophages/microglia	<ul style="list-style-type: none"> • CD68 upregulation, ferritin accumulation • Low to moderate demyelinating activity • Broad rim of foamy/ramified macrophages with extensive inflammation and demyelinating activity, (earlier stage of MS) • Narrow rim of macrophage/microglia containing MBP+ and PLP+ (later stage of MS)
Neurodegeneration	<ul style="list-style-type: none"> • Reduced fast axonal transport and presence of focal axonal swellings or end-bulbs staining for neurofilaments (axonal injury) • Incomplete remyelination • Atrophic changes
Iron deposition	<ul style="list-style-type: none"> • In the core: perivascular iron close to central vessels • In the rim: iron and ferritin match with activated macrophages/microglia at the lesion edge • Iron-containing cells at the peripheral rim: CD68 macrophages/microglia with M1 pro-inflammatory phenotype

Abbreviations: MBP: myelin basic protein; PLP: proteolipid-protein

The chronic active lesions are the leading subtype of plaques in long-standing MS, where they can reach from ~30 % up to 50% of the total lesion burden, as shown in large-scale autoptic analyses (Frischer *et al.*, 2015; Luchetti *et al.*, 2018). In the Vienna autopsy cohort studied by Frischer *et al.*, ~15% of chronic active lesions were identified, with higher rates observed in patients with more than 10 years of disease duration (23%), and the peak of prevalence was at 20-30 years after onset (**Figure 1-7**). In estimation models including age and gender, the highest peak of this lesion type was at 50 years of age, with male predominance (Frischer *et al.*, 2015). Regarding the spatial localisation, there was an equal distribution between the supratentorial and infratentorial compartment, but there were no or few chronic active lesions within the spinal cord or the optic nerve. Considering the MS clinical phenotypes, the highest percentages of chronic active lesions were found in SPMS and PPMS (22% and 28%, respectively). The authors concluded that they are almost exclusively seen among progressive MS patients (with/without relapses), representing a promising marker of neurodegeneration (Frischer *et al.*, 2015).

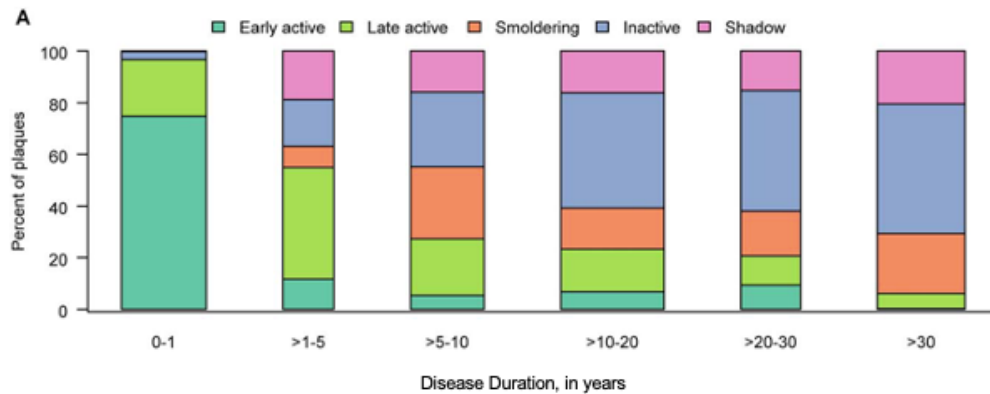


Figure 1-7. Distribution of types of lesions in pathology depending on disease duration.

(from Frischer T. et al., Ann Neurol, 2015)

A further work by Luchetti et al. of the Netherlands Brain Bank analysed 182 MS brain donors (patients with longer disease duration) and confirmed previous findings on chronic active lesions (Luchetti *et al.*, 2018). The authors identified that the majority (57%) of lesions were either active or chronic active and that patients who had a more severe disease course (shorter time to EDSS 6) showed a higher proportion of chronic active lesions, together with a higher lesion load at the time of death. In addition, they also identified that a higher proportion of chronic active lesions were found in progressive MS compared to relapsing disease, and in male compared to female patients.

1.9 Diagnosis of multiple sclerosis

The diagnosis of MS is primarily clinical and relies on the demonstration of symptoms and signs attributable to the presence of multifocal inflammation sites, along with the exclusion of other conditions that may mimic MS. In clinical practice, the neurological examination is integrated with paraclinical studies, including imaging and laboratory tests.

Magnetic resonance imaging (MRI) is the most sensitive tool to detect the demyelinating and neurodegenerative damage in the brain and spinal cord of MS

patients. MRI conventional measures in MS (lesion load, gadolinium enhancement and new/enlarging T2 lesions) are the best surrogate markers used to support the diagnosis and define disease activity, guide treatment decisions and as outcome measures in clinical trials. MRI also provides several measures that correlate with disability and disease progression and new advanced quantitative MRI techniques help to understand the pathogenetic processes underlying neurodegeneration (Filippi *et al.*, 2011).

Testing of cerebrospinal fluid (CSF) provides evidence of chronic inflammation of the CNS and BBB damage, showing mononuclear cells (generally <50 cells/mm³), slightly raised total proteins (not exceeding 100 mg/dl). Two or more unmatched oligoclonal bands detected through isoelectric focusing in CSF but not in serum are found in nearly 90% of MS patients and 68% of CIS patients with a high risk for conversion to clinically definite MS (Dobson *et al.*, 2013). Neurophysiological studies have been used to document reported past episodes or clinically silent lesions in MS in pathways which are not well explored in routine MRI. Visual evoked potentials are useful to assess the extent of demyelination in the optic nerve, and P100 latency prolongation in a patient reporting possible optic neuritis can be considered as a clinical episode supported by paraclinical evidence, which has also moderate ability to predict the clinical evolution of the episode (Kallmann *et al.*, 2006). The evidence of retinal nerve fibre layer thinning at optical coherence tomography (OCT) has been recently employed as alternative suggestive paraclinical data of a visual relapse, as it reflects axonal damage and relates to future disability (Costello, 2011).

The diagnostic criteria have been adjusted over the years according to the advances in the investigation tools available. With reference to the latest 2017 McDonald criteria for the diagnosis of MS, they rely on the combination of dissemination in space (DIS) and dissemination in time (DIT) criteria (Thompson *et al.*, 2017). DIS can be demonstrated by one or more T2-hyperintense lesions (no distinction between symptomatic and asymptomatic MRI lesions is required) in the following areas of the CNS: periventricular, cortical or juxtacortical, infratentorial brain regions, and the spinal cord. DIT can be demonstrated by the simultaneous presence of gadolinium-enhancing and non-enhancing lesions at any time or by a new T2-hyperintense or gadolinium-enhancing lesion on follow-up MRI, with reference to a baseline scan, irrespective of the baseline MRI.

For patients presenting with clinical features suggestive of primary progressive MS, the criteria require evidence of one year of disease progression (retrospectively or prospectively determined) independent of clinical relapse plus two of the three following criteria: 1) One or more T2-hyperintense lesions characteristic of MS in one or more of the following brain regions: periventricular, cortical or juxtacortical, or infratentorial; 2) Two or more T2-hyperintense lesions in the spinal cord; 3) Presence of CSF-specific oligoclonal bands. The terminology of “solitary sclerosis” is used for patients presenting with one inflammatory white matter brain or spinal cord lesion without subsequent new lesion formation, developing progressive disability and showing positive CSF oligoclonal bands.

For POMS, the same diagnostic criteria are applicable to patients who are age 11 or older, whilst under this cut-off, it is important the exclusion of other CNS demyelinating disorders of childhood, such as acute disseminated encephalomyelitis (ADEM), which has usually a monophasic encephalopathic presentation not explained by fever (Krupp *et al.*, 2013). However, some ADEM might be followed by episodes that are non-encephalopathic, and then satisfy the diagnostic criteria for MS. On the other side of the spectrum, 0.5% of adults have disease onset at the age of 60 years or older, who are more likely to have a progressive course at presentation and require careful consideration of alternative diagnoses and comorbidities.

The last revision of the diagnostic criteria stressed the importance of the integration of history, examination, clinical, imaging, and laboratory findings to diagnose MS, focusing on the risk of misdiagnosis (Thompson *et al.*, 2017). The main diseases that should be considered in the work-out are other demyelinating diseases including neuromyelitis optica spectrum disorders (NMOSD) and myelin oligodendrocyte glycoprotein antibody disease (MOGAD) supported by specific MRI and laboratory findings, systemic vasculitis involving CNS, neurodegenerative disorder of the brain and spinal cord (e.g., hereditary cerebellar ataxias), disorders affecting one anatomical site and with either a relapsing or progressive course (especially tumours and other structural lesions), monophasic disorders affecting neuroanatomical sites (e.g., ADEM).

The Magnetic Resonance Imaging in MS (MAGNIMS) research consortium revised the imaging requirements, and recently recommended the inclusion at MRI of a new typical MS localizing area, the optic nerve, in the DIS criteria (Filippi *et al.*, 2016). The potential role of the contribution of cortical lesions has been appreciated, due to the introduction of MRI acquisitions in clinical practice, such as double inversion recovery (DIR), phase-sensitive inversion recovery (PSIR), and magnetization-prepared rapid acquisition with gradient echo sequences (MP-RAGE). The role of more sensitive imaging methods to detect grey matter pathology (particularly to demonstrate subpial cortical and deep grey matter lesions) and techniques to distinguish MS lesions from T2 hyperintensities in other conditions are being explored (eg, central vein sign on susceptibility-weighted, T2*-weighted, or FLAIR* images or paramagnetic rim on T2*-weighted, phase-weighted, or susceptibility-weighted images).

1.10 Therapy

Several disease-modifying treatments (DMTs) have been discovered and the Food and Drug Administration (FDA) and European Medicines Agency (EMA) have approved more than 15 medications over the last decade (**Figure 1-8**), and usually applied within country-specific guidelines.

In general, DMTs target neuroinflammation and could have an indirect effect on neurodegeneration. However, their efficacy for reducing the accumulation of disability in the progressive phase has been moderate, leading to the recommendation of treating in the early phases to delay disability accumulation. Two therapeutic approaches are available in the clinical setting (Montalban *et al.*, 2018). The escalation strategy consists of starting with a first-line DMT (a moderately effective medication) and escalating to a more effective but potentially less safe DMT (second-line, third-line, etc), in cases of persistence of relapsing or progressive activity. The induction strategy involves starting with a highly effective therapy with the aim of obtaining a persistent disease remission in highly active or rapidly evolving disease.

In patients with highly active and severe disabling RRMS, at a young age (< 50 years) and relatively short duration of disease (< 5 years), who failed to respond to multiple lines of treatments, sustained remission and improvements in neurological disability were reported after treatment with high-dose immunosuppressive therapy and autologous haemopoietic stem cell transplantation (Simpson, Mowry and Newsome, 2021).

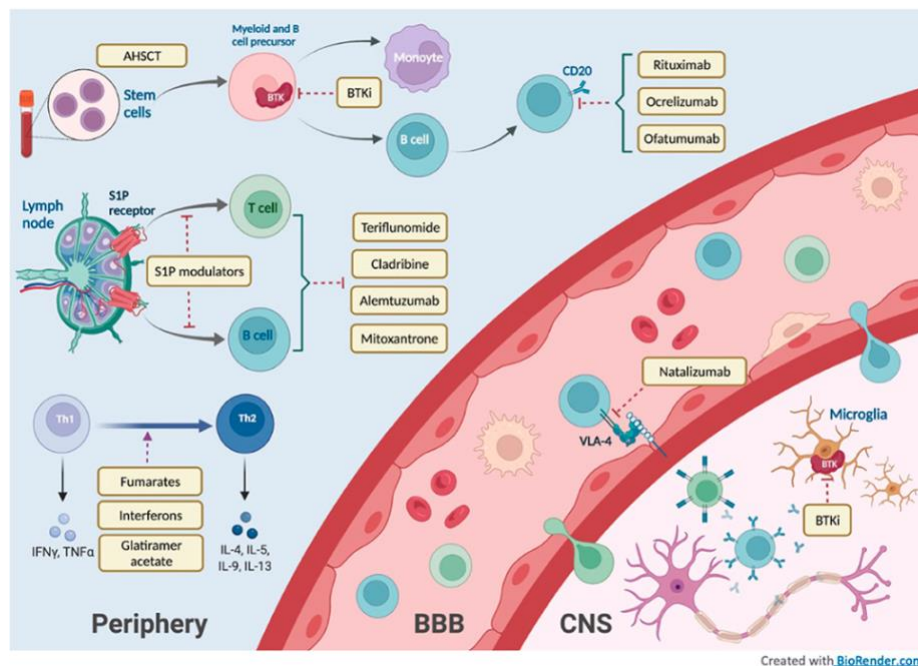


Figure 1-8. Disease-modifying treatments for multiple sclerosis, mechanisms of action.

(from Yang JH et al., *Frontiers in Neurology* 2022)

The Injectables have been the first generation of DMTs applied medications to control exacerbations in RRMS (Signori *et al.*, 2016) and they include interferon- β (various forms including the pegylated) and glatiramer acetate. Those medications can decrease the ARR by slightly more than 30%, reducing brain MRI inflammatory activity, and slowing disease progression as documented by numerous trials (Alan J Thompson *et al.*, 2018). The second generation of DMTs was initiated by the introduction of oral and infusion therapies, with higher efficacy profiles but increased side effects, such as alterations in blood tests, lymphopenia, and risk of infectious conditions due to the

induced immune suppression, such as progressive multifocal leukoencephalopathy (PML).

Among the oral DMTs, the ones currently approved for relapsing MS are the following: dimethyl-fumarate, teriflunomide, cladribine, fingolimod, ozanimod. Fingolimod was the first to be introduced within the sphingosine-1-phosphate receptor (S1P) modulators, acting by stopping the egress of T and B lymphocytes from lymph nodes, and demonstrated in trials ARR reductions of ~50%, and hazard ratio of 0.7 for the reduction of cumulative disability progression, thus being indicated as a second-line drug (Khatri, 2016). The newest and more selective S1P modulators to improve safety and reduce cardiac side effects include ozanimod and ponesimod (Ruggieri, Quartuccio and Prosperini, 2022). Teriflunomide, acting through blockage of the pathway of the pyrimidine synthesis has demonstrated particular efficacy for stabilisation of sustained disability progression (He *et al.*, 2016). Dimethyl-fumarate has been shown to have immunomodulatory and neuroprotective effects (e.g. the expression of detoxification enzymes in microglial cells and the induction of Th2-type cytokines), with a similar efficacy profile as the other oral therapies (Xu *et al.*, 2015).

A group of DMTs have been designed to act through an immune depletion and repopulation strategy, usually defined as immune reconstitution therapies (IRTs), preferentially used in highly active or severe disabling relapsing MS cases as high-potency treatments. Cladribine is an oral IRT, that acts via inhibition of DNA synthesis of the lymphocytes, and showed efficacy in reducing relapse rates by more than 50%, disability progression and MRI activity (Giovannoni *et al.*, 2010).

The infusions DMTs are humanized monoclonal antibodies directed against receptors expressed by immune cells relevant to the MS pathogenesis, and some of them are IRTs. The first one to be licensed was Natalizumab (monthly infusion now available as a subcutaneous formulation), directed against the $\alpha4\beta1-7$ integrins, acting via inhibition of lymphocytes binding to the endothelial receptors (VCAM-1) thus blocking their transmigration into the CNS. This drug reached high rates of ARR reduction by about ~70% and ~90% of MRI activity (Polman *et al.*, 2006). Despite the high efficacy, the use of Natalizumab is associated with a relevant risk for PML (prevalence of ~4 in 1000 (Pitarokoili and Gold, 2017)), increased with the duration

of infusions, prior immunosuppressant treatment, and seropositivity for anti-JC virus antibodies. Alemtuzumab is directed against CD52 to deplete circulating T and B lymphocytes, reaching high efficacy in patients with RRMS as assessed in trials of comparison to interferon beta, showing a lower ARR and fewer patients with worsening disability at 2 to 3 years follow-up (Coles *et al.*, 2012).

Ocrelizumab, a monoclonal antibody targeting the CD20 epitope on B-cells was the first treatment licensed not only for relapsing but also for PPMS, in consideration to the association with lower rates of clinical and MRI progression compared to placebo in trials (Hauser *et al.*, 2017; Havrdová *et al.*, 2018). Rituximab is a similar CD20 B-cell treatment (binding to a different epitope), which was shown to have similar efficacy (Hauser *et al.*, 2008), however, used in MS as an off-label option. Ofatumumab is a fully-humanized anti-CD20, with a subcutaneous formulation that has facilitated patient compliance and that has shown efficacy in reducing relapses and disease progression, and MRI disease activity, compared to Teriflunomide (Hauser *et al.*, 2020). The Bruton's tyrosine kinase (BTK) inhibitors (evobrutinib, tolebrutinib, orelabrutinib) act on a cytoplasmic kinase expressed on cells of the hematopoietic lineage leading to immune modulation via signal transductions from B-cell receptor, which are now under evaluation in phase II-III trials.

For longstanding SPMS with clinical or MRI activity interferon beta-1b and mitoxantrone have indication for relapsing SPMS; however, the role of these two drugs in SPMS is unclear and clinical trials have shown contradictory results. Siponimod, an oral S1P modulator, has been licensed for SPMS due to the efficacy shown in trials of ~20% relative reduction of 3 month confirmed disability progression (Kappos *et al.*, 2018). There are also encouraging results in studies of neuroprotective agents including simvastatin, biotin, phenytoin, ibudilast and reparative agents such as clemastine.

1.11 Rationale for thesis

The purpose of this project is to improve the understanding of the mechanisms that determine disability progression in MS, by developing more specific and sensitive *in vivo* MRI tools.

In the longer term, many patients with MS develop a significant neurological disability, while others have a milder disease course. The mechanisms responsible for the heterogeneity in this disease course remain poorly understood, especially the factors important in the development of disability in progressive MS. There is also the need for improved prognostic markers that can better define the long-term trajectory of MS evolution. Considering that chronic active lesions have been recently shown to represent pathologic markers intrinsically contributing to worsening disability, their imaging correlates need to be studied in all the MS phenotypes and in multiple contexts (e.g. research trials, observational cohorts), through the evaluation of the associations to clinical measures.

Conventional MRI has some limitations in the determination of the persistence of the chronic lesion types in MS, due to the dynamic nature of MS inflammation and remyelination, but recent MRI methodological studies provided evidence of new markers with a potential correlation to the chronic active lesion types. The main aim of this work was to dedicate to the investigation of those new MRI markers in relation to measures of physical and cognitive disability both in relapsing and progressive MS phenotypes and in a wide range of time intervals of longitudinal analyses.

The specific objectives of this project were:

- 1) To contribute to the application of a pilot analysis for detection of the Slowly Expanding Lesions (SELs), a volumetric MRI tool to automatically track constant lesion expansion and extend this application to a trial of secondary-progressive MS. SELs were studied in relation to MS-specific conventional markers, such as the total lesion burden (at T2-weighted or FLAIR) and manually detected new lesions or black holes. Then, this work aimed to assess the spatial localisation and microstructural damage within the SELs through a quantitative analysis of the magnetization transfer ratio (MTR), as a marker of neuroaxonal loss, and their effects on the surrounding tissues and on the global brain volume changes.

2) To investigate the radiological features of SELs in a relapse-onset observational cohort and their relationship to other markers of tissue damage, by implementing a pipeline on the evaluation of T1 hypointensity to detect the persisting black holes (PBHs). This contributed to understanding whether PBHs and SELs were associated, and to confirming the presence of neuroaxonal loss components as assessed by the longitudinal change in T1 intensity. In addition, the impact of SELs on clinical disability has been evaluated on a longer and more heterogeneous follow-up, validating the previous findings, and extending further the application of this technique.

3) To evaluate an alternative MRI marker for the chronic active lesions by analysing the paramagnetic rim lesions (PRLs) at susceptibility imaging. The aim was to assess the relationship between SELs and PRLs, and to evaluate their association with conventional MRI markers, such as total lesion and brain-derived volumes. This analysis was a contribution toward the stratification of patient groups defined by the presence of PRLs and SELs, and to assess the independent and combined contribution of this categorisation on clinical disability evolution.

4) The final work aimed to evaluate the fraction of newly developed lesions which corresponded to SELs, as an explorative analysis of the trajectory of the lesion evolution from their onset. In addition, using data from a trial in progressive MS, another objective included the investigation of the distribution of new lesions and SELs in patients who received treatment versus placebo, to assess whether the expansion of the new lesions and SELs were similarly affected by the exposition to the treatment.

To address all the objectives, I initially conducted a review of the literature in chapter two, including an overview of the imaging markers in MS followed by a focus on the techniques for the analysis of chronic active lesions that I used in the experimental chapters. Then, I continued with the experimental studies, which are described in chapters three to six, followed by the conclusion of this work.

2 Imaging chronic active lesions in MS

2.1 Magnetic resonance imaging markers in MS

Magnetic resonance imaging (MRI) plays a leading role in MS diagnosis, follow-up, and treatment management due to the availability of several biomarkers, assessed through a non-invasive technique. MRI has become central in MS due to the possibility of imaging all the pathological aspects encountered in the disease, among the white and grey matter pathological structural changes, and volumetric measures of expanding inflammation or global and regional brain atrophy (**Figure 2-1**).

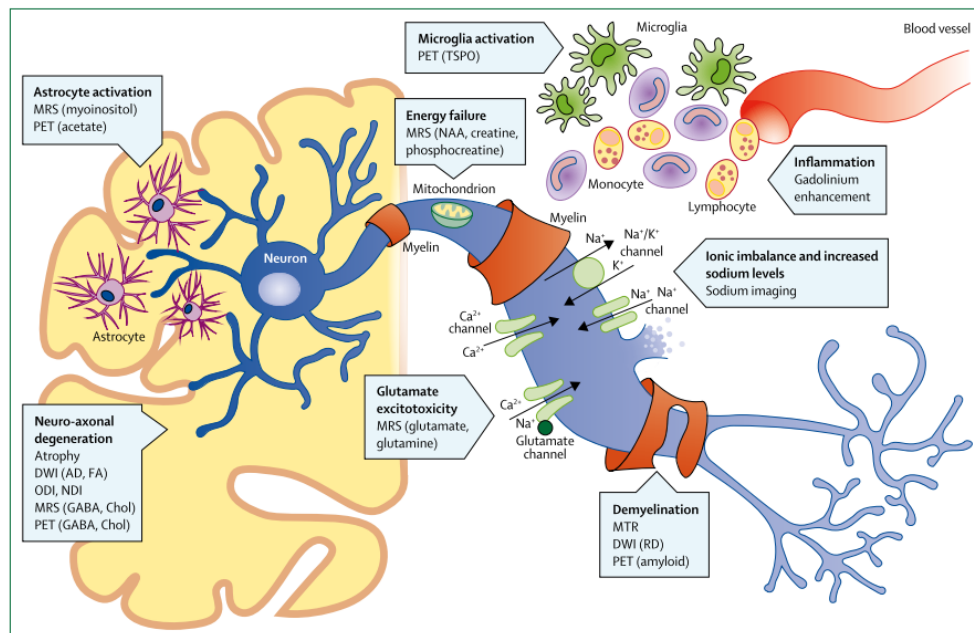


Figure 2-1. Imaging targets for the pathogenetic mechanisms involved in MS.

(Adapted from Thompson AJ. et al. The Lancet 2018)

The hallmark of this neuro-inflammatory condition is the presence of focal white matter lesions with primary demyelination and astrocytic scarring. However, from the pathological background there is an important involvement of several other tissues within the CNS. Lesions are not restricted to the white matter, as they are identified also in the cortical and deep grey matter structures and the spinal cord. There is also

the presence of diffuse neurodegenerative changes in the normal-appearing white and grey matter and all those factors contribute to brain and spinal cord atrophy. MRI has allowed the use of several techniques to acquire images of all the structures and tissues affected in MS, which are discussed in this chapter

2.2 Imaging lesions in MS with conventional MRI

Inflammatory demyelinating lesions of the white matter can be easily visualised on conventional MRI due to the effect of local inflammation, leading to an increase in the amount and mobility of water protons. The MRI correlate is a characteristic signal increase, so-called ‘hyperintensity’, that is at least 3 mm in long axis on T2-weighted spin/fast-spin echo, proton density (PD), and fast fluid attenuated inversion recovery (FLAIR) sequences, and it can also be referred as to ‘T2 lesion’ (**Figure 2-2**).

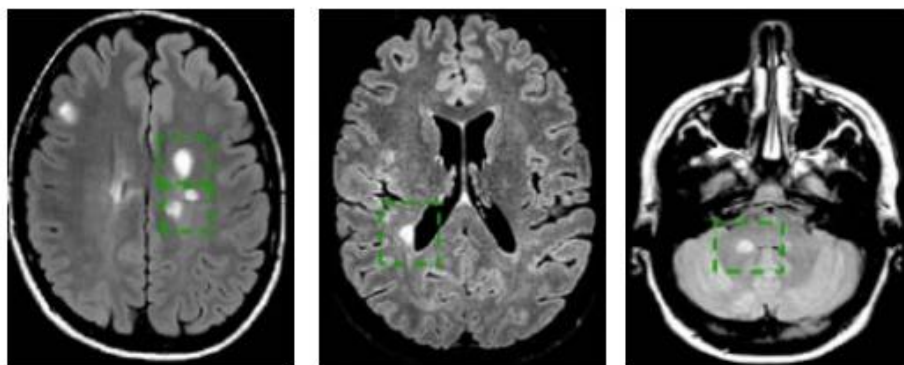


Figure 2-2. Typical supratentorial and infratentorial MS lesions at T2-weighted or FLAIR.

(Adapted from Filippi M et al. Brain 2019)

The high sensitivity of those conventional MRI acquisitions has been extensively demonstrated with good agreement between studies in the detection of MS lesions (Filippi *et al.*, 2012, 2019). However, T2 lesions are not specific to histopathological subtypes and stages, as they can correspond to a wide spectrum of pathological changes, ranging from oedema and demyelination to glial scars and liquid necrosis (De Groot, 2001). Furthermore, they are not entirely MS-specific, as those alterations are similarly found in other neurological inflammatory conditions, or also in migraine and

cerebrovascular disease (Thompson *et al.*, 2017). It is extremely important to note red flags for lesions that might be encountered in other conditions, also defined as MS mimics (Miller *et al.*, 2008). In the recent diagnostic criteria, further emphasis has been given to the evaluation of MS mimics (Alan J. Thompson *et al.*, 2018), which is partially due to the low specificity of the hyperintense lesions at T2-weighted images. For example, the authors claim that vigilance is needed to exclude the alternative diagnoses, particularly NMOSD and MOGAD in populations such as African American, Asian, Latin American and paediatric MS cases. Furthermore, they suggest in certain areas (Latin America) to be aware of infectious diseases and nutritional deficiencies. Moreover, in pathological MS studies, when areas showing hyperintensities at conventional MRI were sampled and analysed, a significant percentage of lesions did not show any demyelination, probably due to the effect of remyelination or very subtle pathology (Kidd *et al.*, 1999; Van Waesberghe *et al.*, 1999; Barkhof, Bruck and De Groot, 2003). Therefore, conventional MRI despite being sensitive to lesions is not specific for histological lesion types.

Several studies have demonstrated a correlation between total T2 lesion burden, conversion to clinically definite MS and worsening disability in the long term (up to 20 years from disease onset) (Brex *et al.*, 2002; Rudick *et al.*, 2006; L. K. Fisniku *et al.*, 2008). Markers including new T2 lesions, change in T2 lesion volume or active lesions, including contrast-enhancing lesions (CELs) or enlarging T2 lesions (manually identified), can capture the cumulative new inflammation occurring in the interval between scans. All those imaging markers and a combination of them (also defined as combined unique active lesions) have been particularly relevant for trials of medications targeting the inflammatory activity in patients with relapse-onset MS, and some of them have been also used in progressive MS. The importance of those markers in MS studies has been shown for their extensive use as primary or secondary outcomes trial measures for inflammatory activity and in clinical routine as a guide towards DMT efficacy assessment (Sormani and Bruzzi, 2013). Despite a correlation to relapses (Tintore *et al.*, 2015), active lesions have been only partially correlated to disability progression in progressive MS phenotypes with variable findings over the long term, with a correlation coefficient from 0.13 to 0.67 (Khaleeli *et al.*, 2008; L. K. Fisniku *et al.*, 2008). The poor prognostic value on disability outcomes is possibly related to the heterogeneity between lesion types that remains undetected (Barkhof,

Bruck and De Groot, 2003). Moreover, the time taken to develop T2 lesion load has been suggested to be more relevant than the actual lesion load in determining disability (Adams *et al.*, 1999), so that a slower accumulation of lesion load may allow more time for repair and recovery of function.

2.2.1 Spatial localisation of MS lesions

The spatial localisation of lesions has been studied since the introduction of MRI in MS. The importance of topographical localisation has been discussed in relation to MS diagnosis, in consideration of the requirements for satisfying the dissemination in space criteria. Over the years the number of lesions needed to allow MS diagnosis has been reduced, while the typical localisations for MS lesions have been extended, also thanks to the improvement in MRI techniques.

Many lesions are clinically silent, and the location of a lesion determines the likelihood that it will be clinically declared or clinically relevant. The presence of infratentorial (e.g. brainstem or within deep white matter) (Tintore *et al.*, 2010) or spinal cord lesions increases the risk of disease progression after a CIS or in established MS (Brownlee *et al.*, 2019), which was confirmed at a long term follow-up reaching 30 years after disease onset (Chung *et al.*, 2020). In those analyses, it has been demonstrated that not only the higher number of lesions is correlated to the development of worse clinical scores, but also the topography of lesions is an independent predictor of disability progression.

Recent studies have identified that lesions localised more caudally along the neuraxis involving the lower parts of the brain and spinal cord (**Figure 2-3**), where a higher number of WM tracts are in the vicinity, associate with greater motor and/ or cognitive disability at baseline and over time (Tur *et al.*, 2022).

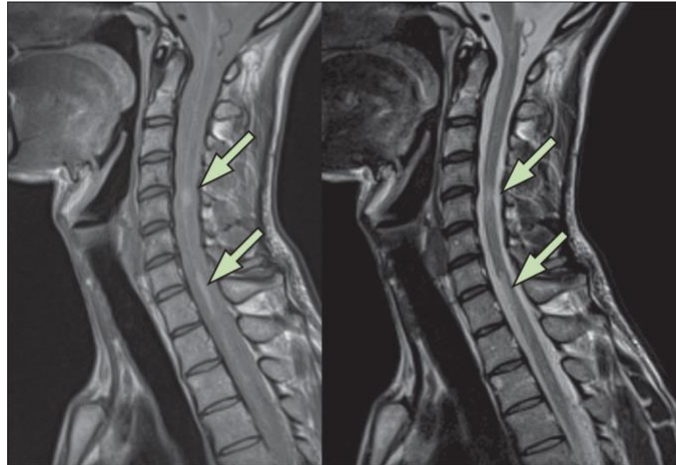


Figure 2-3. Typical spinal cord lesions in MS.

Sagittal intermediate and T2-weighted dual echo fast-spin echo MRI (picture adapted from Filippi M. et al. 2016, Lancet Neurol)

2.2.2 Contrast-enhancing lesions (CELs)

The MS pathogenic processes involved in the onset of lesions start from lymphomonocytic infiltrates surrounding veins. There is also perivascular inflammation around small blood vessels at the edges of lesions and in the surrounding tissues. At pathology newly forming lesions are characterised by at least three concentric areas surrounding a central vein and the perivascular cuff (Henderson *et al.*, 2009): (1) a central region, heavily demyelinated and infiltrated by myelin-containing macrophages; (2) an intermediate region, partly demyelinated; and (3) a peripheral region, with intact myelin, activated microglia, and some oligodendrocyte loss. An important tool to characterize lesions is the evaluation of the disruption and leakage of tight junctions of the blood-brain barrier (BBB) through the identification of CELs (**Figure 2-4**). T1-weighted MRI in combination with low molecular weight gadolinium-based contrast agents (GBCA) can characterize BBB compromise and subset a group of CELs, that have also been termed “active”.

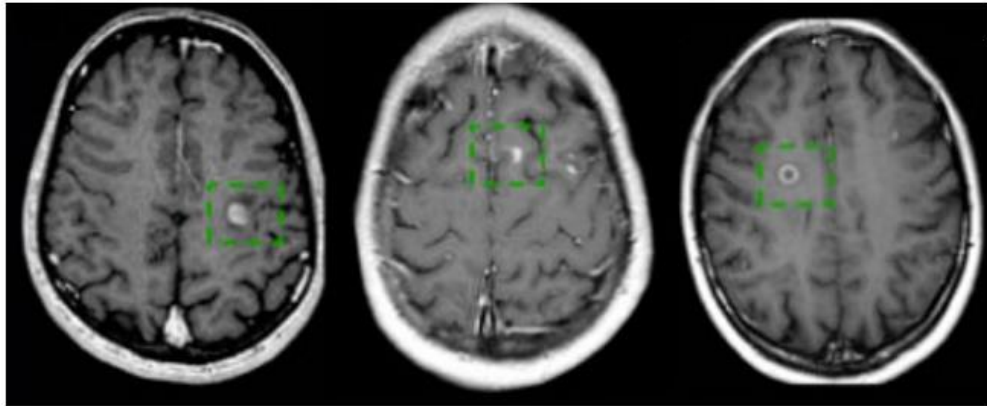


Figure 2-4. Examples of brain typical contrast-enhancing lesions (CELs) in MS. (Adapted from Filippi M. et al. Brain 2019)

There is a good agreement between studies showing that enhancement is a characteristic feature of active inflammation, for its correspondence to intravascular and perivascular inflammatory infiltrates, and cells dysfunction derived from soluble factors in other adjacent lesions in the area surrounding parenchymal micro-vessels. Those are all characteristics of newly forming lesions, as shown in the brain biopsies of early MS cases (Brück *et al.*, 1997). Further studies have demonstrated that BBB permeability to GBCA can also identify the pre-active lesion stage, as it is transiently increased several months prior to new lesion formation (within the preceding 3 to 6 weeks) (Cotton *et al.*, 2003), then a massive increase of permeability during the acute lesion phase, followed by normalisation over 1-2 months after a lesion first appears (or an incomplete normalisation). However, it should be noted that the BBB disruption is not exclusive to the active plaques, as it is also present in inactive lesions and NAWM (Vos *et al.*, 2005). This is justified by the presence in the vicinity of active lesions of numerous vessels, showing leaky endothelial cells due to soluble inflammatory cytokines and chemokines that are liberated from inflammatory cells in the adjacent lesions, destabilizing the surrounding tissues. Despite the high correlation demonstrated by CELs, T2-related measures are preferred in monitoring disease activity, due to the increased costs associated with gadolinium use and the fact that gadolinium infusions entail a risk of rare but severe adverse events (nephrogenic systemic fibrosis).

In some research analyses, CELs have been classified according to their pattern at GBCA, as nodular or ringlike. Nodular lesions have homogeneous hyperintensity

throughout the lesion, while ringlike can have an open or closed shape depending on the presence of an incomplete or complete hyperintense rim surrounding a hypointense centre. Ringlike lesions can be associated with more severe tissue damage, and, in particular open-ring lesions, are described as characteristic of demyelinating diseases (Morgen *et al.*, 1995).

The use of advanced techniques based on dynamic contrast enhancement (DCE), through 4D rapidly acquired repeated post-contrast T1-weighted serial images, has allowed classification of two main subtypes or patterns of enhancement representing stages of the MS lesion development: centrifugal (enhancing from the centre to the periphery, also defined nodular) or centripetal (enhancing from the periphery towards the centre, also defined ring or shell-like). The earliest stages of lesion formation are usually characterised by the centrifugal-DCE pattern, corresponding to the initial opening of BBB (Gaitán *et al.*, 2011, 2013). In an older phase of evolution, the lesions are marked by a centripetal-DCE pattern, reflecting capillary recruitment at the lesion edge and outward expansion. In those studies, centrifugal lesions are smaller, while centripetal are larger. Importantly, centripetal enhancing lesions never became centrifugal, and this process may reflect the typical way in which MS lesions grow.

In the progressive MS phenotypes, CELs are rarer, as reflected by the pathological evidence that the active lesions are also less frequent. In the late MS stages, inflammation becomes trapped or behind a closed or repaired BBB. However, the absence of GBCA does not depict the cessation of inflammation, but most probably a shift towards a chronic and compartmentalized one. Mild disturbance of the BBB, which seems to be below the detection limit of GBCA, is seen in some of the inflamed or not inflamed vessels at this stage. In addition, many vessels with profound perivascular inflammatory infiltrates are seen that do not show any evidence of increased permeability. At this stage of the disease, inflammation also accumulates in the meninges and perivascular spaces in the form of lymph follicle-like structures (Serafini *et al.*, 2004; Magliozzi *et al.*, 2007).

To track chronic MS inflammation, other enhancing substances have been explored. One alternative was introduced with a technique based on ultra-small superparamagnetic particles (USPIO) to track iron-laden macrophages as one of the characteristics of

chronic active lesions, but it has shown safety concerns around the toxic effects of this substance (Gkagkanasiou *et al.*, 2016).

2.3 Imaging tissues beyond white matter lesions in MS

2.3.1 Grey matter damage: cortical lesions and GM atrophy

In pathology there are heterogeneous types of cortical demyelinated lesions in MS and, in general, cortical demyelination may affect up to 80% of the cortical ribbon in the forebrain and up to 95% in the cerebellum; subpial areas are more commonly affected in progressive MS. Cortical lesions (CLs) differ from the white matter lesions as the T- and B-cell infiltrates are mostly in the meninges, while they are sparse or absent within the cortical parenchyma, and BBB disruption is usually absent (except for the cortico-subcortical lesions where there is WM involvement).

At imaging, cortical lesions are nearly invisible by conventional MRI but they can be more readily identified with double inversion recovery (DIR), which uses two inversion pulses to suppress the signal from WM and cerebrospinal fluid (**Figure 2-5**). On DIR they are recognised as focal hyperintensities, compared to adjacent NAGM. However, the double suppression scheme in DIR creates artefacts (flow artefacts, nonuniform magnetic field), thus making it possible to identify only the larger subcortical lesions, and compared to post-mortem assessment, DIR detects only 18% of all GM lesions (Seewann *et al.*, 2012). As an alternative, phase-sensitive inversion recovery (PSIR) sequences have shown some benefits for higher resolution in the detection of cortical lesions, although this has not been confirmed for the subpial lesions. Moreover, increasing field strength with 7T MRI has allowed a more accurate characterisation of cortical lesions using magnetization-prepared rapid acquisition with gradient echo (MPRAGE) sequences.

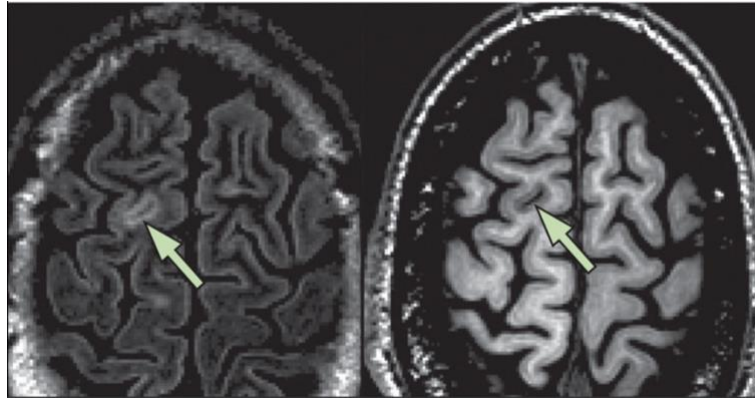


Figure 2-5. Example of cortical lesion in MS.

Diffusion inversion recovery (DIR) on the left and magnetisation-prepared gradient echo (MPRAGE) on the right (figure re-adapted by Filippi M. et al. *Lancet Neurol*, 2016)

Overall, imaging studies have shown that CLs contribute to the identification of patients with CIS who are at risk of evolution to clinically definite MS, and for this reason, they have been added to the most recent version of the diagnostic criteria. Finally, CLs accumulation is strongly associated with disability and cognitive impairment (Harrison *et al.*, 2015).

Atrophy of CGM and DGM structures is recognised in MS, and this has been related to a neuronal loss partially due to inflammatory tissue damage, and to a secondary consequence of axonal transection within WM. The quantification of the extent of tissue loss in the GM and WM, separately, as well as in clinically relevant structures, such as the thalamus, has been facilitated by structural and volumetric MRI longitudinal techniques. GM atrophy starts in early MS and its accumulation is around 10 times greater than controls in RRMS, with the highest values for progressive MS, and a substantial link with disability. Several areas are involved, and thanks to several volumetric MRI techniques (e.g. voxel-based or tensor-based morphometry) it has been possible to identify which regions are more likely to be affected in the long term. All the studies analysing GM atrophy point out that there are patterns of localised atrophy in MS, and the faster rate is seen in DGM areas (such as thalamus, brainstem, basal ganglia structures) and then in CGM (parietal areas such as pre/postcentral regions, temporal pole areas, cingulate cortex) (Eshaghi, Marinescu, *et al.*, 2018;

Eshaghi, Prados, W. J. Brownlee, *et al.*, 2018), including cerebellar cortex. Some of those alterations are already visible, using morphometric advanced MRI techniques, in the short term (i.e. for 1-3 years of follow-up) (Colato *et al.*, 2021; Rocca *et al.*, 2021) and they impact significantly measures of physical and cognitive disability, including MS progression.

2.3.2 Leptomeningeal enhancement

The involvement of the leptomeninges has been progressively recognised in MS, as there is evidence of aggregates of increased numbers of B cells, plasma cells, and follicular dendritic cells in the form of follicles or ectopic tertiary lymphoid tissues, in particular in progressive MS phenotypes (Magliozzi *et al.*, 2010). Those areas are thought to represent one of the sites of autoantigen presentation, which could sustain a compartmentalised smouldering chronic inflammation.

At imaging, standard MRI field strength and FLAIR allow visualisation on 3D of leptomeningeal enhancement (LME) with high variability (1-50% prevalence), however, the use of 7 T MRI has increased the sensitivity (Harrison *et al.*, 2017). At 7 T MRI, there are two main patterns of LME: ‘nodular’ characterised by round areas around the pial surface; ‘spread/fill’ contrast leakage through the subarachnoid space. The presence of spread foci of LME might be related to blood-meningeal barrier breakdown, and there is a relationship with reduced CGM volume in MS patients (Harrison *et al.*, 2017).

2.3.3 Global brain and spinal cord atrophy

MS neurodegeneration is captured on imaging by the presence of irreversible tissue loss globally affecting the whole brain, which can be evaluated through volumetric MRI. In particular, the use of longitudinal scanning has permitted the evaluation of brain volume changes over time, as a marker that take into consideration the evolution over time. One of the main markers studied is the global brain atrophy, usually referred as to percent brain volume change (PBVC), which can be computed automatically using 3D T1-weighted MRI images and application of optimized pipelines using segmentation-based and/or registration-based analyses.

Brain atrophy develops from early MS stages at around a three-fold faster rate than control population (PBVC ranging from -0.5% to -1% per year versus -0.1 to -0.3%, respectively), with the value of -0.4% per year representing a suggested threshold for “pathological” brain volume loss (De Stefano *et al.*, 2010). The limitations of brain atrophy are associated with the presence of a high variability of this measure due to the effect of ageing and other contributing factors related to brain volume loss (e.g. alcohol, smoking), and causes of shifts in tissue water content (dehydration). Moreover, in MS volume reductions are related to the resolution of inflammatory oedema (also defined “pseudoatrophy”) either spontaneous or induced by DMTs. Despite those limitations, brain atrophy is particularly relevant for progressive MS, as indicated by the relevant correlation with long-term disability and cognitive impairment (Leonora K. Fisniku *et al.*, 2008) and a higher performance compared to lesion-related measures. The relevance of PBVC has been observed in several clinical trials, in which the effects on the reduction of the atrophy rate have been observed even in the short-term for most of DMTs, in particular for patients with RRMS or CIS, and consensus recommendations have been proposed by MAGNIMS (Sastre-Garriga *et al.*, 2020).

Recently, imaging of the spinal cord has been implemented to quantify changes in the spinal cord area, which is an elective part of the CNS known to be largely involved in the MS pathological process. It is possible to compute spinal cord atrophy using 3D T1 weighted sequences and estimate through segmentation-based methods the upper cervical cross-sectional area, which is conventionally computed at the C2-C3 level, or the mean area over C1-C2 vertebral bodies. Recently, there has also been introduced a fully automated registration-based technique (using generalized boundary shift integral), which has shown some benefit over alternative semi-automated techniques (Moccia *et al.*, 2019). Overall, spinal cord atrophy changes are highly relevant for their predictive ability on disability accumulation, as it occurs from the early MS stages (Brownlee *et al.*, 2016) and it is more obvious in progressive MS patients. Spinal cord atrophy rates (~1.7%/year) progress faster than brain atrophy, and they might account for a high percentage (reaching 70%) of motor disability as measured by EDSS (Lukas *et al.*, 2014).

2.3.4 Connectivity MRI metrics

Functional MRI (fMRI) utilises the magnetic properties of blood-oxygen proteins and exploits the oxyhaemoglobin to deoxyhaemoglobin ratio in the brain grey matter, also known as the blood-oxygen-level dependent signal (BOLD), acting as endogenous contrast with a gradient-echo sequence. This provides the brain activated areas in two modalities: resting-state default mode network (rs-fMRI) and task-related recruitment.

They are markers for overall brain plasticity and can display a pattern of reorganization of the activation of specific brain areas, which has been thoroughly analysed in MS. fMRI has allowed detecting functional reserve changes that are present beyond and sometimes before the anatomical modifications that can be measured in MS patients.

In particular, several studies demonstrated or increased recruitment of multiple brain regions at resting-state fMRI as either an adaptive compensatory or maladaptive mechanism, from the very early stages of disease (Rocca *et al.*, 2005), which are less evident in the manifest RRMS phase (Roosendaal *et al.*, 2010). On the other hand, task-related fMRI probing visual, cognitive, and sensorimotor systems have consistently demonstrated functional cortical changes with hyperactivation and/or recruitment of additional areas with evidence of a profound bilateral functional cortical reorganisation during simple tasks in manifest relapsing MS (Filippi *et al.*, 2004). In addition, those patterns can discriminate between MS phenotypes (Rocca *et al.*, 2005) and might also add information on the prognosis by revealing more benign or unfavourable outcomes. In the later stages of RRMS and progressive phenotypes, it appears that connectivity tends to decrease in association with MS evolution and it relates to the presence of relevant fatigue and cognitive manifestations, such as working memory deficits or processing speed and executive dysfunction (Vacchi *et al.*, 2017).

2.3.5 MR spectroscopy

Magnetic resonance spectroscopy (MRS) provides 3D quantitative information based on the properties of different nuclei (e.g., ^1H , ^{31}P , ^{13}C , ^{23}Na) and their respective relaxation times. Proton (^1H) MRS has been utilized to characterise MS pathology for at least 30 years and using ^1H shifts major metabolites can be identified with a resonance signal intensity proportional to their relative concentration within the tissue

compartments (neuronal, axonal glial) reflecting specific cellular and biochemical processes, with their changes associated with pathological conditions.

N-acetyl-aspartate (NAA) has been considered a metabolite reflecting cerebral or neuronal integrity, as it is mainly located within the mitochondria of neurons, and its reduction is suggesting neuronal and myelin loss and/or metabolic dysfunction. Pathological-imaging studies have shown that in both early MS stages prior to the formation of acute lesions and in chronic phases there is a reduction in NAA in lesions, but also in NAWM and NAGM (Narayana *et al.*, 1998; Caramanos, Narayanan and Arnold, 2005). The reduction in this metabolite has been correlated to disability, with a variable extent of recovery over time as the marker might partially or completely revert to normal, possibly due to remyelinating effects. Overall, reductions in NAA are usually more pronounced in progressive MS and in cases with higher motor disability level (Moccia and Ciccarelli, 2017).

Glutamate and glutamine (Glu, Glx) products are supposed to increase in MS by enhanced production of inflammatory cells and reduced uptake by glial cells; the accumulation in the extracellular space might contribute to neuroaxonal degeneration via excito-toxicity (Azevedo *et al.*, 2014). Glu has been found raised in MS acute lesions and the NAWM, correlating with clinical disability and other MRI markers of disease activity (Azevedo *et al.*, 2014), while a progressive decline over the course of the disease has been demonstrated, reflecting chronic demyelination (Macmillan *et al.*, 2016), possibly associated with a reduction of the number of Glu synapses.

Gamma-aminobutyric acid (GABA) is the main brain inhibitory neurotransmitter, which has been identified only at reduced levels within CGM of SPMS patients, in association with a consistent clinical motor impairment (Cawley *et al.*, 2015). Therefore, GABA has been suggested as a marker of neurodegeneration, as it reflects an impairment in compensatory mechanisms that have been damaged by MS pathology. Creatine (Cr), a marker of energetic metabolism, has been identified as increased within the corticospinal tract of MS patients and it could be interpreted as a metabolic response to structural tissue damage (Tur *et al.*, 2014).

Choline-containing compounds (Cho) are markers of cell membranes and their increase reflects elevated cell turnover. Cho increase has been identified in NAWM of MS patients preceding the appearance of an enhancing lesion (Narayana *et al.*, 1998), while reductions have been shown in association with worse walking abilities (Tur *et al.*, 2014). Myo-inositol (Myo) is associated with glial (astrocytic) proliferation, which has been identified in acute and chronic MS lesions, and in NAWM, with higher levels have been associated with greater disability (Ciccarelli *et al.*, 2007).

Sodium (^{23}Na) is one of the main extracellular electrolytes and the disbalance within compartments has been used in spectroscopy to identify a further indirect marker of mitochondrial dysfunction, related to neuroaxonal damage. Sodium MRS has allowed estimating the total sodium brain concentration, and reported higher figures within lesions, NAWM and CGM in MS with especially higher concentrations in patients with higher disability level (Paling *et al.*, 2013). Recent use of ultra-high field MRI (7 T) has allowed estimating the Na fractions, and extracellular sodium has shown a reduction in MS-associated to other MRI markers of disease activity and EDSS disability (Petracca *et al.*, 2016).

The main limitations of MRS are related to long acquisition times, low spatial resolution with difficulties in discriminating between tissue compartments, variability in acquisition protocols and variations of the metabolite concentrations dependent on the magnetic field.

2.3.6 Diffusion-weighted imaging (DWI)

Diffusion-weighted imaging (DWI), also called diffusion tensor imaging, allows the extraction of information about the microstructure of tissues, which might not be visible with conventional MRI. This information can be obtained because the measures retrieved using DWI are influenced by membranes, subcellular structures, geometric packing, cell size and shape. DWI measures the average distance water molecules displace during a period of time, and the signal thus reflects the constraints and directionality imposed on water movement by the orientation of white matter fibre bundles, their myelin and axonal structures (Beaulieu, 2002). Therefore, the changes in diffusion parameters are associated with underlying pathological processes in MS and are sensitive to white matter integrity and connectivity. Among the measures

retrieved with DWI, the degree of diffusion, also defined as anisotropy, can be measured through the apparent diffusion coefficient (ADC), which can be computed in different directions. Fractional anisotropy (FA) indicates the degree of diffusion directionality, with values ranging from zero (equal in all directions) to one (movement completely restricted except along one direction). Other measures can be retrieved, such as the axial diffusivity (AD), reflecting the degree of anisotropy in the direction parallel to the fibres, radial diffusivity (RD) exploiting the anisotropy perpendicularly to the fibres, while the mean diffusivity (MD) is a measure of the bulk diffusivity.

Anisotropic diffusion in the white matter has been shown to primarily reflect ‘the dense packing of axons and their inherent axonal membrane’ (Beaulieu, 2002) and a decrease in FA is therefore commonly held to reflect a reduction in white matter tract integrity. Reduced axial diffusivity reflects axonal degeneration due to the damage in regions of the white matter with high coherence, which was shown in the animal model of MS (Kim *et al.*, 2006). Multiple studies have replicated the presence of a reduction of FA and/or an increase in RD within lesional tissues and NAWM of MS patients, with several brain pathways that are more often involved and are associated with cognitive impairment (Roosendaal *et al.*, 2008) or progression of physical disability (Bodini *et al.*, 2014). In addition, low values of FA were found in contrast-enhancing lesion (M Filippi *et al.*, 2001) and highest ADC values within the black holes (Nusbaum *et al.*, 2000). More recently, the degree of chronic lesion volume expansion measured through volumetric MRI has been associated to an increase in the core lesional MD measured longitudinally (Klistorner *et al.*, 2021), and with an increase of the peri-plaque white matter RD (Klistorner *et al.*, 2022).

2.3.7 Positron emission tomography (PET)

Positron emission tomography (PET) is a non-invasive technique that enables targeted quantitative imaging of physiological and pathological processes, based on isotope-labelled ligands (a positron-emitting molecule, also called radioligand or tracers) with a short half-life (i.e. ^{11}C , ^{15}O , ^{18}F), which accumulates into target tissues. PET use has been lately extended from neuro-oncology to neurodegenerative diseases, due to the development of specific tracers to target specific receptors. In MS, the extension to the research of PET markers provides functional *in vivo* information about axonal degeneration, demyelination, remyelination, microglial activation and astrogliosis.

The most studied tracer, the translocator protein (TSPO or ^{11}C -PK11195) is a macromolecular complex expressed in the outer mitochondrial membrane, which is strongly upregulated in activated microglial cells. Several reports described increased TSPO uptake within active MS lesions and in the NAWM, but also the deep grey matter structures (e.g. thalamus) in the perilesional areas, with a correlation to other structural MRI metrics and disability (Airas, Rissanen and Rinne, 2017). Recent evidence suggests that this radioligand can be used as one of the markers for the chronic active lesions (Kaunzner *et al.*, 2019), due to affinity for cells that are particularly populating the rim of those lesions, when the overall inflammation level might be not detectable by other MRI markers (**Figure 2-6**).

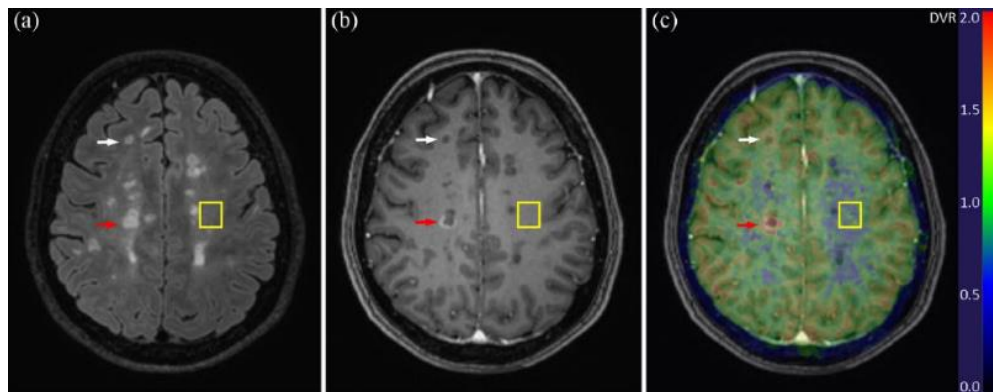


Figure 2-6. Example of lesion in active and chronic stage at axial views of FLAIR (a), gadolinium T1-weighted (b) and ^{11}C -PK11195 PET (c).

(From Airas L. et al. MSJ 2017)

Second generation TSPO tracers have been explored, and they are expected to overcome the low unspecific uptake of some of the tracers and improve the targeting of specific molecules or structures of interest. However, they might have heterogeneous binding to TSPO due to genetic polymorphism, which complicates the interpretation of the results. Amyloid tracers (^{11}C -PiB and ^{18}F -florbetaben) studied in dementia for their affinity to β -amyloid have also been used in MS due to their affinity to myelin within white matter and correlation with demyelination (Stankoff *et al.*, 2011), with the future prospect in their use for tracking remyelination. PET tracking

glucose metabolism with fludeoxyglucose (^{18}F -FDG) has been initially linked to higher metabolism within lesions undergoing acute inflammation (Schiepers *et al.*, 1997); more recently hypometabolism in several cortical and deep grey matter areas has been associated with patients with cognitive impairment and fatigue severity (Blinkenberg *et al.*, 2000). Several new targets have been undergoing investigations, including cannabinoid and purinergic receptors, or compounds related to neuronal synaptic/dendritic damage and glial/astrocyte activation, in an attempt to find imaging correlates for degenerating cellular populations and signalling pathways involved in MS and other neurodegenerative disorders.

2.4 MRI markers for chronic lesions in MS

In MS imaging research, quantitative MRI imaging techniques can determine tissue parameters quantitatively, enabling the detection of microstructural processes related to tissue remodelling. Such approaches can be directed specifically to quantify the progressive damage over time occurring within chronic lesions as a key factor related to the progression of disability in MS.

Quantitative MRI studies have been centred on evaluating the pathological characteristics seen in MS biopsies and their correlation with various imaging modalities. One of the main strategies is directed to the identification of tissue damage, such as chronic demyelination and neuro-axonal loss, as features occurring when the neurodegenerative process has become predominant in the MS lesion evolution.

In the following paragraphs, relevant MRI markers related to the chronic active lesions applied in MS research and trials are described, with a focus on the newest techniques that have been explored within this doctoral work.

2.4.1 T1 hypointensity and the black holes

The extensive use of MRI for diagnosis and follow-up in MS, including T1-weighted acquisitions, has promoted the evaluation of specific characteristics of the tissues at this imaging modality. A subset of the T2 lesions appears also dark compared to the surrounding tissues on T1-weighted, also defined lesions with T1 hypointensity or

'black holes' (BHs), initially noted by Uhlenbrock et al. (Uhlenbrock and Sehlen, 1989), as a differential characteristic in MS compared to vascular lesions. This feature has been pathologically associated with areas of axonal loss and gliosis within the chronic MS lesion types, and becomes prominent in the later disease stages (Van Walderveen *et al.*, 2001).

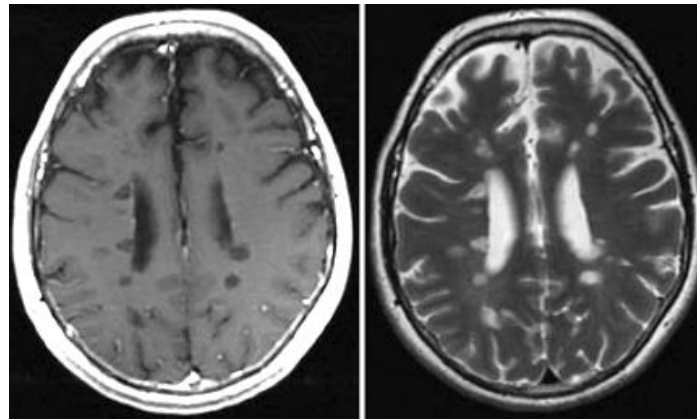


Figure 2-7. Example of black holes (BHs).

On the left axial T1-weighted post-gadolinium scan, with some of them corresponding on the T2-weighted image to hyperintense lesions (from Sahraian M et al. *Acta Neurol Scand*, 2010)

Several histopathological studies replicated this finding, including the associations between the total T1 hypointense volume and disability, and with other MRI markers of neurodegeneration. Van Waldeerven et al. performed an imaging-pathological correlation study through the analysis of 19 lesions from five MS patients and identified correlation to complete loss of axons and severe T1 hypointensity (van Walderveen *et al.*, 1998). The authors identified that the degree of lesion hypointensity (manually retrieved), ranging from mild (i.e., similar to GM) to severe (i.e., similar to CSF), has a relevant correlation with the degree of pathological severity. Truyen et al. analysed 46 MS patients and found correlations between baseline EDSS and T1 hypointense baseline volume (Spearman rank correlation 0.46, $p=0.001$) (Truyen *et al.*, 1996). In SPMS patients, higher correlations were found between change in EDSS and percent change in T1 volume (Spearman rank correlation 0.81, $p<0.001$) (Truyen *et al.*, 1996). Sailer et al. confirmed similar results on 29 MS patients and identified associations between T1 hypointense lesion volume and brain atrophy (Sailer *et al.*,

2001). The correlation between T2 lesion volumes and T1 hypointense volumes indicates that there is an interaction of the two markers and that a higher total lesion burden correlates to an accumulation of tissue damage (Adams *et al.*, 1999). Some of those studies have also demonstrated that T1 hypointense lesion load correlates better with disability progression compared to the T2 lesion volume.

For its relevance and the high reproducibility, as shown in multicentric cohort evaluation (Molyneux *et al.*, 2000), the T1 hypointense volume has been introduced as a valid marker in MS treatment trials, due to the evidence of its efficacy in demonstrating treatment responses (M. Filippi *et al.*, 2001). Together with the T2 lesion related measures, the T1 hypointense volume changes have been analysed over time to better discern their impact on MS disability and the combination of those markers has been explored. Indeed, black holes at baseline and new T2 lesions were able to predict, respectively, the severity of executive deficits and slowed information processing 7 years later (Summers *et al.*, 2008). In a study involving RRMS patients, the combination of the BH count (at baseline) and the relative increase in T1 hypointense volume, was the best predictor of the EDSS worsening over 10 years (Giorgio *et al.*, 2014).

Despite those descriptions, T1 hypointensity has limitations due to low specificity and high variability, since it is found in association with several other pathological processes that cause an expanded extracellular space, such as in other neurodegenerative conditions or in vascular lesions (Uhlenbrock and Sehlen, 1989). Moreover, low T1 values are not only characteristic of the late stages of MS lesions, as they are also found in newly forming MS lesions, and they have been associated with the presence of oedema and increased extracellular free water associated with the local acute inflammation (Van Walderveen *et al.*, 1998).

2.4.2 Persisting black holes (PBHs)

The importance of lesions with persistence of T1 hypointensity has been noted since the first cross-sectional MRI-pathological correlation studies (Bitsch *et al.*, 2001). Active demyelinating lesions can become either less or more T1 hypointense over time, which is associated with their stages of development. Lesions may either proceed directly into remyelination or become inactive and stay demyelinated. The earlier

remyelination starts, the more effective and complete it appears to be, which favours a normalisation of the extracellular space and compaction of the tissue, thus favouring a return to isointense T1 signal (Lassmann *et al.*, 1997). On the other hand, in completely demyelinated and susceptible lesions, the failure of remyelination (or a late and incomplete repair process) favours ongoing axonal destruction with neurodegenerative changes, corresponding to the persistence of T1 hypointensity (Lassmann *et al.*, 1997).

The extension of MRI analyses to longitudinal time-series studies in MS has allowed better characterising of the patterns of evolution of BHs from their onset. In the early stages of lesion formation, T1 hypointensity is related to the acute inflammation, thus lesions with this feature have been referred to as acute black holes (ABHs). The majority of ABHs correspond to CELs (~80%), which demonstrate a relation to the BBB damage occurring in the early stages of lesion formation (Bagnato *et al.*, 2003). A fraction (~60%) of these ABHs corresponding to CELs are reversible and once contrast enhancement ends may become isointense to the NAWM, probably as a result of the resolution of oedema and repair or remyelination (Bagnato *et al.*, 2003). It is not clear the exact time of the resolution of the acute T1 hypointensity but it might coincide with the correspondence of enhancement.

The rest of the lesions that maintain T1 hypointensity for a prolonged time (at least greater than 6 months), have been referred to as persisting black holes (PBHs) (Bagnato *et al.*, 2003). The first data on the PBHs originated from clinical trials on a follow-up of 1 to 2 years documented that there is an increase in the rate of formation of new PBHs accompanied by the increase in the number of CELs converting into PBHs (Bagnato *et al.*, 2003). The authors found that within lesions a longer persistence of the enhancement (> 1 month) defines a greater chance of evolution into a PBH with longer time duration. Finally, they noted that a majority of PBHs would disappear within the first year of formation, while it appeared unlikely that a PBH could disappear after persisting for more than 2 years (Bagnato *et al.*, 2003).

A wide percentage between 10% and 40% of ABHs evolve into PBHs, which is linked to the variable length of follow-up of the studies, limited tissue contrast of T1-weighted

images, and the visual threshold evaluated for determining an area of T1 hypointensity (M. Filippi *et al.*, 2001).

Despite PBHs having been usually referred to as markers for a chronic stage of the lesion formation, and thus predominate in the progressive MS phenotypes, they have also been identified from disease onset and CIS, and their accumulation has been correlated to a higher risk of conversion to CDMS (Mitjana *et al.*, 2014).

2.5 Quantitative and volumetric MRI measures

Quantitative MRI methods refer to those imaging techniques that assess a quantifiable metric, which can relate to the physical structure of specific substances. In MS, they have been mainly conducted for the evaluation of myelin and axonal density and to identify markers for the chronic active lesions.

On the other hand, volumetric MRI techniques assess the longitudinal evolution in the dimensions and shape of the lesions. In the following paragraphs, the focus is on those markers relevant for the chronic active lesions: magnetization transfer, volumetric MRI and susceptibility techniques.

2.5.1 Magnetization transfer ratio (MTR)

Magnetization transfer imaging (MTI) provides an indirect estimate of tissues macromolecular structure, and this metric in MS has been well established as a marker of myelin content, due to the histopathological correlation with severely demyelinated areas and axonal loss (Schmierer *et al.*, 2004). This technique probes magnetization exchange between freely mobile water protons and those that are bound to macromolecules within the tissues, providing a measure of the amount of macromolecular structure in tissue.

In conventional MRI, only signals from “free” intra- or extra-cellular mobile water protons that have sufficiently long T2 relaxation times can be directly detected. By contrast, protons bound to macromolecules, such as myelin proteins and lipids, have extremely short T2 relaxation times of about 10 μ s, too short to be detected directly.

They can be imaged indirectly with MTI by exploiting the transfer of magnetization between both proton pools, which is caused by dipolar coupling and chemical exchange mechanisms. When applying an off-resonance radio-frequency pulse, the bound pool magnetization becomes saturated. Through magnetization transfer, this saturation is then transferred to the magnetic resonance visible water proton pool and causes a decrease of the longitudinal magnetization and consequently a decrease of the signal intensity. The extent of the magnetization transfer induced signal decrease is usually assessed by the magnetization transfer ratio (MTR). The MTR increases with the rate of magnetization exchange and with the size of the bound pool, and it is usually measured in percent units (pu). MS lesions have been characterized using MTR, as this measure is very sensitive to detect tissue changes occurring throughout the lesion development in different phases (**Figure 2-8**).

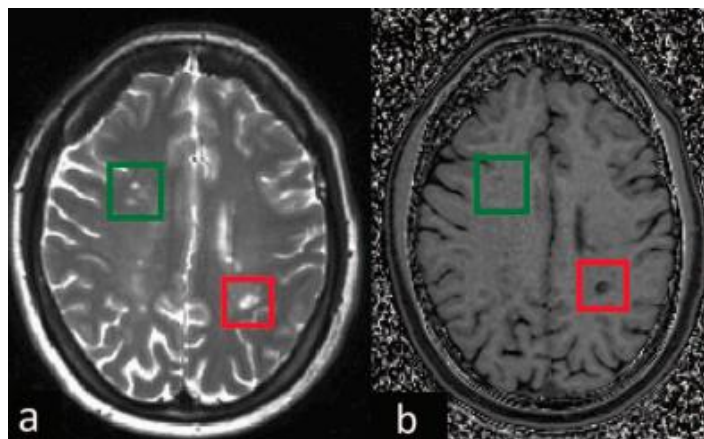


Figure 2-8. Example of MTR map (on right - b) and the corresponding T2-weighted scan (on the left - a).

A lesion in the red box corresponds on MTR to hypointense signal suggestive of demyelination, while the lesions in the green box do have a isointense signal, thus they might correspond to remyelination. (From Mallik S. et al. JNNP, 2014)

A first pattern is a short-term (3–12 months) MTR reduction which detects the acute phase of the active MS lesions, reflecting the presence of early inflammation and associated oedema, preceding the appearance of enhancement and CELs or new T2 lesions (Filippi *et al.*, 1998). In a subset of those lesions, MTR can go back to initial values, and this could correspond to the resolution of inflammation and successful remyelination. As a result, this marker has been suggested for treatment monitoring,

as an increase in MTR values may reflect remyelination. However, fluctuations in MTR values are highly variable, and changes can be also found in the NAWM in MS patients compared to healthy controls (Loevner *et al.*, 1995), underlying the presence of areas preceding the formation of lesions. Moreover, MTR can be sensitive of changes within cortical lesions through the measurement of grey matter areas (Hayton *et al.*, 2012).

A second pattern is the finding of a deep decrease and persistence of MTR reduction in a subset of chronic lesions, which is highly correlated to the evolution of a lesion into PBHs (van Waesberghe *et al.*, 1998; Van Waesberghe *et al.*, 1998). The persistent reduction of MTR represents a signature of severe and permanent tissue damage within the chronic lesion subtypes. This marker is also predictive of significant disability at EDSS after long-term follow-up (Filippi *et al.*, 1998), as MTR values are more profoundly affected in progressive MS phenotypes (Filippi *et al.*, 1999; Rovaris, 2003). There is evidence suggesting that MTR correlates better with physical and cognitive impairment than conventional MR measures (Filippi *et al.*, 2000), and the association between MTR and clinical disability has been used to assess treatment effects in phase II-III clinical trials (Hayton *et al.*, 2012).

2.5.2 Volumetric MRI basics: segmentation and registration

Volumetric imaging analyses rely on longitudinal or time-serial MRI, which refers to collecting multiple scans for each subject at subsequent time points and retrieving measures of the volume changes within tissues. The tissues need to be classified at MRI and delineated before evaluating the volumetry and subsequent follow-up scans follow a registration in the same space. In MS studies, the segmentation phase identifies regions of interest (ROIs), and it allows the differentiation of what is considered the lesion volume from the other tissues or regional brain volumes (i.e., GM and NAWM) and the CSF.

Lesion segmentation refers to the delineation of ROIs around MS lesions, also called ‘lesion masks’, through the application of manual, semi- or fully automatic techniques. The manual approach based on visual inspection is the gold standard, but it is time-consuming and imprecise due to high intra/inter-observer variability (Danelakis, Theoharis and Verganelakis, 2018). The automatic segmentation aims to analyse a

single-time MRI of the lesion volume relying on intensity homogeneities to identify the MS lesions. The automatic techniques can be supervised, requiring manually segmented training images used as references for automatic segmentation of new images. On the other hand, unsupervised algorithms perform automatically the segmentation by employing clustering techniques to separate the voxels into different classes (or clusters) based on different extracted features (García-Lorenzo *et al.*, 2013).

Registration refers to the process that brings multiple images into spatial alignment at the basis of the time series (or 4D) longitudinal MRI analyses. Registration can be rigid-model (linear) or deformable-model based (non-linear) and several parameters affect the registration process, such as the similarity functions used for the image transformation. One of the most widely used similarity functions is the normalised mutual information (NMI), a measure of statistical dependency between two data sets based on information theory, which is an accurate and reliable method for serial MRI analyses in MS (Leng Tan *et al.*, 2002).

Change quantification techniques have been extensively applied in longitudinal MRI, and for the case of MS studies they have been optimised to quantify volumetric lesion modifications to consider both large and more localised changes (Bosc *et al.*, 2003). The general problems associated with this analysis are related to lesion shapes, as usually, ill-defined boundaries can be ambiguous, and the lesion position, since they can appear or disappear arbitrarily and may shrink or enlarge over time. Those change detection methods have been classified essentially in intensity-based or deformation-based (Lladó *et al.*, 2012).

The intensity-based ones consist of analysing two successive scans by means of subtraction techniques based on deterministic approaches that exploit the direct intensity differences between the scans. With this approach it has been shown that there was a better agreement for positive activity, facilitating the detection of new/enlarging lesions (Tan *et al.*, 2002). The application of this technique has been the basis of the identification of the new T2 or “active” lesions in MS studies, which is an efficient marker for the high inter-observer agreement and increased power to assess treatment efficacy as compared to other lesion-based markers such as CELs (Moraal *et al.*, 2010).

Within the intensity-based methods, other more sophisticated techniques are based on statistical approaches to reduce the inaccurate results obtained by direct point-to-point subtraction, or temporal analysis based on the detection of active voxels through a time-series analysis in more than two sessions (Lladó *et al.*, 2012).

Finally, the deformation-based approaches aim to obtain a deformation field from a non-rigid registration process between successive time points, which can be directly used to perform the lesion detection and evolution (Lladó *et al.*, 2012). In a recent literature review, the change detection methods have been classified more extensively as follows: data-driven methods (thresholding and spatial approaches), statistical (estimation of probability density functions), intelligent (involving neural network) and deformation-based volume estimations (Mortazavi, Kouzani and Soltanian-Zadeh, 2012).

As methodological general consideration in volumetric MRI studies, it is essential to consider that a different scanner may be used in a follow-up scan with different signal characteristics or operating software. Thus, the volume change detection requires as an essential component in the process not simply the detection of change but the separation of acquisition-related change from disease-related change (Patriarche and Erickson, 2004).

2.5.3 Deformation-based analysis

An MS lesion is generally seen as the combination of two different effects, tissue transformation and tissue deformation (Thirion and Calmon, 1999). Tissue transformation refers to the intensity change in the tissue of the lesion, while tissue deformation refers to the modification of its surrounding tissue, due to lesion expansion or contraction. Therefore, using only approaches based on intensity changes between serial scans to evaluate the evolution of lesions may not give satisfactory results, since the surrounding tissue deformation due to the presence of the lesion is not considered. In order to consider this phenomenon, also defined as the mass effect of the lesions, deformation-based approaches have been employed in volumetric MRI.

Deformation analysis is based on a non-linear registration, which leads to the computation of tissue displacement due to expansion or contraction in a four-

dimensional spatiotemporal dataset (Mortazavi, Kouzani and Soltanian-Zadeh, 2012). This technique allows visualizing volume changes by deforming the baseline scan onto their subsequent scans (warping algorithms), using the deformation map to quantify local changes. Vector displacement fields were initially used to identify semi-automatically both divergence and norm of the displacement vector to be sensitive to deformation and intensity change (Thirion and Calmon, 1999).

Improvements in deformation analysis enabled a precise quantification of volume change based on computing the deformation field as the spatial transformations required to match the image acquired on the follow-up to the baseline time point (Ashburner and Friston, 2000). By taking the gradients at each element of the vector field, a Jacobian matrix field is obtained, in which each element is a tensor describing the relative positions of the neighbouring elements (determinant of Jacobian matrix or Jacobian). The field obtained by taking the determinants at each point gives a map of volumes relative to those of a reference image. A Jacobian operator larger than 1 indicates a local expansion, while smaller values indicate local shrinking. Deformation analysis has been recently applied in MS research studies to determine local volume changes, and initial applications on lesion masks showed that high divergence indicated the presence of expanding lesions (Rey *et al.*, 2002).

2.5.4 Susceptibility MRI

The susceptibility of a material is a measure of whether an applied magnetic field creates a larger or smaller field within that material. In MRI acquisitions, after a radio-frequency excitation pulse, the net magnetization returns from the transverse plane to the longitudinal plane and induces a voltage in the MR receiver coil. The magnitude of the transverse component decays with a time constant of this decay called $T2^*$, which is always shorter than $T2$. This occurs due to the magnetic field inhomogeneity, imperfections in the windings of the coil itself and the differences in magnetic susceptibility between adjacent regions (Ge, Grossman and Haacke, 2011). Therefore, $T2^*$ represents a measure of variations in the magnetic field susceptibility, as it depends on the interface of the tissues assessed. In MRI, compounds can have paramagnetic or diamagnetic properties, as they all interact with the local magnetic field distorting it and thus altering the phase of local tissue which, in turn, results in a change of signal.

The applications of susceptibility MRI in human pathophysiology are widespread and they have been linked to the possibility of tracking compounds of interest with specific paramagnetic properties (Haacke and Reichenbach, 2011). Susceptibility MRI sequences include the following: T2* and the computation of the inverse measure as quantitative transverse relaxation rate (R2*); post-processing of gradient-echo phase and magnitude sequences, such as susceptibility-weighted imaging (SWI) and quantitative susceptibility mapping (QSM).

T2* imaging has been applied to identify paramagnetic substances accumulating within the CNS, and in particular iron-containing compounds. Initial studies using T2* showed that the strongest signals were found within the deep grey matter brain areas and they suggested accumulation of iron, which increased as a function of age and was more pronounced in MS (Drayer *et al.*, 1986). The presence of lesions with hypointense rims (rim-positive) at T2* and the relative increase in R2* was found to correlate with brain atrophy and to be predictive of MS disability progression (Khalil *et al.*, 2009). While T2* imaging has proven sensitive in the qualitative detection of the presence of rim-positive lesions in MS, R2* is affected by both myelin (diamagnetic) and iron (paramagnetic) concentrations, and in isolation, this makes it difficult to discern the evolution of these features. For example, myelin and iron changes can be greatly variable with reference to the chronic lesion subtypes.

SWI is a post-processing image derived by a 3D high-resolution gradient-echo (GRE) sequence that uses magnitude and phase data both separately and together to enhance information about local tissue susceptibility (Haacke *et al.*, 2004). In particular, the post-processing requires that a filtered mask phase image is multiplied into the magnitude image to enhance contrast in susceptibility-shifted areas. SWI is very sensitive to iron deposition in the form of hemosiderin, ferritin, and deoxyhemoglobin (Haacke *et al.*, 2004).

A novel susceptibility MRI post-processing method is the QSM. The acquisition sequence for QSM is typically a 3D GRE similar to that used for routine SWI, but multiple echoes are used to allow for detection of weak susceptibility changes and correction for multi-exponential T2*-decay (Langkammer *et al.*, 2012). This technique shows benefits in terms of accuracy in quantification and localization of

brain iron and fewer artefacts as compared to other MRI with gradient-echo approaches. QSM shows the highest disease-related changes in deep grey matter in MS compared to other gradient-echo approaches (Langkammer *et al.*, 2013). Furthermore, with QSM the diamagnetism of myelin components counteracts the paramagnetism of iron, and it contributes to it additively. Therefore, using QSM severe or complete demyelination can increase susceptibility up to zero, while positive values indicate contributions from paramagnetic material, such as iron (Khalil *et al.*, 2013). Recent imaging-pathological correlation studies have found a positive QSM value indicating iron deposition within chronic active lesions (Wisnieff *et al.*, 2015).

2.6 Markers for chronic active lesions

2.6.1 Paramagnetic rim lesions at susceptibility MRI

Lesions surrounded by a rim of hypointense signal, also addressed as ring-like or rim-positive or paramagnetic rim lesions (PRLs), were initially described on visual inspection of either T2* or SWI images as a qualitative feature of a subgroup of lesions in MS. Several histopathological-imaging studies in all MS phenotypes confirmed an association between PRLs at susceptibility MRI and correspondence on pathological specimens to chronic active lesions (Bagnato *et al.*, 2011; Yao *et al.*, 2012; Absinta *et al.*, 2013). A pilot study on 27 MS patients initially identified a variety of lesional features at SWI allowing the development of a classification into six patterns according to the intensity level and distribution (Haacke *et al.*, 2009). One of those patterns was defined as “*lesions surrounded by a rim of hypointense signal*”. Similarly, Hammond *et al.* studied the lesions in 19 RRMS patients with GRE phase images at 7T (Hammond *et al.*, 2008) and found that 8% of the overall lesions showed higher contrast in the phase images as a peripheral field shift, corresponding to a rim. The identification of paramagnetic rims has been assessed at 3T to perform well, with good intra-rater and inter-rater agreement for clinical MRI evaluation (Absinta *et al.*, 2018) (**Figure 2-9**).

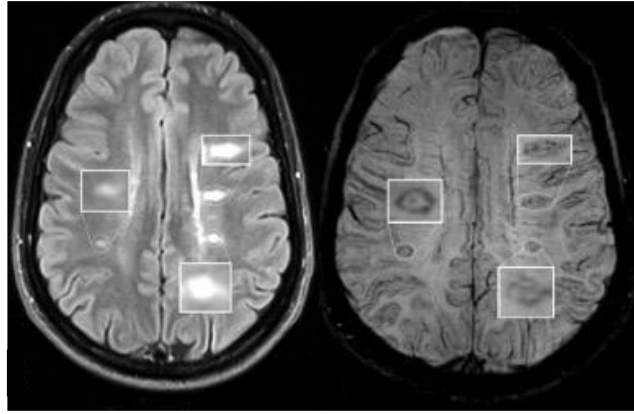


Figure 2-9. Example of paramagnetic rim lesions in the periventricular white matter. FLAIR (left) and SWI (right) images (from Clarke M.A. et al. AJNR, 2020)

In accordance with those descriptions, a study described up to 5 lesion patterns at GRE phase and quantitative R2* maps (Yao *et al.*, 2012), two of them being defined ‘ring-like’, due to the presence of a rim with different contrast (hypointense or hyperintense) compared to the inner lesion part and the perilesional area. The more common lesion type was characterized by a generalized reduction of the R2* and normal phase shift (~ 60% of the whole lesions), while a subset of the lesions (~8%) was characterized by the presence of a negative phase shift and R2* increase localized on the rim.

Combined histopathological and susceptibility MRI analyses assessed the localisation of iron at pathology in MS. Those studies found a correspondence between PRLs and the deposition within the peripheral area of ferritin derived from oligodendrocytes and macrophages/microglia, which co-localised with the peripheral areas of the chronic active lesions (Bagnato *et al.*, 2011; Yao *et al.*, 2012). In a subsequent study, MS lesions were further characterised on the basis of their appearance on susceptibility MRI and at pathology (Yao *et al.*, 2012). The histochemical staining confirmed that the rim was coincident with a positive Perl’s stain and increased ferritin, suggesting the presence of iron was co-localising with the chronic active lesions. Conversely, a reduced R2* in the centre of the lesions was found in concomitance with a reduction of myelin staining, and to a lesser extent, with reduced iron staining.

Susceptibility MRI research in MS patients followed the evaluation of cohorts including longitudinal scans. A pilot study involving 5 RRMS patients investigated the evolution of phase-contrast on the lesions, scanning with serial 7T MRI scans for ~2.5 years (average of 3.2 scans per subject) (Bian *et al.*, 2013). Among the overall lesions, phase images were able to differentiate two subgroups: a majority of nodular and uniform hypointense lesions, and a small number of rim-positive lesions or PRLs. By combining DCE and susceptibility imaging studies, new “transient” PRLs were found since the initial stage of lesion formation (Yao *et al.*, 2015), which could reflect the first infiltration of macrophages/microglia carrying paramagnetic substances. Active lesions with rims were more often associated with a centripetal pattern on DCE, and this finding was related to the opening of the BBB at the lesion edge towards a central vein (Absinta *et al.*, 2013). However, PRL persistence was more frequently found in concomitance with the shell-enhancing or centrifugal DCE pattern (i.e. a later stage of the lesion evolution) (Absinta *et al.*, 2016). About 10-20% of the overall lesions were characterized by PRL persistence over time, and this fraction might represent ongoing chronic inflammation. In addition, rim thickness and lesion dimensions allowed differentiating the lesion stage, as acute lesions had smaller diameters and had thinner rims compared to the chronic lesions (Absinta *et al.*, 2013). Only in chronic lesions was the rim thickness proportionally correlated to the diameter. However, the morphological characteristics of the lesion rims in chronic lesions did not change in a longitudinal analysis up to 2.5 years of follow-up (Bian *et al.*, 2013).

As an alternative MRI susceptibility assessment, the characterisation of MS lesion subtypes at QSM confirmed the presence of PRLs with this different acquisition. Studies focused on MS lesions found a positive QSM value only in correspondence to significant iron deposition, allowing differentiating from the presence of isolated demyelination (Wisnieff *et al.*, 2015). Lesions on longitudinal MRI were stratified according to the QSM intensity pattern, as QSM values were similar to NAWM in new active lesions, progressively increased in the early chronic stage and finally returned to initial values in the late chronic stage (Chen *et al.*, 2014).

A further step forward in susceptibility MRI research has been done with the inclusion of clinical data in those studies assessing PRLs in MS. In a longitudinal MS cohort, Absinta *et al.* found that clinically progressive MS was more prevalent in patients

having ≥ 4 PRLs and those patients developed motor and cognitive disability at a younger age and increased brain atrophy (Absinta *et al.*, 2019).

Overall the cross-sectional susceptibility-weighted MRI studies in MS consistently described the presence of up to 10-20% of rim-positive lesions (Hammond *et al.*, 2008; Yao *et al.*, 2012). Longitudinal studies found at least one rim in the majority of patients, in either relapsing or progressive MS (Bian *et al.*, 2013; Yao *et al.*, 2015). Rim positivity was associated with the lower rate of total lesion volume reduction and progressing accumulation of T1 intensity (Absinta *et al.*, 2016). Thus, rim-positivity is regarded as a marker for lesions evolving towards the chronic active stage, due to the most frequent association of the presence of rims in long-standing non-enhancing MS lesions, showing the highest susceptibility values (Absinta *et al.*, 2013; Zhang *et al.*, 2016). In the most recent longitudinal susceptibility-MRI analysis, rim-positive lesions have been found over more than 10 years follow-up (Absinta *et al.*, 2019), which might suggest that rims could persist for even longer times within chronic active lesions.

Recently, a retrospective volumetric evaluation of MS lesions identified an overall expansion in rim-positive lesions, which has also been confirmed in a prospective MRI study (Dal-Bianco *et al.*, 2017) (**Figure 2-10**). With those analyses, the evaluation of combined markers for the chronic active lesions has been started including both susceptibility and volumetric MRI metrics, as similar and alternative techniques to detect chronic inflammatory activity in MS.

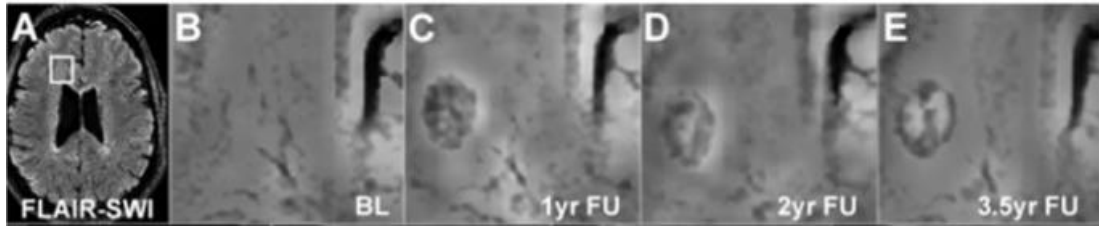


Figure 2-10. Example of a nascent lesion developing a paramagnetic rim over a follow-up on a 7T FLAIR-SWI.

The lesion appeared from B to C, then showed a slow increase of the volume over time (Adapted from Dal Bianco A. et al. *Brain*, 2021)

2.6.2 Slowly expanding lesions (SELs) at volumetric MRI

Based on the assumption of demyelination at advancing lesion edges and the pathological basis of the ongoing inflammation in chronic MS stages, the identification of expanding lesions in MS through volumetric MRI has been further exploited to extract potential markers for the chronic active lesions. Several techniques have been explored to identify this subset of MS lesions.

An initial technique was described by Fox et al. using the voxel-guided morphometry (VGM) approach, based on a non-linear transformation to register images from two time points on a voxel-by-voxel basis (Fox *et al.*, 2016). VGM allowed sub-selecting at least three types of lesions, which were defined as radiologically ‘active’ (new lesions, chronic enlarging, and chronic shrinking), using a cut-off of 5% of volume increase or decrease. The authors identified that all those active lesion types correlated to local atrophy in the surrounding and functionally related brain areas, including the corpus callosum (Fox *et al.*, 2016). In a subsequent study integrating VGM and spectroscopy, the total sodium concentration within chronic active lesions was significantly higher than the other lesion types, as a further indicator of ongoing inflammation leading to tissue damage in those lesions with changes in their volumes (Eisele *et al.*, 2021).

Recent MRI studies have applied deformation-based techniques to select the so-called slowly expanding lesions (SELs), through the analysis of imaging data on large, pooled trial cohorts from mixed relapsing and progressive MS patients. Elliott et al. developed

a method on more than 2000 patients to identify and quantify the lesional volume change over time characterized by constant radial enlargement, using only conventional T1-weighted and T2-weighted MRI data (Elliott, Wolinsky, *et al.*, 2019). The authors applied a Jacobian analysis retrieving the non-linear deformation field between a reference and follow-up scans as described by Nakamura et al (Nakamura *et al.*, 2014). In their work, the T2 lesions were initially identified in baseline scans using a semi-automated method, and then the identification of SELs was done as a two-stage process:

- 1) SEL candidates were selected as areas corresponding to contiguous regions of a T2 lesion undergoing local expansion;
- 2) Individual SEL candidates were heuristically scored, to favour those undergoing concentric and constant change, consistent with gradual inside-out radial expansion.

Before computing the SELs, some preliminary steps need to be followed: resampling of images to 1-mm isotropic space and linear (affine) registration between a reference and follow-up timepoint for global alignment of a scan in a halfway space. Then, a non-linear registration is applied between linearly aligned timepoints (using the T1-weighted and T2-weighted images simultaneously) to generate a deformation field which describes the local displacement that best aligns the two images, where the registration is performed. The computation of the Jacobian corresponds to the 3D spatial derivative of the deformation field at each voxel, while the determinant of the Jacobian, provides a single scalar value describing the magnitude of local volume change at each voxel as a percentage.

To retrieve the SEL candidates, the pre-existing T2 lesions that have a minimum rate of expansion greater or equal to a cut-off of Jacobian Expansion (or JE1, set to 12.5%/year) so that voxels with those characteristics are grouped to form initial boundaries of SEL candidates. Then, SEL candidates are further defined into the definite (also high-probability or high confidence) SELs, by iteratively considering neighbouring voxels that have a minimum rate of local expansion (and JE2 to 4%/year) to generate final boundaries of SELs and ensure that distinct expansions are considered as separate discrete entities (**Table 2-1**).

Table 2-1. SEL detection algorithm steps and subtypes of SEL lesions obtained

Step of SEL algorithm	Subtype of lesion detected	Description of the characteristics of the lesion subtype
1	Pre-existing T2 lesions	Automatic segmentation of hyperintense lesions. Resampling to isometric space (1mm x 1mm x 1mm). Affine registration baseline and follow-up scans. Non-linear registration baseline and follow-up scans. Exclusion of lesions ≤ 10 voxels.
2	candidate SELs	Grouping voxels in (1) with rate of expansion \geq JE1 (12.5%/year) based on connected-component analysis.
3	definite SELs	Dilating the boundaries from (2) by iteratively considering neighbouring voxels with minimum rate of local expansion \geq JE2 (4%/year).

SEL candidates with a total volume of less than 10 voxels in size (voxel size is 3 mm³) were discarded to ensure that the JE are reliable. The second stage of SEL detection scores each SEL candidate in turn, based on the concentricity and constancy of expansion across time. Considering local expansion at all intermediate scans allows the identification of SEL candidates undergoing constant and gradual expansion across time (increasing value ≥ 0), while measuring concentricity allows the identification of SEL candidates exhibiting inside-out radial expansion and a positive concentricity score (cut-off set as ≥ 0).

In Elliott’s study, the proportion of patients with at least one SEL was similar in PPMS (71.9%) and RRMS patients (68.2%). PPMS patients had a higher mean number of SELs compared to RRMS patients (6.3 vs 4.6, $p = 0.002$), a higher mean T2 volume of SELs (baseline: 1838 vs 1223 mm³, $p < 0.001$), and a higher mean proportion of baseline total T2 lesion burden identified as SELs (11.3% vs 8.6%, $p < 0.001$) (Elliott, Wolinsky, *et al.*, 2019). Also, the percentage of voxels showing Gd enhancement was higher in areas of pre-existing T2 lesions at baseline not classified as SEL (non-SEL) (1.5%, $p < 0.001$) and in new focal T2 lesions (8.9%, $p < 0.001$), compared with regions identified as SELs (0.3%). Both among RRMS and PPMS patients, SELs had a lower normalized T1 intensity at baseline compared to the non-SELs, and the

longitudinal evaluation over the 96 weeks of the trials showed a significantly larger decrease in normalized T1 intensity in SELs compared with non-SELs in these two MS phenotypes. Finally, the anatomical distribution of SELs was respecting the preferentially periventricular maximal probability of T1/T2 lesion occurrence across MS disease phenotypes, with a higher heat map density in patients with PPMS, and a more posterior distribution pattern of SELs along the periventricular region.

In a subsequent study conducted on the PPMS trial population only (n = 732), the authors observed that most of the total brain non-enhancing T1 hypointense lesion volume accumulation was derived from chronic lesion activity within pre-existing T2 lesions rather than new T2 lesions (Elliott, Belachew, Jerry S Wolinsky, *et al.*, 2019). A larger decrease in T1 signal intensity and a greater relative accumulation of T1 hypointense volume was found within SELs compared with non-SELs. In addition, T1 hypointense lesion volume accumulation within SEL predicted clinical progression on a composite disability measure (based on 12-weeks confirmed 20% increase in EDSS, T25FW and NHPT). In contrast, whole-brain volume loss and acute lesion activity measured by longitudinal T1 hypointense lesion volume accumulation in new focal T2 lesions did not predict subsequent composite disability progression. The authors assessed also the treatment effect, as in the Ocrelizumab arm they found reduced longitudinal measures of chronic lesion activity (i.e. T1 hypointense lesion volume accumulation and mean normalized T1 signal intensity decrease) both within SELs and non-SELs.

The analysis of SELs was also extended to evaluate their association with multiparametric MRI quantitative measures within MS trials. For example, a study assessed SELs and their features at MTR and diffusion-weighted imaging (DWI) in both RRMS and SPMS patients within the SYNERGY trial (assessing Opicinumab when used concurrently with Beta-interferon) (C. Elliott *et al.*, 2020). In accordance with previous analyses, the authors found higher numbers of SELs in SMPS compared to RRMS (median 7.0 versus 4.0), but the associated T2 lesion-volume was similar in the two phenotypes, after accounting for demographic and baseline total lesion volume. In line with the hypothesis of their correspondence to chronic active lesions, SELs had a lower MTR and greater radial diffusivity at DWI from baseline up to 72

weeks, as markers of axonal-loss and reduced tissue integrity consistent with MS-specific chronic demyelination.

A recent observational study has confirmed the relevance of SELs for RRMS patients (n=52) for their relation to future clinical evolution (Preziosa *et al.*, 2022), and also assessed T1 signal intensity and MTR, as measures of microstructural integrity of the MS lesions. MRIs were acquired at baseline, and after 6, 12 and 24 months, while a further clinical evaluation was performed at 9 years follow-up. Median numbers of SELs were higher in patients with worsening EDSS compared with stable patients (4 vs 0). EDSS worsening at follow-up associated with the presence of more than 4 SELs, a higher proportion of SELs among baseline lesions and lower MTR of SELs. These last two metrics, and a higher T1 signal intensity decline, were also significant independent predictors of EDSS worsening at follow-up and predicted SPMS conversion.

The effects on SEL occurrence related to exposure to DMTs have been assessed in a recent prospective longitudinal non-randomized cohort study, over a follow-up of 2 years (Preziosa *et al.*, 2020). In this study, SELs and their structural changes on T1 intensity and MTR were assessed with respect to two treatment groups, RRMS patients following Natalizumab or Fingolimod (n= 28 and n=28, respectively). The authors identified that cross-sectionally in both treatment groups, SELs versus non-SELs showed lower MTR and T1 signal intensity. Longitudinally, non-SEL MTR increased while T1 signal intensity decreased in both treatment groups.

2.6.3 Conclusions on the current MRI markers for progression in MS

In conclusion, in this sub-chapter, conventional MRI markers related to disease progression in MS were presented. Currently, one of the most important markers to depict the global neurodegenerative effects is the percentage of brain volume change (PBCV), as a measure of brain atrophy. However, the quantification of chronic active lesion types has been demonstrated to be an additional feature of neurodegeneration. A focused review was provided on the use of T1 hypointensity to manually identify the subtype of lesions with chronic changes (i.e. the black holes) as compared to the overall hyperintense lesions in T2-weighted scans. More recently, implementation has been provided by tracking those hypointense lesions over time (i.e. persistent black

holes) by confirming them on subsequent follow-ups, or by using the dynamic contrast-enhanced (DCE) patterns, thus being more suitable to represent the chronic lesion types. Subsequently, one of the quantitative MRI markers has been presented, as this was used throughout the analyses of this thesis, the magnetization transfer ratio (MTR). In the last sections, novel MRI markers were presented. With the advent of volumetric non-linear registration and susceptibility MRI techniques, together with PET, it was possible to better characterise the chronic active lesions in MS. All the specific characteristics of those markers, including their limitations are presented in **Table 2-2**.

Table 2-2 Features and limitations of markers for progression in multiple sclerosis

Type of marker	Association to pathological substrate in MS	Features of the marker	Limitations
Percentage Brain volume change (PBVC)	Global brain atrophy	Represent the global outcome of neurodegenerative processes	High variability, effect of other contributors (ageing, alcohol, smoking, dehydration)
Dynamic contrast enhancement (DCE)	Chronic lesions (unspecified)	Older and larger lesions are marked by a centripetal-DCE (shell) pattern	Not consistently replicated and validated in imaging-pathological correlation studies
Persisting Black Holes (PBHs)	Chronic lesions (unspecified)	T1 hypointensity lasting for at least 6–12 months, associate to myelin damage	Not consistently correlate with axonal loss, due to effects of oedema/remyelination
Magnetization transfer ratio (MTR)	Chronic lesions (unspecified)	MTR reductions are associated to myelin damage	Possible inter-subject and inter-scanner variability
Paramagnetic rim lesions (PRLs)	Chronic active lesions	Rim associate to iron accumulation within macrophages	Paramagnetic/diamagnetic substances biasing effects
Slowly expanding lesions (SELs)	Chronic active lesions	Pattern of expansion likely depicts the activated macrophages	Arbitrary cut-off selected for the expansion rate. No imaging-pathological correlation available
PET with translocator protein (TSPO)	Chronic active lesions	Affinity of the tracker to the activated macrophages	Difficult access and feasibility in the clinical context

3 Characterising the slowly expanding lesions in secondary-progressive MS

3.1 Introduction and aim of the study

The first part of this work was dedicated to the application of a new technique for the analysis of one of the markers for chronic active lesions, by computing the Slowly Expanding Lesions (SELs) in a progressive MS cohort. Data from pathology suggests that those lesion subtypes are more prevalent with longer disease duration. Therefore, a SPMS population was identified from the MS-SMART (NCT01910259) (Chataway *et al.*, 2020), a phase IIB randomized multi-arm trial comparing the efficacy on disease progression of Amiloride 10mg/day or Riluzole 100mg/day or Fluoxetine 40mg/day versus placebo). I took part in the data collection as assessor neurologist, and clinical and imaging data analysis with the research team at Queen Square MS Centre. The aim of this study was to investigate the associations of SELs with physical and cognitive disability scores in secondary-progressive MS (SPMS). A structural analysis of MTR was also included, in order to explore the development of tissue damage within SELs in a subset of patients. The investigation included a descriptive radiological analysis of SELs, including their relationship with other conventional MRI inflammatory and neurodegeneration markers, such as T2 lesion volume change, manually detected new or enlarging T2 lesions, new PBH, and brain atrophy.

3.2 Pilot analysis

This work was addressed to study the applicability of the SEL detection algorithm. A pilot study was set with the aim of developing the algorithm to extract SELs and evaluate the performance on the pilot population, by running some methodological variations. A sample of patients was selected, a subgroup of the MS-SMART trial cohort whilst the trial was still ongoing. The eligibility criteria to be included in the pilot study were the following: the availability of at least 3 consecutive MRI scans at all trial time points including T1/T2-weighted scans and clinical data. 79 patients were

enrolled as they fulfilled the eligibility criteria and passed a satisfactory MRI quality check.

3.2.1 The SEL detection algorithm

The SEL detection algorithm was an in-house version of the pipeline proposed by Elliott et al. (C. Elliott, J.S. Wolinsky, S.L. Hauser, L. Kappos, F. Barkhof, C. Bernasconi, S. Belachew, Arnold, 2017), using a non-linear registration analysis of T2-defined lesions on volumetric T1 images in a two-stage process. This method was based on the method of Elliott et al. which was previously described in paragraph 2.6.2. Practically, baseline and follow-up scans are firstly aligned in a rigid registration to a common mid-space. Then, a non-rigid registration is applied so that the baseline scan is warped into the follow-up scan, thus each voxel on the image grid will undergo a deformation. The local 3D deformation field is derived on a voxel-by-voxel basis to get a Jacobian expansion value (JE, the determinant of the non-linear deformation field) and the relative Jacobian map visualizes the volume change on a heat map: the red colour corresponds to expansion and positive JE, while areas in blue with negative JE are related to contraction/shrinkage (**Figure 3-1**).

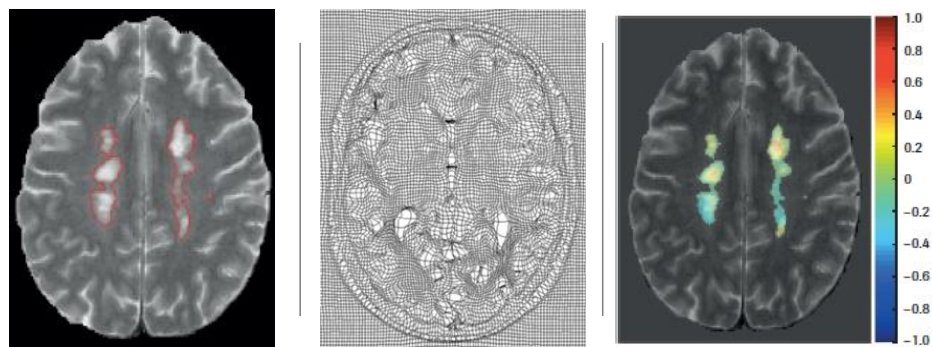


Figure 3-1. Lesion segmentation, deformation field map and Jacobian heat map. (figure re-adapted from Elliott C. et al., MSJ, 2018)

Firstly, ‘candidate’ SELs were identified from the baseline T2 lesion masks propagated to subsequent scans. A lesion with a positive JE and size of at least 10 mm³, was classified as SEL candidate. The remainder of the lesions with a negative JE were classified as non-SELs. The second step identified ‘definite’ SELs, through a

further sub-selection from the SEL candidates. This was based on both the constancy over time and concentricity of their expansion, as calculated by the z-score sum of those parameters greater than zero. SEL candidates, which did not satisfy the full two-stage criteria, were designated as ‘possible’ SELs (**Figure 3-2**). The rationale behind this new method stands in excluding the steps of defining a minimal expansion (JE1 and JE2 as in Elliott et al.) from the pipeline, as they were considered heuristic scores and the cut-offs were set without a biological justification. For this reason, those parameters could have affected the classification of the lesional voxels, due to the grouping and dilation phases affecting the lesion counts and possibly reflecting an unrealistic number of SELs. Overall, the reliability and robustness of this method stand in the use of a unique acquisition (T1-weighted) and a simplified algorithm, which relies on the evaluation of a unique value (the Jacobian determinant) using a cut-off of 0, which was set based on the simple concept of a positive value reflecting a volumetric increase of any extent. Therefore, this method is characterised by high sensitivity in detecting the smallest expansion within MS lesions. This is related to the biological mechanism observed for the chronic active lesions, i.e., the presence at pathology of active macrophages at the periphery contributing to slow growth of the lesion boundaries.

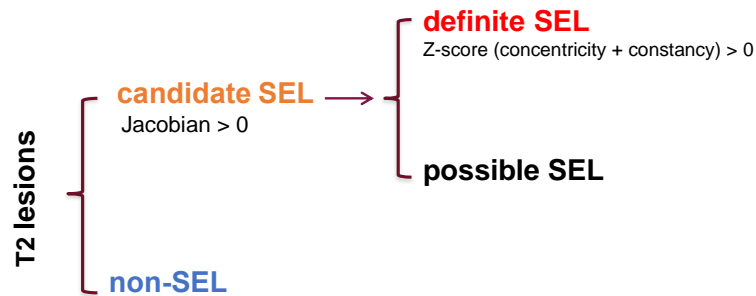


Figure 3-2. Classification of lesions according to the SEL detection algorithm.

The ‘constancy’ parameter was measured through the amount of lesion expansion determined by JE as a function of time, using the least square linear fit to the data points as determined by forcing a 0 intercept, since the baseline scan is assumed to be the reference (**Figure 3-3**). The residual squared error between the linear fit and the actual data points is measured including the average over all time points and it is

normalized by the amount of actual expansion. The constancy parameter favours lesions that show gradual positive volume change, excluding lesions with large volumetric, but not constant changes

The ‘concentricity’ parameter is applied to capture a concentric inside-out spatial expansion pattern, based on the assumption that the expansion advances towards the periphery. Practically, the voxels within each lesion were subdivided into concentric bands from the central core, and the mean JE values in each band were plotted against the distance from the edge, allowing calculation of the slope of the least-squares linear fit (**Figure 3-3**). This is taken as the raw measure of concentricity, and the JE gradient from the outside towards the inner layers should be positively increasing. The mean fit residual is computed and the raw concentricity is normalized by the residual, to penalize poor linear fits and give the final concentricity score.

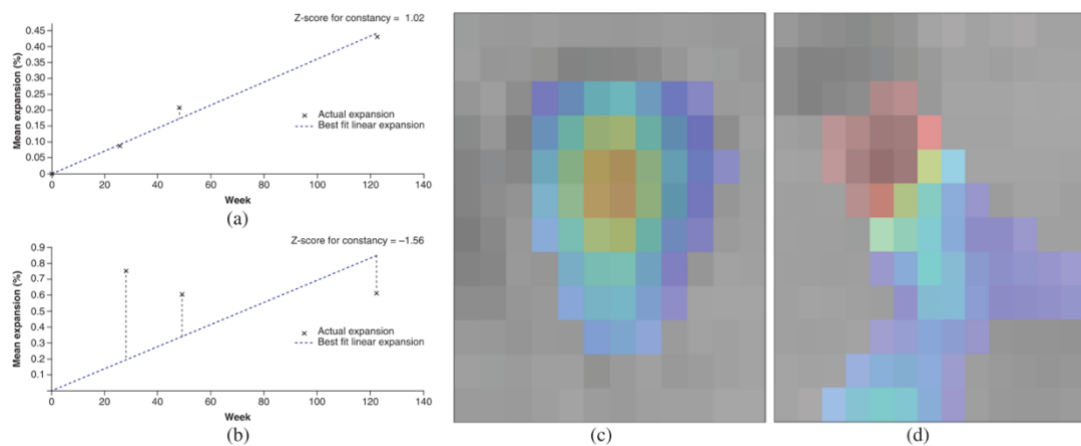


Figure 3-3. Constancy and concentricity of expansion

(a), (b) Plots of the amount of expansion as a function of time: dotted line represents the linear best fit of expansion as a function of time and markers (X) represent the actual expansion as measured by the Jacobian determinant at each time point. The plots represent examples of lesions with a constant expansion (a) and a poorly constant expansion (b). Other examples in which colours represent per cent local expansion are shown in (c) and (d): concentric pattern of expansion (c) and a poorly concentric pattern of expansion (d) (Figure re-adapted from Elliott C. et al. MSJ, 2018)

3.2.2 Methods and Results of the pilot study

Before performing the SEL analysis on the pilot population, I first manually segmented the lesion masks using a semi-automated technique. As there is no gold standard for a SEL, several variations of the algorithm were performed, in which combinations of the use of different sequences (e.g. 3D T1 versus 2D T2-weighted) and registration optimisation methods (local normalized correlation coefficient or LNCC, and normalised mutual information or NMI) were applied.

Some initial trials of the SEL algorithm on a pilot population were assessed to evaluate the performance of the deformation analysis when using as the main sequence 2D T2-weighted or 3D T1-weighted. Thus, the deformation maps, obtained through the non-linear registration, were assessed firstly using one or the other as the main sequence to retrieve the Jacobian values. In line with the work on SELs by Elliott et al., a trial to evaluate the combination of the T1 with the T2 sequence was applied, but this was not satisfactory because it didn't provide any improvement in comparison with the use of a single sequence. The results, as examples of the deformation maps, and graphs of the frequency distribution after the classification of lesions in the SEL-derived categories were reviewed by an expert consensus. The PhD Supervisors were asked to determine which variation on the algorithm most consistently identified lesions that expanded over time. Moreover, two different optimisation functions were applied for the registration, including the LNCC, which didn't provide optimal results with T1 images because of the low T1 signal within most of the lesions. Finally, the use of the NMI registration method, which is the most used in the literature, was the one that retrieved more optimal results.

Here are reported the two main SEL algorithms evaluated during the pilot work, i.e. the preliminary and the optimised one. In the preliminary SEL algorithm, the main reference image used to extract the main sequence to calculate the deformation was 2D PD/T2-weighted with the LNCC registration. Thus, the same acquisition in which the lesion masks were obtained was also used to obtain the deformation map. On the other hand, the optimised algorithm included a resampling of the images to isotropic voxels (1 mm x 1 mm x 1 mm) to increase the sensitivity of the technique in identifying the lesion boundaries and the use of the NMI registration method. Afterwards, lesion masks, originally delineated on PD/T2-weighted images, were co-registered to the T1

space using a pseudo-T1 image generated by subtracting the PD from the T2-weighted image. (Hickman *et al.*, 2002). They were then transformed from native space to 3D-T1 space using nearest-neighbour interpolation (Prados *et al.*, 2016). This implied that the deformation maps, in this alternative approach, were calculated based on the longitudinal T1 intensity change over time. The combination of the NMI registration algorithm using 3D T1-weighted sequences performed best, thus this alternative approach was defined as the optimized SEL algorithm.

The application of this optimized SEL algorithm led to the identification of a higher number of all lesion types, except for non-SELs, and an increase in the overall mean lesion volume per patient without significant changes of the mean sum volumes per patient by lesion type, using a paired t-test (*Table 3-1*).

Table 3-1. Pilot analysis: lesion counts and volumes by type with preliminary and optimized SEL algorithm

	Sum number per patient mean, (IQR)			Sum volume per patient ml (% of total lesions)		
	Pilot	Optimized	p-value*	Pilot	Optimized	p-value*
Total lesions	60.62 (36.5 – 75.0)	80.90 (52.0 – 99.0)	<0.001	12.85 (100%)	13.18 (100%)	<0.001
non-SEL	45.77 (26.0 – 59.0)	46.71 (29.0 – 61.0)	0.273	5.50 (45%)	6.17 (47%)	0.380
possible SEL	12.66 (7.5 – 15.0)	19.96 (12.0 – 25.0)	<0.001	3.20 (26%)	4.12 (31%)	0.100
definite SEL	1.77 (1.0 – 3.0)	15.12 (8.0 – 18.0)	<0.001	3.60 (29%)	2.89 (22%)	0.170

*paired t-test; Abbreviations: SEL=slowly expanding lesions

In the pilot study, 4756 lesions were manually segmented and the SEL algorithm applied to PD/T2-weighted scans as the main sequence to compute the deformation field within each lesion. After the first step of the algorithm, 1140 lesions were classified as SEL candidates (24% of the total T2 lesions) and the rest as non-SELs. Following the second step, 140 (3% of the total) lesions were categorised as definite SELs and the remaining 1000 (21% of total) classified as possible SELs. Each patient had a mean sum number of definite SELs around 2 and a mean sum volume of SEL candidates of 3.60 ml (SD 5.83), which accounted for 29% of the total lesion volume.

In this exploratory work, the analysis was restricted to a simple univariate correlation analysis, and included some linear regressions to identify the associations between SELs and other conventional MRI markers in MS. A simple linear regression model between definite SELs and total lesion volumes showed a positive association between those markers (beta=1.85, 95% CI 1.30 to 2.40, $p < 0.001$), suggesting that having a higher definite SEL volume was associated with higher total lesion volume load. In addition, a positive strong correlation coefficient between candidate SELs and total lesion volume was found (Spearman rho=0.73, $p < 0.001$; **Figure 3-4**).

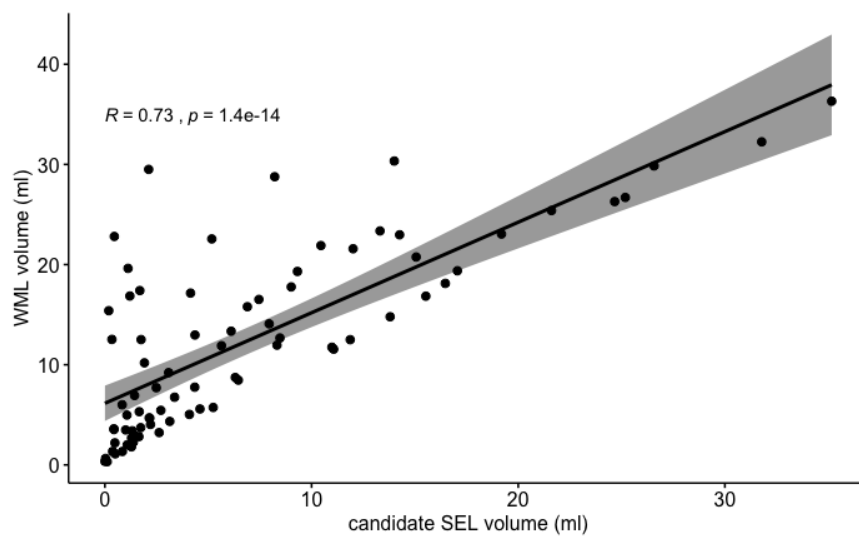


Figure 3-4. Regression line of the candidate SEL volume and total white matter lesion (WML) volume, and 95% CI in the grey area.

R correspond to Spearman correlation coefficient.

The pilot study population was classified into two groups according to presence or absence of definite SELs: SEL-positive patients, if definite SEL volume was greater than zero; SEL-negative patients, if definite SEL volume was equal to zero. The SEL-positive group demonstrated a significantly higher total lesion volume load compared to SEL-negative patients (t-test 13.83 ml, SD 9.1 versus 7.12 ml, SD 7.6; $p = 0.006$).

In addition, in linear regressions SEL-positive patients were characterised by higher physical disability, measured by the MSFC z-score (adjusted difference -0.42; 95% CI -0.68 to -0.12; $p = 0.007$) after correcting for total lesion volume, normalised brain

volume, age and gender. There was some evidence of a trend towards developing worse cognitive performance at follow-up in SEL-positive patients, measured by the SDMT (adjusted difference -5.28; 95% CI -11.75 to -0.32; $p=0.065$).

3.3 Extension to the SEL study population

At the conclusion of the MS-SMART trial, the analysis that was started in the pilot study was extended to the overall trial population. The main eligibility inclusion criteria for this study were defined as follows: availability of clinical data and MRI scans (of sufficient quality for SEL analysis) at all the three trial study assessments (baseline, week 24 and week 96). Out of the full MS-SMART cohort ($n=445$) enrolled in the trial, after applying those eligibility criteria, 352 were sub-selected for the enrolment in the SEL study, and the others were discarded due to missing scans or because there were image artefacts ($n=93$).

As a second step in the selection of the SEL study population, a participant was defined as a ‘MRI outlier’ when the total T2 volume was outside of two standard deviations of the mean, either above or below. The MRI outliers were carefully checked and the decision to discard them from the analysis depended on the fact that the extremely high lesion burden (and or presence of an extreme brain atrophy rate) represented a different behaviour outside of the average identified, after the manual check, and by the judgement of the raters. An example of images obtained from subjects who were considered outliers with an extremely high lesion load that could have affected the computation of the deformation maps is provided in **Figure 3-5**.

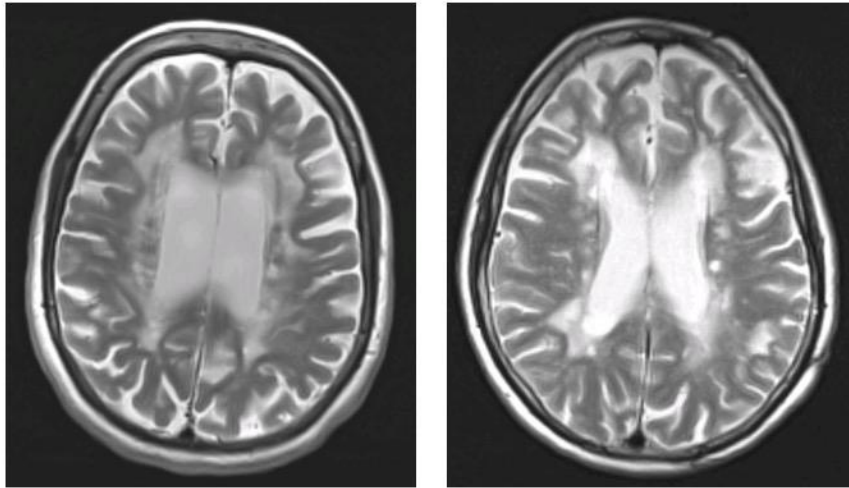


Figure 3-5. Example of outliers discarded from the SEL analysis.

Therefore, another group of outlier patients with those extreme characteristics (n=7) were discarded, thus possibly driving the results of the analysis. All patients that were not included in the study did not have any difference in the demographic features compared to the ones included (**Table 3-3**).

The flow-chart of the enrolment on this analysis, to select the population defined ‘SEL study’ is presented in **Figure 3-6**. A sub-set of the overall MS-SMART patients did follow the advanced MRI protocol as a sub-study run only in some trial sites, therefore another subset (n=106) did follow the acquisition of an extra MTR sequence out of the usual trial MRI protocol.

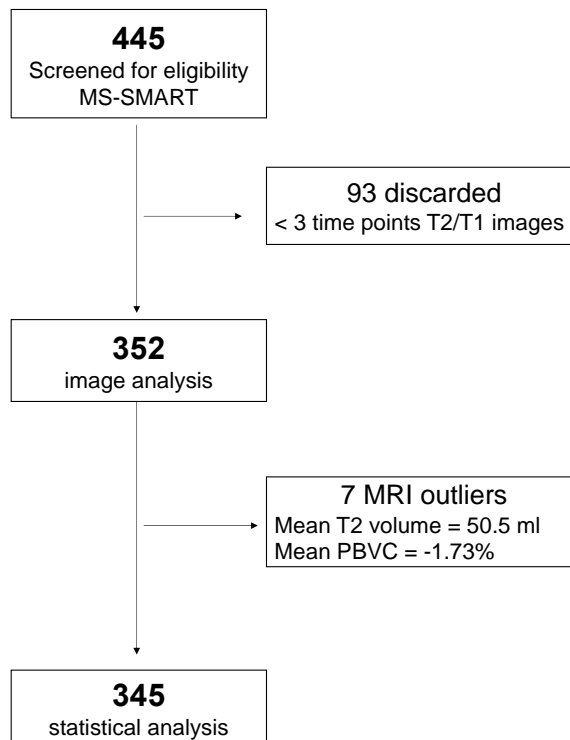


Figure 3-6. Flowchart showing the enrolment of subjects into the SEL extension study.

3.3.1 Methods

3.3.1.1 Data collection & clinical assessments

Data were collected after written informed consent was obtained and the study was approved by the local research ethics committee at University College London (UCL). Then, fully anonymized clinical and MRI data were analysed at Queen Square MS Centre, Department of Neuroinflammation. All the demographical data were collected (age at baseline, sex), including MS-specific clinical information, such as disease duration and progression duration (as defined by the onset of the secondary-progressive phase of the disease). Clinical data included in this analysis were measured with the following scores: EDSS, SDMT and MSFC. The latter was calculated as the composite of z-scores of the three subcomponents, as previously described (Cutter *et al.*, 1999): NHPT, T25FW and PASAT. The disability progression at the end of the trial was defined as a binary measure (presence or absence of clinical deterioration), as follows: 1-point increase in EDSS (considering the EDSS change from baseline to

week-96) if the baseline score was ≤ 5.0 , or a 0.5-point increase if the baseline score was > 5.0 , as previously described in other trials (Lublin *et al.*, 2016; Kappos *et al.*, 2018).

3.3.1.2 MRI acquisitions

The trial involved 13 UK sites with multiple MRI scanners, including Philips 3T and 1.5T (Philips Healthcare, Best, the Netherlands), Siemens 3T and 1.5T (Siemens Healthineers, Erlangen, Germany), GE 3T (General Electric Healthcare, Chicago, IL). All patients were scanned using 1.5T or 3T MRI scanners with the core protocol, including scans at baseline, week 24 and week 96, with the following acquisitions: 3D isotropic T1-weighted (T1); 2D proton density (PD) and T2-weighted (T2); 2D fluid-attenuated inversion recovery (FLAIR). As part of the advanced MRI protocol of the trial, a subset of 106 patients scanned in London and Edinburgh trial sites also had 3D MTR imaging at baseline and week 96. The details of the MRI acquisition parameters are shown in **Table 3-2**.

Table 3-2. MRI acquisition parameters

Sequences	Repetition time (ms)	Echo time (ms)	Flip angle (α)	Field of view (mm^2)	Voxel size (mm^3)	No. of slices
PD/T2 weighted 2D TSE	3500	19/85	90°	240 x 240	1x1x3	50
T1 weighted 3D	7.0	3.1	8°	180 x 256	1x1x1	256
MTR 3D FFE	6.4 35*	2.7/4.3 4.07/9.49*	9°	180 x 256 256 x 256*	1x1x1	256 176*

Abbreviations: TSE=turbo spin-echo; MTR= magnetization transfer ratio; FFE= fast field echo. MTR parameters are referred to London site, while * denotes the parameters used at Edinburgh site.

3.3.1.3 T2 lesion segmentation, SEL detection and tissue segmentation

T2-weighted, PD and FLAIR baseline images were used to delineate the T2 hyperintense lesions through a manual identification technique using a semi-automated edge finding tool (JIM v7.0, Xinapse Systems, Aldwinckle, UK). From the manually outlined lesions, T2 lesion volumes were acquired. Then, the SEL detection algorithm technique described before in the pilot analysis allowed stratifying lesions in the following categories: candidate SELs, including definite SELs and possible

SELS, and the non-SELS. The term ‘SEL-derived volumes’ was used to describe the lesion volumes at baseline, in the categories as defined after applying the SEL detection. For the evaluation of spatial localisation, lesion probability maps (LPM) were separately obtained for the SEL-derived categories, after registering all subjects to a common anatomical atlas, as described in previous works (Kincses *et al.*, 2011).

New/enlarging T2 lesions were manually identified using subtraction of the PD/T2 images at baseline and 24/96 weeks. Similarly, new Persistent black holes (PBH) were manually selected and reported as the number of new T2 lesions at 24 weeks that were persistently T1 hypointense at 96 weeks. For brain extraction, tissue segmentation and parcellation, Geodesical Information Flows (GIF) method was used on the lesion-filled 3D T1 scans, (Cardoso *et al.*, 2015) providing the following metrics: normalised brain volume (NBV); normal-appearing white matter (NAWM), cortical grey matter (CGM) and deep grey matter (DGM) volumes; lesion-filling was used in this step using a multi-time-point patch-based method to avoid segmentation bias (Prados *et al.*, 2016). The Percent Brain Volume Change (PBVC) from baseline to week 24 and from baseline to week 96, as a measure of brain atrophy, was calculated using the Structural Image Evaluation using Normalization of Atrophy (SIENA) technique (Smith *et al.*, 2002).

3.3.1.4 Structural analysis of MTR within lesion types

Magnetization transfer ratio (MTR), as percent units (pu), was computed within all the lesion masks previously outlined at baseline and week 96 at the lesion level. Then, the difference between the two measures was calculated as the longitudinal MTR change. For each participant, the mean MTR within each of the segmented lesions was calculated. MTR was also analysed at the single lesion level within the subgroups of definite, possible, and non-SELS. To account for the presence of registration inaccuracies, MTR values greater or less than two standard deviations from the mean were excluded from this analysis, as considered possible misregistration not pertaining to the region of interest analysed.

3.3.1.5 Statistical analysis

The statistical analysis was performed with STATA version 13.1 and all the actual p values obtained were reported. Firstly, the distribution and the normality assumptions of all the clinical, demographic and MRI variables were evaluated. Differences in EDSS from baseline to the last follow-up (week 96) were assessed using the Wilcoxon signed ranked test. Clinical scores were evaluated through their longitudinal changes by subtracting the baseline from week 96 values. Differences in the conventional MRI measures (such as T2 lesion volume and PBVC at each trial interval) were compared using paired t-tests. Lesion counts were assessed at the patient level by calculating the total number and volume of the SEL-derived measures (definite SELs, the possible SELs and the non-SELs, respectively). As the distribution of SEL-derived volumes was positively skewed, they were all log-transformed (using logarithm on base 10 of the value + 1) to normalise the data. Pearson and partial correlations were assessed between SEL volumes, other MRI measures and clinical scores to assess the magnitude and direction of associations. Simple linear regressions, with SEL volumes as predictors and demographic and clinical features (age, sex, disease duration, progression duration, EDSS, MSFC, NHPT, T25FW, PASAT, SDMT) as outcome variables, were performed. Through this association analysis, an evaluation of the relationship between the clinical outcomes and the MRI metrics was carried out with Direct Acyclic Graphs (DAGs) to identify confounders to include in the final statistical models. For example, **Figure 3-7.** illustrates the procedure used for the definite SEL volume and the EDSS (at final follow-up), which were assessed as the exposure and the outcome variables, respectively.

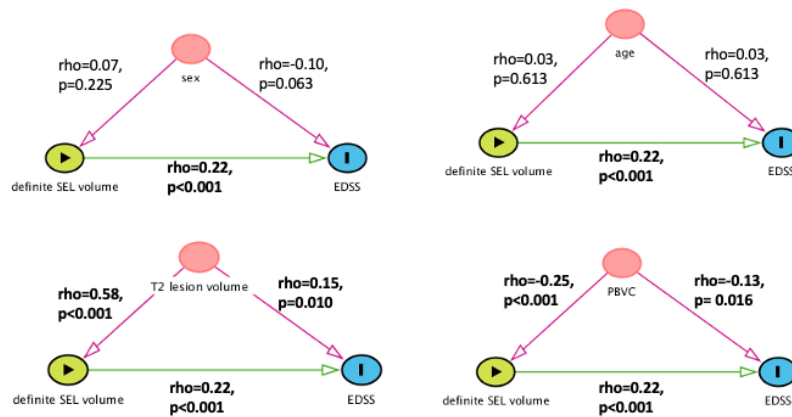


Figure 3-7. Direct Acyclic Graphs (DAGs) showing the relationship between the variables included in the statistical models.

The relationship between these two was then observed in concomitance to possible confounders, by analysing the Spearman correlation coefficients (shown on the connecting arrows). In the bottom DAGs, the variables T2 lesion volume (at final follow-up) and percentage brain volume change (PBVC) are significantly associated to both exposure (definite SEL volume) and outcome (EDSS), thus those two variables can be considered confounders and they were included in our models. In the top DAGs, the two demographic variables, sex and age, did not show significant correlation with either the exposure or outcome variable. However, in consideration of extensive literature data of their association to the outcomes, they were kept as confounders in all the models. The same analyses were replicated for all the other SEL-derived variables and clinical outcomes. The volumetric and structural MTR analysis was performed at the single lesion level by applying mixed-effects regression models to take into account within subject variability, and they were also adjusted for age, gender and trial centre (to account for scanner differences).

Multiple linear regression models were run to explore whether SEL-derived volumes could independently predict disability outcomes. The added value of SEL-derived volumes was evaluated in comparison with conventional MRI measures, using a backward stepwise selection process. All models were adjusted for age and sex, T2 lesion volume change and PBVC, keeping the variables in the models if statistically

significant, always forcing age and sex into the models and using a boot-strap approach, and including robust standard errors. The final model included the clinical measure at final follow-up (week 96) as the dependent variable, adjusting for the clinical measure at baseline, and the SEL-derived volumes as independent variable, to assess the ability of SEL-derived volumes to predict longitudinal clinical changes. The stability of the final model was confirmed in a forward selection process. In addition, logistic regression models were built to assess the ability of SEL-derived volumes to predict the development of disability progression. All the models' residuals were checked for normality. The validation of the relationship between SEL and the clinical variable measurements was undertaken across trial time points, using repeated-measures mixed-effects models. In those models, the dependent variable was the value of the clinical variable (one at a time) at each time point, and the explanatory variables included the time point, SEL-derived volumes, and an interaction term between them. Whenever the interaction terms were significant, an association between the clinical variable and the SEL-derived volume was assumed, for the time point explored. To take into account the multicentre structure of the trial, all the mixed-effects models were nested at the centre level.

3.3.2 Results

3.3.2.1 Clinical-demographic and conventional MRI metrics

Demographics, clinical characteristics and radiological parameters at baseline and their longitudinal changes within the SEL study population and the patients excluded from the study are reported **Table 3-3**.

Table 3-3. Demographic, clinical, and radiological characteristics of the patients whose scans contributed to the SEL study

	Clinical and radiological characteristics	SEL study	Excluded
Demographics and clinical measures	Number of patients	345	100
	Age, median [y] (IQR)	55.9 (50.0 – 60.4)	54.6 (48.8 – 58.2)
	Female n (%)	230 (67%)	68 (68%)
	Baseline disease duration, median [y] (IQR)	21 (15 – 22)	18 (14 – 26)
	Baseline progression duration, median [y] (IQR)	6 (3 – 8)	6 (3 – 9)
	Number of patients allocated to the treatment arms, n (% total):		
	– Fluoxetine	90 (26.1%)	21 (21%)
	– Riluzole	85 (24.6%)	26 (26%)
	– Amiloride	86 (24.9%)	25 (25%)
	– Placebo	84 (24.4%)	28 (28%)
	EDSS at baseline, median (IQR)	6.0 (5.5 – 6.5)	6.0 (6.0 – 6.5)
	EDSS change from baseline to week 96, mean (SD)	0.11 (0.72)	0.25 (0.78)
	Patients with disability progression over time, number (%)	126 (37%)	72 (72%)
	MSFC z-score at baseline, mean (SD)	-0.02 (0.85)	-0.26 (1.16)
	MSFC z-score change, mean (SD)	-0.41 (1.40)	-0.53 (1.64)
	NHPT at baseline, mean [sec ⁻¹] (SD)	0.03 (0.01)	0.03 (0.01)
	NHPT z-score change, mean (SD)	-0.12 (0.58)	0.05 (0.59)
	T25FW at baseline, mean [sec] (IQR)	11.2 (8.2 – 17.5)	11.8 (8.8 – 23.8)
	T25FW z-score change, mean (SD)	-1.17 (3.86)	-1.53 (4.71)
	PASAT score at baseline, mean (SD)	38.8 (14.9)	37.43 (14.33)
PASAT z-score change, mean (SD)	0.09 (0.69)	-0.11 (0.70)	
SDMT score at baseline, mean (SD)	44.4 (12.5)	43.31 (12.16)	
SDMT change, mean (SD)	0.58 (7.13)	-0.37 (10.61)	
MRI metrics	T2 lesion volume at baseline, mean [ml] (SD)	12.54 (10.85)	16.52 (16.50)
	T2 lesion volume at week 96, mean [ml] (SD)	12.78 (10.99)	17.92 (19.49)
	New/enlarging T2 lesions at week 96, mean number (SD)	2.67 (6.23)	3.80 (8.53)
	New PBH at week 96, mean number (SD)	0.32 (1.14)	0.28 (0.67)
	NBV at baseline, mean [ml] (SD)	1421 (85)	1430 (79)
	CGM at baseline, mean [ml] (SD)	790 (44)	788 (44)
	DGM at baseline, mean [ml] (SD)	45 (4)	45 (4)
	NAWM at baseline, mean [ml] (SD)	588 (44)	596 (42)
	PBVC, mean [%] (SD)		
	– week 24 to week 96	-0.94 (1.20)	-0.57%
– baseline to week 96	-1.35 (1.27)	-1.34%	

Abbreviations: EDSS=expanded disability status scale, MSFC=multiple sclerosis functional composite, NHPT=nine-hole peg test, T25FW=timed 25-foot walk test, PASAT=paced auditory serial addition test, SDMT=symbol digit modalities test, PBH=persisting black hole, NBV=normalised brain volume, CGM=cortical grey matter, DGM=deep grey matter, NAWM=normal-appearing white matter, PBVC=percent grain volume change

After applying the eligibility criteria, in the retained SEL study cohort, EDSS significantly increased from baseline to the final follow-up (Wilcoxon signed-ranked test, $p < 0.001$) and 36.5% of the patients developed disability progression. The mean T2 lesion volume increased significantly from baseline to week 96 (12.54 ml and 12.78 ml, respectively, paired t-test, $p < 0.001$). The mean NBV was 1421 ml at baseline, and PBVC from baseline to week 96 was greater than PBVC from week 24 to week 96 (-1.35% and -0.92% respectively, paired t-test, $p < 0.001$).

3.3.2.2 Descriptive analysis of SEL-derived metrics.

The total T2 lesions, and then lesion measures for each SEL category were analysed at the patient level and they are shown in **Table 3-4**. The ratio to total T2 lesions is the number of lesions in a given SEL-derived category relative to the total number of T2 lesions. 340 of the 345 patients (99%) were defined as SEL-positive, i.e. they had at least one definite SEL, while only 5 did not have any SEL (also called SEL-negative). The mean number of T2 lesions per patient was around 67, of which ~20 (29%) of them were categorised as definite SELs. The mean T2 lesion volume of definite SELs was ~4 ml, which accounts for 36% of the overall T2 lesion volume.

Table 3-4. SEL-derived metrics at the patient level (n= 345)

Lesion type		Number of lesions per patient, mean (range)	Ratio to total T2 lesions	Lesion volume per patient, mean [ml] (range)	Ratio to total T2 lesion volume
T2 lesion		67.2 (3 – 352)	NA	12.3 (0.1 – 71.4)	NA
SEL category	non-SEL	41.2 (1 – 284)	0.61	5.6 (0.1 – 37.7)	0.46
	possible SEL	6.4 (0 – 36)	0.10	2.3 (0 – 38.8)	0.18
	definite SEL	19.5 (0 – 94)	0.29	4.4 (0 – 39.7)	0.36

Abbreviations: SEL=slowly expanding lesions

The volumes of the lesions were analysed at the single lesion level from mixed-effects model to analyse the differences between each SEL-derived category: the definite

SELs were significantly larger than non-SELs (0.25 ml, 95% confidence interval (CI) [0.18 to 0.31] vs 0.14 ml [0.07 to 0.20], respectively, $p=0.019$).

Then, to assess the actual expanding portion as a quantitative measure, the JE values were analysed for each SEL-derived category. The mean annualised JE change in the individual lesion volumes was 3% (SD 2.9) for definite SELs, 1.5% (SD 3) for possible SELs, and 1.5% (SD 2.2) for non-SELs. Finally, the visual inspection of the lesion probability maps (LPM) revealed that the spatial localisation showed higher probability in the periventricular areas, while no regional differences were found between definite SELs, possible SELs and non-SELs, although the latter were more prevalent overall (**Figure 3-8**).

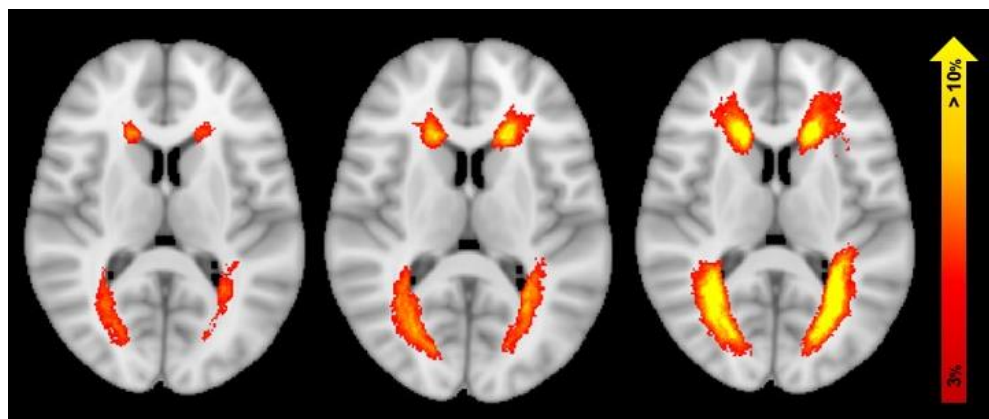


Figure 3-8. Lesion probability map (LPM).

From left to right, LPM for definite SEL, possible SEL and non-SELs where red indicates a lower probability starting at 3% and yellow bigger than 10%.

The analysis of the SEL-derived metrics was extended to include the treatment-allocation as assigned in the MS-SMART trial. All the conventional MRI measures, including the SEL-derived metrics, were described for each one of the three treatment arms and the placebo group (**Table 3-5**). No differences between treatment arms were observed in terms of counts and volumes of T2 lesions, or any of the SEL-derived categories.

Table 3-5. SEL-derived metrics at the patient level by treatment allocation arm.

	Treatment allocation				p value
	Fluoxetine (n=90)	Riluzole (n=85)	Amiloride (n=86)	Placebo (n=84)	
Total T2 lesion count	65.3 (6 – 176)	66.6 (3 – 201)	68.2 (4 – 352)	68.7 (7 – 266)	p=0.94
Non-SEL count (n)	37.4 (4 – 97)	41.5 (1 – 158)	43.5 (2 – 234)	42.5 (4 – 206)	p=0.52
Possible SEL count (n)	7.2 (0 – 28)	6.2 (0 – 27)	6.4 (0 – 36)	5.9 (0 – 25)	p=0.45
Definite SEL count (n)	20.7 (0 – 76)	18.9 (2 – 51)	18.3 (0 – 94)	20.3 (1 – 47)	p=0.56
Total T2 volume (ml)	13.6 (0.1 – 71.4)	11.3 (0.1 – 37.9)	12.5 (0.2 – 51.6)	11.6 (0.2 – 51)	p=0.49
Non-SEL volume (ml)	5.1 (0.1 – 37.7)	5.9 (0.1 – 31.6)	5.9 (0.2 – 29.5)	5.5 (0.1 – 27.8)	p=0.47
Possible SEL volume (ml)	2.9 (0 – 38.8)	2.0 (0 – 35.3)	2.3 (0 – 25.7)	1.9 (0 – 23.9)	p=0.32
Definite SEL volume (ml)	5.6 (0 – 38.2)	3.3 (0.1 – 19.6)	4.2 (0 – 39.7)	4.3 (0.1 – 25.5)	p=0.09

Abbreviations: SEL=slowly expanding lesions

3.3.2.3 Association between SEL and conventional MRI metrics

To evaluate the relationship of the SEL-derived metrics with other conventional MRI measures, an initial association analysis was carried out. In particular, positive correlations were found between definite SEL volume and T2 lesion volume change ($r=0.24$, $p<0.001$), the number of manually obtained new/enlarging T2 lesions at week 96 ($r=0.26$, $p<0.001$), and the number of new PBHs at week 96 ($r=0.19$, $p<0.001$). In addition, a positive correlation was found between definite SEL volume and baseline T2 lesion volume ($r=0.55$, $p<0.001$). This association was still significant in partial correlations, after accounting for the effect of the number of new/enlarging T2 lesions and new PBHs at week 96. Finally, the definite SEL volume negatively correlated with percentage of brain volume reduction over time ($r=-0.26$, $p<0.001$). An example of a patient from this study with a high proportion of SELs (relative to total lesion count), worsening of disability and high PBVC is shown in **Figure 3-9**.

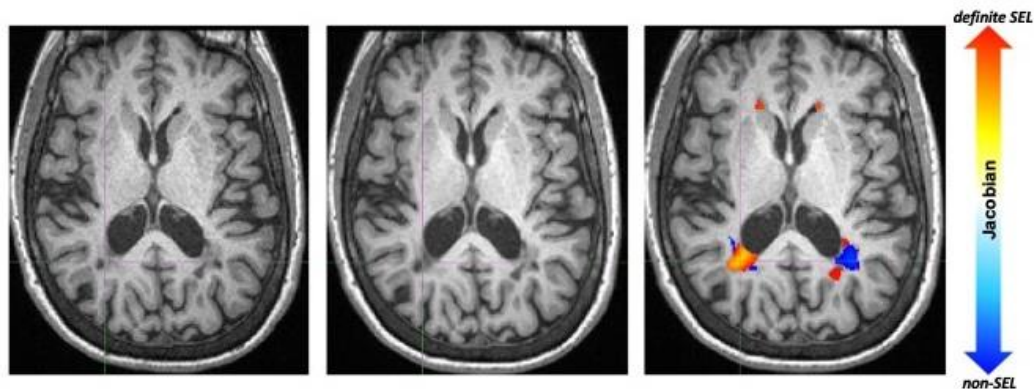


Figure 3-9. Example of patient with high number of SELs.

From left to right: T1 at baseline, T1 at week 96 and registered T1 with Jacobian maps overlaid; out of 27 total T2 lesions identified, 16 were definite SELs (59%). EDSS at baseline was 5.5 and EDSS at week 96 was 8. PBVC from baseline to week 96 was -2.5%.

3.3.2.4 MTR analysis within SEL-derived lesion types

Data on lesional MTR were available in a subset of 106 patients from the SEL study population, in which 6,938 T2 lesions were retrieved. The mean MTR was computed at baseline and at the end of the trial, and then it was evaluated using a mixed-effects model to account for within-subject variability, age, gender and site, and total lesion volume, as shown in **Table 3-6**.

Table 3-6. Magnetization Transfer Ratio (MTR) at baseline and 96 weeks follow-up, and MTR changes over time in the different lesion types.

T2 Lesion types	MTR in individual lesions (n=6,938)			
	MTR baseline, pu	MTR week 96, pu	MTR change	p value
non SEL (n= 4395)	29.77 (29.22 – 30.32)	30.03 (29.47 – 30.58)	0.26 (0.14, 0.37)	p<0.001
possible SEL (n= 659)	27.91 (27.27 – 28.54)	27.80 (27.17 – 28.43)	-0.11 (-0.40, 0.18)	p=0.351
definite SEL (n= 1884)	28.77 (29.20 – 29.34)	28.50 (27.93 – 29.07)	-0.27 (-0.44, -0.10)	p=0.002

Abbreviations: MTR=magnetization transfer ratio, SEL=slowly expanding lesions

The definite SELs had significantly lower MTR compared to non-SELs cross-sectionally, both at baseline and at week 96 ($p < 0.001$). Moreover, the difference between MTR longitudinal changes over time were also identified between those lesion categories. A higher rate of MTR reduction from baseline to week 96 was found in the definite SELs when compared with the non-SELs (mean adjusted difference 0.52, 95% CI [0.38 to 0.67], $p < 0.001$).

3.3.2.5 Associations between SELs, demographic and clinical features

An association analysis similar to the one described before for radiological measures was extended to the analysis of the demographic and clinical measures. A higher volume of definite SELs at baseline, correlated with a higher increase in EDSS over time (Pearson $r=0.18$, $p < 0.001$). Similarly, when the MSFC and its sub-components were analysed, a higher definite SEL volume correlated with increasing disability over time, as assessed by changes in the z-scores of the MSFC, T25FW and PASAT: Pearson r ranging from -0.18 to -0.22 , $p < 0.001$. On the other hand, definite SEL volumes did not show any significant association with the demographic features available (age, sex, disease duration and progression duration).

3.3.2.6 SELs and clinical disability outcomes

The main analysis in this part of the work was carried out through stepwise multiple linear regression models to check whether the SEL-derived volumes correlated with a deterioration of clinical scores at the end of the trial. With this work, a higher SEL burden was associated with worsening disability at follow-up in the majority of clinical scores assessed in the trial, and in particular the EDSS (**Figure 3-10**).

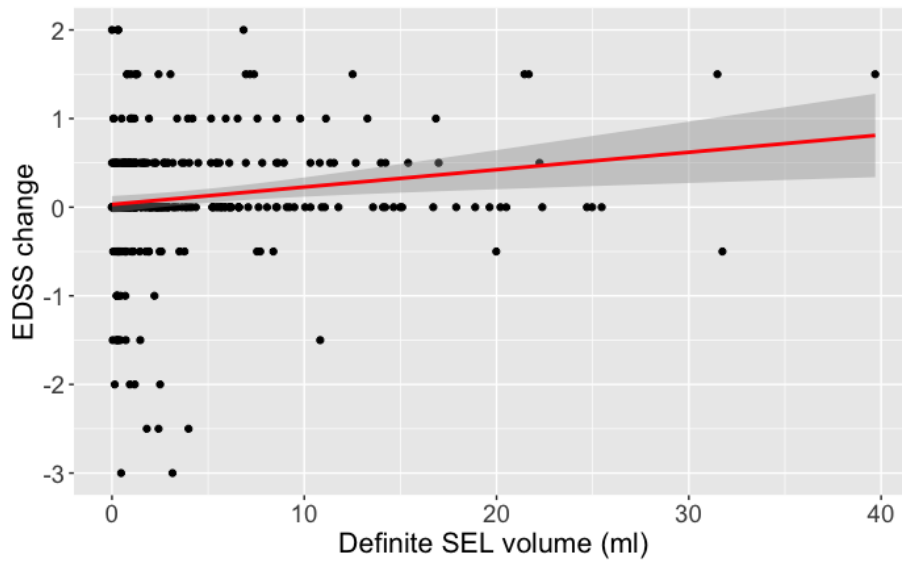


Figure 3-10. Regression line, drawn using R, showing the relationship between EDSS change from baseline to week 96 and baseline definite SEL volume (ml).

All the multiple linear regression models are shown in **Table 3-7** (in bold the significant results set as p-value <0.05), and they were computed after adjusting for demographic covariates, T2 volume change and PBVC.

Table 3-7. Multiple linear/logistic regressions between SEL-associated log-volumes and clinical scores.

	Non SEL log-volume beta or OR (95% CI) p value	Possible SEL log-volume beta or OR (95% CI) p value	Definite SEL log-volume beta or OR (95% CI) p value
EDSS	beta=-0.04(-0.25,0.16), p=0.695	beta=0.07 (-0.12, 0.27), p=0.461	beta=0.23 (0.04, 0.43), p=0.020
MSFC z-score	beta=-0.04(-0.37,0.28), p=0.809	beta=-0.24 (-0.79, 0.18), p=0.323	beta=-0.47 (-0.98, -0.03) p=0.048
NHPT z-score	beta=-0.12(-0.31,0.06), p=0.180	beta=-0.13 (-0.31, 0.03), p=0.127	beta=-0.09 (-0.28, 0.08), p=0.313
T25FW z-score	beta=-0.53(-1.42,0.40), p=0.263	beta=-0.69 (-2.19, 0.69), p=0.340	beta=-2.10 (-3.43, -0.85), p=0.001
PASAT z-score	beta=-0.06(-0.25,0.12), p=0.533	beta=-0.18 (-0.37, 0.01), p=0.056	beta=-0.27 (-0.50, -0.10), p=0.006
SDMT	beta=-3.02(-5.18, -1.12) p=0.004	beta=-2.77 (-5.05, -0.22), p=0.026	beta=-2.06 (-4.08, 0.29), p=0.067
Disability progression	OR=0.84 (0.47, 1.48), p=0.537	OR=1.43 (0.75, 2.71), p=0.276	OR=1.92 (1.08, 3.39), p=0.025

Abbreviations: SEL=slowly expanding lesion, EDSS=expanded disability status scale, MSFC=multiple sclerosis functional composite, NHPT=nine-hole peg test, T25FW=timed 25-foot walk test, PASAT=paced auditory serial addition test, SDMT=symbol digit modalities test, disability progression= 1-point increase in EDSS if the baseline score was ≤ 5.0 , or a 0.5-point increase if the baseline score was >5.0

For example, for each unit (ml) increase in definite SEL log-volume, there was an increase in EDSS at follow-up ($p=0.020$, adjusted $R^2=0.56$) and a tendency toward a decrease of MSFC z-score ($p=0.048$, adjusted $R^2=0.38$). In addition, a higher definite SEL log-volume was associated with worsening of all the MSFC subcomponents: T25FW z-score ($p=0.001$, adjusted $R^2=0.20$), PASAT z-scores ($p=0.006$, $R^2=0.66$). Neither non-SEL nor possible SELs log-volumes were significantly associated with any of those clinical scores. Interestingly, T2 volume change was not independently associated with change in the clinical measures, while PBVC remained significantly associated with worsening in EDSS and MSFC z-score in the models assessed. In the logistic regressions, an increase in the definite SEL log-volume was associated with an increased risk of developing disability progression ($p=0.025$, pseudo- $R^2=0.03$). No significant associations between all the SEL-derived measures and changes in the NHPT z-score were found. For the SDMT only, increase in non-SEL and possible SEL log-volumes were associated with a worsening in the cognitive score.

The associations observed in clinical disability and SEL measures were further confirmed through repeated-measures mixed-effects models across the trial time intervals (baseline to week 24 and baseline to week 96) and after adjusting for age at baseline, sex, total baseline lesion volume, PBVC between baseline and week 96 (**Table 3-8**).

Table 3-8. Association between SEL-derived volumes and clinical outcomes over time using mixed-effects regression models

	Mixed-effect repeated measures models interaction term:		
	beta (95%CI), p-value		
	Non SEL log-volume	Possible SEL log-volume	Definite SEL log-volume
EDSS change			
baseline – wk24	-0.04 (-0.21,0.13), p=0.647	0.11 (-0.09,0.31), p=0.274	0.30 (0.13,0.47), p=0.001
baseline – wk96	0.02 (-0.14,0.19), p=0.775	0.01 (-0.19,0.21), p=0.938	-0.07 (-0.24,0.10), p=0.431
MSFC z-score change			
baseline – wk24	0.01 (-0.31,0.33), p=0.961	-0.12 (-0.50,0.25), p=0.519	-0.14 (-0.46,0.19), p=0.405
baseline – wk96	-0.15 (-0.47,0.18), p=0.375	-0.25 (-0.63,0.12), p=0.185	-0.80 (-1.13,-0.48), p<0.001
NHPT z-score change			
baseline – wk24	-0.06 (-0.20,0.08), p=0.433	0.02 (-0.14,0.19), p=0.776	-0.01 (-0.14,0.14), p=0.995
baseline – wk96	-0.13 (-0.28,0.01), p=0.065	-0.11 (-0.27,0.05), p=0.184	-0.13 (-0.28,0.01), p=0.075
T25FW z-score			
baseline – wk24	0.16 (-0.72,1.05), p=0.716	-0.51 (-1.54,0.51), p=0.327	-0.59 (-1.48,0.31), p=0.199
baseline – wk96	-0.30 (-1.19,0.59), p=0.504	-0.59 (-1.62,0.44), p=0.265	-2.02 (-2.91,-1.13), p<0.001
PASAT z-score			
baseline – wk24	-0.10 (-0.29,0.08), p=0.269	0.12 (-0.09,0.33), p=0.269	0.06 (-0.13,0.24), p=0.548
baseline – wk96	-0.01 (-0.19,0.18), p=0.964	-0.07 (-0.29,0.14), p=0.502	-0.31 (-0.49,-0.12), p=0.001
SDMT change			
baseline – wk24	-0.88 (-2.78,1.01), p=0.364	-1.00 (-3.27,1.28), p=0.390	-1.19 (-3.13,0.74), p=0.226
baseline – wk96	-2.47 (-4.37,-0.57), p=0.011	-2.51 (-4.83,-0.20), p=0.033	-2.63 (-4.59,-0.67), p=0.009

Abbreviations: SEL=slowly expanding lesion, EDSS=expanded disability status scale, MSFC=multiple sclerosis functional composite, NHPT=nine-hole peg test, T25FW=timed 25-foot walk test, PASAT=paced auditory serial addition test, SDMT=symbol digit modalities test

With this work a validation that higher SEL-derived log-volumes associated with greater worsening in the clinical outcome over time was again found for all the explored measures, except for the NHPT, in the interval from baseline to last time point (week 96). For the EDSS case, the association between SEL-derived volumes and clinical changes over time could only be confirmed for the first-time interval (between baseline and week 24). Regarding SDMT, there was a decrease in the performance from baseline to final time point associated with an increase in all the SEL-derived volumes. The SEL-derived volumes and the other MRI and clinical measures were highly reproducible and not influenced by the study centre, as all the models took into account the multicentre structure, which was confirmed by intraclass correlation coefficients (ICC) computation. In fact, all ICC retrieved from the mixed-effects regression models between the evaluated outcome variables, with the variable of the centre nested in the model, were between 0.005 and <0.001 .

Finally, to retrieve the values of the SEL-derived volumes for the missing subjects, a multivariate imputation by chained equations (predictive mean matching) was used. As a result, all patients enrolled in the trial ($n=445$) were included and the multiple linear regressions were repeated with the SEL-associated volumes as predictors (definite SEL, possible SEL and non-SEL log-volumes) and the clinical measure (at baseline and week 96) as response variable (**Table 3-9**). All models were adjusted for age, gender, T2 lesion volume change and percentage brain volume change. The results of this analysis confirmed the associations previously found between the definite SEL volumes and all the clinical scores, except for NHPT.

Table 3-9. Multiple linear regression using a multiple imputation model

	Non SEL volume beta (95% CI) p value	Possible SEL volume beta (95% CI) p value	Definite SEL volume beta (95% CI) p value
EDSS	-0.03 (-0.22, 0.16) p=0.76	0.10 (-0.12, 0.32) p=0.35	0.23 (0.03, 0.42) p=0.03
MSFC z-score	-0.14 (-0.61, 0.33) p=0.57	-0.26 (-0.81, 0.29) p=0.36	-0.64 (-1.13, -0.15) p=0.001
NHPT z-score	-0.15 (-0.34, 0.05) p=0.15	-0.15 (-0.38, 0.09) p=0.22	-0.11 (-0.32, 0.10) p=0.31
T25FW z-score	-0.15 (-1.56, 1.25) p=0.83	-0.97 (-2.61, 0.65) p=0.24	-1.71 (-3.17, -0.25) p=0.02
PASAT z-score	-0.20 (-0.39, -0.02) p=0.03	-0.17 (-0.38, 0.05) p=0.12	-0.37 (-0.56, -0.18) p=0.001
SDMT	-4.31 (-6.86, -1.78) p=0.001	-2.41 (-5.33, 0.52) p=0.11	-2.95 (-5.60, -0.29) p=0.03

Abbreviations: SEL=slowly expanding lesion, EDSS=expanded disability status scale, MSFC=multiple sclerosis functional composite, NHPT=nine-hole peg test, T25FW=timed 25-foot walk test, PASAT=paced auditory serial addition test, SDMT=symbol digit modalities test

3.3.3 Discussion

In this study, for the first time, SELs were analysed in a large trial cohort of SPMS. Definite SELs were associated with more severe lesional damage, as measured by MTR (a marker of myelin and neuroaxonal loss) and they showed a predictive value on physical and cognitive disability progression.

This work demonstrated that SELs are common in SPMS, as the proportion of patients with at least one SEL was remarkably high (99%), and greater than that observed in PPMS or RRMS (72% and 68%). (Elliott, Wolinsky, *et al.*, 2019) In addition, the mean number of definite SELs (19.5) was also higher than in PPMS and RRMS (6.3 and 4.6, respectively). (Elliott, Wolinsky, *et al.*, 2019) In line with other clinical trials in SPMS (Tur *et al.*, 2018), there was a substantial T2 lesion volume, as a marker of inflammatory burden. Out of the total lesion burden, the fraction of definite SELs was remarkable (36%), indicating that they account for a substantial proportion of lesions. A novelty of this work not previously assessed was the evaluation of the annualised volume change of definite SELs, as represented by the Jacobian expansion, which was on average 3% per year. The comparison of observations on SELs in SPMS with those in other MS phenotypes suggests that chronic inflammatory activity accumulates over

the course of the disease, although differences in techniques may influence the absolute numbers derived from different studies.

In relation to the lesion level, previous analysis has shown that SELs have a preferential distribution in the periventricular areas (Elliott, Wolinsky, *et al.*, 2019). However, there have not been previous studies investigating the morphological or dimensional features of SELs. With this work, the spatial localisation of SEL was also in periventricular areas, but no difference was noted in lesion distribution between non-SEL, possible and definite SELs. In addition to previous work, here the definite SELs were significantly bigger than non-SELs, suggesting that there is a greater tendency for ongoing lesion expansion in larger lesions, but this may also reflect prior lesion enlargement. In this population, which was enrolled as a part of the MS-SMART study cohort (n=345), a positive correlation between definite SELs volume and change in the overall T2 lesion volume was found ($r=0.24$, $p<0.001$). This finding suggests that SELs might represent markers for chronic inflammatory activity and they can be a significant contributor to the global lesion burden, in line with pathological studies, where chronic active lesions are associated with a higher lesion load. (Luchetti *et al.*, 2018)

Moreover, in this work, a moderate correlation between higher SEL volume and new PBH was found ($r=0.18$, $p<0.001$), as also suggested by previous studies that demonstrated an association with a lower and more rapidly decreasing T1 hypointensity within SELs (Elliott, Belachew, Jerry S Wolinsky, *et al.*, 2019; Elliott, Wolinsky, *et al.*, 2019), reflecting chronic axonal loss in MS. (Van Waesberghe *et al.*, 1999; Van Walderveen *et al.*, 2001) In a recent work in RRMS (involving 52 patients) a correlation between SELs, normalised brain volume and PBVC was reported (Preziosa *et al.*, 2020), as markers of neurodegeneration linked with worse disability accrual. As a novel research finding, higher definite SEL volume was associated with greater brain atrophy ($r=-0.26$, $p<0.001$) for the SPSM phenotype. These results support the hypothesis that SELs contribute significantly to the neurodegenerative process in SPMS.

To further investigate the damage involving the different lesion types, a quantitative advanced MRI measure, MTR, was also analysed in a subsample of 106 patients. As

expected, MTR, whose reductions are associated with reduced myelin and axonal density, was lower within SELs than in non-SELs at baseline. In addition, over time a greater decline in MTR was found in the definite SELs, compared to non-SELs. In line with this finding, a previous analysis in RRMS found a lower baseline MTR in SELs and an increase in MTR in non-SELs after 24 months follow-up (Preziosa *et al.*, 2020). In this analysis, a strong association between SELs and disability in SPMS was demonstrated. Similarly, previous research by Elliott et al. found that SELs were able to explain 12-week confirmed disability progression as measured by EDSS, and a 20% greater increase in T25FW and NHPT in a PPMS trial cohort (n = 732). (Elliott, Belachew, Jerry S Wolinsky, *et al.*, 2019) In this study, this evidence was also extended to SPMS, as SEL-derived volumes could significantly explain a proportion of clinical worsening and the development of disability progression based on EDSS change from baseline to the end of the trial (week 96) in multiple linear regressions, and in the first interval of the trial (baseline to week 24) using mixed-effects models.

As a further relevant clinical finding, SEL-derived volumes were also associated with worsening MSFC z-score and increased odds for disability progression. Interestingly, in the multiple linear regression, SEL volumes explained clinical progression in both the MSFC subcomponents assessing walking and cognitive functions (i.e. T25FW and PASAT). However, only in the mixed-effects models was a significant association with hand function (NHPT) found. Finally, SDMT worsening, as alternative test assessing the cognitive function, was associated with increases in all the SEL-derived volumes in the mixed-effects models only. Overall, the results of the regression models indicated that SEL accumulation is associated with disability in secondary-progressive MS, and that this is independent of other conventional MRI markers associated to inflammation and neurodegeneration, such as the total lesion burden and brain atrophy.

Nevertheless, there are some study limitations related to methodological aspects of this study. Firstly, SEL analysis can be influenced by resolution and field strength, the number of time points used, registration and deformation algorithms used. Then, the definitions (e.g. size, rate of growth) of lesion subtypes can be arbitrarily set. Regarding the SEL definition, a volume threshold of 10 mm³ was set, recognising that the computation of non-linear deformations in smaller spatial areas reduces reliability. However, in contrast to the previous study from Elliott et al., the algorithm used in this

work did not use a threshold for lesions based on rates of expansion. Moreover, after a review of the confluent lesions, they were analysed without separating them from the ones that would have subsequently merged, as the pipeline was based on the baseline lesion masks. On the other hand, an added value of the SEL pipeline used in this study is that it is highly reproducible across centres, using common pipelines and conventional MRI sequences (PD/T2-weighted and T1-weighted). The robustness of this technique compared to other SEL algorithm presented previously (Elliott, Wolinsky, *et al.*, 2019) is related to the exclusion of heuristically-set scores of expansion, which could have impacted on the final number of each of the lesion subtypes, without a real representation of the actual counts at the patient level. Furthermore, the use of a unique sequence to retrieve the deformation map and a single cut-off of the expansion rate (Jacobian greater than zero) reflects a simple positive value. Thus, a high sensitivity is expected in picking up the expansion of any extent. In the clinical practice this aspect is important, because it would allow to detect even the smallest volumetric expansion within a lesion and confidently represent the actual picture of the state of the lesion. This could be finally beneficial to assess the treatment response for an individual subject followed in the clinical context.

With regards to other limitations related to the MRI acquisitions, post-contrast T1-weighted scans were not available in this study, so it was not possible to assess the relationship between SELs and contrast-enhanced lesions. However, this was not an objective of this work, considering that in SPMS the frequency of gadolinium enhancing lesions is low (10% as reported in SPMS trials) (Kappos *et al.*, 2018) and a previous study showed that contrast-enhancement is not a common feature of SELs (Elliott, Wolinsky, *et al.*, 2019). For the statistical analysis part, the magnitude associations and effect sizes were to some extent small or borderline significant. However, given the nature of this exploratory study, analysing the impact of a novel MRI marker, any sign of association to the disability measures, even if weak, were considered valuable. Out of 445 enrolled in the trial, 100 patients had to be excluded due to incompatibility with the inclusion criteria (i.e. missed MRI scans), which did not allow computing SELs in this subset. However, the robustness of the results of the multiple linear regression including the clinical outcome variables was accounted for by using a multiple imputation model for the missing data.

In previous studies, SELs have been observed over periods of 2-3 years as they were assessed in trials, and in this study as well on a period of 96 weeks. However, there have been no investigations yet reporting that SELs remain active perpetually, and it could be speculated that they might eventually become so over a longer period of time. In contrast to the evidence of the presence of lesions with expansion such as SELs, it has been previously shown that over decades some lesions may also shrink or even disappear. (Sethi *et al.*, 2016; Pongratz *et al.*, 2019) In addition to the T1 and MTR reductions observed in previous studies and confirmed in this work, other microstructural and cellular properties of SELs could be investigated, using advanced quantitative MRI or targeted PET techniques, providing greater insights into the pathobiology of SELs.

As an alternative imaging marker for chronic active MS lesions the presence of a rim surrounding MS lesions on susceptibility-weighted MRI is also used, (Bagnato *et al.*, 2011; Yao *et al.*, 2012; Wisnieff *et al.*, 2015) and retrospective volumetric analyses have provided evidence that paramagnetic rim lesions have a tendency to expand (Absinta *et al.*, 2016; Dal-Bianco *et al.*, 2017). Similar to the evidence on SELs, a greater number of rim lesions appears to be associated with clinical severity, (Absinta *et al.*, 2019) and their persistence is associated with a worse prognosis (Absinta *et al.*, 2016), although the temporal dynamics of rim appearance and persistence are not entirely clear. Furthermore, using quantitative susceptibility mapping (QSM), as with SELs, hyperintense rims appear to be more common in progressive MS, and in patients with higher levels of disability (Harrison *et al.*, 2016).

4 Slowly Expanding Lesions and Persisting Black Holes

4.1 Background and objectives

In MS the characteristic multifocal inflammatory demyelinating lesions show variable degrees of neurodegenerative changes. The dichotomization of lesions into acute and chronic, and their classification into at least four subtypes (active, remyelinated, chronic active, inactive) reflect the presence of pathological changes over time.

The usual formation of lesions follows distinct steps. Initially, newly forming active lesions typically surround veins, with inflammation and demyelination seen concurrently over days to weeks. (Alan J Thompson *et al.*, 2018) This is followed by variable degrees of remyelination usually seen after weeks and months following their formation (so-called remyelinated lesions). (Barkhof, Bruck and De Groot, 2003) A fraction of them can evolve into a chronic active (or mixed active-inactive) stage, characterised by a hypocellular centre and activated iron-enriched macrophages-microglia at the lesion border. (Kuhlmann *et al.*, 2017) This process leads to a radial expansion of the lesions, in combination with further myelin damage, axonal loss, and gliosis, in the core of the lesions. (Prineas *et al.*, 2001; Frischer *et al.*, 2009) Finally, chronic lesions can evolve into an inactive stage, where cellularity is reduced, and tissue damage and gliosis are dominant.

The MS clinical spectrum is heterogeneous and this variety is in part explained by the different distribution of lesion subtypes, which accumulate over the course of the disease. (Kuhlmann *et al.*, 2017) There is a peak of the active lesion types in RRMS, while the chronic active lesions increase with longer disease duration when there is a higher probability of developing SPMS. (Lassmann, 2019) Therefore, it is important to understand the evolution of the phenotypes of MS lesions and their characteristics.

On MRI, T2-weighted and FLAIR sequences sensitively detect all MS lesion subtypes, but they are not specific for any of the histopathological subtypes. Chronic axonal loss and demyelination have been associated with hypointensity on T1-weighted sequences (van Walderveen *et al.*, 1998; Van Waesberghe *et al.*, 1999) and low magnetization

transfer ratio (MTR) (Schmierer *et al.*, 2004; Kapoor *et al.*, 2010) values. Black holes (BHs) can be defined as lesions with T1 intensity darker than the grey matter (GM) and surrounding tissues. (Molyneux *et al.*, 2000) Persisting black holes (PBHs), represent a significant proportion of the overall lesions (20-40%), (Bagnato *et al.*, 2003; van den Elskamp *et al.*, 2008) and are associated with future disability progression and brain atrophy accrual, (Truyen *et al.*, 1996; Sailer *et al.*, 2001; Van Walderveen *et al.*, 2001) therefore possibly representing lesions at the end-stage of their evolution. Magnetic resonance spectroscopy (Mader *et al.*, 2000), diffusion-weighted imaging (DWI) (Enzinger *et al.*, 2015) and myelin imaging at MRI, (Faizy *et al.*, 2016; Jung *et al.*, 2018) together with positron emission tomography (PET), (Högel *et al.*, 2018) all provide quantitative and microstructural information on the degree of damage within and around lesions, however, none of these methods has been consistently used as *in vivo* correlates of chronic active lesions. (Calvi *et al.*, 2020)

The compartmentalized inflammation is supposed to be one of the mechanisms that is a main contributor for MS neurodegeneration, thus novel imaging markers have been investigated to identify chronic active lesions affected by chronic inflammatory events. The slowly expanding lesions (SELs), detected using volumetric MRI are imaging markers of chronic lesion activity in MS. SELs, identified automatically using routinely acquired volumetric MRI, offer practical advantages as a biomarker for the chronic active lesions. (Elliott, Wolinsky, *et al.*, 2019; Dal-Bianco *et al.*, 2021) Compared with manually outlined lesion masks, prone to inter and intra-rater variability, (Vrenken *et al.*, 2013) the automated longitudinal computation of a deformation field in SELs allows the acquisition of a quantitative measure of MS lesion expansion, hence it could provide a marker for chronic inflammatory activity to measure the predisposition to develop disability.

SELs are seen in all MS phenotypes, but more commonly in the progressive ones and less frequently in RRMS (median 7 vs. 4 per patient, respectively), and they evolve independently of gadolinium enhancement. (Elliott *et al.*, 2017; C Elliott *et al.*, 2020) Compared with other lesions, SELs show a progressive decline in T1 intensity suggestive of ongoing neuro-axonal damage. (Elliott *et al.*, 2017; Elliott, Belachew, Jerry S Wolinsky, *et al.*, 2019) In a study assessing patients with RRMS and SPMS,

SEs had a lower MTR and greater radial diffusivity in DWI from baseline up to 72 weeks, (C. Elliott *et al.*, 2020) consistent with MS-specific chronic demyelination.

The aims of this study were: 1) To compute SEs in a relapse-onset observational cohort over a long-term follow-up; 2) To identify whether there is a relationship between PBHs and SEs; 3) To assess changes in T1 intensity contrast ratio and MTR values within SEs vs. non-SEs; 4) To evaluate whether the increase in number and volume of SEs are associated with worsening disability over time or higher risk of MS progression.

4.2 Material and methods

4.2.1 Participants and MRI acquisitions

A retrospective observational cohort of early relapse-onset patients involved two centres from a collaborative MAGNIMS initiative between the Queen Square MS Centre (QSMSC) University College London (UK), the University of Siena (Italy) and the University of Milan (Italy). All patients gave written consent for their data to be used in post-hoc studies, which were approved by the local Ethics Committee.

To be included the criteria were: confirmed diagnosis of RRMS according to the revised 2017 McDonald criteria (Alan J. Thompson *et al.*, 2018) and availability of at least three consecutive MRI longitudinal images, including FLAIR or T2-weighted scans at baseline, and 3D acquired T1 at all time points, with adequate image quality. For a subset of patients MTR sequences were also available.

The scans from the University of Siena were collected on a Gyroscan operating at 1.5 T (Philips Healthcare, Best, the Netherlands), while those from the University of Milan were acquired on an Achieva 3T scanner (Philips, Eindhoven, The Netherlands). The acquisition parameters are shown in **Table 4-1**. Each patient was scanned consistently with the same machine throughout the trial. An initial number of 139 patients with MS were identified, but data from 4 patients had to be discarded due to image artefacts (final sample n=135). A subset of 83 patients (provided from the University of Siena) also had MTR at baseline and final follow-up, although a machine upgrade meant this

could only be analysed cross-sectionally at both timepoints rather than longitudinally between them.

Table 4-1. MRI acquisition parameters

Sequences	Repetition time (ms)	Echo time (ms)	Flip angle (α)	Field of view (mm^2)	Voxel size (mm^3)	No. of slices
T2 weighted 2D*	2492	78	90°	256x256	0.97x0.97x3	50
FLAIR[§]	11000	125	90°	250x250	0.56x0.56x0.56	300
T1 weighted – 2D*	35	10	-	256x256	0.97x0.97x3	50
T1 weighted – 3D[§]	9.9	4.6	8°	240x240	1.0x1.0x1.0	163
MTR*	MT pulse 1.2 ms	Radio-frequency field strength 20 microT	-	256x256	0.97x0.97x3	50

*Acquisitions from University of Siena site (1.5 T) [§] Acquisitions from University of Milan site (3 T). Abbreviations: FLAIR= fluid attenuated inversion recovery; MTR= magnetization transfer ratio

4.2.2 Clinical assessments

Patients were clinically assessed at each scanning session using the Expanded Disability Status Scale (EDSS) (Kurtzke, 1983), obtained by an MS specialist. The EDSS change was calculated as the difference between EDSS at last scanning session and EDSS at baseline. Confirmed disability progression (CDP) was defined by an EDSS score change ≥ 1.0 or ≥ 0.5 , when baseline EDSS score was < 5.5 or ≥ 5.5 (cut-offs as previously used in phase III trials (Lublin *et al.*, 2016)), respectively, which was confirmed in the following 6 months after the last follow-up visit.

4.2.3 T2 lesion, tissue segmentation and SEL detection

A semi-automated edge finding tool (JIM v7.0, Xinapse Systems, Aldwinckle, UK) was used to manually delineate T2 hyperintense lesions on the dual-echo T2 or FLAIR baseline images. The original T2 images acquired in 2D with a voxel resolution of $(1 \times 1 \times 3) \text{ mm}^3$ were resampled into a 1-mm isotropic space, and lesions were co-registered to the 3D-T1 images using a pseudo-T1 image generated by subtracting the 2 echoes of the T2-weighted sequence. (Hickman *et al.*, 2002)

As described in the previous chapter for brain extraction, tissue segmentation and parcellation, Geodesic Information Flows (GIF) method was used on the lesion-filled T1 scans (3D acquired) (Cardoso *et al.*, 2015). This provided the following metrics: normalised brain volume (NBV), normalised normal-appearing white matter (NAWM, i.e. the white matter volume after subtracting the T2 lesion volume), and normalised cortical grey matter (CGM) and normalised deep grey matter (DGM) volumes. Percent Brain Volume Change (PBVC) from baseline to intermediate follow-up and from baseline to the last follow-up, as a measure of brain atrophy, was calculated using the SIENA method. (Smith *et al.*, 2002) To identify SELs a non-linear registration of volumetric T1 images was used as described in the previous Chapter 3, thus obtaining possible SEL, definite SELs and non-SELs.

4.2.4 T1 ratios and MTR within lesion types

After registering the T1-weighted with the T2-weighted/FLAIR images, in the lesion masks space, the T1 intensity ratio values were calculated according to the image intensity. In detail, they corresponded to the mean T1 value within the respective lesion mask area, after dividing each value by the mean T1 value within the grey matter ($T1_{ratioGM} = T1_{LESION}/T1_{GM}$). The lesion-specific T1 was computed independently at each time point. For a subset of patients, the MTR was computed at the baseline and last follow-up in percent unit (pu). In consideration of a long time to the last follow-up for most of the MTR subcohort, which included an upgrade of the scanner, the longitudinal MTR was discarded from the analysis to avoid any bias. T1 and MTR were analysed after applying the SEL detection algorithm within the SEL metrics at the single lesion level (average values of all the voxels in the specific mask).

4.2.5 PBH detection

To retrieve the black holes at each time point an automated pipeline was created for the analysis on a voxel-by-voxel level of the local $T1_{ratioGM}$ value within each lesion mask. This method was based on a previous definition of BH as a region with signal intensity similar to or reduced relative to the signal intensity of the grey matter (GM) and corresponding to a lesion mask drawn on T2-weighted image. (Van Walderveen *et al.*, 2001) After testing several thresholds, an evaluation of the cut-off was reached

by the expert consensus of the PhD supervisors. The formula used identified the upper threshold of T1 intensity below which a lesion is classified as a BH:

$$T1 \text{ intensity threshold} = \text{mean } T1 \text{ ratio}_{GM} - (SD \ T1 \ \text{ratio}_{GM})$$

The T1 intensity threshold was defined for each subject, so that each lesion was evaluated with a normalization at the patient-level. A persisting black hole (PBH) was defined when the lesion fulfilled the criteria of having the mean T1 intensity under the patient-specific threshold at each time point from baseline to the last follow-up. In order to avoid the inclusion of small artefactual hypointensities, the T1 hypointense volume had to cover an area greater than 10% of the total lesion volume. I conducted the manual check of the obtained PBHs and the doubtful cases were reviewed with my Supervisor, as a neuroradiologist (FB), to ensure accuracy.

4.2.6 Statistical analysis

STATA version 16 was used for the statistical analysis and significance reported at $p < 0.05$, while frequency distributions and plots were drawn using R (a language and environment for statistical computing R Core Team [2020]). The Wilcoxon signed rank test assessed the differences in EDSS over time between baseline and last follow-up. At the lesion level, a descriptive analysis was performed for each lesion type, including the SEL-derived metrics and the hypointense lesions (total BH and PBH) and the frequency distributions were visually assessed. Then, lesion counts, and volumes were analysed at the patient level calculating the sum of the number and volume of the respective lesion types. Each specific lesion volume type was log-transformed (base 10) in order to meet the normality assumption. The associations were computed with Pearson (for normally distributed variables, i.e. log-transformed lesion volumes) or Spearman (for non-normally distributed variables, i.e. lesion counts) correlation coefficients. A Gaussian mixture model (GMM) was built in order to identify the underlying components, and to categorise subpopulations of patients according to their total SEL count number, using the possible SEL type, as this was the more numerous subgroup (*Figure 4-1*).

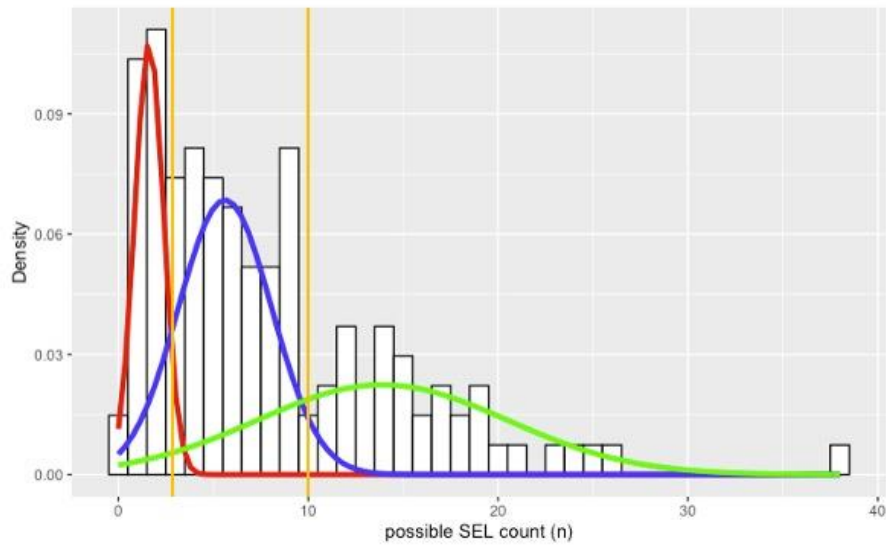


Figure 4-1. Patient clusters according to SEL counts. The yellow vertical bars indicate the cut-offs defined by the Gaussian mixture model on the distribution of the possible SEL counts. The first cut-off is set at $n=2$ SELs, the second cut-off at $n=10$ SELs.

The GMM was used to define the optimal number of clusters of patients divided according to the SEL counts. The analysis retrieved three underlying Gaussian curves on the density distribution of possible SELs counts. The optimal cluster number was 3 with the highest performance and the best accuracy, as estimated by analysing the within-cluster sum of squares at an increasing number of clusters (variance for the GMM did not change for higher values), corresponding to the maximisation of the negative BIC. A lower BIC is associated with higher performance of the model. The cut-offs for the SEL count clusters were defined by the evaluation of the posterior probability of the GMM for each one of the three components. The definition of cut-offs of the clusters was obtained by analysing the frequency distribution of SEL count on a unit-by-unit increase together with the highest probability of each one of the predicted components.

T1 and MTR were analysed using a mixed-effects regression model, assessing their values one at a time on a lesion-by-lesion basis as the outcome variable; the random effect components included the patient-specific identification number, the study centre and a unique lesion identifier in order to take into account the within-subject variability. Mixed-effects regression models were based on the clinical outcome

(EDSS) adjusted for MRI conventional measures (baseline total T2 lesion volume and PBVC) and they assessed the relationship with SELs, using the interaction term between each SEL-derived metric (i.e. definite SEL, possible SEL and non-SEL), and the random effects including the patient-level and the time at follow-up. A subset of patients, defined ‘early-onset MS subcohort’, were grouped using a filter to identify those with short disease duration at baseline (≤ 5 years), using a similar mixed-effects regression model. Multiple logistic regressions, adjusted for demographic covariates (age at baseline, gender, time to last follow-up) were applied to investigate the risk of CDP explained by within-patient counts or log-volumes of SELs. The odds ratio (OR) and p values are reported. The performance of the models using conventional MRI or SEL-derived metrics was assessed using the Bayesian information criterion (BIC) which is an estimate of the performance of the statistical model.

4.3 Results

4.3.1 Cohort demographics and clinical features

Patients’ demographical data and clinical measures are reported in **Table 4-2**. The mean disease duration since the initial diagnosis was 5.5 years and the mean age at study onset was 35.5 years. There was variability of time intervals from the baseline to the subsequent follow-up MRI scans due to the multi-centric nature of this study. At baseline, 49% of patients (n=66) were on any DMTs, while at last follow-up 75% used DMTs (n=102). Global brain and regional brain volumes at baseline, and brain atrophy (PBVC), were consistent with a relapsing-onset MS population. EDSS had significantly increased at final follow-up compared to baseline (Wilcoxon signed-rank test, $p=0.035$). Overall, 37 patients (27%) demonstrated CDP and 6 patients (0.4%) had developed SPMS by the end of the study. 85 patients out of 135 (63%) had a short disease duration at study onset (≤ 5 years). The clinical characteristics of the early onset MS subcohort were the following: 61 were female (71%), mean disease duration at baseline was 1.43 years (range = [0 – 4.7]) and mean EDSS change 0.11 (SD=1.40).

Table 4-2. Clinical-demographic and radiological characteristics of the patients enrolled in the study.

Number of patients	135
Female, n (%)	99 (73 %)
Age at baseline, mean (SD) [years]	35.5 (9.0)
Disease duration at baseline, mean (range) [years]	5.5 (0 – 32.5)
Time to MRI scan follow-up, mean (range) [years]	
- at intermediate follow-up	2.9 (0.4 – 10.5)
- at last follow-up	6.5 (1.0 – 12.5)
EDSS, median (range)	
- at baseline	1.5 (0 – 5.5)
- at last follow-up	2.0 (0 – 8.0)
EDSS change, mean (SD)	0.30 (1.34)
MS phenotype	
- at baseline	RRMS = 135
- at last follow-up	RRMS = 129; SPMS = 6
Number (%) of patients treated	
- at baseline	66 (49%)
- at last follow-up	102 (75%)
Number (%) of patients with CDP	37 (27%)
NAWM volume at baseline [ml], mean (SD)	656.1 (31.2)
CGM volume at baseline [ml], mean (SD)	819.6 (42.1)
DGM volume at baseline [ml], mean (SD)	48.8 (3.6)
NBV at baseline [ml], mean (SD)	1524.5 (59.5)
BPF at baseline, mean (SD)	0.72 (0.03)
PBVC baseline to last follow-up, mean (SD)	-0.18% (0.49)

Abbreviations: EDSS=expanded disability status scale, NAWM=normal-appearing white matter, CGM=cortical grey matter, DGM=deep grey matter, NBV=normalised brain volume, BPF=brain parenchymal fraction, PBVC=percent grain volume change

4.3.2 Descriptive analysis of MRI metrics

The MRI metrics of all the cohort at baseline are summarised in **Table 4-3**. Out of a total of 4007 lesions on T2-weighted or FLAIR images manually segmented, definite SELs were 408 (ratio to total lesions=0.10), possible SELs were 1061 (ratio to total lesions=0.26), and the non-SELs were 2538 (ratio to total lesions=0.64). The median baseline total lesion count per patient was 23, of which 2 and 6 were classified as definite SELs and possible SELs (9% and 26% out of the total lesion count, respectively) and their volume corresponded to 13% and to 24%, respectively, out of the total lesion volume. The median baseline total BH count per patient was 6, of which 4 were PBHs. Patients with at least one definite SEL and one possible SEL represented

86% (n=116) and 99% (n=133), respectively. At least one PBH was identified in 89% of patients (n=121).

Table 4-3. Lesion counts and volumes, by SEL types, total BH and PBH at the patient level

Lesion-specific MRI metrics			
Counts	T2 lesion count at baseline [n], median (IQR)		23 (13 – 41)
	SEL-derived	non-SEL count [n], median (IQR)	13 (6 – 26)
		possible SEL count [n], median (IQR)	6 (3 – 12)
		definite SEL count [n], median (IQR)	2 (1 – 4)
	Total BH count at baseline [n], median (IQR)		6 (3 – 10)
	PBH count [n], median (IQR)		4 (2 – 6)
	New T2 lesions between baseline and intermediate follow-up [n], median (IQR)		4 (1 – 8)
	New T2 lesions between intermediate and last follow-up [n], median (IQR)		3 (1 – 7)
Volumes	T2 lesion volume at baseline [ml], median (IQR)		3.77 (1.56 – 9.74)
	SEL-derived	non-SEL volume [ml], median (IQR)	1.49 (0.45 – 3.81)
		possible SEL volume [ml], median (IQR)	0.89 (0.32 – 2.10)
		definite SEL volume [ml], median (IQR)	0.51 (0.15 – 2.00)
	Total BH volume at baseline [ml], median (IQR)		0.19 (0.09 – 0.50)
	PBH volume at last follow-up [ml], median (IQR)		0.22 (0.08 – 0.69)
	New T2 lesion volume between baseline and intermediate follow-up [ml], median (IQR)		0.23 (0.06 – 0.71)
	New T2 lesion volume between intermediate and last follow-up [ml], median (IQR)		0.22 (0.04 – 0.53)

Abbreviations: SEL=slowly expanding lesion, PBH=persisting black hole

An example of a patient showing a PBH, that corresponds also to a SEL is shown in **Figure 4-2**. The patient shown in the figure was enrolled in the study at 53 years old (baseline) with a diagnosis of RRMS and EDSS 4.5, which progressed to 6.0 (last follow-up).

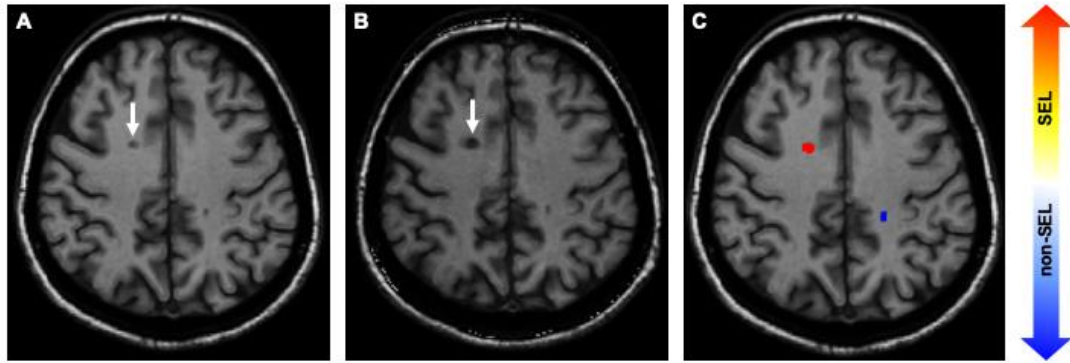


Figure 4-2. Example of patient with SEL and PBH.

Image A is the baseline T1-weighted scan, image B is the last follow-up scan. The white arrow indicates a lesion that was T1 hypointense at baseline and over a follow-up of 9.3 years thus represent a PBH, and in C the Jacobian map indicates that the same lesion corresponds to a SEL.

4.3.3 High, intermediate and low SEL count clusters

Based on the best performance of the GMM model, three clusters were identified (**Figure 4-1**), using counts of possible SELs as the reference due to their higher numerosity. The ‘low SEL counts’ cluster included patients with up to 2 SELs (n=31 out of 135, 23%); the ‘intermediate SEL count’ had counts ranging from 3 to 10 SELs (n= 65, 48%); the ‘high SEL count’ had >10 SELs (n=39, 29%). A test of the differences in the demographical, clinical and radiological characteristics within the three clusters was performed, and those characteristics by groups are presented in **Table 4-4**.

All the MRI measures were analysed at baseline (except for PBVC). As a result, the demographical characteristics were not different in the three groups. Conversely, a higher EDSS at the last follow-up was identified in the high SEL count compared to the other groups analysed (p=0.026). Moreover, the T2 lesion volume and T2 lesion counts at baseline were higher in the high SEL count cluster (p<0.001). In accordance with those results, the global and cortical brain volumes (NBV, CGM and DGM) had the lowest figures within the high SEL count. Finally, no differences in brain atrophy (PBVC) were identified between the groups analysed.

Table 4-4. Clinical demographics and radiological characteristics by high, intermediate and low SEL count clusters

	Low SEL count (n=31)	Intermediate SEL count (n=65)	High SEL count (n=39)	p value*
Female n (%)	24 (77%)	46 (71%)	29 (74%)	p=0.778
Age at baseline, mean (SD) [years]	35.3 (8.4)	36.3 (8.4)	34.3 (10.3)	p=0.573
Disease duration at baseline, mean (SD) [years]	4 (5.6)	5.5 (7.0)	6.8 (7.0)	p=0.236
EDSS, median (range)				
- at baseline	1.5 (0 – 5)	1.5 (0 – 5.5)	1.5 (1 – 5)	p=0.237
- at last follow-up	1.25 (0 – 5.5)	2 (0 – 8)	2 (0 – 7)	p=0.026
EDSS change, mean (SD)[§]	-0.03 (0.86)	0.27 (1.41)	0.64 (1.48)	p=0.313
Number (%) of patients with confirmed disability progression[°]	3 (10%)	6 (9%)	2 (5%)	p=0.324
T2 lesion volume [ml], mean (SD)	1.9 (2.4)	8.9 (11.7)	10.6 (9.2)	p<0.001
T2 lesion count [n], median (range)	7 (1 – 41)	21 (4 – 75)	45 (20 – 113)	p<0.001
NAWM volume [ml], mean (SD)	669.3 (24.6)	651.7 (31.6)	651.2 (32.1)	p=0.024
CGM volume [ml], mean (SD)	836.2 (35.1)	818.5 (43.2)	808.3 (43.4)	p=0.027
DGM volume [ml], mean (SD)	51.2 (2.6)	48.5 (3.5)	47.3 (3.2)	p<0.001
NBV [ml], mean (SD)	1556.7(46.8)	1518.7 (58.6)	1506.8 (61.1)	p=0.002
PBVC baseline to last follow-up, mean (SD)	-0.17% (0.43)	-0.20% (0.41)	-0.16% (0.64)	p=0.928

Abbreviations: EDSS=expanded disability status scale, NAWM=normal-appearing white matter, CGM=cortical grey matter, DGM=deep grey matter, NBV=normalised brain volume, PBVC=percent grain volume change

4.3.4 Associations between T1-black holes, PBHs and SELs

The associations between radiological metrics were firstly analysed at the lesion level. Among the T2 lesions retrieved from all the cohort (n=4007), 10% were classified as PBHs (n=449) and they represented the majority (52%) of the BHs (n=851). The analysis of the counts of the total BHs and PBHs according to their SEL-derived volumetric category (definite SEL, possible SEL, non-SEL), and the relative percentage of PBHs to the total BHs is presented in **Table 4-5**. When grouped into the three SEL-derived categories, PBHs were more common among possible and definite SELs, as compared to non-SELs (61% and 52% versus 44%, respectively, Pearson's Chi-squared test, $p < 0.001$). In the correlation analysis, the highest positive correlations were identified between the baseline total BH counts and possible SEL counts (Spearman $\rho = 0.48$, $p < 0.001$), and between PBH counts with possible SEL counts (Spearman $\rho = 0.47$, $p < 0.001$). Similarly, the sum of PBH volume at last follow-up positively correlated with possible SEL log-volumes (Pearson $r = 0.53$, $p < 0.001$). On the other hand, a low correlation was found between baseline total BH volumes and possible SEL log-volumes (Pearson $r = 0.18$, $p = 0.04$).

Table 4-5. Distribution of black holes counts divided by the SEL-derived categories

Lesion category		Total BH, count (n=851)	PBH count (n=449)	% PBH over the total BH corresponding category
SEL-derived	Non-SEL	336	147	44%
	Possible SELs	375	229	61%
	Definite SELs	140	73	52%

Abbreviations: BH=black hole, PBH=persisting black hole, SEL=slowly expanding lesion

4.3.5 Associations between SELs and brain volumes

The correlation analysis was extended to the global brain and cortical volumes at baseline. As a result, SEL log-volumes were negatively associated with NBV (highest absolute values for possible SEL, Pearson $r = -0.35$, $p < 0.001$) and with normalised CGM and DGM volumes (highest absolute values for possible SEL, Pearson $r = -0.41$,

$p < 0.001$; $r = -0.48$, $p < 0.001$; respectively). Similarly, at last follow-up (possible) SEL log-volumes negatively correlated with NBV (Pearson $r = -0.40$, $p < 0.001$) and both CGM and DGM volumes (Pearson $r = -0.44$, $p < 0.001$; $r = -0.49$, $p < 0.001$). Those results indicated that higher possible SEL volumes would be correlated to lowest brain and cortical measures both at baseline and at last follow-up. However, no significant associations in the correlation analysis were found between possible SEL log-volumes and PBVC (Pearson $r = 0.02$, $p = 0.83$).

4.3.6 T1 intensity ratio and MTR within SELs

The data of the T1 intensity ratio, analysed on 4007 lesions, were computed as adjusted mean (95% confidence intervals) obtained from the mixed-effects model taking into account time to follow-up and using as covariates the baseline age, gender, baseline T2 lesion volume, and PBVC. The results are presented in **Table 4-6** for the T1 intensity ratio values at baseline, at last follow-up and for the longitudinal change between those time points.

Table 4-6. Cross-sectional and longitudinal T1 intensity ratio within lesion types

Lesion category	T1 baseline (95% CI)	T1 at last follow-up (95% CI)	T1 change beta (95% CI)
Non-SEL (n=2538)	1.284 (1.234, 1.333)	1.286 (1.236, 1.336)	0.002 (0.002, 0.003) $p < 0.001$
Possible SEL (n=1061)	1.215 (1.165, 1.264)	1.211 (1.161, 1.261)	-0.004 (-0.005, -0.003) $p < 0.001$
Definite SEL (n=408)	1.220 (1.169, 1.271)	1.217 (1.166, 1.268)	-0.003 (-0.004, -0.002) $p < 0.001$

Abbreviations: SEL=slowly expanding lesion

Definite and possible SELs had lower cross-sectional T1 ratio values compared to non-SELs both at baseline and last follow-up. Longitudinally, the T1 intensity ratio was also computed using a similar mixed-effects model, by including the interaction term with the time at MRI follow-up. The results of the longitudinal analysis showed that T1 decreased over time in both possible and definite SELs while it increased within non-SELs. The differences in T1 change between SELs and non-SELs were

significant, with the greatest T1 decrease within the possible SELs (-0.004 [95% CI: -0.005 to -0.003], $p < 0.001$).

Figure 4-3 shows the relationship between the predicted T1 intensity ratio change and time at last follow-up from baseline at the lesion level, as obtained from the model described above. The lines visualised were drawn on R by plotting the predicted values obtained by the mixed effect model, considering the three lesion categories.

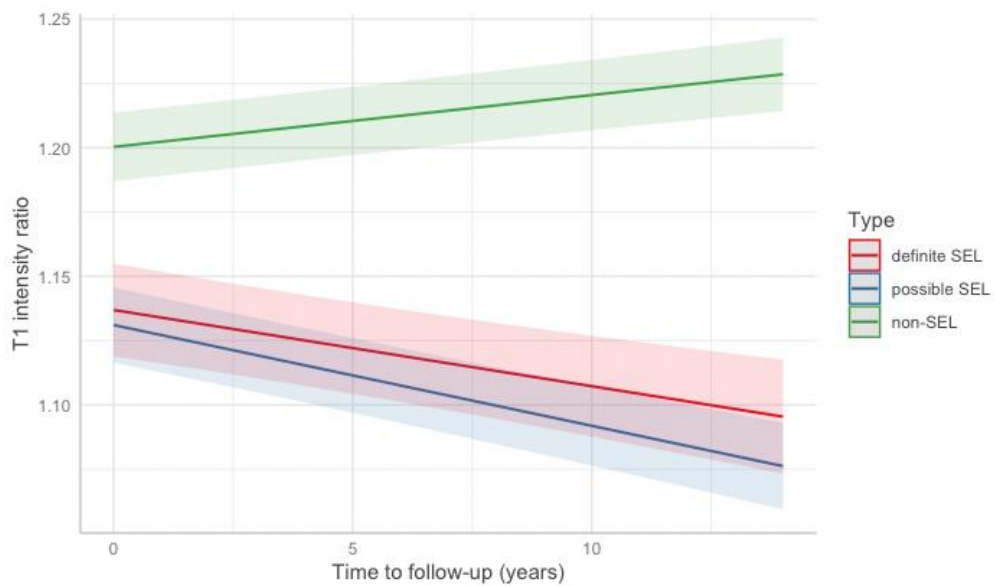


Figure 4-3. T1 change over time within SEL-derived lesion metrics.

In the subcohort of patients with MTR acquisitions ($n=83$), over 2352 lesions 10% ($n=232$) were definite SELs, 25% ($n=572$) were possible SELs, and 65% non SELs ($n=1548$), respecting the previously shown fractions. The MTR values were computed cross-sectionally at baseline and last follow-up using mixed-effects models to take into account subject and centre variability and they are shown in **Table 4-7**.

Table 4-7. Cross-sectional MTR at baseline and last follow-up within lesion types

Lesion category	MTR baseline (95% CI)	MTR difference with non-SELs, (95%CI), p-value	MTR at last follow-up (95% CI)	MTR difference with non-SELs, (95%CI), p-value
Non-SEL (n=1548)	28.6 (24.5 – 32.8)	NA	28.3 (24.3 – 32.3)	NA
Possible SEL (n=572)	27.3 (23.1 – 31.5)	-1.3 (-1.9, -0.8) p<0.001	26.7 (22.7 – 30.8)	-1.6 (-2.1, -1.1) p<0.001
Definite SEL (n=83)	27.1 (22.9 – 31.3)	-1.5 (-2.2, -0.8) p<0.001	26.9 (22.9 – 30.9)	-1.4 (-2.1, -0.7) p<0.001

Abbreviations: MTR=magnetization transfer ratio, SEL=slowly expanding lesion

Those values were lower within SELs compared to non-SELs (difference between SEL and non-SEL up to -1.5 percent unit [pu]; at follow-up up to -1.6 [pu]), when adjusted for demographical and MRI covariates (age, gender, baseline T2 lesion volume, and PBVC).

4.3.7 SEL associations to disability and risk of progression

The associations with clinical measures were analysed with models to predict disability evolution over time using mixed-effects regressions, and adjusting for demographic and MRI covariates (age, gender, disease duration, time at follow-up evaluation, total baseline lesion volume and PBVC). As a first major result, EDSS worsening over time was associated with higher possible SEL volumes (interaction term: beta=0.11, 95% CI 0.03 to 0.20, p=0.01), when the other MRI variables, i.e. baseline total lesion volume and PBVC, were not significantly associated. To better understand whether this result was due to the very long follow-up time, this analysis was replicated in the early onset MS subcohort (n=85). As a result, the EDSS was still predicted by an increase in possible SEL volumes (interaction term: beta= 0.14, 95% CI 0.04 to 0.25, p=0.008).

To evaluate the risk of incurring in clinical disability the outcome variable of the development of CDP at the last follow-up was used. For every additional unit increase in SEL (possible SEL log-volume), when assessed independently and adjusting for demographic characteristics, a five-fold higher risk for CDP was found (logistic

regression OR=5.15, 95% CI 1.60 to 16.60, $p=0.006$, pseudo- $R^2=0.11$). When the other MRI variables were analysed independently, total baseline lesion volume was also independently able to predict CDP, indicating that those markers demonstrate collinearity. However, after an assessment of the Bayesian Information Criterion (BIC), which was significantly reduced, SEL volumes performed better (156.14 vs 157.10). In addition, when this last analysis was extended to the early onset MS subcohort, a higher risk of CDP was confirmed only when using as explanatory metric SEL (CDP explained by possible SEL log-volume OR=13.38, 95% CI 1.56 to 114.60, $p=0.018$, pseudo- $R^2=0.25$), and not with the total baseline lesion volume.

4.4 Discussion

The accumulation of chronic active lesions in MS is a factor contributing to the worsening of clinical disability. In this retrospective observational study, with up to 12 years of follow-up, the results suggested that lesion expansion as measured through SELs was associated with increasing T1-hypointensity and with MTR reduction at follow-up, markers of both demyelination and axonal loss. Moreover, SELs were associated with disability progression, independent of conventional lesion measures or brain atrophy, highlighting their relevance as a therapeutic target in MS.

In this study, involving relapse-onset MS patients, SELs represented a very common finding, considering that from 86 up to 99% of the total cohort had at least one definite or one possible SEL, respectively. In addition, out of the total lesion count between 9% (definite SELs) and 26% (possible SELs) showed evidence of chronic activity, as both lesion types expressed an expansion as measured by the deformation maps, and the per-patient lesion count was a median of 6 SELs. From previous studies that used another SEL analysis technique in relapsing-onset MS trials, slightly lower counts were reported (median number of SELs = 4.6, proportion of lesions defined as SELs = 8.6%): (Elliott, Wolinsky, *et al.*, 2019) which could be due to a shorter follow-up period of observation (up to 96 weeks).

In the subsequent descriptive analysis of the distribution of the SEL-derived lesion counts, three subpopulations were found based on the evaluation of the possible SEL

type, which was the more numerous and they will be referred to as SEL to simplify. A high number of patients (48%) had a number between 3 to 10 SELs and they were defined as intermediate counts, while the rest were nearly split between high SEL counts (>10, 29%) and low SEL counts (0 to 2, 23%). The clusters with intermediate and high SEL counts had a higher EDSS at last follow-up, as well as consistent MRI metrics of inflammatory activity such as higher baseline T2 lesion volume and T2 lesion counts, and of neurodegenerative activity, such as lower values in brain and cortical volumes. A recent study involving alternative markers of chronic activity at susceptibility MRI has similarly identified a classification of patients depending on a low versus a high number of paramagnetic rim lesions (PRLs). (Absinta *et al.*, 2019) However, the authors identified higher percentages (30-40%) of patients without any rims or with low PRL counts. (Absinta *et al.*, 2019) The overall lower percentages of PRLs found in MRI longitudinal studies might suggest that only a subset of the chronic active lesions defined as SELs would develop PRLs.

Recently, MRI protocols using fully automatic segmentation techniques have allowed efficient detection of PBHs, promoting a stratification of MS lesion types through the assessment of their T1 intensity ratio to the surrounding tissues. (Datta *et al.*, 2006; Wu *et al.*, 2006; Khayati *et al.*, 2008; Spies *et al.*, 2013; Giorgio *et al.*, 2014; Valcarcel *et al.*, 2018) In the present study, PBHs were automatically determined using a newly developed in-house developed pipeline, taking into consideration previous works analysing the same lesion type. (Khayati *et al.*, 2008; Tam *et al.*, 2011; Spies *et al.*, 2013; Valcarcel *et al.*, 2018)

As a major result, a relevant positive correlation between the SEL counts or volumes and PBHs was found. Moreover, from 52 up to 61% out of the total T1 hypointense lesions (or BHs) that were PBHs also coincided with SELs. Those results suggest that there might be an evolution from a chronic active initial stage (SELs) towards the accumulation of a higher degree of neuro-axonal damage, typical of PBHs. Then, other MRI markers of neurodegeneration were also investigated, and the higher SEL burden, was consistently associated with reductions in global and regional brain volumes (both at baseline and at last follow-up). However, SELs were not directly correlated to brain atrophy measures in this study. Overall, the presence of both PBHs and SELs could

impact separately as additive risk factors, to develop a worse clinical outcome in relapsing-onset MS.

The structural MRI characteristics of MS lesions were assessed through a lesion-level quantitative analysis. In line with previous studies conducted on trial populations, including both relapsing and progressive MS patients, (Elliott *et al.*, 2017; Elliott, Belachew, Jerry S Wolinsky, *et al.*, 2019) SELs demonstrated a significant T1 intensity reduction over time. As a novelty of this analysis, in the current study, the subjects enrolled were in a very early disease stage at baseline, therefore the results could be implied to be relevant for MS since early diagnosis. Interestingly, the highest T1 intensity ratio change was identified within possible SELs. Similarly, the results of the MTR analysis (lower MTR at follow-up within SELs vs non-SELs) were consistent with previous studies showing that SELs are characterised by microstructural damage. (C Elliott *et al.*, 2020) As T1 and MTR reductions have been associated with neuro-axonal loss, (Van Walderveen *et al.*, 1998; Van Waesberghe *et al.*, 1999; Schmierer *et al.*, 2004) therefore SEL might be thought to present those characteristics related to tissue damage, however, this evaluation would require a confirmation at pathology. Nonetheless, it seems plausible that the possible SEL could represent an earlier step of the MS lesion evolution towards the chronic stage. In this dynamic stage, there might be a tendency toward a mixture of demyelination and remyelination, reflected by a higher degree and variability of T1 and MTR changes. Definite SELs could be seen as a later stage of the lesion evolution when significant tissue damage is reached including irreversible neuro-axonal loss, as confirmed by their generally lower MTR values. Overall, the accumulation of SELs could drive other pathological processes relevant to disease progression in MS, such as global tissue loss and microstructural lesion damage.

From a clinical perspective in this relapsing-onset MS cohort a higher disability level, as measured by an increase in the EDSS score at follow-up, was independently associated with higher possible SEL volumes (beta=0.11, p=0.01), and this was independent of the other MRI metrics including T2 lesion volume and brain atrophy. Furthermore, a five times higher risk of CDP was predicted by higher possible SEL volumes (OR=5.15, p=0.006). Those results might imply an active role for SELs in determining a change in clinical outcome, which were as well confirmed when the

analysis was restricted to a subcohort of patients with an early onset MS (≤ 5 years, $n=85$).

Overall, the ‘possible’ SEL types metrics were better correlated to clinical measures compared to the ‘definite’ SELs. This result was interpreted as higher flexibility due to less restriction in the algorithm to select this SEL subtype, thus a higher possibility of representing a dynamic stage. For example, they might represent chronic active lesions with a higher potential to expand, as an intermediate evolution step of MS lesions. From the SEL pipeline definition, the definite SEL types need to satisfy arbitrary restrictions, which might not have a clear correlation to the pathobiological processes occurring within the chronic active MS lesions. For example, the definite SEL selection criteria stipulate that there be a homogeneous expansion in all directions but in pathological studies lesion boundaries might also evolve into different shapes, depending on the degree of local and spatial specific chronic demyelination or remyelination. (Bramow *et al.*, 2010)

There are several comments on the methodology of this work. As a retrospectively selected observational cohort, SEL counts were higher compared to the figures identified in previous trials (Elliott, Wolinsky, *et al.*, 2019). Those results might be related to a longer observation time to the last follow-up MRI scan (reaching up to 12 years). Additionally, the SEL pipeline used in this work did not use an arbitrary cut-off of a minimal annualised expansion rate, used in other studies as a further inclusion criteria (Preziosa *et al.*, 2020), which may have further increased the number of SELs detected. Currently, there is not a gold standard for SEL identification (or any threshold of minimal expansion), and a study to evaluate different techniques and their sensitivity would benefit appropriate comparisons of the results.

A limitation of the work is related to the retrospective nature of this study, in which the time intervals at each follow-up were variable. This heterogeneity of the follow-up time might have impacted the overall computation of SELs, which requires the normalization (z-score computation) of the expansion rate within all subjects. However, a further analysis restricted to the early onset MS subcohort, evaluating only patients with disease duration lower or equal to 5 years at baseline, was confirmed in our main findings. As another methodological point, the MRI structural analysis found

a high degree of T1 hypointensity within SEL lesions, which was an expected finding. This could represent also a possible bias of the increase in sensitivity of the technique standing with the methodology itself, as the deformation field is obtained through the analysis of T1-weighted images. The lower T1 signal in SELs compared to other lesion types could be expected as a consequence of the inclusion criteria as part of the SEL detection algorithm. Moreover, T1-weighted images offer a better resolution and when they were available in 3D acquisition the lesion boundaries were more distinct, improving the computation of the deformation field as compared to the 2D FLAIR/T2-weighted sequences. Another limitation was the absence of the evaluation of the effect of disease-modifying treatment (DMT) use with regards to the SEL-derived lesion counts. However, due to the nature of the observational study, this was a very heterogenous cohort, thus the evaluation of the relationship between DMTs and SELs was not achievable. The evaluation of the effects of treatments on SEL would have required a balanced population including treated and non-treated subjects.

As a future step, it would be of interest to further develop a multiparametric analysis of SELs, including other quantitative MRI markers, such as diffusion-weighted MRI and network integrity metrics, in order to better characterise subtypes of MS lesions, their impact on the functional global brain level, and how they evolve over time.

In conclusion, SELs are a common finding in relapse-onset MS. On this longitudinal evaluation over time this type of MRI marker of chronic lesions not only expands but also shows associated T1 and MTR features of pathological MS-specific tissue damage. Importantly, they correlate independently with clinical outcomes and therefore might serve as an imaging marker of MS progression. Further work is required to determine if they can help identify a transition from relapsing to secondary-progressive MS, which can be clinically challenging, or play a useful role in MS clinical trials.

5 Relationship between Paramagnetic Rim Lesions and Slowly Expanding Lesions

5.1 Introduction

In relapse-onset MS, there is a predominance of focal acute new lesions, as described in chapter one (neuropathology section). Despite that, recent histopathological studies have shown that between 15% to 30% of lesions are classified as chronic active lesions (Frischer *et al.*, 2015; Luchetti *et al.*, 2018). They are characterised by progressive tissue matrix damage and a rim of iron-laden activated microglia/macrophages with myelin breakdown and reactive astrocytes (Bagnato *et al.*, 2011; Popescu *et al.*, 2017). Chronic active lesions, which are seen in all MS spectrum, are thought to contribute to driving clinical progressive (relapse independent) disability by inducing neuro-axonal damage.

On MRI, the iron-enriched areas at the edge of chronic active lesions can be visualised due to paramagnetic properties of iron-enriched cells at the edges combined with demyelination. As described in chapter two, hypointense rims surrounding lesions have been assessed in several studies in all MS phenotypes using either T2*-weighted or phase (Yao *et al.*, 2015), susceptibility-weighted imaging (SWI) (Clarke *et al.*, 2020) as well as quantitative susceptibility mapping (QSM) (Zhang *et al.*, 2016). Using those modalities, it has been shown that paramagnetic rim lesions (PRLs) can discriminate MS from the other neuroinflammatory conditions (Maggi *et al.*, 2020). In addition, PRLs comprise 9.8% of the global lesion count (Sinnecker *et al.*, 2016), which might represent a low estimate due to a limited MRI sensitivity in detecting iron inside inflammatory cells (Dal-Bianco *et al.*, 2017). In a recent study, the pooled prevalence estimation for PRL occurrence reached up to 40% among MS patients (Kwong *et al.*, 2021). PRLs can be identified at all disease stages and since disease onset, although it is debated whether they preferentially accumulate in certain clinical phenotypes (Mehta *et al.*, 2013; Harrison *et al.*, 2016). The accumulation of PRLs correlates with disease progression, as confirmed by higher EDSS and younger age to reach motor and cognitive disability in patients with ≥ 4 PRLs (Absinta *et al.*, 2019).

The retrospective evaluation of PRLs in vivo in combination with histopathological studies has allowed researchers to demonstrate on MRI that the chronic active lesions slowly expand over time (Dal-Bianco *et al.*, 2017). Thus, the slowly expanding lesions (SELs) have been developed as alternative markers to detect the slow expansion in chronic active lesions using deformation-based longitudinal volumetric MRI. As shown in previous chapters and in previous trials (Elliott, Wolinsky, *et al.*, 2019), SELs are a common lesion type among the whole MS spectrum including relapse-onset MS (Elliott, Wolinsky, *et al.*, 2019), but a higher number of SELs is found in progressive MS, in which the SEL count reaches up to 29 lesions per patient. Previous studies by Elliott *et al.* have determined that SELs are related to greater T1 hypointense volume (Elliott, Belachew, Jerry S Wolinsky, *et al.*, 2019), MTR reductions (Preziosa *et al.*, 2020) and diffusivity measures (Klistorner *et al.*, 2021). A further contribution has been made in this PhD work by demonstrating that SELs are also associated with MTR reductions and PBHs (Calvi, Tur, *et al.*, 2022), adding to the literature that those markers exhibit relevant neuro-axonal damage compared to non-SELs, and they correlate with disability as assessed by physical and cognitive measures (Elliott, Belachew, Jerry S. Wolinsky, *et al.*, 2019). Recent analyses found that lesions with rims grew significantly more than all the other lesions (Weber *et al.*, 2022), and that in those lesions that share the features of the SELs and PRL there are signs of more severe tissue damage, as assessed by lower magnetization transfer ratio (Elliott *et al.*, 2021). While both markers represent chronic active lesions, it is unclear whether SELs or PRLs reflect an identical population of lesions.

In this chapter, the main objectives were: (1) to investigate the relationship between PRLs, identified on the baseline SWI, and SELs, computed using volumetric MRI, in MS; (2) to evaluate their association with other radiological markers (i.e. total lesion and brain-derived volumes); (3) to evaluate groups defined by the presence of PRLs and SELs (4) to assess the independent and combined contribution of PRLs and SELs on clinical disability evolution.

The hypothesis behind this work are the following: (1) lesions with paramagnetic rims would be more likely to undergo expansion and be classed as SELs, (2) both lesion types would be associated with a higher lesion volume and lower brain-derived metrics

at baseline and (3) patients with both PRLs and SELs would have a worse clinical prognosis than patients without.

5.2 Materials and methods

5.2.1 Participants, MRI acquisitions and clinical assessments

This is a retrospective study from an observational cohort of MS conducted at Centre d'Esclerosis Multiple de Catalunya (CEMCAT) and Section of Neuroradiology, Vall d'Hebron Barcelona Hospital Campus (Barcelona, Spain). The study was a collaborative project within the Magnetic Resonance Imaging in MS (MAGNIMS) initiative, and it received the approval of the local Ethical Committees of Vall d'Hebron Barcelona Hospital Campus and the Queen Square MS Centre, University College London. The patients who took part in this observational study had given informed consent for use of their data for other research. The following inclusion criteria were adopted to include patients with: (1) confirmed diagnosis of relapsing-remitting (RRMS) or clinically isolated syndrome (CIS) according to the revised 2017 McDonald criteria; and availability of (2) baseline SWI and FLAIR images; (3) at least three consecutive 3D magnetization-prepared rapid gradient-echo (MPRAGE) scans of sufficient image quality and absence of artefacts.

The scanner used for this study was a 3T magnet (Tim Trio; Siemens, Erlangen, Germany) with a 12-channel phased-array head coil. The acquisition parameters, as previously described⁶ were: (1) transverse fast FLAIR (TR=9000 ms, TE=87 ms, TI=2500 ms, flip angle=120°, voxel size=0.49×0.49×3.0 mm³); (2) sagittal T1-weighted 3D MPRAGE (TR=2300 ms, TE=2.98 ms, TI=900 ms, voxel size=1.0×1.0×1.2 mm³); (3) transverse SWI (TR= 33 ms, TE₁=6.08 ms, TE₂=24.6 ms, flip angle=15°, voxel size=0.65×0.65×3 mm).

All patients included in the cohort had been assessed with the Expanded Disability Status Scale (EDSS) at all three sessions by MS neurologists. The EDSS change was calculated as the difference between EDSS at the last session and baseline EDSS. Confirmed disability progression (CDP) was defined as an EDSS change greater than 1.5 or greater than 1.0 when the baseline EDSS score was 0 or greater than 0,

respectively, which had to be confirmed in the following 6 months after the last session.

5.2.2 Lesion and brain segmentation, SEL detection

For the acquisition of the MS lesions an automated technique was used, the lesion prediction algorithm (LPA) from the lesion segmentation tool (LST) (Roura *et al.*, 2015) for Statistical Parametric Mapping (SPM) framework, based on the analysis of the baseline FLAIR images. The lesion masks computed automatically followed a subsequent manual quality check and were corrected, if needed, in Jim v7.0 (Xinapse Systems, Aldwinckle, UK) by experienced raters (myself and Margareta Clarke). The FLAIR images originally acquired in 2D were resampled to 1-mm isotropic space. Then, the 3D-MPRAGE images followed a registration to the lesion masks using a pseudo-T1 image generated by subtracting the 2 echoes of the FLAIR sequence (Hickman *et al.*, 2002).

After that, as previously described in chapters three and four, the SEL-derived metrics were retrieved. To account for the heterogenous interval time at follow-up, the SEL pipeline used a normalisation by evaluating the z-score of the Jacobian expansion values as previously described. The only differences consisted in the acquisition used in this work, as the deformation field was acquired using the MPRAGE and lesions were acquired with FLAIR. Similar to the previous chapters, for brain extraction, tissue segmentation and parcellation, Geodesic Information Flows (GIF) (Cardoso *et al.*, 2015) technique was applied on MPRAGE, using a multi-time-point patch-based lesion-filling method to avoid segmentation bias (Prados *et al.*, 2016). From these segmentations, the normalised brain volume (NBV), and the cortical volumes were obtained: normalised cortical grey matter (CGM) and normalised deep grey matter (DGM) volumes.

5.2.3 PRL detection on SWI

FLAIR and SWI images were rigidly aligned using *NiftyReg* software package, and consecutively labelled lesions were transformed to SWI space using a neighbour interpolation method to perform the PRL analysis. Lesions were independently manually reviewed by two raters (myself and Margareta Clarke) using the software *slicer* to allow for the simultaneous visualisation of the lesion masks on

the registered SWI and FLAIR images to identify the PRLs. The criteria for the definition of a PRL were: (1) the presence of a partial or complete rim of hypointense signal on SWI relative to the lesion core (being either hyper- or isointense) or the surrounding white matter; (2) the correspondence of the rim to the lesion's edge on the registered FLAIR; (3) the rim needed to be visible on at least two consecutive slices. A conservative approach was used by removing the inclusion of PRLs which did not correspond to the lesion's edges or to hypointense areas on the FLAIR. Moreover, care was taken not to mistake veins and signals from the white/grey matter border for PRLs, by tracing the path of the signal. The raters initially independently reviewed 20 scans before reviewing the data together for any disagreements and to identify the most common patterns of signal, which led to it. After that, they proceeded to review the remaining cases independently and blindly. In both cases, any disagreements were subsequently settled by two highly experienced radiologists (AR and FB). There was a low rate of disagreement between raters in a small number of lesions (<1%), which corresponded to a high inter-rater agreement (Cohen's Kappa = 0.87).

5.2.4 Lesions and categories according to SELs and PRLs

An initial classification was performed at the lesion level by separating lesions by category (i.e. SELs, PRLs, or both). Then, patients were stratified according to the presence of at least one SEL or one PRL, as assessed independently. After that, the presence or the absence of SEL and PRL were assessed in combination, by categorising patients into three mutually exclusive subgroups, as follows:

- Presence of at least one SEL and at least one PRL, also called SEL+PRL+ (positive for both markers);
- Presence of at least one SEL but without PRLs, called SEL+PRL- (SEL positive only)
- Absence of SELs, called SEL- (SEL negative);

Since the number of SEL negative patients was small, those with and those without PRLs were not considered separately in that subgroup only.

5.2.5 Statistical analysis

The statistical analysis of this chapter was performed using a combination of STATA and R. All the lesions were labelled individually, each one was classified in the SEL-

derived category and the presence or absence of PRL was recorded, in order to obtain the counts and the volumes of each category. The individual identification of each lesion evaluated the spatial correspondence between SEL and PRL.

A descriptive analysis was followed to identify PRL and SEL-related measures at the lesion level for each category. Then, the lesion counts, and volumes (by type) were analysed at the patient level, reporting median and range, or mean and standard deviation (SD). As previously done, each specific lesion volume type was log-transformed (base 10) to meet the normality assumption.

The correlations among all the radiological measures retrieved were initially assessed with Spearman (' ρ ') coefficients. Then, Poisson and linear regressions were applied to confirm the associations (for the counts and the volumes, respectively) and for each variable, the normality of the residuals was checked. The odds ratio (OR) or beta coefficients and p values (limit set as $p < 0.05$) are reported in the results. To assess the differences in the proportions of lesions that were PRLs according to the SEL-derived category, the Chi-square test was used. Differences in the subgroups of patients classified according to the combinations of SEL/PRL were assessed using linear regressions. The radiological analysis was repeated taking into consideration the treated and the non-treated population at the end of the study. This analysis was also repeated by sub-selecting the group of patients with short follow-up (< 2 years) from those with a longer follow-up (≥ 2 years).

As a final step, mixed-effect regression models adjusted for age, gender and baseline total lesion volume and treatment status were used to assess the relationship between the EDSS (dependent variable) and the MRI measures as independent variables, i.e., counts and log-volumes of SELs and presence of PRLs or combined presence of PRLs and SELs, using the interaction term between each metric and the time at follow-up, while the random effects were taking into account the variability within each subject. Multiple logistic regressions, adjusted for demographic covariates (age at baseline, gender, time to the last follow-up) were applied to investigate the risk of CDP explained by within-patient counts or log volumes of SELs. Statistical significance was reported at $p < 0.05$.

5.3 Results

5.3.1 Cohort demographics and clinical features

The demographical and clinical characteristics of the cohort enrolled in this study are reported in **Table 5-1**.

Table 5-1. Clinical-demographic characteristics of the patients enrolled in the study.

Demographics and clinical features	
Number of patients	61
Female, n (% over total)	42 (69 %)
Age at baseline, median (range), years	34.4 (14.1 – 64.9)
Disease duration, median (range), years	0.4 (0.1 – 16.6)
Time to intermediate scan, median (range), years	0.8 (0.4 – 6.4)
Time to final scan, median (range), in years	3.2 (0.7 – 8.3)
EDSS at baseline, median (range)	1.5 (0 – 4.5)
EDSS at final session, median (range)	1.5 (0 – 5.5)
EDSS change[§], mean (SD)	0.16 (1.33)
MS phenotype at baseline	CIS=6; RRMS=55
MS phenotype at last follow-up	CIS=6; RRMS=53; SPMS=2
Number (%) of patients with CDP*	14 (23%)
Number (%) of patients treated at baseline	16 (26%)
Number (%) of patients treated at last follow-up	51 (84%)

Abbreviations: EDSS= Expanded Disability Status Scale; CIS=clinically isolated syndrome; RRMS=relapsing-remitting multiple sclerosis; SPMS=secondary-progressive multiple sclerosis. [§] EDSS change calculated as the difference between EDSS at final session and EDSS at baseline. * Confirmed Disability Progression (CDP) was defined by an EDSS change ≥ 1.5 if baseline EDSS=0 or EDSS change ≥ 1.0 when baseline EDSS>0, respectively, and confirmed at least > 6 months after the last session.

At baseline, the median age was 34.4 years (range 14.1 to 64.9) and the median disease duration was 0.4 years (range 0.1 to 16.6), thus indicating an RMS cohort at an early stage since the onset of MS symptoms. Most patients enrolled were female (n=42). There was some heterogeneity in this cohort with respect to the time to the final MRI scan (median was 3.2 years). The following subgroups at baseline were recognised: 6 with CIS and 55 with RRMS; at the final follow-up, there were 6 CIS, 53 were RRMS

and 2 converted to secondary-progressive (SPMS). Median EDSS at baseline was 1.5 (range 0 to 4.5), and the mean EDSS change was 0.16 (SD=1.33). Patients with MS who developed CDP by the end of the study were 14 (23%). At baseline patients who were receiving any disease-modifying treatment (DMT) were a minority (16%), while 84% had been treated with any DMTs at the final session.

5.3.2 Patient categories according to SELs and PRLs

Patients were grouped according to the studied imaging markers, by evaluating the presence or absence of SELs and PRLs, and a combination of the two, as reported in **Table 5-2**. When those markers were analysed separately at the patient level, nearly all patients had at least one SEL (92%, n=56), while slightly more than half had at least one PRL (56%, n=34).

Table 5-2. Patient categories according to presence or absence of SELs and PRLs

		Presence of SELs	
		SEL+ (≥ 1 SEL) n=56	SEL- n=5
Presence of PRL	PRL+ (≥ 1 PRL) n=34	SEL+ PRL+ n=31	SEL- PRL+ n=3
	PRL- n=27	SEL+ PRL- n=25	SEL- PRL- n=2

Abbreviations: SEL slowly expanding lesions, PRL paramagnetic rim lesions

On the other hand, when those imaging markers were analysed in combination, the majority of patients had both SELs and PRLs (SEL+PRL+, n=31, 51%). Then, considering the numerosity they were followed by the group of patients with SELs but no PRLs (SEL+PRL-, n=25, 41%) and finally, patients without SELs (SEL-, n=5, 8%).

5.3.3 SELs and PRLs correspondence and radiological descriptive analysis

After applying the automatic lesion segmentation, an overall total number of 1492 lesions were identified. This was followed by a descriptive analysis after applying the SEL algorithm: 616 were SELs (41%), while 876 were non-SEL (59%).

The spatial correspondence analysis between SEL and PRL for each of the individual lesions was conducted. On the baseline SWI acquisitions, a total number of 80 PRLs were identified, which corresponded to 5% (80/1492) of the whole lesion number. Forty-three lesions belonged to both the SEL and PRL categories, representing 54% (43/80) of all the PRLs and 7% (43/616) of all the SELs (**Figure 5-1**).

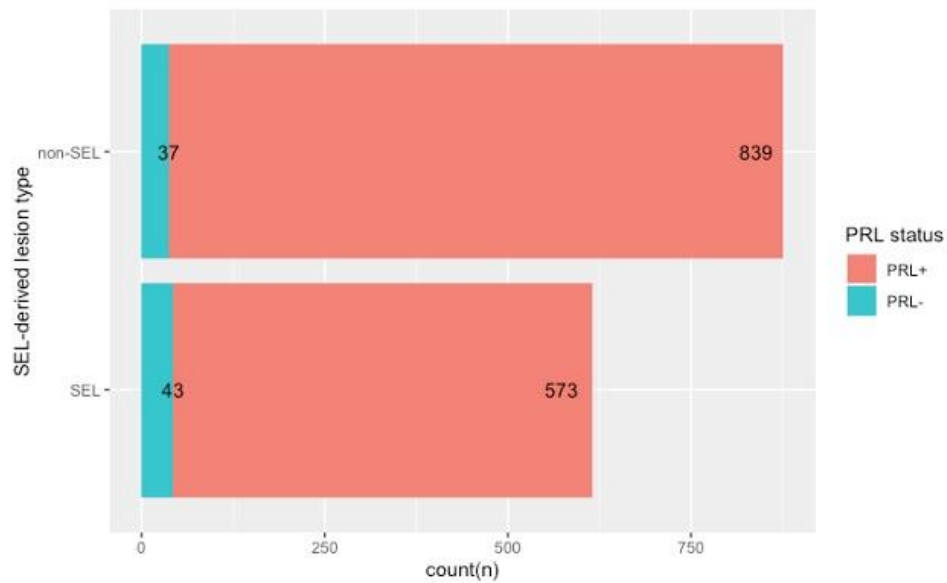


Figure 5-1. Stacked bar plot of PRL and SEL counts.

The plot, drawn with R, shows the counts of lesions divided in the SEL and the non-SEL, and the correspondent PRL in each subtype.

The proportion of PRLs was higher among the SELs (43/473, or 8%) than among the non-SELs (37/839, or 4%, Chi-square test $p=0.027$). Following this analysis, the figures of SEL and PRL, i.e. their relative counts and volumes were described at the subject level, by summing together each measure of the same type for each subject. Out of a median of 20 total lesions per patient, SEL were 5 and they accounted for 27% of the lesion volume (0.6 ml/2.2 ml).

Then, the GIF segmentation was performed and all the radiological measures were calculated. The radiological characteristics of the cohort at the patient level are presented in **Table 5-3**.

Table 5-3. Radiological measures: counts and volumes and brain-derived measures

Radiological measures	
Total lesion count at baseline (n), median [range]	20 [1 – 80]
SEL count (n), median [range]	5 [0 – 41]
non-SEL count (n), median [range]	10 [0 – 55]
PRL count at baseline (n), median [range]	1 [0 – 8]
Total lesion volume at baseline, median [range], ml	2.2 [0.1 – 67.0]
SEL volume, median [range], ml	0.6 [0 – 65.3]
Non-SEL volume, median [range], ml	0.9 [0 – 27.1]
PRL volume at baseline, median [range], ml	0.03 [0 – 1.0]
Gadolinium-enhancing lesions at baseline, count (n), median [range]	0 [0 – 40]
New lesions at final session, count (n), median [range]	1 [0 – 24]
NBV volume at baseline, mean (SD), ml	1505.7 (75.1)
CGM volume at baseline, mean (SD), ml	839.9 (47.9)
DGM volume at baseline, mean (SD), ml	49.4 (3.7)
BPF at baseline, mean (SD)	0.77 (0.02)

All the measures are referred at the patient level. Abbreviations: SEL= slowly expanding lesion; NBV = normalised brain volume; CGM = cortical grey matter; DGM = deep grey matter; NAWM = normal-appearing white matter; BPF = brain parenchymal fraction.

On **Figure 5-2** an example of a correspondence between a PRL and a SEL is shown in a woman enrolled in the study, diagnosed with CIS at baseline (45 years old). The MRI was executed at 4 months since onset (EDSS 0). At last follow-up she converted to RRMS and EDSS increased to 1.5.

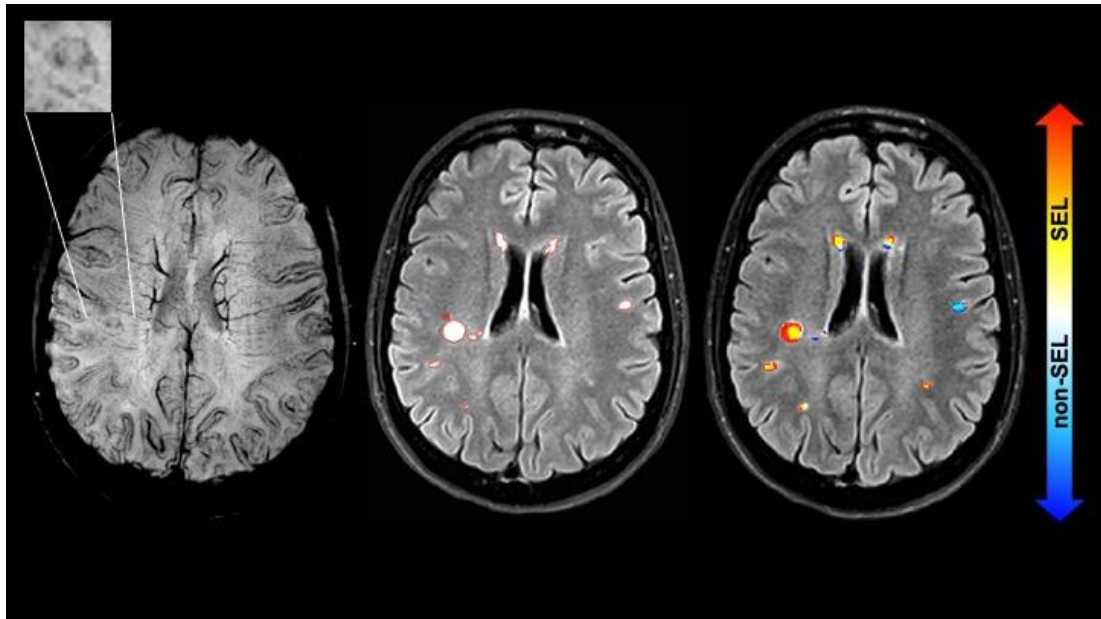


Figure 5-2. Example of a PRL+ at baseline and the correspondence to a SEL.

The images show from left to right: SWI at baseline (the arrow indicates the paramagnetic rim lesion), FLAIR with lesion mask countered in red, Jacobian map indicating that the PRL correspond to a SEL.

5.3.4 SELs and PRL in treated versus non-treated, and in short versus long time intervals

In this analysis all the radiological markers of interest, the SEL and PRL-derived measures, were assessed in the group of patients who received treatment and the ones who were untreated by the end of the study observation interval time. This analysis is presented in **Table 5-4**. Patients who were treated at final follow-up (n=51) had a higher baseline total lesion burden, together with higher non-SEL and PRL counts and volumes. However, there was a tendency towards higher SEL volumes in the treated population, but this was borderline significant (p=0.056).

Table 5-4. SEL- and PRL-derived metrics at baseline at the patient level in the treated and non-treated population

	Treated at final follow-up (n=51)	Not treated at final follow-up (n=10)	p value*
Total lesions count at baseline (n), median [range]	21 [1 – 80]	4 [1 – 38]	0.002
SEL count (n), median [range]	7 [0 – 41]	2 [1 – 20]	0.061
Non-SEL count (n), median [range]	14 [1 – 55]	2 [0 – 18]	<0.001
PRL count at baseline (n), median [range]	1 [0 – 8]	0 [0 – 1]	0.002
Total lesion volume at baseline (ml), median [range]	2.8 [0.1 – 66.9]	0.3 [0.1 – 4.3]	0.003
Total SEL volume (ml), median [range]	0.7 [0 – 65.3]	0.1 [0.1 – 2.56]	0.056
Non-SEL volume (ml), median [range]	1.6 [0.1 – 27.1]	0.2 [0 – 1.7]	<0.001
PRL volume at baseline (ml), median [range]	0.1 [0 – 1.0]	0 [0 – 0.1]	<0.001

*unpaired sample t-test (for the normally distributed variables) or Mann-Whitney test (for the non-normally distributed variables). Abbreviations: SEL slowly expanding lesions, PRL paramagnetic rim lesions

Those radiological measures were also assessed in the groups of patients with long or short interval time at final follow-up. No differences between patients followed for a short time interval (< 2 years) compared to the ones with a longer follow-up (≥ 2 years) were identified. The analysis is presented in **Table 5-5**.

Table 5-5. SEL- and PRL-derived metrics at the patient level in the short- and long-time range interval sub-cohorts

	Short-time range sub-cohort (< 2 years) [n=15]	Long-time range sub-cohort (≥ 2 years) [n=46]	p value*
Total lesions count at baseline (n), median [range]	18 [2 – 80]	20 [1 – 77]	0.750
SEL count (n), median [range]	5 [0 – 41]	5 [0 – 41]	0.960
Non-SEL count (n), median [range]	16 [1 – 55]	9 [0 – 50]	0.580
PRL count at baseline (n), median [range]	1 [0 – 6]	1 [0 – 8]	0.750
Total lesion volume at baseline (ml), median [range]	2.3 [0.1 – 9.7]	2.1 [0.1 – 66.9]	0.624
SEL volume (ml), median [range]	0.6 [0 – 3.8]	0.6 [0 – 65.3]	0.496
Non-SEL volume (ml), median [range]	1.6 [0.1 – 6.4]	0.9 [0 – 27.1]	0.863
PRL volume at baseline (ml), median [range]	0.1 [0 – 0.8]	0.1 [0 – 1.0]	0.828

*unpaired sample t-test (for the normally distributed variables) or Mann-Whitney test (for the non-normally distributed variables). Abbreviations: SEL slowly expanding lesions, PRL paramagnetic rim lesions

5.3.5 Association analysis of SELs, PRLs and radiological measures

A positive correlation was identified between the SEL counts and PRL counts ($\rho=0.28$, $p=0.03$) and between SEL volumes and PRL counts ($\rho=0.29$, $p=0.02$). However, when a partial correlation between PRL and SEL counts or volumes was computed taking into account the total lesion burden, no significant associations were found. The global brain and regional brain volumes were then assessed for their associations with the SELs and PRLs. There was a negative association between baseline BPF and SEL volume ($\rho=-0.48$, $p<0.001$), which was similarly driven by the association to the total lesion volumes in the partial correlations. No significant associations were found with any of the regional baseline brain volumes (CGM, DGM). No associations were found between the count or volumes of the PRLs and the global or regional brain volumes.

5.3.6 Radiological and clinical measures by patient groups according to SEL & PRLs

To assess the differences in groups the radiological and clinical measures were described among patients classified as SEL+PRL+, SEL+PRL- or SEL- (**Table 5-6**)

Table 5-6. Clinical-demographic and radiological characteristics in groups according to the presence of SEL and PRLs.

	SEL+PRL+ (n=31)	SEL+PRL- (n=25)	SEL- (n=5)	p-value*
EDSS at baseline, median [range]	1.5 [0; 4.5]	1 [0; 3]	1 [0; 2]	0.187
EDSS at final follow-up, median [range]	1.5 [1; 5.5]	1 [0; 5.5]	1 [1; 2]	0.106
EDSS change, mean [SD]	0.27 [1.12]	0.06 [1.62]	0.00 [1.00]	0.806
Age at baseline, median [range]	37.2 [17.7; 67.6]	34.2 [17.5; 47.4]	35.7 [23.5; 41.9]	0.325
Disease duration, median [range]	0.2 [0.1 – 16.7]	0.4 [0.1 – 13.5]	0.3 [0.1; 0.3]	0.518
Total lesion count, median [range]	28 [4 – 80]	9 [1 – 77]	5 [1 – 24]	0.006
Non-SEL count, median [range]	15 [1 – 55]	5 [0 – 44]	5 [1 – 24]	0.029
SEL count, median [range]	9 [1 – 41]	4 [1 – 39]	0 [0]	0.008
Total lesion volume at baseline, median [range]	3.7 [0.5 – 66.9]	0.7 [0.02 – 6.0]	0.5 [0.1 – 27.1]	0.005
Non-SEL volume, median [range] at baseline	2.1 [0.1 – 18.3]	0.4 [0 – 2.5]	0.5 [0.1 – 27.1]	0.020
SEL volume, median [range]	1.2 [0.1 – 65.3]	0.2 [0.01 – 4.2]	0 [0]	0.007
NBV at baseline, mean [SD]	1497.2 [83.4]	1512.4 [64.8]	1525.1 [77.9]	0.636
CGM volume at baseline, mean [SD]	834.2 [55.8]	846.5 [38.6]	841.6 [39.6]	0.638
DGM volume at baseline, mean [SD]	49.0 [4.2]	49.8 [3.0]	50.5 [3.8]	0.552
BPF at baseline, mean [SD]	0.76 [0.02]	0.77 [0.01]	0.77 [0.02]	0.130

*multiple linear regression models. Abbreviations: SEL= slowly expanding lesion; NBV=normalised brain volume, CGM=cortical grey matter, DGM=deep grey matter, BPF=brain parenchymal fraction

Among those groups, SEL+PRL+ patients had overall the highest total lesion counts (median 28, $p=0.001$) and the highest total lesion volume (median 3.7 ml, $p=0.005$). In accordance with those findings, similar results were also found in a multiple linear regression model, where the total lesion volume was explained by the SEL patient group category when the group categories were converted into continuous numbers (beta=5.7 ml, 95% CI [0.8 – 10.6], $p=0.025$). No differences were identified between the SEL & PRL combination groups with regard to the baseline NBV and regional brain volumes.

5.3.7 SELs and PRLs relationship to demographics

The correlation analysis was extended to the demographic features, i.e. sex, age at baseline, and disease duration. Both the SEL count and the SEL volume were positively associated with the age at baseline ($\rho=0.37$, $p=0.004$; $\rho=0.36$, $p=0.004$, respectively). In linear regressions, SEL lesion counts and volumes were higher in patients with longer disease duration (beta=0.10, 95% CI [0.07; 0.14], $p<0.001$) and higher age at baseline (beta=3.0, 95% CI [1.7 – 4.3], $p<0.001$). Conversely, PRL lesion count and volume were not associated with any of the demographic factors explored. No associations were found between gender and either the SEL-derived or PRL measures.

5.3.8 EDSS progression in relation to SELs and PRLs

In mixed-effect regression models adjusted for age at baseline, gender, disease duration, treatment status at the end of the study, and the baseline lesion counts and volumes, a greater EDSS increase over time was associated with higher baseline definite SEL counts (beta=0.01/year, 95% CI [0.001; 0.03], $p=0.040$) and volumes (beta=0.01/year, 95% CI [0.001; 0.01], $p=0.034$). In addition, the presence of at least one PRL at baseline was associated with a greater increase in EDSS over time (beta=0.02/year, 95% CI [0.03; 0.33], $p=0.018$) compared to patients without PRLs.

Those SEL+PRL+ patients had greater increases in EDSS scores over time than SEL+PRL- (SEL+PRL+ beta=0.18/year, 95% CI [0.07; 0.29], $p=0.002$ vs SEL+PRL- beta=-0.02/year 95% CI [-0.13; 0.09], $p=0.699$). No differences in EDSS progression

were found between the SEL+PRL+ and SEL- group (beta=-0.11/year, 95% CI [-0.44; 0.22], p=0.513) or between SEL+PRL- and SEL- group (beta=-0.09/year, 95% CI [-0.42;0.24] p=0.580). These associations were confirmed when the categories were assessed as binary variables, and all the models are presented in **Table 5-7**. In the logistic regressions that assessed CDP status using baseline SEL or PRL counts and volumes, no significant associations were found.

Table 5-7. Association between the SEL-PRL measures and categories with EDSS over time using mixed-effects regression models

MRI and patient category (Independent variables)	EDSS (Dependent variable)	
	Beta coefficient [95% CI]	p value
Interaction terms with time		
SEL count* (n)	beta=0.01/year [0.001; 0.03]	p=0.040
SEL volume* (ml)	beta=0.01/year [0.001; 0.01]	p=0.034
SEL+ (category: binary)	beta=0.01/year [-0.32,0.33]	p=0.973
PRL count at baseline (n)	beta=0.04/year [-0.01,0.08]	p=0.078
PRL volume at baseline (ml)	beta=0.03/year [-0.001,0.05]	p=0.062
PRL+ (category: binary)	beta=0.02/year [0.03; 0.33]	p=0.018
SEL+PRL+ (category: binary)	beta=0.19/year [0.04; 0.34]	p=0.012
SEL+PRL- (category: binary)	beta=-0.19/year [-0.34; -0.04]	p=0.012
SEL- (category: binary)	beta=-0.01/year [-0.33; 0.32]	p=0.973
SEL count* (n)	beta= 0.01[-0.002; 0.02]	p=0.117
PRL+ (category: binary)	beta=0.13[-0.03; 0.03]	p=0.103
SEL volume* (ml)	beta=0.01[-0.001; 0.01]	p=0.106
PRL+ (category: binary)	beta=0.13[-0.03; 0.29]	p=0.103
PRL+ (category: binary)	beta=0.04 [-0.33; 0.40]	p=0.848
SEL+PRL+ (category: binary)	beta=0.16 [-0.20; 0.52]	p=0.384

The table shows the interaction terms between time and the independent variables, MRI measures or patient categories, while the clinical score (EDSS) was the dependent variable. Whenever the interaction term is significant, we assume that there is a significant association between the MRI measure/patient category and the change in the clinical variable over time. *SEL here refers to the definite SEL category.

5.4 Discussion

In this work, associations between MRI markers of the chronic active lesions in patients with MS were assessed. A moderate association between slowly expanding lesions (SELs) and the presence of SWI visible rim lesions at baseline was found, and SELs outnumbered PRLs by a factor of 10. In addition, this work suggests that the co-occurrence of both MRI markers is an adverse prognostic factor.

This was an early MS cohort, in which the vast majority (92%) developed at least one SEL over the follow-up observation time (median 3 years), and 56% had at least one PRLs at SWI, in line with previous reports (Absinta *et al.*, 2019; Clarke *et al.*, 2020). Patients in this cohort on average developed 5 SELs (40% of the overall lesions), despite being early in their disease course, comparable to more heterogeneous MS phenotypes (4 to 19.5 SELs per patient, with higher figures in the progressive phenotypes) (Elliott, Wolinsky, *et al.*, 2019; C Elliott *et al.*, 2020; Calvi, Carrasco, *et al.*, 2022). By contrast, only a low number of baseline lesions were PRLs (80/1492, 5%), suggesting that close to disease onset only a small subset of MS lesions are characterised by ring-like iron deposition. A study evaluating up to 7 years after baseline has recently demonstrated that PRLs can persist in progressive disease stages, and a high percentage (50%) of them show a slow volume growth, presenting with more destructive MRI features (Dal-Bianco *et al.*, 2021). However, it was also suggested that, after this growing phase, PRLs reach a stabilization period with reduced susceptibility and rim attenuation thereafter, becoming than non-PRLs.

This work indicates a moderate association between PRLs and lesion expansion, as measured by SEL, in early relapse-onset MS. Despite that, the proportion of PRLs that were also classified as SELs exceeded the proportion among the non-SELs. Moreover, the group of patients having both SELs and PRLs (SEL+PRL+) had the highest lesion counts and volumes, in comparison to patients with SELs only or without SELs. PRLs and SELs were positively associated in this cohort, however, their correlation was mainly driven by the total lesion load, consistent with previous observations that PRL counts are related to lesion burden (Absinta *et al.*, 2019; Dal-Bianco *et al.*, 2021). In accordance with the hypothesis of a link between these two markers of chronic active lesions, a previous study on 7T MRI found an association between lesion expansion and PRLs (Dal-Bianco *et al.*, 2017). Further, supportive evidence described that newly

developed lesions with PRLs had 30% of volume expansion over 3 years (Dal-Bianco *et al.*, 2017). Moreover, in studies assessing up to 7-10 years after the baseline scan, up to 50% of the PRLs showed an expansion with a growth rate greater than 10% of their initial volume (Dal-Bianco *et al.*, 2021), and a yearly growth rate up to 2.5% (Absinta *et al.*, 2019). In this study, there were trends in reductions in brain volumetrics in association with higher SEL volumes, suggesting that there is an association between chronic inflammation and global neuro-axonal damage. However, no clear differences in the baseline global brain or regional brain volumes were found for the group of SEL+PRL+ patients. This result could be linked to the early age range and short disease duration of this early relapse-onset MS cohort.

From a clinical perspective, these results suggest that there is an association between SELs, higher age at baseline and longer disease duration, which are well-known predictors for a worse prognosis in MS (Cree *et al.*, 2016; Dekker *et al.*, 2019). Those associations can be partially explained by the fact that a higher baseline total lesion burden is related to higher SEL accumulation. The presence of SEL and PRLs in combination correlated with the evolution of clinical disability, as measured by the EDSS, reflecting that as additive factors they might be involved in the perpetuation of inflammation and in a reduced remyelination potential. The early deposition of paramagnetic materials within PRLs could also indicate a specific adverse pathogenetic process, such as a more aggressive macrophages-microglia profile, favouring expansion and conversion to SELs. All those factors could be implicated in a reduced recovery potential from relapses or in progression independent of relapsing activity.

This work has several limitations linked to the methodological aspects and the characteristics of the cohort. First of all, the MRI scans were retrospectively collected from an observational cohort, thus increasing the heterogeneity of the MRI scanning schedule and the short interval of observation time for a subgroup of this cohort could have impacted the accuracy of SEL detection. In addition, the acquisitions had different image resolutions (2D or 3D), which could affect the computation of SELs and the visualisation of PRLs. A limitation is also related to the criteria for SEL definition and pipeline used that differ between centres, thus making a comparison across trials difficult. In the descriptive analysis, we combined ‘possible’ and ‘definite’

SELs, which differs from the work in the previous chapters that included only definite SELs. However, the mixed-effect models evaluating the clinical impact of the markers were all evaluated for the definite SELs. This analysis was also limited to SWI only on the baseline scan and the persistence of PRLs on the follow-up scans was not assessed, which represents an objective for a future evaluation. Finally, an evaluation of treatment exposure based on the first or second lines was not conducted, as this was not an objective of the study and due to the relatively small sample size. However, in an initial evaluation of the differences between treated and non-treated subjects by the end of the study, the results of the analysis were not materially changed by the treatment effect.

Overall both SEL and PRL hold promise for being used in the future as markers for the chronic active lesion in MS. SELs represent a very common finding and this technique could be applied with simple acquisitions (T2 and T1-weighted), therefore facilitating the standardisation between MS centre. However, due to the high prevalence of SELs within the cohort, an assessment of patients based on the presence or absence SELs alone could be of limited clinical value. On the other side, PRLs could have a higher specificity due to the fact that several imaging-pathological correlation studies have provided supporting evidence for their association with the chronic active lesion phenotypes in MS. Despite this, recent studies have also confirmed that a high proportion of PRL is not persistent and would eventually disappear (Dal-Bianco *et al.*, 2021), thus reducing the sensitivity of this method.

In conclusion, this study suggests that SELs are a common finding and a subset of them can coincide with PRLs. Despite a modest association between PRLs and SELs, their combination, in association with the overall increase in lesion burden, could have a prognostic meaning and impact as a predictor of MS severity since disease onset.

6 Evolution patterns of the new lesions in primary-progressive MS

6.1 Introduction and aim of the study

The main cause of progressive disability in MS remains unknown. In progressive MS, brain lesions have been considered to play a relatively minor role, whereas, in the relapsing forms of MS, new lesions are the main cause of symptoms (Barkhof, 1999). However, pathological studies have demonstrated that there are chronic active lesions in progressive MS phenotypes, which would explain neurodegeneration (Prineas *et al.*, 2001). Therefore, it is important to identify MRI markers related to the lesions from their onset, evaluate how they dynamically evolve over time and understand their relation to the formation of chronic active lesions.

New lesions can be visualized *in vivo* at MRI and they represent those focal lesions at their onset usually recorded as a new hyperintensity in relation to a baseline scan on T2-weighted (including PD and FLAIR) images or as contrast-enhancing lesions on T1-weighted post-gadolinium images. These markers have been described in chapter 2 and they have been extensively used as primary (in phase II trials) or secondary outcome measures (in phase III trials) to evaluate treatment response in MS. The development of these MRI markers has emerged from the limitation in observing clinical changes in MS, as relapses can be undetected in the clinical context of disease progression or might be silent and difficult to record. A previous study has demonstrated that in relapse-onset MS over 80% of the between-trial variability in treatment effects on the clinical relapse is explained by the variability in treatment effects on new T2 lesions (Sormani *et al.*, 2009). Moreover, treatment effects on relapse can be predicted by treatment effects on lesion-related MRI outcome measures in phase II/III trials of the drug (Sormani and Bruzzi, 2013).

Despite the importance of new MRI lesions, there are several limitations to using them as markers, especially in progressive MS phenotypes. Indeed, the load of new T2 lesions is usually lower in progressive than relapse-onset MS, and there might be virtually zero new lesions appearing between interval scans. Moreover, manual

techniques to detect them are limited by the low sensitivity of the detection of new lesions and high intra- and inter-rater variability, leading to poor interobserver reproducibility. However, the use of automated image subtraction protocols, having optimal registration techniques through serial scan analysis, has been shown to overcome technical issues by providing good visualization and quantification of the fraction of new MRI lesions in longitudinal studies of MS patients.

The fraction of slowly expanding lesions (SELs) as opposed to non-SELs has been previously shown to represent a valuable volumetric MRI marker correlating with disability in both progressive and relapsing MS, and it is a surrogate for chronic inflammatory activity. In the previous chapters, the analysis of SELs was conducted in RRMS and SPMS through quantification of the deformation field, characterised by the Jacobian values, and confirming that there was positive expansion within SELs. However, the analysis was extended to the whole population of lesions without distinction between the lesions already present at the beginning of the study and newly formed lesions.

In this chapter, automatic detection of new lesions has been combined with the identification of SELs in a PPMS cohort from the INFORMS trial evaluating patients under placebo and fingolimod (FTY). The main objective was to study the evolution of the fraction of the new lesions into SELs, to analyse their deformation quantified by the Jacobian expansion, and whether this process was influenced by the treatment effect.

The overall aim of this study was to identify new lesions in PPMS and describe them in relation to lesion expansion. Specific objectives were: (1) to evaluate the numbers of new lesions which correspond to SEL versus non-SEL, (2) to investigate the distribution of new lesions and SELs in patients who received treatment versus placebo, (3) to confirm the relationship between lesion expansion, as measured quantitatively and through SELs, and clinical scores, and (4) to assess whether the expansion of the new lesions and SELs are affected by the exposition to the treatment.

6.2 Definition of the cohort

A cohort of suitable cases was retrospectively selected from the INFORMS trial (NCT 00731692), a multicentre, double-blind, placebo-controlled, parallel-group study involving 148 centres in 18 countries worldwide in PPMS comparing the efficacy on disease progression of Fingolimod (FTY) 1.25 mg or 0.5 mg versus placebo. The analysis was conducted at Queen Square MS Centre, University College London (UCL) through the Oxford Big Data Initiative (BDI) and the INFORMS trial was selected for the availability of a frequent MRI scanning schedule from screening and including yearly time points. The flow chart to select the cohort for the analysis of the current study of the expansion of new lesions is shown in **Figure 6-1**.

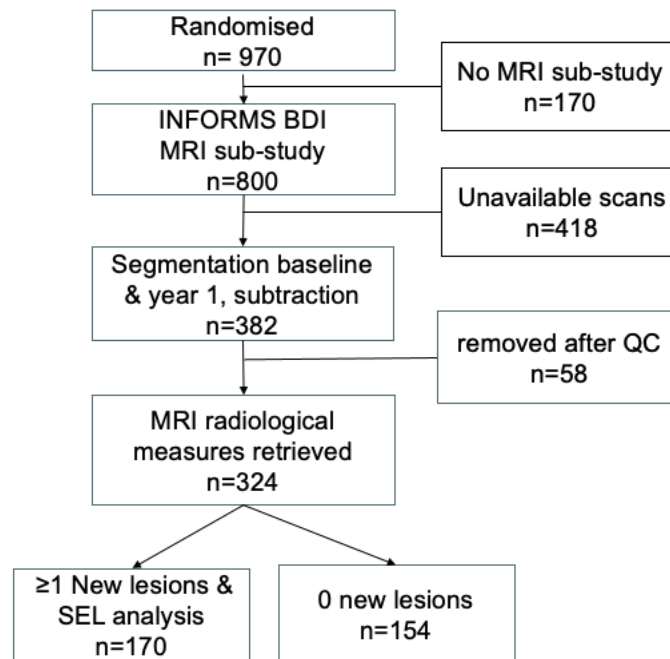


Figure 6-1. Flowchart showing the enrolment of subjects into the SEL study.

From the initial number of 970 patients randomised PPMS patients, 800 participated in the MRI sub-study and their scans were available for imaging analysis. The initial inclusion criteria to run the first part of this analysis were the following: availability of clinical/demographical data and both T1-weighted and FLAIR images at screening and at least up to the end of the trial (not required to participate in the extension phase). Therefore, each subject enrolled had fulfilled MRI scans in all the trial time-points (screening, year 1, year 2, and year 3). T1-weighted post-contrast images were

discarded due to the possibility of interference with the segmentation and registration. After applying these criteria, 382 patients were included for further analysis. An initial MRI analysis was conducted for all 382 patients. From this cohort, 58 patients were excluded due to issues in the segmentation phase (artefacts) or during the MRI deformation analysis. Thus, 324 patients were included in the second step of the analysis of new lesions. The final sub-cohort of 170 patients who had at least one new lesion at year 1, also called the PPMS 'active', were available for the analysis of the new lesion expansion, while the rest (n=154) were discarded as they had no new lesions. In total, 646 patients were excluded.

6.3 Methods

6.3.1 Data collection, trial information, clinical assessments

The data from the INFORMS trials were available as part of the Oxford BDI. Written informed consent was obtained from all subjects and the study was approved by the local research ethics committee. Fully anonymized clinical and MRI data were analysed at Queen Square MS Centre, Department of Brain Repair and Rehabilitation, UCL.

Patients were included in this analysis according to the INFORMS trial criteria (Lublin *et al.*, 2016), which are as follows: diagnosis of PPMS according to the 2005 revised McDonald criteria with 1 year or more of disease progression and two of the following criteria: positive brain MRI, positive spinal cord MRI, or positive CSF. Additional criteria included time of 2-10 years from first reported symptoms before study entry, evidence of disability progression documented by an increase in EDSS of 0.5 points or more in the past 2 years, objective evidence of disability measured by EDSS score of 3.5–6, pyramidal functional system score of 2 or more, and a 25FWT of less than 30 s.

Patients were initially randomly assigned (1:1) to receive either fingolimod (FTY) 1.25 mg or placebo once daily but after the decision to select the 0.5 mg dose for submission to regulatory authorities (November 2009), all patients on FTY 1.25 mg were switched

to FTY 0.5 mg. In this study, the differentiation was not considered and all patients who took either dose were defined as treated in comparison to the placebo group.

Demographic data available (age at baseline and sex) and clinical data were collected, including the following scores: Expanded Disability Status Scale (EDSS), Paced Auditory Serial Addition Test (PASAT) score, Nine Hole Peg Test (NHPT) measured in seconds, and Timed 25-Foot Walk (T25FW) also in seconds. Confirmed disability progression (CDP) at the end of the trial was defined as a binary measure to indicate the presence or the absence of clinical deterioration, as follows: 1-point increase in EDSS (considering the EDSS change from baseline to week-96) if the baseline score was ≤ 5.0 , or a 0.5-point increase if the baseline score was > 5.0 as previously described in other trials (Lublin *et al.*, 2016; Kappos *et al.*, 2018).

6.3.2 MRI acquisitions

All patients were scanned at baseline and yearly up to the third year (end of the trial) with the following acquisitions: 2D isotropic T1-weighted (T1) and 2D FLAIR both with 1x1x3 mm resolution and field of view 192x192x40 voxels. Due to the nature of the international multicentre trial, the characteristics of the MRI scanners were very diverse involving several machines and vendors at different field strength (1.5T and 3T) and software versions. Overall, the study involved 148 centres in 18 countries worldwide, which have been reported previously and they are available in the appendix of the published INFORMS publication (Lublin *et al.*, 2016).

6.3.3 MRI analysis: new lesions and tissue segmentation

The cohort for the MRI analysis of this study initially comprised 324 subjects, who followed the lesion and tissue segmentation phases. An automatic lesion segmentation approach was used based on a cascade of two 3D patch-wise convolutional neural networks (CNN), which has been shown to outperform other lesion segmentation techniques in previous studies (Valverde *et al.*, 2017). The segmentation was used to outline lesions on the FLAIR images at screening and at all subsequent time points. From the automatically outlined lesions, the lesion volumes were acquired and after using an automatic subtraction pipeline the new lesions at year 1 were computed and labelled. All images following this analysis were manually quality checked by three

experienced raters (myself, a medical student Zoe Mendelsohn, and a neuroradiology fellow Dr Weaam Hamed).

The MRI measures to obtain the global and regional brain volumes were obtained through Geodesical Information Flows (GIF) using the lesion-filled 2D T1 scans, (Cardoso *et al.*, 2015) providing the following metrics: normalised brain volume (NBV); white matter (WM), normalised cortical grey matter (CGM) and normalised deep grey matter (DGM) volumes; lesion-filling was used in this step using a multi-time-point patch-based method to avoid segmentation bias (Prados *et al.*, 2016). All those measures were assessed at screening and at the final time point (year 3), and the change was calculated as the subtraction between the final to the screening value. The Percent Brain Volume Change (PBVC) from baseline to year 3, as a measure of brain atrophy, was calculated using the Structural Image Evaluation using Normalization of Atrophy (SIENA) technique (Smith *et al.*, 2002).

6.3.4 MRI volumetric deformation analysis

From the cohort of patients who followed the initial MRI analysis, only those with at least one new lesion at year 1 (n=170), which were defined as ‘active PPMS’, entered into the deformation analysis phase on the segmented new lesions. The rest of the subjects who did not show any new lesions at year 1 were classified as ‘inactive’ PPMS and were discarded.

The deformation maps were computed through a non-linear registration of the T1-weighted scans up to year 3, as described in the previous chapter. Then, as an additional part of the pipeline, the Jacobian expansion value (across all the study intervals: screening to year 1, year 1 to year 2, year 2 to year 3 and screening to year 3) was computed within each labelled new lesion. In addition, all the new lesions were stratified in the SEL-derived categories (definite SELs, possible SELs, and non-SELs) as described in the previous chapters. A unique patient-specific value for the Jacobian expansion was retrieved as the mean of the sum of the Jacobian values of each lesion categorised according to the SEL type.

6.3.5 Statistical analysis

For the statistical analysis STATA version 16 was used and the significance reported at $p < 0.05$, while all the graphical displays for distributions were drawn using R. Initially, all the demographical variables were evaluated within the sub-cohorts as divided by the first and second analysis steps followed in this work. The demographical (sex and age at screening) and the clinical characteristics, i.e. EDSS (at screening, at final time point, and the EDSS change as the difference of the two) were analysed in the all trial randomized patients ($n=970$), and the cohort of active PPMS ($n=170$) who had ≥ 1 new lesions and the inactive PPMS ($n=154$), who had no new lesions at year 1 compared to screening.

At the lesion level, a descriptive analysis was performed for the population of the new lesions and they were divided in each SEL-derived lesion types. Then, lesion counts, and volumes were analysed at the patient level calculating the sum of the number and volume of the respective lesion types. Each specific lesion volume type was log-transformed (base 10) in order to meet the normality assumption. The Wilcoxon signed rank test assessed the differences between the counts of the different types of lesions (as non-normally distributed) while the t-test or a linear model was used for the normally distributed variables.

6.4 Results

6.4.1 Clinical-demographic characteristics

Demographics, clinical characteristics and radiological parameters at baseline and their longitudinal changes within the active and inactive sub-cohorts, and the patients excluded for incompatibility with the MRI inclusion criteria are reported in **Table 6-1**. **Table 6-1**. Demographic and clinical characteristics

In the cohort of active PPMS patients (with ≥ 1 new lesions), EDSS, T25FW and PASAT significantly increased, thus signifying a worsening, from screening to the final follow-up (Wilcoxon signed-ranked test, $p < 0.001$), and 42% of them developed

disability progression. The mean NHPT population did not increase from screening to final follow-up (Wilcoxon signed-ranked test, $p=0.1659$).

No differences were found with regards to the clinical and demographical characteristics between the active and the inactive populations. A higher EDSS at screening was found in the discarded for MRI criteria population compared to the active subgroup ($p=0.002$), but not at year 3. In addition, in the discarded population higher NHPT ($p=0.01$) and 25FWT at screening ($p=0.002$) were found.

Table 6-1. Demographic and clinical characteristics

	Active ≥ 1 new lesion (n=170)	Inactive 0 new lesions (n=154)	Not included in the analysis (n=646)	p value[°]
Female n [%]	95 [56%]	72 [47%]	302 [47%]	$p=0.096$
Age at Screening, median [range]	48 [27 – 64]	48 [24 – 66]	49 [24 – 67]	$p=0.089$
EDSS median [range] At screening At year 3	4.0 [3.0 – 6.5] 5.0 [2.0 – 8.0]	4.5 [3.0 – 6.5] 5.0 [2.0 – 8.0]	4.5 [2.5 – 6.5] 6.0 [0 – 10.0]	$p=0.002$ $p=0.071$
EDSS change*, mean [SD]	0.47 [1.01]	0.34 [1.03]	0.46 [1.06]	$p=0.900$
NHPT (sec), mean [SD] At screening At year 3	26.3 [7.0] 29.7 [15.4]	27.7 [10.16] 32.6 [21.5]	29.7 [14.4] 31.0 [16.6]	$p=0.011$ $p=0.526$
T25FW (sec), mean [SD] At screening At year 3	8.5 [13.8] 12.6 [11.2]	8.3 [4.5] 16.6 [26.3]	9.1 [5.4] 12.5 [12.6]	$p=0.002$ $p=0.983$
PASAT score, mean [SD] At screening At year 3	42.3 [12.2] 49.2 [12.4]	44.3 [12.4] 51.5 [10.6]	40.6 [13.8] 48.9 [12.1]	$p=0.256$ $p=0.547$
Number [%] with CDP[§]	71 [42%]	61 [40%]	198 [31%]	$p=0.006$
Number [%] on FTY	90 [53 %]	77 [50%]	316 [49 %]	$p=0.464$

*EDSS change defined as the difference between EDSS at end of trial (year 3) and EDSS at screening [§]CDP defined as a 1-point increase in EDSS if the score at screening was ≤ 5.0 , or a 0.5-point increase if the score at screening was > 5.0 .

[°]chi-square test (for the categorical variables) or Wilcoxon signed-ranked test.

Abbreviations: EDSS=expanded disability status scale, NHPT=nine-hole peg test, T25FW=timed 25-foot walk test, PASAT=paced auditory serial addition test, CDP=confirmed disability progression

6.4.2 MRI characteristics

A descriptive analysis of all the MRI measures available after the first step analysis is presented in **Table 6-2**. All the MS-specific radiological measures were retrieved and

analysed in the group of PPMS patients who followed the first step of the MRI analysis (n=324), and the differences between the group of active and inactive were analysed. The lesion counts are referred to as the overall lesion number obtained through the automatic segmentation of the FLAIR images after the manual check was completed. Active PPMS patients had a higher lesion count compared to the inactive patients at screening (median 27 and 22, p=0.007) and after one year (median 25 and 19, p<0.001). Similarly, the lesion volume in active patients was also significantly higher both at screening and at year 1 (p<0.001). Regarding the brain and regional volumes, no significant differences were identified in all the MRI measures assessed, except for PBVC which declined more steeply in the active sub-cohort, indicating a higher brain atrophy rate in active PPMS patients.

Table 6-2. MRI measures in the active and inactive PPMS cohort

	Active PPMS ≥ 1 new lesion (n=170)	Inactive PPMS 0 new lesions (n=154)	p value*
Lesion count at screening (n), median [IQR]	27 [19 – 36]	22 [16 – 31]	0.007
Lesion volume at screening (ml), median [IQR]	8.1 [4.6 – 16.7]	5.6 [2.9 – 10.2]	<0.001
New lesion count at year 1 (n), median [IQR]	3 [2 – 5]	0 [0]	/
New lesion volume at year 1 (ml), median [IQR]	0.10 [0.05 – 0.23]	0 [0]	/
NBV (ml), mean [SD] at screening	1472.4 [84.3]	1460.8 [84.4]	0.217
at year 3	1453.8 [84.4]	1443.7 [86.4]	0.322
NBV change (ml), mean [SD]	-10.6 [29.8]	-6.6 [33.5]	0.294
CGM volume (ml), mean [SD] at screening	768.4 [52.8]	759.4 [51.7]	0.125
at year 3	752.8 [51.8]	746.3 [49.8]	0.280
CGM change (ml), mean [SD]	-8.7 [20.5]	-8.4 [23.4]	0.903
DGM volume, mean [SD] at screening	45.8 [3.3]	46.2 [3.5]	0.203
at year 3	45.4 [3.5]	45.6 [3.5]	0.718
DGM change (ml), mean [SD]	-0.20 [1.7]	-0.1 [1.9]	0.740
PBVC screening - year 3, mean [SD]	-0.63 % [1.42]	-0.28 % [1.32]	0.032

Abbreviations: NBV=normalised brain volume, CGM=cortical grey matter, DGM=deep grey matter, PBVC=percent grain volume change

*Univariate linear regression, adjusted for age and gender.

6.4.3 Descriptive analysis of new lesions and SELs, lesion level

556 new lesions at year 1 were obtained after the subtraction pipeline was applied on the lesion masks, among the active cohort (n=170). The mean volume for the new lesions was 0.1 ml (SD=0.2), thus consisting of mostly small size lesions, as the confluent ones at the following time points were not computed. After applying the SEL detection algorithm, the types of lesions were retrieved and the counts and proportions out of the totals of new lesions and their mean volumes are described in **Table 6-3** and **Figure 6-2**. The mean volume for a new lesion was ~0.1 ml. After applying a mixed-effects model to account for the fact that each lesion belonged to a particular subject (nested design), no differences in the size of the lesions were found between the three SEL-derived categories.

Table 6-3. Descriptive analysis of the SEL-derived lesion types and volumes

Lesion type		Total lesions	Percentage of the new lesions (%)	Mean volume, ml (SD)
New lesion		556	100%	0.10 (0.24)
SEL category	Non-SEL	350	63%	0.12 (0.28)
	Possible SEL	67	12%	0.07 (0.10)
	Definite SEL	139	25%	0.07 (0.07)

Abbreviations: SEL=slowly expanding lesions

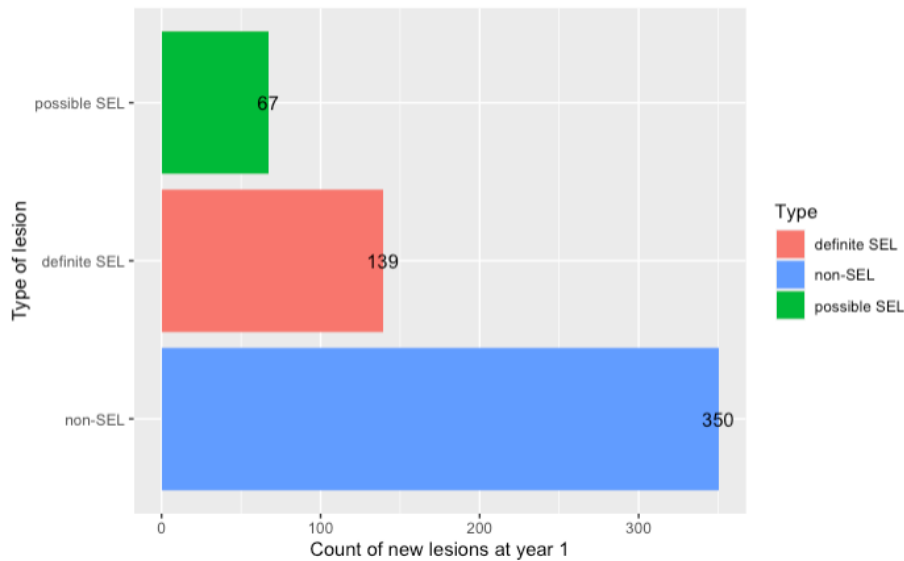


Figure 6-2. Bar plot showing the distribution of the new lesions (year 1) by type. The bar chart shows the total counts of the new lesions retrieved by subtraction (at year 1), divided in the categories as obtained with the SEL algorithm.

6.4.4 Descriptive analysis of the Jacobians

The mean Jacobian expansion value (or Jacobian) at the lesion level in the first trial interval (year 1 \rightarrow 2) was 0.05 (SD=0.04), while the mean within the second interval (year 2 \rightarrow 3) was 0.02 (SD=0.06). Overall, the mean Jacobian computed from the start to the end of the observation time (year 1 \rightarrow 3) was -0.01 (SD=0.05).

Then, the Jacobian values were categorised and were described according to the SEL-derived categories, after applying mixed-effects models accounting for the subject level and the volume of the lesions, as shown in **Table 6-4** and **Figure 6-3**. The Jacobian in the interval year 1 \rightarrow 3 was significantly higher within the definite SELs as compared to all the other lesion types (adjusted difference with the possible SEL -0.03 95% CI -0.05 to -0.01, $p=0.002$; with the non-SELs -0.12 95% CI -0.13 to -0.10, $p<0.001$). Considering the first and second trial intervals, the Jacobians were consistently positive only within the definite SELs.

Table 6-4. Jacobian expansion in the SEL-derived categories

Lesion type		Jacobian, mean [95% CI] year 1 → 2	Jacobian, mean [95% CI] year 2 → 3	Jacobian, mean [95% CI] year 1 → 3
SEL category	non-SEL (n= 350)	-0.06 [-0.08, -0.05]	-0.04 [-0.06, -0.03]	-0.06 [-0.07 – 0.05]
	possible SEL (n= 67)	0.03 [0.01, 0.04]	-0.01 [-0.02; 0.01]	0.03 [0.01 – 0.04]
	definite SEL (n=139)	0.06 [0.04, 0.07]	0.05 [0.04; 0.06]	0.06 [0.04 – 0.07]

Abbreviations: SEL=slowly expanding lesions

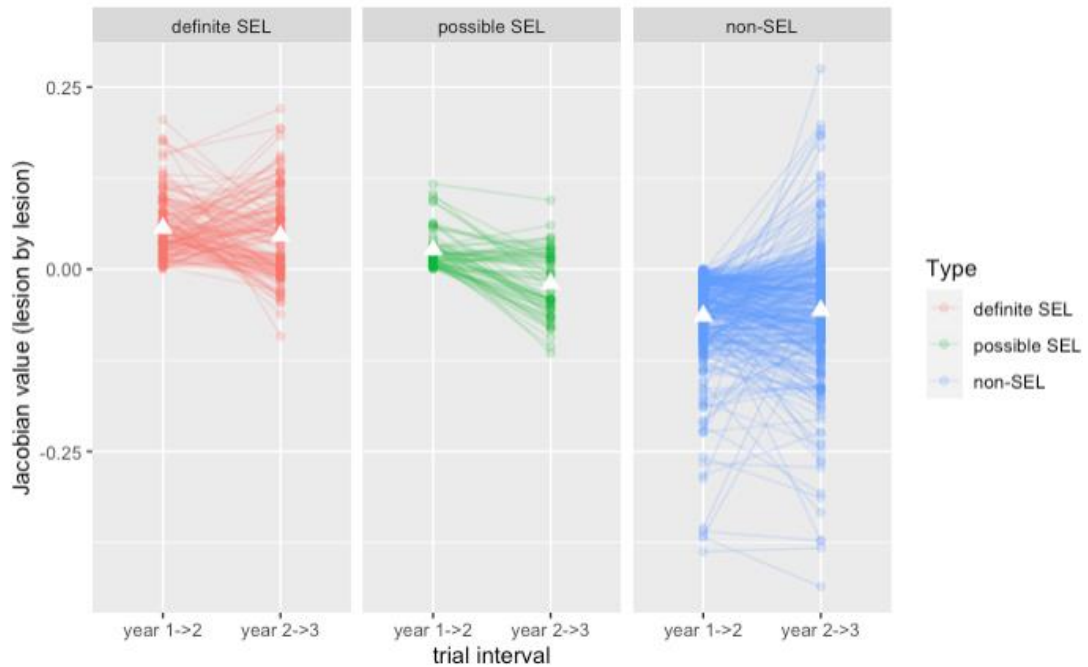


Figure 6-3. Jacobian expansion in the SEL-derived lesion types

The line plots are showing the Jacobian values at the lesion level of the three lesion types as derived from the SEL algorithm, as measured in the first time interval (year 1 to 2) and the second interval (year 2 to 3), respectively.

6.4.5 Descriptive analysis of SELs at the patient level

A descriptive analysis was carried out at the patient level, by summing up all the lesions as classified by their type (new lesions and the SEL-derived categories) for each subject enrolled in the active PPMS group (n=170). In **Table 6-5** all the counts

and the volumes are reported, and for the SEL-derived categories, the proportions of each measure calculated out of the new lesion volume were computed as percentages. As a result, out of a median of 2 new lesions per patient, which corresponded to a mean volume of 0.33 ml, 15% was occupied by the definite SELs and 9% by the possible SELs. An example of a patient with a new lesion detected as a SEL is shown in **Figure 6-4**.

Table 6-5. Patient-level descriptive analysis of the new lesions and the SEL categories

Lesion type		Count (n), mean; median [range]	Volume (ml), mean; median [SD]	Percentage of the new lesion volume [%]
New lesions (FLAIR)		3.3; 2 [1 – 31]	0.33 [1.50]	NA
SEL category	non-SEL	2.06; 1 [0 – 29]	0.25 [1.45]	76%
	possible SEL	0.39; 0 [0 – 8]	0.03 [0.13]	9%
	definite SEL	0.82; 0 [0 – 5]	0.05 [0.10]	15%

Abbreviations: SEL=slowly expanding lesions

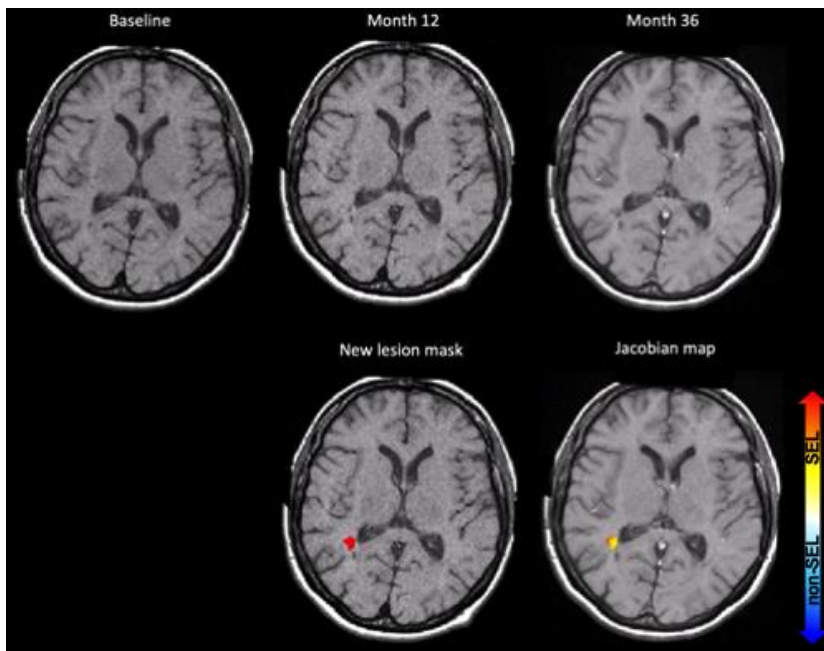


Figure 6-4. Example of a new lesion corresponding to a SEL

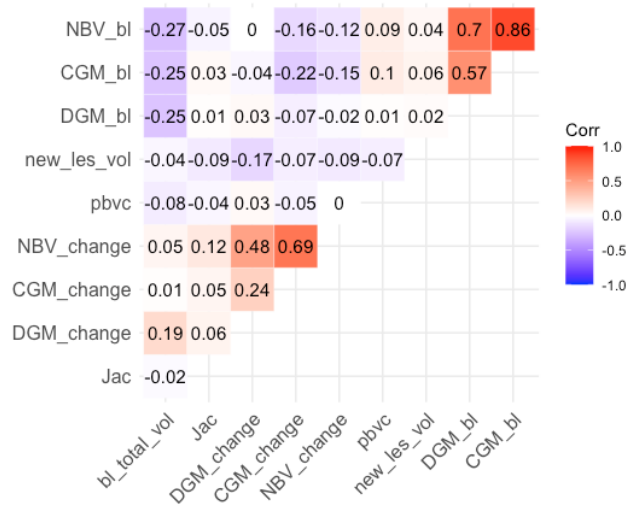
In the first row the images from left to right are: baseline, year one and year two T1-weighted scans from a subject enrolled. In the bottom row and from left to right, the mask of a new lesion at year 1 is superimposed on the corresponding T1-weighted scan and the deformation map shows that the new lesion corresponds to a SEL.

6.4.6 Association between Jacobians and SELs with MRI metrics

The cross-sectional associations between the mean Jacobians and the other relevant MRI measures were analysed cross-sectionally through correlation coefficients (Pearson or Spearman depending on the normality of the variables). No significant

associations were found between the mean Jacobians and PBVC, or the volumes of lesions at screening and their changes over time, as shown in the correlation matrix (Table 6-6). When the changes in all the global and regional brain volumes were analysed with the SEL volumes, no significant associations were found.

Table 6-6. Correlation Matrix showing the correlation coefficients (Spearman) between all the MRI radiological measures included in the study.



Abbreviations: NBV_bl = normalised brain volume at baseline, CGM_bl = cortical grey matter volume at baseline, DGM_bl= deep grey matter at baseline, new_les_vol= new lesion volume, pbvc = percent brain volume change, NBV_change = normalised brain volume change from baseline to year 3, CGM_change = cortical grey matter volume change from baseline to year 3, DGM_change = deep grey matter volume change from baseline to year 3, Jac = Jacobian expansion value

6.4.7 Cross-sectional and longitudinal associations between Jacobian and SELs with clinical measures

A cross-sectional association analysis was performed by computing the correlations between the Jacobians, the SEL-derived counts and volumes with the clinical measures (i.e. EDSS and the mean T25FW, NHPT and PASAT). With regards to the Jacobian values and the SEL-derived volumes, no associations were found with any of the explored clinical or demographic measures, both at screening and at the final time point (year 3). However, a significant mild positive association (Pearson $r=0.18$, $p=0.01$) and the EDSS at final follow-up was found with the SEL candidates (i.e. the sum of the definite SELs and the possible SELs). Then, a longitudinal analysis to

evaluate the effects on the clinical scores over time derived from the Jacobian and SELs was evaluated using mixed-effect models. As a result, no significant changes in the clinical scores were found in association with the Jacobian (**Table 6-7**). Using as explanatory variables SEL log-volumes, a worsening of the EDSS was associated with both the candidate and definite SELs ($p < 0.001$). The longitudinal increase of the T2FW over time, as a measure of a reduction in the walking performance, was associated with a higher candidate SEL volume ($p = 0.034$), as shown in **Table 6-7**. Finally, in logistic regression the risk for patients to reach CDP status was associated with increased SEL volumes (for candidates SEL $p = 0.038$ and for definite SEL $p = 0.028$).

Table 6-7. Mixed-effect regression models to investigate association between clinical scores and Jacobians and SEL volumes

	Interaction term: beta (95% CI), p value		
Dependent variable	Jacobian year 1 → year 3 (new lesions) beta or OR (95% CI) p value	Candidate SEL volume beta or OR (95% CI) p value	Definite SEL volume beta or OR (95% CI) p value
EDSS	0.03 (-0.58, 0.64), p=0.922	1.2 (0.7; 1.6), p<0.001	1.7 (1.0; 2.4), p<0.001
NHPT	0.94 (-13.05, 14.92), p=0.896	8.7 (-0.9, 18.3), p=0.079	15.0 (-3.2; 33.2), p=0.107
T25FW	-1.72 (-9.38, 5.93), p=0.659	6.1 (0.5, 11.7), p=0.034	8.9 (-1.3, 19.0), p=0.086
PASAT	4.21 (-3.10, 11.52), p=0.241	0.1 (-5.4, 5.6), p=0.969	4.2 (-6.1, 14.6), p=0.424
CDP	0.04 (0.001, 28.7), p=0.331	39.3 (1.2, 1251.9), p=0.038	81.89 (1.6, 4163.9), p=0.028

Abbreviations: EDSS=expanded disability status scale, NHPT=nine-hole peg test, T25FW=timed 25-foot walk test, PASAT=paced auditory serial addition test, CDP=confirmed disability progression

6.4.8 Conventional MRI measures and treatment effect

To evaluate the treatment effect on the radiological conventional metrics, the MRI measures (at baseline), brain atrophy values (i.e. PBVC) and the new lesion count/volumes at year 1 obtained through the lesion and brain segmentations were investigated in the active PPMS cohort, after grouping patients in the treated (n=90)

versus the non-treated (n=80), as shown in **Table 6-8**. No significant differences were identified in any of the radiological measures, except for the new lesion counts at year 1 which were lower within the treated patients compared to the non-treated (3 versus 2, p=0.037 Mann-Whitney test). However, the volume of new lesions at year 1 were not significantly different in the two groups classified by the treatment status.

Table 6-8. MRI measures in treated and non-treated patients of the active PPMS sub-cohort

	Treated (n=90)	Non-treated (n=80)	P value*
Baseline lesions, count (n), median [IQR]	25 [17; 36]	28 [21; 36]	0.119
New lesions at year 1, count (n), median [IQR]	2 [1; 4]	3 [2; 6]	0.037
Baseline lesion volume, median [IQR], in ml	8.96 [4.23; 16.79]	7.70 [4.71; 16.52]	0.993
New lesion volume at year 1, median [IQR], in ml	0.10 [0.06; 0.22]	0.11 [0.05; 0.35]	0.299
NBV at baseline, mean [SD], in ml	1472.5 [87.8]	1472.4 [80.7]	0.869
CGM volume at baseline, mean [SD], in ml	769.4 [56.4]	767.1 [48.8]	0.891
DGM volume at baseline, mean [SD], in ml	45.8 [3.2]	45.7 [3.4]	0.724
PBVC from baseline to year 3, mean [SD]	-0.53% [1.38]	-0.55% [1.50]	0.785

Abbreviations: NBV=normalised brain volume, CGM=cortical grey matter, DGM=deep grey matter, PBVC=percent grain volume change

6.4.9 Jacobian, SELs and treatment effect

The analysis of the Jacobian and the SEL-derived measures was extended to include the effects on the active cohort by assessing the differences in the treated versus the non-treated patients, which is reported in **Table 6-9**. In addition, mixed-effect models were also run to analyse the Jacobian values at the lesion level, by considering the subject's nested structure. The mean Jacobian of all the new lesions did not show any significant difference between the treated and the non-treated group, both at the patient and the lesion level. The definite SEL count and SEL volume were both significantly

lower in the treated cohort as compared to the non-treated group. In detail, the median definite SEL count in treated versus non-treated patients was 0 and 1 respectively (Mann-Whitney test, $p=0.018$), and the median definite SEL volume was 0 versus 0.02 ml (unpaired t-test, $p=0.011$).

Table 6-9. Differences in SEL-derived measures between the treated and non-treated

	Treated (n=90)	Non-treated (n=80)	P value*
Jacobian, median [IQR]	-0.02 [-0.03, 0.02]	-0.01 [-0.03, 0.01]	$p=0.615$
Definite SEL, count (n), median [IQR]	0 [0; 1]	1 [0; 1.25]	$p=0.018$
Possible SEL, count (n), median [IQR]	0 [0; 1]	0 [0; 1]	$p=0.136$
Non-SEL, count (n), median [IQR]	1 [1; 2]	1 [1; 3]	$p=0.608$
Definite SEL volume, median [IQR], in ml	0 [0; 0.05]	0.02 [0; 0.09]	$p=0.011$
Possible SEL volume, median [IQR], in ml	0 [0; 0.02]	0 [0; 0.02]	$p=0.296$
Non-SEL volume, median [IQR], in ml	0.06 [0.03; 0.12]	0.07 [0.02; 0.18]	$p=0.741$

*Mann-Whitney test was used for the non-normal (count variables) while the unpaired t-test was used for the volumes (log-transformed). Abbreviations: SEL=slowly expanding lesions

6.5 Discussion

This work aimed to analyse on MRI the fraction of new lesions in PPMS and follow their evolution from the formation up to the end of the 3-year trial observation. The deformation longitudinal analysis applied to the subgroup of the new lesions allowed a detailed assessment of their expansion. Thus, the main evidence of this work is that new lesions exhibit a growth phase in the first trial interval. In addition, with this analysis, there is some evidence that Fingolimod has a benefit to the reduction of accumulation of SELs in PPMS.

In this study, patients included had to fulfil the MRI inclusion criteria including the availability of at least three follow-up scans after screening (minimum of four sessions) to follow then the image registration and subtraction phase. Interestingly, after

applying those techniques, 52% (170/324) of patients were found to have at least one new lesion. This was a slightly higher percentage compared to the numbers identified in the publication of INFORMS trial study (Lublin *et al.*, 2016). The authors reported that a percentage between 20 to 40% (on the Fingolimod and on the placebo arm, respectively) were not free of new or newly enlarging T2 lesions at the end of the study. This difference might be related to the automatic segmentation technique, characterised by a higher sensitivity in detecting the new lesions as compared to the fully manual detection. In addition, that analysis used T2 images while in this work FLAIRs were used, which could also have accounted for the higher detection rate.

Patients having at least one or more new lesions, also defined as active PPMS, had different radiological measures with higher lesion load compared to the inactive population. This might be related to the fact that, also in PPMS, there is a sub-group of patients who develop a higher degree of inflammatory activity. This activity is considered a limited phenomenon compared to the other MS phenotypes, despite data showing that even with a low white matter lesion count a high cortical lesion load can be found in PPMS (Calabrese *et al.*, 2009).

The fraction of active patients (n=170) had a median of 3 new lesions, with an interquartile range from 2 to 5. This was different from in the initial INFORMS trial investigation, in which the mean count of new/enlarging T2 lesions (obtained with fully visual detection) reached counts from 0.13 to 0.50, in the treated and the placebo cohort, respectively. Thus, the subtraction technique used in this study might have an increased sensitivity in new lesion detection, as expected for an automatic method.

Interestingly, the active PPMS sub-cohort showed higher lesion counts and volumes (both at screening and at year 1) and brain atrophy as assessed by a reduction in PBVC compared to the inactive sub-cohort, thus demonstrating that those patients have a profile of not only sustained inflammatory activity but also a combination with neurodegeneration. Despite that, no changes were found in the global and regional brain volumes as assessed cross-sectionally between the active and inactive sub-cohorts.

The presence of relevant inflammatory activity in progressive MS has been recently described in pathological studies, which demonstrated that it is common to identify a high lesion load at the time of autopsy (Luchetti *et al.*, 2018). However, previous research using conventional MRI measures (i.e. T2-weighted manual lesion evaluation) showed that on average PPMS have a lower lesion load compared to relapsing MS (Thompson *et al.*, 1991). Despite that, in the short-term and at diagnosis, contrast-enhancing lesions can be identified between 14% (M. Filippi *et al.*, 2001) up to ~40% (Ingle *et al.*, 2005) of PPMS patients, which have also been associated with a worse future prognosis (Ingle *et al.*, 2005). However, long-term MRI longitudinal studies were not able to show that the total brain lesion load is a predictor of the long-term clinical outcomes in PPMS (Khaleeli *et al.*, 2008).

More recently, trials have demonstrated that inflammatory markers at MRI are also relevant in PPMS. For example, in the ORATORIO trial (evaluating the efficacy of Ocrelizumab) the number of new/enlarging T2 lesions reached up to ~4 per patient in the placebo population. From the perspective of the brain-related volume changes from previous data the PBVC reduction in PPMS is substantial (from -0.73% up to -1.53% in the INFORMS and ORATORIO trials), accompanied by more severe neurological deficit (De Stefano *et al.*, 2010) and greater rates compared to RRMS. In this study, a substantial PBVC reduction of up to -0.60% was found. Overall, those findings again indicate that there is substantial inflammatory and neurodegenerative activity detected at MRI in PPMS in contrast with the studies conducted in the past.

As a novel addition to this chapter, a quantitative measure of the deformation within each lesion was provided by computing the Jacobian determinant within the spatial area of each individual lesion. The results of this analysis have demonstrated that an expansion tendency is characteristic of the first stage of lesion formation, as demonstrated by higher Jacobian values in the first trial interval (0.02 up to 0.06) compared to the second one (-0.02 up to 0.04). This pattern can reflect the fact that gliotic or atrophying mechanisms leading to an involution, and compression, are supposed to follow the acute phase of new lesion formation in combination with remyelinating processes that might impact a stabilisation of the expansion and possibly lead to a future lesion shrinkage.

The new lesions assessed were categorised using the SEL algorithm presented in the previous chapters. Here, in PPMS, the relative proportions of SELs (possible and definite as a sum, or SEL candidates) reached up to 37% of the lesion counts. At the patient level, 24% of the new lesion volume was occupied by possible and definite SELs. In chapter 4, in the RMS cohort studied including a more heterogeneous cohort with a longer follow-up (up to 6.5 years), a similar count of SELs was found (up to 6 SELs, and up to 37% of the total lesion volume). In the recently published work by Elliott et al., the mean SEL number reached 6.3 in the ORATORIO cohort, including PPMS, while this figure was 4.6 in the pooled OPERA I and II trials of RRMS (Elliott, Wolinsky, *et al.*, 2019). As expected for the criteria used in the SEL algorithm, the highest Jacobian values were found within the definite SELs. It is important to notice that those results only refer to active PPMS, therefore lower percentages of SELs or reduced Jacobian values would be expected if the analysis was extended to the non-new lesions and to the inactive sub-cohort. Overall, these data stand for supporting evidence of a substantial presence of chronic active lesions in the form of SELs, in line with data supporting a role of chronic inflammatory activity in the progression evolution in PPMS.

In the association analysis including all the radiological measures evaluated, the Jacobian had a negative correlation with the global brain and the deep grey matter volumes. This might imply that a higher expansion pattern in the MS lesions is a characteristic of patients that develop also an initial degenerative process, as shown by the correlation with lower brain volumes.

Finally, the mixed models to investigate the relationship of the clinical scores confirmed the results of the previous chapter by indicating a role for SELs in predicting disability progression. The results of this part of the analysis suggest that the increase in SEL volumes was related to a higher global disability and walking function, as measured by the EDSS and T2FW, respectively. Despite that, the Jacobian was not able to explain any of the assessed clinical scores. Therefore, it can be postulated that there are multiple aspects related to lesion expansion, and their combination could contribute to explain the complexity of disease progression in PPMS.

As a further step assessed in this chapter, the assessed novel MRI measures were investigated as a function of the treatment effect. The new lesions count was higher in the placebo population, similar to the results of the trial demonstrating the impact of Fingolimod on the reduction of the new or enlarging T2 lesions. In addition, a major finding consisted of the identification of a higher volume and count of definite SELs within the placebo compared to the treated group. Those observations are new supporting evidence for Fingolimod efficacy in the reduction of chronic active inflammation. In previous trials, only a limited effect on the MRI measures was found before by exposition to disease-modifying treatments in PPMS. For example, Glatiramer Acetate was only able to temporarily reduce the counts of contrast-enhancing lesions or T2 lesion volume (M. Filippi *et al.*, 2001). More recently, Rituximab and Ocrelizumab have shown a steady effect on reduction of those MRI measures in PPMS trials (Hawker *et al.*, 2009; Elliott, Belachew, Jerry S Wolinsky, *et al.*, 2019). Moreover, Ocrelizumab demonstrated an effect on the reduction of T1-hypointense volume associated to SEL (Elliott, Belachew, Jerry S. Wolinsky, *et al.*, 2019), as a measure of the tissue damage within the areas identified as chronically active. Despite that, in the present work it was not possible to identify a change in the Jacobian between treated and non-treated populations. Overall, evaluating SELs and other MRI markers for the chronic active lesions in MS would be needed as a future tool to use in the clinical practice context to evaluate treatment response in progressive MS forms, which would complement the use of other biological and clinical markers for disease progression.

As a first and main limitation of this work, the unavailability of scans for all trial time points allowed to study only a subgroup of the whole trial cohort (324/850), due to incompatibility with the MRI inclusion criteria. In addition, there was inhomogeneity of the scans, as the method required at least two modalities for each session, including the FLAIR and T1-weighted images, which were not available for certain patients for each of the time points. Then, the new lesions as computed by the pipeline had some artefacts related to the misidentification of hyperintense areas close to the cerebral ventricles, which are well-known false positives found in every automatic segmentation technique (García-Lorenzo *et al.*, 2013). Moreover, the evaluation of the Jacobian determinant was limited by the presence of the artefactual identification of

areas recognised as lesions but in the vicinity of the boundaries to the skull or to the ventricles, which could have affected the overall quantification of the measure.

As a future perspective, the successful segmentation technique used in this work for the identification of new lesions in MS, should then be applied to other samples and compared to manual techniques in order to then evaluate a standardisation of the method to translate to clinical practice. Moreover, further evaluation is warranted with regards to the evaluation of the Jacobian to clarify its role as a quantitative measure, with the need to standardise the measurement and apply this as an outcome for research trials. In addition, the importance of understanding the implications of this work, such as the evolution of the lesions in MS from their onset, would need to be coupled with the biological evaluation, such as the analysis from the animal models. The combined MRI deformation and pathobiological studies could help to evaluate whether there is a determinate mechanism implied in the formation and maintenance of chronic active lesions.

As in the treatment effect analysis, there was a sign of Fingolimod effectively reducing the presence of SELs. As a future work other trials assessing alternative DMTs, and using other MRI markers of chronic inflammatory activity, should be analysed to replicate and discuss the findings.

Overall, this work has shown that PPMS is characterized by a frequent occurrence of new lesions, which show a pattern of growth of their volume in the short term, by analysing their deformation longitudinally. Fingolimod might be useful in reducing the presence of chronic active lesions and the impact on PPMS clinical future outcomes.

7 Discussion, conclusion, and future directions

7.1 Thesis overview

A major need for the clinicians who work for people with multiple sclerosis (MS) is to identify useful biomarkers for investigations of the pathogenetic mechanisms, prognostication and treatment response evaluation. In MS clinical practice more than fifteen disease-modifying therapies (DMTs) are approved and new treatments, now under trial evaluation, will become available to fight disease progression.

In this thesis, a study was conducted to evaluate the heterogeneity of some recently developed radiological markers for chronic active lesions, which represent a key target responsible for MS progression. This work consisted of the application of several imaging techniques to a wide range of cohorts of MS patients. The specific goals were (1) to contribute to the development and application of an advanced volumetric MRI analysis pipeline to extract the Slowly Expanding Lesions (SELs) in a pilot cohort; (2) to extend the SEL analysis to a trial cohort of secondary-progressive MS patients and to evaluate their association with markers of neurodegeneration and their clinical relevance in terms of physical and cognitive disability; (3) to assess alternative markers for MS progression by evaluating the persisting black holes (PBHs) and the paramagnetic rim lesions (PRLs); (4) to extract the fraction of new lesions from their formation and to analyse their pattern of evolution to the chronic active stage.

As a first step, an in-depth review of the literature was conducted, focused on the imaging markers for chronic active lesions. The relevance of this topic has been consolidated by recently published research providing evidence that chronic active lesions are common in histopathological MS studies, and they contribute to disability. In this part, as outlined in the first two chapters, together with the general current knowledge of MS from a clinical and pathobiological perspective, more widely available imaging markers in use for MS research and clinical practice were reviewed.

One of the main works was to conduct a pilot study to add substantial methodological elements to the existing literature on SELs. The pipeline to compute SELs was

optimised and firstly applied in an academic trial setting involving people with secondary-progressive MS, then this was extended to the whole population of the trial. Currently, the gold standard for markers of inflammatory activity in MS clinical practice and trial evaluations has been the manual acquisition of new or enlarging T2/FLAIR lesions (Fahrbach *et al.*, 2013). However, in the last decade, there was an exponential increase in automatic detection techniques (García-Lorenzo *et al.*, 2013). SELs have been demonstrated to be a feasible marker, as it is possible to extract with high precision the fraction of MS lesions that manifest a tendency of constant and peripheral expansion. This initial descriptive analysis contributed to providing insights into the pathophysiological processes occurring within chronic active lesions. Their individual volumes and spatial localisation were assessed, and the analysis showed that SELs are generally bigger than other lesions and are located preferentially in the periventricular areas. Subsequently, SEL microstructure was estimated through the magnetization transfer ratio (MTR), whose reductions compared to the other lesions suggested a more extensive neuro-axonal loss, as a manifestation of ongoing tissue damage. Furthermore, SELs have been related to brain atrophy, thus implying a close link with a global neurodegenerative process and they were associated with MS progression, as assessed by several clinical scores of physical and cognitive disability.

In the following project, my work has contributed to the current literature on this topic towards the characterisation at MRI of the chronic active lesions from disease onset in the early disease phenotype, the relapse-onset MS (RMS). Moreover, the application of SELs as markers for chronic active lesions was extended to a retrospective observational cohort, outside of the trial context to understand the application in a real-life context. With a heterogeneous follow-up and time to the latest scan reaching up to 12 years, it was possible to detect SELs, thus representing a reproducible technique. In addition, the relevance of this marker has been reinforced by the nature of an international multi-centric design, involving multiple types of sequences and scanners. A significant association between SELs and clinical disability (i.e. the Expanded Disability Status Scale – EDSS) and a higher risk to reach confirmed disability progression (CDP) were similarly found in this analysis. As a continuation of the work, I contributed to the evaluation of the structural damage within MS lesions by evaluating the T1 intensity values within those lesions and focusing on another marker, the persisting black holes (PBHs). This analysis was based on the evidence from

previous literature on the importance of T1 signal reduction, as a marker of neuro-axonal loss in MS (Van Waesberghe *et al.*, 1999). With this work, a relevant longitudinal decrease in T1 intensity was found within the SELs compared to the other lesion types. Furthermore, PBHs computation, assessing longitudinally the T1 hypointensity of the lesions, was automatized for future application in trials and clinical practice. Interestingly, positive moderate associations between SELs and PBHs have been observed (correlation coefficient reached values up to +0.53), outlining the importance of the classification of subtypes of lesions in MS, through the evaluation of their volumetric and structural characteristics together.

The project has progressed further to the analysis of other *in vivo* markers of chronic active lesions, by including an evaluation of the paramagnetic rim lesions (PRLs), one of the main alternative markers to SELs. The results reported that both markers are frequently encountered in MS since early disease onset, with SELs substantially outnumbering the PRLs. Interestingly, for a lesion, being classified as SEL was associated with a higher possibility of also being a PRL. There was some evidence suggesting an association between age and disease duration, which are known determinants of worse outcomes, with the SEL-derived measures, thus implying that those markers could similarly be prognostic factors. Overall, more than half of the patients had a combination of the two markers (called PRL+SEL+ status) and the group of patients with this condition had a higher total lesion load. Such results were expected, in consideration that both markers were associated with an increased lesion burden, as a manifestation of the presence of inflammatory activity. Nonetheless, these results imply that there might be a tendency for accumulating SELs, accompanied by a concomitant increase of PRLs. This could represent two converging factors of the evolution of a lesion towards the chronic active stage. Finally, in patients characterized by a SEL+PRL+ status, an association with worsening of the disability outcome (assessed by the Expanded Disability Status Scale) was found. As a result, this analysis was the first contribution to assess the prognostic value of those novel markers together.

The last analysis described in this project was accomplished with the main aim of evaluating the evolution of new lesions from their formation in a primary-progressive (PPMS) trial cohort. The main question to answer was whether a specific subset of

lesions is more likely to develop into the chronic active subtype. Initially, the focus was to identify the newly developed lesions by discarding the ones already present at baseline. Therefore, as a novelty of this study, only the subset of new lesions was followed-up through the computation of their longitudinal deformation, in order to focus on the pattern of evolution from the ‘real’ onset. In this way, the bias of analysing lesions at different ages was removed. The results suggested that there may be a particular period of maximal expansion during the first year after onset, subsequently followed by a stabilisation and a possible shrinkage. Firstly, the subpopulation of patients defined as ‘active’ (i.e. showing at least one new lesion) had a higher global lesion load, and a higher level of brain atrophy compared to the ‘inactive’ PPMS, as previously reported (Lublin *et al.*, 2016). In this work, in addition to the definition of lesion subtypes by the volumetric MRI technique, the computation of Jacobian values within lesions promoted the evaluation of a quantitative metric, as opposed to the qualitative identification of SELs versus non-SELs. However, only the SEL-derived measures were able to predict global disability accrual over time, as assessed by the EDSS and higher risk for CDP, together with worse physical walking function. The main finding of this work was the identification of a treatment effect (fingolimod versus placebo) on some of the MRI markers assessed. More in detail, both the new lesions and the SELs (i.e. definite SEL counts and volumes) had higher figures in the placebo population, suggesting that there is a potential for the reduction of chronic active lesion activity with the use of DMTs.

7.2 Clinical relevance and future directions

The improvements in the understanding of MS derive from several research areas: the primary experimental studies that investigate the pathogenetic mechanisms, and the translational research directed to evaluating and assessing relevant biomarkers. A biomarker is defined by the UK Medical Research Council as “an objective measurement acting as an indicator of pathological processes or pharmacologic responses to treatment intervention”. Those are measures that reflect the pathological changes in MS and serve as a tool to understand the clinical evolution, the factors responsible for the progression of disability and the treatment effects.

Together with other international MS organisations, one of the main priorities of the International Progressive MS Alliance is to promote our understanding of progression as a way to improve the well-being of people with MS (Thompson *et al.*, 2022). In view of this, they suggested developing and validating biomarkers signalling progression that are scientifically sensitive and specific enough to justify their use in phase II and phase III clinical trials, to make those trials less time- and resource-consuming. MRI markers played an important, if not key, role in this direction and their application in the clinical trials setting has contributed to the development of new treatments. However, there is still a paucity of drugs that could halt the progression and neurodegeneration, despite the recent regulatory approval for two treatments in progressive MS (Liu *et al.*, 2021) (e.g., ocrelizumab (Montalban *et al.*, 2017) and siponimod (Kappos *et al.*, 2018)) and recent trials showing promise in neuroprotection and remyelination (e.g, simvastatin (Chataway *et al.*, 2014) and clemastine (Green *et al.*, 2017)), together with treatments targeting the inhibition of the microglial activity (Bruton's tyrosine kinase inhibitors, or BTKi (Montalban *et al.*, 2019)).

7.2.1 Insights on the pathogenetic mechanisms within chronic active lesions

Regarding the pathogenetic basis, in the first chapter, I provided supporting evidence that chronic active lesions are relevant biomarkers for MS progression as they manifest signs of ongoing neuro-axonal injury and low-burning demyelination. Indeed, the accumulation of chronic active lesions has been confirmed by large histopathological MS studies, and they are responsible for a relevant level of inflammation seen up to the late disease stages (Frischer *et al.*, 2015; Luchetti *et al.*, 2018). Moreover, they contribute to driving clinical deterioration, together with meningeal inflammation and subpial cortical lesions, which all represent aspects of the compartmentalized and resident central nervous system (CNS) inflammation (Lassmann, Brück and Lucchinetti, 2007). Then, another characteristic of those lesions is the accumulation of neuro-axonal loss, as the outcome of the interplay of numerous factors promoting neurodegeneration, including oxidative damage, mitochondrial dysfunction and energy failure (Giovannoni *et al.*, 2022).

Prineas *et al.* initially described the 'progressive plaques', lesions with evidence of widespread ongoing demyelination of an unusual type and inflammatory cells in the periplaque white matter (Prineas *et al.*, 2001). These unusual lesions, subsequently

called mixed active-inactive or smouldering, have been meticulously studied over the years and distinctive pathological features were recognised. Among them are a low degree of inflammation, T and B cells at the core, a dense network of activated iron-enriched microglia/macrophages expressing pro-inflammatory markers, damaged axons and proliferating oligodendrocytes at the lesion edge (Dal-Bianco *et al.*, 2017; Popescu *et al.*, 2017; Luchetti *et al.*, 2018). Recent analyses have shown that those plaques present a preferential accumulation of CNS-resident microglia of the pro-inflammatory M1 phenotype, and an upregulation of genes involved in immune defence, metabolic and transcription or translation processes (Jäckle *et al.*, 2020). The current recognition of those factors has contributed to the awareness that chronic inflammatory activity impacts the whole MS spectrum, while inflammation was initially thought to be seen only in the context of relapses of MS.

7.2.2 Contribution of the thesis

In this work, the main accomplishment has been to develop *in vivo* MRI markers of the chronic active lesions for MS characterisation, by improving their quantification in combination with other radiological markers and assessing their impact on clinical disability.

The characterization of the chronic active lesions through advanced imaging analysis has helped to broaden the knowledge on the evolution of chronic inflammatory activity, as one of the mechanisms contributing to disability progression. This work has contributed to the implementation of pipelines for the acquisition of imaging markers for chronic active lesions for trial evaluation and has contributed to providing the evidence of their clinical impact in MS. Therefore, this could represent an initial point for the industry to improve information technology tools, such as lesion segmentation and registration techniques, and to adapt them for the clinical practice

As an indirect contribution of this work, the evidence of the key role of chronic active lesions has stimulated experimental research on the cell network involved in forming those lesions. For example, recent research studies were conducted on the control of pathological astrocytes by microglia (Liddelow *et al.*, 2017), as one of the principal cell types involved in the expansion of chronic active lesions, and on the mechanisms of iron accumulation as a contributor to the neurodegenerative processes (LeVine and

Chakrabarty, 2004), which have been hypothesised to impact not only MS but also other neurodegenerative conditions. Moreover, the knowledge acquired has stimulated the research on new targeted drugs used to reduce progression in MS. For example, recently several trials have been conducted with disease-modifying treatments (DMTs) to counteract the microglial activation (i.e. BTKi) (Montalban *et al.*, 2019), and pilot studies for treating excess iron levels (Lynch, Peters and LeVine, 1996) and oxidative damage.

The principal focus at the start of this work was the study of SELs, linked to the main objective to implement a marker derived from an automatic tool and to exploit the benefits of computational technologies of this method. The results have established that SELs are common in all MS forms, they predominate in progressive MS, and can impact physical and cognitive disability. Moreover, the application of SELs as biomarkers in the trial context has indicated that they can be extended to clinical practice for the feasibility of the technique, requiring only conventionally acquired MRI acquisitions. SELs are more sensitive and quantifiable measures compared to previously used manually retrieved markers for expanding MS lesions (new/enlarging T2/FLAIR lesions), and they have a significant impact on physical and cognitive progression. Therefore, those biomarkers are expected to become in the nearest future a standard marker for trials to develop new treatments for MS, and they can provide the tools with which to measure in clinical practice the effects of DMTs.

Other MRI surrogates for MS progression, such as the persisting black holes (PBHs) and brain atrophy, markers of tissue damage within lesions and neurodegeneration, were investigated in combination with SELs. The significant correlation of all those markers supported the notion that chronic active lesions can be affected by higher tissue damage within lesions and are associated with global neurodegeneration. Then, the analysis of the paramagnetic rim lesions (PRLs), as alternative MRI markers, provided evidence that there are multiple aspects of the evolution of chronic active lesions that are still unknown and need further evaluation. Indeed, the presence of several imaging markers to detect them suggested that there is a complexity in the evolution of the plaques in MS. In the final chapter, the focus of the investigation was centred on the fraction of the new lesions, to disentangle the trajectory of evolution to SELs and to better understand the implication of lesion ‘age’. Thus, this work provided

evidence that the newly developed lesions have an initial tendency toward volume growth, and a high proportion evolves into SELs. Therefore, it can be postulated that in MS the mechanisms leading to chronic inflammatory activity can start in the early phases of lesion formation, and there is a relevant risk for lesions to evolve into the chronic active stage.

7.2.3 Commentary from recent literature

During the completion of this PhD, the scientific MS community has largely directed the research efforts towards better measurement of chronic active lesions, and this has currently become an active field of MRI research. There have been also recent publications evaluating the impact of this topic among the expert community of MS researchers. For example, Absinta et al. wrote in the context of the issue ‘Controversies in MS’ debating the recognition of slowly expanding lesions as a marker for progressive MS (Absinta and Dal-Bianco, 2021). The authors supported the notion that all studies focused on imaging markers of the chronic active lesion, from the susceptibility-based techniques (to identify the paramagnetic rims) to the longitudinal volumetric studies of SELs have demonstrated that they are frequently found in about 50% of MS patients. They added that those markers are common in both progressive and relapse-onset phenotypes, and in the early cases of CIS or RIS. Most importantly, there is evidence from trials and observational studies of a risk to reach higher disability scores in patients harbouring several chronic active lesions at MRI (Elliott, Wolinsky, *et al.*, 2019; C. Elliott *et al.*, 2020).

On the other hand, in the same journal issue, the group of Arnold et al. (Arnold *et al.*, 2021) debated the view of the limitations of those new imaging markers for chronic active lesions. A major limitation is linked to differences in the acquisitions (T1/T2-weighted and susceptibility) and the methodological techniques used by research laboratories. With regards to SELs, it is important to note that the complexity of the technique is influenced by the image registration, deformation algorithms, computing processing methods and the time window of selection of a required minimum number of time points for the image acquisition. However, despite some limitations, the main novelty of computing SELs compared to previous volumetric MRI techniques (i.e. new/enlarging T2 lesions) is that the longitudinal nature of this marker and the need to satisfy constant expansion at each subsequent scan represents an aspect coinciding

with the nature of the smouldering inflammation, that requires a persistent inflammatory activity at lesion edges.

Finally, a commentary provided by Dr Simmons et al. on Neurology has provided a comprehensive view of our current knowledge on biomarkers of chronic active lesions (Simmons and Ontaneda, 2022). The authors described the main differences between distinct imaging markers (SELs total volume, T1-hypointense volume change within SELs and PRLs) and stated that each of them likely captures only a distinct subset of the total chronic active lesion burden. However, in the minority of those MRI lesions that share the features of the two MRI markers, there are signs of more severe tissue damage, as assessed by lower magnetization transfer ratio (Elliott *et al.*, 2021). Overall, regardless of the type of imaging marker, it is still unknown why some of these lesions progressively expand. In conclusion, there is recognition that the presence of chronic active lesions likely results in deleterious clinical effects, and a future research priority will be to understand how different radiological biomarkers of chronic active lesions affect disability and behave in clinical trials to be used for therapeutic development.

7.2.4 Future directions

All the techniques assessed in this thesis need to be evaluated and compared among the imaging techniques available to identify a common marker for chronic active lesions. It is also important to state that a simplification is needed to facilitate the applicability of those techniques. This standardisation is needed to make the measures comparable and widely used with the common view of drawing objective conclusions on the analyses. As a result, the use of standardised markers for chronic active lesions could in the future benefit clinicians and patients. A future perspective would be to evaluate those issues in an expert panel committee, and initially identify standardized and optimized pipelines (including the type of sequences and scanners) with the best outcomes. Similarly, for all the markers discussed in the thesis (e.g. SELs, PBHs, PRLs), there should be a common definition of the criteria, so that there is homogeneity facilitating comparisons of the results between centres and translation to the clinical practice. This work towards standardisation has been initiated by presentations related to this topic within the Magnetic Resonance Imaging in MS (MAGNIMS) collaborative initiative during the annual meetings of the last two years.

Another important future step will be to assess the time evolution of MS lesions and to investigate the factors related to the transition into the chronic active stage. The final chapter of this thesis is a starting point toward an accurate study of the trajectories of lesion volume evolution at MRI, such as a long-term evaluation using growth analysis. Furthermore, this work could also favour the identification of other lesions that manifest a volumetric shrinkage, as a possible marker of response to DMTs, or to the shift to a final atrophic state. Recent studies have also shown the importance of evaluating different phenotypes of patients as defined by MRI-based characteristics and suggested that the subtypes characterised by lesion accumulation have also a higher disability level and present treatment response in trials (Eshaghi *et al.*, 2021). Thus, this evidence supports that the further characterisation of the lesion evolution and the profiles of patients that present chronic burden, as confirmed by accurate computation tools, could be critical for improving our understanding of MS progression.

This work will also stimulate the understanding of the pathological components contributing to the endurance of an inflammatory state, by employing other data from quantitative imaging techniques analysing the microstructural components of chronic active lesions. Recent studies have demonstrated that those lesion types can be visualized with other imaging techniques in MS. For example, chronic active lesions have been detected at quantitative susceptibility mapping (QSM) and the presence of lesions with rims (and higher susceptibility values) was associated with tracer deposition at PET (using ligand ^{11}C -PK11195) indicating the presence of active macrophages/microglia (Kaunzner *et al.*, 2019). Both modalities should be analysed further, and in combination with the currently available markers for chronic active lesions.

Recent imaging studies are in line with the work described in this thesis, as they are all indicating that there is extensive tissue damage and defective remyelination within the chronic active lesions, as shown by multiple MR modalities, from the T1 hypointensity (Elliott, Belachew, Jerry S Wolinsky, *et al.*, 2019) and magnetization transfer reductions (Preziosa *et al.*, 2022) to increased radial diffusivity (C Elliott *et al.*, 2020). Furthermore, recent works have also described the association of chronic active lesions at imaging to other peripheral biological markers of neurodegeneration,

such as serum neurofilaments (Maggi *et al.*, 2021). Overall, reflecting on those studies, a complex and heterogeneous frame for all the factors contributing to the clinical outcomes has emerged and the integration of several markers is now a major need in MS research. This future work would be stimulated by the establishment of robust data-sharing platforms that leverage machine learning and related artificial intelligence tools to develop new insights into biological pathways contributing to progressive disease.

7.3 Final considerations

In this thesis, by exploring a combination of several MRI markers for the chronic active lesions in MS, I promoted the implementation of newly developed pipelines using advanced computational technologies. Together with recent research studies from other imaging centres, the results of this work provide further evidence of the clinical validity and the potential added value of markers of chronic MS activity and have paved the way for its integration into future clinical practice.

The findings acquired in this work and the relevant associations found with the clinical outcomes, promoted our understanding of mechanisms driving disability progression. Multiple factors are contributing, as this represents a complex and dynamic process that can be better captured by multiple markers in such a complex disease as MS. The investigation needs to continue and involve all the pathobiological aspects of the disease with the final objective to understand the potential link between neuroinflammatory and neurodegenerative processes. In-use evaluation of the measures analysed in this work will need to be exploited with the objective of improving our understanding of the pathogenetic process leading to progression, such as the involvement of specific cell subtypes in the maintenance of a chronic compartmentalised inflammation and the role of a dysregulated remyelination, which are plausible factors related to the occurrence of neurodegeneration.

Imaging research will advance further towards the full automatization and standardisation of MRI and, more generally, imaging markers in MS. This would favour a more objective quantification, with the aim of translating those measures for

practical use in the clinics. To approach clinical use a standardisation of the measures applied in trials is necessary. The complexity and the multitude of imaging biomarkers reinforce the principle that those quantitative measures should be used as complementary additional information for the neurologist to assimilate into their assessment.

In conclusion, there are reasons to support that there is a need for integration of imaging markers of chronic inflammatory activity with other MS-specific markers to help to understand the temporal evolution of inflammation and neurodegeneration, and to identify patterns that will be more clearly associated with disability. Understanding the interplay between factors promoting disability in a complex disease with large heterogeneity requires the use of multimodal information. The future systematic analysis and integration of those markers into combined scores might inform the risk of developing a progressive course and provide an efficient way to evaluate treatment response.

Bibliography

Absinta, M. *et al.* (2013) 'Seven-tesla phase imaging of acute multiple sclerosis lesions: A new window into the inflammatory process', *Annals of Neurology*, 74(5), pp. 669–678. Available at: <https://doi.org/10.1002/ana.23959>.

Absinta, M. *et al.* (2016) 'Persistent 7-tesla phase rim predicts poor outcome in new multiple sclerosis patient lesions', *The Journal of Clinical Investigation*, 126(7), pp. 2597–2609. Available at: <https://doi.org/10.1172/JCI86198>.

Absinta, M. *et al.* (2018) 'Identification of chronic active multiple sclerosis lesions on 3T MRI', *American Journal of Neuroradiology*, 39(7), pp. 1233–1238. Available at: <https://doi.org/10.3174/ajnr.A5660>.

Absinta, M. *et al.* (2019) 'Association of Chronic Active Multiple Sclerosis Lesions With Disability In Vivo', *JAMA Neurology* [Preprint]. Available at: <https://doi.org/10.1001/jamaneurol.2019.2399>.

Absinta, M. and Dal-Bianco, A. (2021) 'Slowly expanding lesions are a marker of progressive MS – Yes', *Multiple Sclerosis Journal*. SAGE PublicationsSage UK: London, England, pp. 1679–1681. Available at: <https://doi.org/10.1177/13524585211013748>.

Adams, H.P. *et al.* (1999) 'Hypointense and hyperintense lesions on magnetic resonance imaging in secondary-progressive MS patients', *European Neurology*, 42(1), pp. 52–63. Available at: <https://doi.org/10.1159/000008069>.

Airas, L., Rissanen, E. and Rinne, J. (2017) 'Imaging of microglial activation in MS using PET: Research use and potential future clinical application', *Multiple Sclerosis*. SAGE Publications Ltd, pp. 496–504. Available at: <https://doi.org/10.1177/1352458516674568>.

Alonso, A. and Hernán, M.A. (2008) 'Temporal trends in the incidence of multiple sclerosis: A systematic review', *Neurology* [Preprint]. Available at: <https://doi.org/10.1212/01.wnl.0000316802.35974.34>.

Amato, M.P. and Ponziani, G. (2016) 'Quantification of impairment in MS: discussion of the scales in use', <http://dx.doi.org/10.1177/135245859900500404>, 5(4), pp. 216–219. Available at: <https://doi.org/10.1177/135245859900500404>.

Arnold, D.L. *et al.* (2021) 'Slowly expanding lesions are a marker of progressive MS – No', *Multiple Sclerosis Journal*, 27(11), pp. 1681–1683. Available at: <https://doi.org/10.1177/13524585211017020>.

Ascherio, A. *et al.* (2014) 'Vitamin D as an early predictor of multiple sclerosis activity and progression', *JAMA Neurology*, 71(3), pp. 306–314. Available at: <https://doi.org/10.1001/jamaneurol.2013.5993>.

Ascherio, A. and Munger, K.L. (2007) 'Environmental risk factors for multiple sclerosis. Part I: The role of infection', *Annals of Neurology*, 61(4), pp. 288–299. Available at: <https://doi.org/10.1002/ana.21117>.

Ascherio, A., Munger, K.L. and Lünemann, J.D. (2012) 'The initiation and prevention of multiple sclerosis', *Nature Reviews Neurology*, pp. 602–612. Available at: <https://doi.org/10.1038/nrneurol.2012.198>.

Ashburner, J. and Friston, K.J. (2000) 'Voxel-based morphometry - The methods', *NeuroImage*, 11(6 I), pp. 805–821. Available at: <https://doi.org/10.1006/nimg.2000.0582>.

Azevedo, C.J. *et al.* (2014) 'In vivo evidence of glutamate toxicity in multiple sclerosis', *Annals of Neurology*, 76(2), pp. 269–278. Available at: <https://doi.org/10.1002/ANA.24202>.

Babbe, H *et al.* (2000) 'Clonal expansions of CD8(+) T cells dominate the T cell infiltrate in active multiple sclerosis lesions as shown by micromanipulation and single cell polymerase chain reaction.', *The Journal of experimental medicine*, 192(3), pp. 393–404. Available at: <https://doi.org/10.1084/JEM.192.3.393>.

Babbe, Holger *et al.* (2000) 'Clonal Expansions of Cd8⁺ T Cells Dominate the T Cell Infiltrate in Active Multiple Sclerosis Lesions as Shown by Micromanipulation and Single Cell Polymerase Chain Reaction', *The Journal of Experimental Medicine*, 192(3), pp. 393–404. Available at: <https://doi.org/10.1084/jem.192.3.393>.

Bagnato, F. *et al.* (2003) 'Evolution of T1 black holes in patients with multiple sclerosis imaged monthly for 4 years', *Brain*, 126(8), pp. 1782–1789. Available at: <https://doi.org/10.1093/BRAIN/AWG182>.

Bagnato, F. *et al.* (2011) 'Tracking iron in multiple sclerosis: a combined imaging and histopathological study at 7 Tesla', *Brain*, 134(12), pp. 3602–3615. Available at: <https://doi.org/10.1093/brain/awr278>.

Ban, M. *et al.* (2008) 'Investigation of the role of mitochondrial DNA in multiple sclerosis susceptibility', *PLoS ONE*, 3(8), p. e2891. Available at: <https://doi.org/10.1371/journal.pone.0002891>.

Barkhof, F. (1999) 'MRI in multiple sclerosis: Correlation with expanded disability status scale (EDSS)', in *Multiple Sclerosis*, pp. 283–286. Available at: <https://doi.org/10.1177/135245859900500415>.

Barkhof, F., Bruck, W. and De Groot, C.J.A. (2003) 'Remyelinated Lesions in Multiple Sclerosis', *Arch Neurol*, 60, pp. 1073–1081.

Barnett, M.H. and Prineas, J.W. (2004) 'Relapsing and remitting multiple sclerosis: Pathology of the newly forming lesion', *Annals of Neurology*, 55(4), pp. 458–468. Available at: <https://doi.org/10.1002/ANA.20016>.

Beaulieu, C. (2002) 'The basis of anisotropic water diffusion in the nervous system - a technical review', *NMR in Biomedicine*, 15(7–8), pp. 435–455. Available at: <https://doi.org/10.1002/nbm.782>.

Belbasis, L. *et al.* (2015) 'Environmental risk factors and multiple sclerosis: an umbrella review of systematic reviews and meta-analyses', *The Lancet Neurology*, 14, pp. 263–273. Available at: [https://doi.org/10.1016/S1474-4422\(14\)70267-4](https://doi.org/10.1016/S1474-4422(14)70267-4).

Berer, K. *et al.* (2011) ‘Commensal microbiota and myelin autoantigen cooperate to trigger autoimmune demyelination’, *Nature*, 479(7374), pp. 538–541. Available at: <https://doi.org/10.1038/nature10554>.

Bian, W. *et al.* (2013) ‘A serial in vivo 7T magnetic resonance phase imaging study of white matter lesions in multiple sclerosis’, *Multiple Sclerosis Journal*, 19(1), pp. 69–75. Available at: <https://doi.org/10.1177/1352458512447870>.

Bitsch, A. *et al.* (2001) ‘A longitudinal MRI study of histopathologically defined hypointense multiple sclerosis lesions’, *Annals of Neurology*, 49(6), pp. 793–796. Available at: <https://doi.org/10.1002/ana.1053>.

Blinkenberg, M. *et al.* (2000) ‘Cortical cerebral metabolism correlates with MRI lesion load and cognitive dysfunction in MS’, *Neurology*, 54(3), pp. 558–558. Available at: <https://doi.org/10.1212/WNL.54.3.558>.

Bö, L. *et al.* (1994) ‘Detection of MHC class II-antigens on macrophages and microglia, but not on astrocytes and endothelia in active multiple sclerosis lesions’, *Journal of Neuroimmunology*, 51(2), pp. 135–146. Available at: [https://doi.org/10.1016/0165-5728\(94\)90075-2](https://doi.org/10.1016/0165-5728(94)90075-2).

Bø, L. *et al.* (2003) ‘Subpial demyelination in the cerebral cortex of multiple sclerosis patients’, *Journal of Neuropathology and Experimental Neurology*, 62(7), pp. 723–732. Available at: <https://doi.org/10.1093/jnen/62.7.723>.

Bodini, B. *et al.* (2014) ‘A novel approach with “skeletonised MTR” measures tract-specific microstructural changes in early primary-progressive MS’, *Human Brain Mapping*, 35(2), pp. 723–733. Available at: <https://doi.org/10.1002/HBM.22196>.

Bosc, M. *et al.* (2003) ‘Automatic change detection in multimodal serial MRI: Application to multiple sclerosis lesion evolution’, *NeuroImage*, 20(2), pp. 643–656. Available at: [https://doi.org/10.1016/S1053-8119\(03\)00406-3](https://doi.org/10.1016/S1053-8119(03)00406-3).

Bramow, S. *et al.* (2010) ‘Demyelination versus remyelination in progressive multiple sclerosis’, *Brain*, 133(10), pp. 2983–2998. Available at: <https://doi.org/10.1093/brain/awq250>.

Brex, P.A. *et al.* (2002) ‘A Longitudinal Study of Abnormalities on MRI and Disability from Multiple Sclerosis’, *New England Journal of Medicine*, 346(3), pp. 158–164. Available at: <https://doi.org/10.1056/NEJMoa011341>.

Browne, P. *et al.* (2014) ‘Atlas of Multiple Sclerosis 2013: A growing global problem with widespread inequity.’, *Neurology*, 83(11), pp. 1022–4. Available at: <https://doi.org/10.1212/WNL.0000000000000768>.

Brownlee, W.J. *et al.* (2016) ‘Association of asymptomatic spinal cord lesions and atrophy with disability 5 years after a clinically isolated syndrome.’, *Multiple sclerosis (Houndmills, Basingstoke, England)*, pp. 1–10. Available at: <https://doi.org/10.1177/1352458516663034>.

Brownlee, W.J. *et al.* (2019) ‘Early imaging predictors of long-term outcomes in relapse-onset

multiple sclerosis', *Brain*, 142(8), pp. 2276–2287. Available at: <https://doi.org/10.1093/BRAIN/AWZ156>.

Brück, W. *et al.* (1995) 'Monocyte/macrophage differentiation in early multiple sclerosis lesions', *Annals of Neurology*, 38(5), pp. 788–796. Available at: <https://doi.org/10.1002/ana.410380514>.

Brück, W. *et al.* (1997) 'Inflammatory central nervous system demyelination: Correlation of magnetic resonance imaging findings with lesion pathology', *Annals of Neurology* [Preprint]. Available at: <https://doi.org/10.1002/ana.410420515>.

Von Büdingen, H.C. *et al.* (2001) 'Immune responses against the myelin/oligodendrocyte glycoprotein in experimental autoimmune demyelination', *Journal of clinical immunology*, 21(3), pp. 155–170. Available at: <https://doi.org/10.1023/A:1011031014433>.

C. Elliott, J.S. Wolinsky, S.L. Hauser, L. Kappos, F. Barkhof, C. Bernasconi, S. Belachew, Arnold, D. (2017) 'Detection and characterisation of slowly evolving lesions in multiple sclerosis using conventional brain MRI', in *ECTRIMS Online Library. Elliott C. Oct 27 2017; 202544*, p. 53. Available at: <https://onlinelibrary.ectrims-congress.eu/ectrims/2017/ACTRIMS-ECTRIMS2017/202544/colm.elliott.detection.and.characterisation.of.slowly.evolved.lesions.in.html>.

Calabrese, M. *et al.* (2009) 'Cortical lesions in primary progressive multiple sclerosis', *Neurology*, 72(15), pp. 1330–1336. Available at: <https://doi.org/10.1212/WNL.0B013E3181A0FEE5>.

Calabrese, M., Filippi, M. and Gallo, P. (2010) 'Cortical lesions in multiple sclerosis', *Nat Rev Neurol*, 6(8), pp. 438–444. Available at: <https://doi.org/nrneurol.2010.93> [pii]r10.1038/nrneurol.2010.93.

Calvi, A. *et al.* (2020) 'In vivo imaging of chronic active lesions in multiple sclerosis', *Multiple Sclerosis Journal*. SAGE Publications Ltd, p. 135245852095858. Available at: <https://doi.org/10.1177/1352458520958589>.

Calvi, A., Carrasco, F.P., *et al.* (2022) 'Association of Slowly Expanding Lesions on MRI With Disability in People With Secondary Progressive Multiple Sclerosis', *Neurology*, 98(17), pp. E1783–E1793. Available at: <https://doi.org/10.1212/WNL.0000000000200144>.

Calvi, A., Tur, C., *et al.* (2022) 'Slowly expanding lesions relate to persisting black-holes and clinical outcomes in relapse-onset multiple sclerosis.', *NeuroImage. Clinical*, 35, p. 103048. Available at: <https://doi.org/10.1016/j.nicl.2022.103048>.

Caramanos, Z., Narayanan, S. and Arnold, D.L. (2005) '1H-MRS quantification of tNA and tCr in patients with multiple sclerosis: a meta-analytic review', *Brain*, 128(11), pp. 2483–2506. Available at: <https://doi.org/10.1093/BRAIN/AWH640>.

Cardoso, M.J. *et al.* (2015) 'Geodesic Information Flows: Spatially-Variant Graphs and Their Application to Segmentation and Fusion', *IEEE Transactions on Medical Imaging*, 34(9), pp. 1976–1988. Available at: <https://doi.org/10.1109/TMI.2015.2418298>.

Cawley, N. *et al.* (2015) ‘Reduced gamma-aminobutyric acid concentration is associated with physical disability in progressive multiple sclerosis’, *Brain*, 138(9), pp. 2584–2595. Available at: <https://doi.org/10.1093/BRAIN/AWV209>.

Charo, I.F. and Ransohoff, R.M. (2006) ‘The many roles of chemokines and chemokine receptors in inflammation’, *The New England journal of medicine*, 354(6), pp. 610–621. Available at: <https://doi.org/10.1056/NEJMRA052723>.

Chataway, J. *et al.* (2014) ‘Effect of high-dose simvastatin on brain atrophy and disability in secondary progressive multiple sclerosis (MS-STAT): A randomised, placebo-controlled, phase 2 trial’, *The Lancet*, 383(9936), pp. 2213–2221. Available at: [https://doi.org/10.1016/S0140-6736\(13\)62242-4](https://doi.org/10.1016/S0140-6736(13)62242-4).

Chataway, J. *et al.* (2020) ‘Efficacy of three neuroprotective drugs in secondary progressive multiple sclerosis (MS-SMART): a phase 2b, multiarm, double-blind, randomised placebo-controlled trial’, *The Lancet Neurology*, 19(3), pp. 214–225. Available at: [https://doi.org/10.1016/S1474-4422\(19\)30485-5](https://doi.org/10.1016/S1474-4422(19)30485-5).

Chen, W. *et al.* (2014) ‘Quantitative susceptibility mapping of multiple sclerosis lesions at various ages’, *Radiology*, 271(1), pp. 183–192. Available at: <https://doi.org/10.1148/radiol.13130353>.

Chiaravalloti, N. and DeLuca, J. (2008) ‘Cognitive impairment in multiple sclerosis’, *The Lancet Neurology*, 7(12), pp. 1139–1151.

Chung, K.K. *et al.* (2020) ‘A 30-Year Clinical and Magnetic Resonance Imaging Observational Study of Multiple Sclerosis and Clinically Isolated Syndromes’, *Annals of Neurology*, 87(1), pp. 63–74. Available at: <https://doi.org/10.1002/ANA.25637>.

Ciccarelli, O. *et al.* (2007) ‘Spinal cord spectroscopy and diffusion-based tractography to assess acute disability in multiple sclerosis’, *Brain*, 130(8), pp. 2220–2231. Available at: <https://doi.org/10.1093/BRAIN/AWM152>.

Clarke, M.A. *et al.* (2020) ‘Value of 3T Susceptibility-Weighted Imaging in the Diagnosis of Multiple Sclerosis’, *American Journal of Neuroradiology*, 41(6), pp. 1001–1008. Available at: <https://doi.org/10.3174/AJNR.A6547>.

Cohen, J.A. *et al.* (2012) ‘Disability outcome measures in multiple sclerosis clinical trials: current status and future prospects’, *www.thelancet.com/neurology*, 11, p. 467. Available at: <http://www.neurostatus.net> (Accessed: 24 September 2021).

Colato, E. *et al.* (2021) ‘Predicting disability progression and cognitive worsening in multiple sclerosis using patterns of grey matter volumes’, *Journal of Neurology, Neurosurgery & Psychiatry*, 92(9), pp. 995–1006. Available at: <https://doi.org/10.1136/JNNP-2020-325610>.

Coles, A.J. *et al.* (2012) ‘Alemtuzumab for patients with relapsing multiple sclerosis after disease-modifying therapy: A randomised controlled phase 3 trial’, *The Lancet*, 380(9856), pp. 1829–1839. Available at: [https://doi.org/10.1016/S0140-6736\(12\)61768-1](https://doi.org/10.1016/S0140-6736(12)61768-1).

Compston, A. (1988) ‘The 150th anniversary of the first depiction of the lesions of multiple

sclerosis.’, *Journal of Neurology, Neurosurgery, and Psychiatry*, 51(10), p. 1249. Available at: <https://doi.org/10.1136/JNRP.51.10.1249>.

Compston, A. and Coles, A. (2008) ‘Multiple sclerosis’, *The Lancet*, 372, pp. 1502–1517. Available at: [https://doi.org/10.1016/S0140-6736\(08\)61620-7](https://doi.org/10.1016/S0140-6736(08)61620-7).

Corfield, F. and Langdon, D. (2018) ‘A Systematic Review and Meta-Analysis of the Brief Cognitive Assessment for Multiple Sclerosis (BICAMS)’, *Neurology and Therapy*. Springer Healthcare, pp. 287–306. Available at: <https://doi.org/10.1007/s40120-018-0102-3>.

Correale, J. (2014) ‘The role of microglial activation in disease progression’, *Multiple Sclerosis*, 20(10), pp. 1288–1295. Available at: <https://doi.org/10.1177/1352458514533230>.

Costello, F. (2011) ‘Evaluating the Use of Optical Coherence Tomography in Optic Neuritis’, *Multiple Sclerosis International*, 2011, pp. 1–9. Available at: <https://doi.org/10.1155/2011/148394>.

Cotton, F. *et al.* (2003) ‘MRI contrast uptake in new lesions in relapsing-remitting MS followed at weekly intervals’, *Neurology* [Preprint]. Available at: <https://doi.org/10.1212/01.WNL.0000046587.83503.1E>.

Cree, B.A.C. *et al.* (2016) ‘Long-term evolution of multiple sclerosis disability in the treatment era’, *Annals of Neurology*, 80(4), pp. 499–510. Available at: <https://doi.org/10.1002/ana.24747>.

Cutter, G.R. *et al.* (1999) ‘Development of a multiple sclerosis functional composite as a clinical trial outcome measure’, *Brain*, 122(5), pp. 871–882. Available at: <https://doi.org/10.1093/brain/122.5.871>.

Dal-Bianco, A. *et al.* (2017) ‘Slow expansion of multiple sclerosis iron rim lesions: pathology and 7 T magnetic resonance imaging’, *Acta Neuropathologica*, 133(1), pp. 25–42. Available at: <https://doi.org/10.1007/s00401-016-1636-z>.

Dal-Bianco, A. *et al.* (2021) ‘Long-term evolution of multiple sclerosis iron rim lesions in 7 T MRI’, *Brain: a journal of neurology*, 144(3), pp. 833–847. Available at: <https://doi.org/10.1093/brain/awaa436>.

Danelakis, A., Theoharis, T. and Verganelakis, D.A. (2018) ‘Survey of automated multiple sclerosis lesion segmentation techniques on magnetic resonance imaging’, *Computerized Medical Imaging and Graphics*, 70, pp. 83–100. Available at: <https://doi.org/10.1016/j.compmedimag.2018.10.002>.

Datta, S. *et al.* (2006) ‘Segmentation and quantification of black holes in multiple sclerosis’, *NeuroImage*, 29(2), pp. 467–474. Available at: <https://doi.org/10.1016/j.neuroimage.2005.07.042>.

Dekker, I. *et al.* (2019) ‘Predicting clinical progression in multiple sclerosis after 6 and 12 years’, *European Journal of Neurology* [Preprint]. Available at: <https://doi.org/10.1111/ene.13904>.

Dobson, R. *et al.* (2013) ‘Cerebrospinal fluid oligoclonal bands in multiple sclerosis and clinically isolated syndromes: A meta-analysis of prevalence, prognosis and effect of latitude’, *Journal of Neurology, Neurosurgery and Psychiatry*, 84(8), pp. 909–914. Available at: <https://doi.org/10.1136/jnnp-2012-304695>.

Drayer, B. *et al.* (1986) ‘MRI of brain iron.’, *AJR. American journal of roentgenology*, 147(1), pp. 103–110. Available at: <https://doi.org/10.2214/ajr.147.1.103>.

Eisele, P. *et al.* (2021) ‘Characterization of chronic active multiple sclerosis lesions with sodium (²³Na) magnetic resonance imaging—preliminary observations’, *European Journal of Neurology*, 28(7), pp. 2392–2395. Available at: <https://doi.org/10.1111/ENE.14873>.

Elliott, C. *et al.* (2017) ‘Detection and characterisation of slowly evolving lesions in multiple sclerosis using conventional brain MRI’, *Multiple Sclerosis Journal*, 23(3_suppl), p. 52. Available at: <https://doi.org/10.1177/1352458517731283>.

Elliott, C., Belachew, S., Wolinsky, Jerry S., *et al.* (2019) ‘Chronic white matter lesion activity predicts clinical progression in primary progressive multiple sclerosis’, *Brain*, 142(9), pp. 2787–2799. Available at: <https://doi.org/10.1093/brain/awz212>.

Elliott, C., Belachew, S., Wolinsky, Jerry S., *et al.* (2019) ‘Chronic white matter lesion activity predicts clinical progression in primary progressive multiple sclerosis’, *Brain*, 142(9), pp. 2787–2799. Available at: <https://doi.org/10.1093/BRAIN/AWZ212>.

Elliott, C., Wolinsky, J.S., *et al.* (2019) ‘Slowly expanding/evolving lesions as a magnetic resonance imaging marker of chronic active multiple sclerosis lesions’, *Multiple Sclerosis Journal*, 25(14), pp. 1915–1925. Available at: <https://doi.org/10.1177/1352458518814117>.

Elliott, C. *et al.* (2020) ‘Patterning chronic active demyelination in slowly expanding/evolving white matter MS lesions’, *American Journal of Neuroradiology*, 41(9), pp. 1–8. Available at: <https://doi.org/10.3174/ajnr.A6742>.

Elliott, C. *et al.* (2020) ‘Patterning Chronic Active Demyelination in Slowly Expanding/Evolving White Matter MS Lesions’, *American Journal of Neuroradiology*, 41(9), pp. 1584–1591. Available at: <https://doi.org/10.3174/AJNR.A6742>.

Elliott, C. *et al.* (2021) ‘MRI Characteristics of Chronic MS Lesions by Phase Rim Detection and/or Slowly Expanding Properties (4101)’, *Neurology*, 96(15 Supplement).

van den Elskamp, I.J. *et al.* (2008) ‘Persistent T1 hypointensity as an MRI marker for treatment efficacy in multiple sclerosis’, *Multiple Sclerosis*, 14(6), pp. 764–769. Available at: <https://doi.org/10.1177/1352458507087842>.

Enzinger, C. *et al.* (2015) ‘Nonconventional MRI and microstructural cerebral changes in multiple sclerosis’, *Nature Reviews Neurology*, 11(12), pp. 676–686. Available at: <https://doi.org/10.1038/nrneurol.2015.194>.

Eshaghi, A., Prados, F., Brownlee, W.J., *et al.* (2018) ‘Deep gray matter volume loss drives disability worsening in multiple sclerosis’, *Annals of Neurology*, 83(2), pp. 210–222. Available at: <https://doi.org/10.1002/ana.25145>.

Eshaghi, A., Prados, F., Brownlee, W., *et al.* (2018) ‘Deep grey matter volume loss drives disability worsening in multiple sclerosis’, *Annals of Neurology* [Preprint]. Available at: <https://doi.org/10.1002/ana.25145>.

Eshaghi, A., Marinescu, R. V., *et al.* (2018) ‘Progression of regional grey matter atrophy in multiple sclerosis’, *Brain*, 141(6), pp. 1665–1677. Available at: <https://doi.org/10.1093/BRAIN/AWY088>.

Eshaghi, A. *et al.* (2021) ‘Identifying multiple sclerosis subtypes using unsupervised machine learning and MRI data’, *Nature Communications*, 12(1). Available at: <https://doi.org/10.1038/s41467-021-22265-2>.

Fahrbach, K. *et al.* (2013) ‘Relating relapse and T2 lesion changes to disability progression in multiple sclerosis: A systematic literature review and regression analysis’, *BMC Neurology*, 13(1), pp. 1–14. Available at: <https://doi.org/10.1186/1471-2377-13-180/TABLES/3>.

Faizy, T.D. *et al.* (2016) ‘Heterogeneity of multiple sclerosis lesions in multislice myelin water imaging’, *PLoS ONE*, 11(3), p. 151496. Available at: <https://doi.org/10.1371/journal.pone.0151496>.

Fernández-Menéndez, S. *et al.* (2016) ‘Epstein–Barr virus and multiple sclerosis. From evidence to therapeutic strategies’, *Journal of Neurological Sciences*, 361, pp. 213–219. Available at: <https://doi.org/10.1016/j.jns.2016.01.013>.

Filippi, M. *et al.* (1998) ‘Magnetization transfer changes in the normal appearing white matter precede the appearance of enhancing lesions in patients with multiple sclerosis’, *Annals of Neurology*, 43(6), pp. 809–814. Available at: <https://doi.org/10.1002/ana.410430616>.

Filippi, M. *et al.* (1999) ‘Comparison of MS clinical phenotypes using conventional and magnetization transfer MRI.’, *Neurology*, 52(3), pp. 588–94. Available at: <https://doi.org/10.1212/WNL.52.3.588>.

Filippi, M. *et al.* (2000) ‘Changes in the normal appearing brain tissue and cognitive impairment in multiple sclerosis’, *Journal of Neurology Neurosurgery and Psychiatry*, 68(2), pp. 157–161. Available at: <https://doi.org/10.1136/jnnp.68.2.157>.

Filippi, M. *et al.* (2001) ‘Diffusion tensor magnetic resonance imaging in multiple sclerosis’.

Filippi, M. *et al.* (2001) ‘Glatiramer acetate reduces the proportion of new MS lesions evolving into “black holes”’, *Neurology*, 57(4), pp. 731–733. Available at: <https://doi.org/10.1212/WNL.57.4.731>.

Filippi, M. *et al.* (2004) ‘Simple and complex movement-associated functional MRI changes in patients at presentation with clinically isolated syndromes suggestive of multiple sclerosis’, *Human Brain Mapping*, 21(2), pp. 108–117. Available at: <https://doi.org/10.1002/HBM.10160>.

Filippi, M. *et al.* (2011) ‘Magnetic resonance techniques in multiple sclerosis: The present and the future’, *Archives of Neurology*, pp. 1514–1520. Available at: <https://doi.org/10.1001/archneurol.2011.914>.

Filippi, M. *et al.* (2012) ‘Association between pathological and MRI findings in multiple sclerosis’, *The Lancet Neurology*, 11(4), pp. 349–360. Available at: [https://doi.org/10.1016/S1474-4422\(12\)70003-0](https://doi.org/10.1016/S1474-4422(12)70003-0).

Filippi, M. *et al.* (2016) ‘MRI criteria for the diagnosis of multiple sclerosis: MAGNIMS consensus guidelines’, *The Lancet Neurology*, 15(March), pp. 292–303. Available at: [https://doi.org/10.1016/S1474-4422\(15\)00393-2](https://doi.org/10.1016/S1474-4422(15)00393-2).

Filippi, M. *et al.* (2019) *Association between pathological and MRI findings in multiple sclerosis*, *The Lancet Neurology*. Available at: [https://doi.org/10.1016/S1474-4422\(18\)30451-4](https://doi.org/10.1016/S1474-4422(18)30451-4).

Fischer, J.S. *et al.* (1999) ‘The multiple sclerosis functional composite measure (MSFC): An integrated approach to MS clinical outcome assessment’, in *Multiple Sclerosis*, pp. 244–250. Available at: <https://doi.org/10.1177/135245859900500409>.

Fisniku, L. K. *et al.* (2008) ‘Disability and T2 MRI lesions: A 20-year follow-up of patients with relapse onset of multiple sclerosis’, *Brain*, 131(3), pp. 808–817. Available at: <https://doi.org/10.1093/brain/awm329>.

Fisniku, Leonora K. *et al.* (2008) ‘Gray matter atrophy is related to long-term disability in multiple sclerosis’, *Annals of Neurology*, 64(3), pp. 247–254. Available at: <https://doi.org/10.1002/ana.21423>.

Fleming, J.O. and Cook, T.D. (2006) ‘Multiple sclerosis and the hygiene hypothesis’, *Neurology*, 67(11), pp. 2085–2086. Available at: <https://doi.org/10.1212/01.wnl.0000247663.40297.2d>.

Fox, J. *et al.* (2016) ‘Individual assessment of brain tissue changes in MS and the effect of focal lesions on short-term focal atrophy development in MS: A voxel-guided morphometry study’, *International Journal of Molecular Sciences*, 17(4), pp. 1–15. Available at: <https://doi.org/10.3390/ijms17040489>.

Frischer, J.M. *et al.* (2009) ‘The relation between inflammation and neurodegeneration in multiple sclerosis brains’, *Brain*, 132(5), pp. 1175–1189. Available at: <https://doi.org/10.1093/brain/awp070>.

Frischer, J.M. *et al.* (2015) ‘Clinical and pathological insights into the dynamic nature of the white matter multiple sclerosis plaque’, *Annals of Neurology*, 78(5), pp. 710–721. Available at: <https://doi.org/10.1002/ana.24497>.

Gaitán, M.I. *et al.* (2011) ‘Evolution of the blood-brain barrier in newly forming multiple sclerosis lesions’, *Annals of Neurology*, 70(1), pp. 22–29. Available at: <https://doi.org/10.1002/ana.22472>.

Gaitán, M.I. *et al.* (2013) ‘Initial investigation of the blood-brain barrier in MS lesions at 7 tesla’, *Multiple Sclerosis Journal*, 19(8), pp. 1068–1073. Available at: <https://doi.org/10.1177/1352458512471093>.

García-Lorenzo, D. *et al.* (2013) ‘Review of automatic segmentation methods of multiple

sclerosis white matter lesions on conventional magnetic resonance imaging’, *Medical Image Analysis*, pp. 1–18. Available at: <https://doi.org/10.1016/j.media.2012.09.004>.

Ge, Y., Grossman, R.I. and Haacke, E.M. (2011) ‘Susceptibility Weighted Imaging in Multiple Sclerosis’, *Susceptibility Weighted Imaging in MRI: Basic Concepts and Clinical Applications*, pp. 249–264. Available at: <https://doi.org/10.1002/9780470905203.CH15>.

Gilmore, C.P. *et al.* (2009) ‘Regional variations in the extent and pattern of grey matter demyelination in multiple sclerosis: A comparison between the cerebral cortex, cerebellar cortex, deep grey matter nuclei and the spinal cord’, *Journal of Neurology, Neurosurgery and Psychiatry*, 80(2), pp. 182–187. Available at: <https://doi.org/10.1136/jnnp.2008.148767>.

Giorgio, A. *et al.* (2014) ‘Relevance of hypointense brain MRI lesions for long-term worsening of clinical disability in relapsing multiple sclerosis’, *Multiple Sclerosis*, 20(2), pp. 214–219. Available at: <https://doi.org/10.1177/1352458513494490>.

Giovannoni, G. *et al.* (2010) ‘A placebo-controlled trial of oral cladribine for relapsing multiple sclerosis.’, *The New England journal of medicine*, 362(5), pp. 416–426. Available at: <https://doi.org/10.1056/NEJMoa0902533>.

Giovannoni, G. *et al.* (2022) ‘Smouldering multiple sclerosis: the “real MS”’, *Therapeutic Advances in Neurological Disorders*, 15. Available at: <https://doi.org/10.1177/17562864211066751>.

Gkagkanasiou, M. *et al.* (2016) ‘USPIO-Enhanced MRI Neuroimaging: A Review’, *Journal of Neuroimaging*, 26(2), pp. 161–168. Available at: <https://doi.org/10.1111/jon.12318>.

Goldschmidt, T. *et al.* (2009) ‘Remyelination capacity of the MS brain decreases with disease chronicity.’, *Neurology*, 72(22), pp. 1914–21. Available at: <https://doi.org/10.1212/WNL.0b013e3181a8260a>.

Green, A.J. *et al.* (2017) ‘Clemastine fumarate as a remyelinating therapy for multiple sclerosis (ReBUILD): a randomised, controlled, double-blind, crossover trial’, *The Lancet*, 390(10111), pp. 2481–2489. Available at: [https://doi.org/10.1016/S0140-6736\(17\)32346-2](https://doi.org/10.1016/S0140-6736(17)32346-2).

De Groot, C.J.A. (2001) ‘Post-mortem MRI-guided sampling of multiple sclerosis brain lesions: Increased yield of active demyelinating and (p)reactive lesions’, *Brain* [Preprint]. Available at: <https://doi.org/10.1093/brain/124.8.1635>.

Grossi, P. *et al.* (2020) ‘The minimal neuropsychological assessment of MS patients (MACFIMS): normative data of the Italian population’, *Neurological Sciences* 2020 41:6, 41(6), pp. 1489–1496. Available at: <https://doi.org/10.1007/S10072-020-04251-6>.

Haacke, E.M. *et al.* (2004) ‘Susceptibility weighted imaging (SWI)’, *Magnetic Resonance in Medicine*, 52(3), pp. 612–618. Available at: <https://doi.org/10.1002/mrm.20198>.

Haacke, E.M. *et al.* (2009) ‘Characterizing iron deposition in multiple sclerosis lesions using susceptibility weighted imaging’, *Journal of Magnetic Resonance Imaging*, 29(3), pp. 537–544. Available at: <https://doi.org/10.1002/jmri.21676>.

Haacke, E.M. and Reichenbach, J.R. (2011) 'Introduction to Susceptibility Weighted Imaging', *Susceptibility Weighted Imaging in MRI: Basic Concepts and Clinical Applications*, pp. 1–16. Available at: <https://doi.org/10.1002/9780470905203.CH1>.

Halliwell, B. (2006) 'Oxidative stress and neurodegeneration: where are we now?', *Journal of Neurochemistry*, 97(6), pp. 1634–1658. Available at: <https://doi.org/10.1111/J.1471-4159.2006.03907.X>.

Hammond, K.E. *et al.* (2008) 'Quantitative in vivo magnetic resonance imaging of multiple sclerosis at 7 Tesla with sensitivity to iron', *Annals of Neurology*, 64(6), pp. 707–713. Available at: <https://doi.org/10.1002/ana.21582>.

Harrison, D.M. *et al.* (2015) 'Association of cortical lesion burden on 7-T magnetic resonance imaging with cognition and disability in multiple sclerosis', *JAMA Neurology*, 72(9), pp. 1004–1012. Available at: <https://doi.org/10.1001/jamaneurol.2015.1241>.

Harrison, D.M. *et al.* (2016) 'Lesion heterogeneity on high-field susceptibility MRI Is associated with multiple sclerosis severity', *American Journal of Neuroradiology*, 37(8), pp. 1447–1453. Available at: <https://doi.org/10.3174/ajnr.A4726>.

Harrison, D.M. *et al.* (2017) 'Leptomeningeal Enhancement at 7T in Multiple Sclerosis: Frequency, Morphology, and Relationship to Cortical Volume', *Journal of Neuroimaging*, 27(5), pp. 461–468. Available at: <https://doi.org/10.1111/JON.12444>.

Hauser, S.L. *et al.* (2008) 'B-cell depletion with rituximab in relapsing-remitting multiple sclerosis.', *The New England journal of medicine*, 358(7), pp. 676–688. Available at: <https://doi.org/10.1056/NEJMoa0706383>.

Hauser, S.L. *et al.* (2017) 'Ocrelizumab versus Interferon Beta-1a in Relapsing Multiple Sclerosis', *New England Journal of Medicine*, 376(3), pp. 221–234. Available at: <https://doi.org/10.1056/NEJMoa1601277>.

Hauser, S.L. *et al.* (2020) 'Ofatumumab versus Teriflunomide in Multiple Sclerosis', *New England Journal of Medicine*, 383(6), pp. 546–557. Available at: https://doi.org/10.1056/NEJMOA1917246/SUPPL_FILE/NEJMOA1917246_DATA-SHARING.PDF.

Havrdová, E. *et al.* (2018) 'No evidence of disease activity (NEDA) analysis by epochs in patients with relapsing multiple sclerosis treated with ocrelizumab vs interferon beta-1a', *Multiple Sclerosis Journal - Experimental, Translational and Clinical*, 4(1), p. 205521731876064. Available at: <https://doi.org/10.1177/2055217318760642>.

Hawker, K. *et al.* (2009) 'Rituximab in patients with primary progressive multiple sclerosis: Results of a randomized double-blind placebo-controlled multicenter trial', *Annals of Neurology*, 66(4), pp. 460–471. Available at: <https://doi.org/10.1002/ANA.21867>.

Hawkes, C. and Macgregor, A. (2009) 'Twin studies and the heritability of MS: a conclusion', *Multiple Sclerosis Journal*, 15(6), pp. 661–667. Available at: <https://doi.org/10.1177/1352458509104592>.

Hayton, T. *et al.* (2012) ‘Longitudinal changes in magnetisation transfer ratio in secondary progressive multiple sclerosis: Data from a randomised placebo controlled trial of lamotrigine’, *Journal of Neurology*, 259(3), pp. 505–514. Available at: <https://doi.org/10.1007/s00415-011-6212-9>.

He, D. *et al.* (2016) ‘Teriflunomide for multiple sclerosis’, *Cochrane Database of Systematic Reviews*, 2016(3). Available at: <https://doi.org/10.1002/14651858.CD009882.pub3>.

Hemmer, B., Kerschensteiner, M. and Korn, T. (2015) *Role of the innate and adaptive immune responses in the course of multiple sclerosis*, www.thelancet.com/neurology. Available at: [https://doi.org/10.1016/S1474-4422\(14\)70305-9](https://doi.org/10.1016/S1474-4422(14)70305-9).

Hemminki, K. *et al.* (2008) ‘Risk for multiple sclerosis in relatives and spouses of patients diagnosed with autoimmune and related conditions’, *neurogenetics 2008 10:1*, 10(1), pp. 5–11. Available at: <https://doi.org/10.1007/S10048-008-0156-Y>.

Hempel, S. *et al.* (2017) ‘A systematic review of modifiable risk factors in the progression of multiple sclerosis’, *Multiple Sclerosis Journal*. Available at: <https://doi.org/10.1177/1352458517690270>.

Henderson, A.P.D. *et al.* (2009) ‘Multiple sclerosis: Distribution of inflammatory cells in newly forming lesions’, *Annals of Neurology*, 66(6), pp. 739–753. Available at: <https://doi.org/10.1002/ana.21800>.

Hickman, S.J. *et al.* (2002) ‘Technical note: The comparison of hypointense lesions from “pseudo-T1” and T1-weighted images in secondary progressive multiple sclerosis’, *Multiple Sclerosis*, 8(5), pp. 433–435. Available at: <https://doi.org/10.1191/1352458502ms824xx>.

Hobart, J. *et al.* (2001) ‘The Multiple Sclerosis Impact Scale (MSIS-29)’, *Brain*, 124(5), pp. 962–973. Available at: <https://doi.org/10.1093/brain/124.5.962>.

Högel, H. *et al.* (2018) ‘Positron emission tomography imaging in evaluation of MS pathology in vivo’, *Multiple Sclerosis Journal*, pp. 1399–1412. Available at: <https://doi.org/10.1177/1352458518791680>.

van Horssen, J. *et al.* (2012) ‘Clusters of activated microglia in normal-appearing white matter show signs of innate immune activation’, *Journal of Neuroinflammation*, 9. Available at: <https://doi.org/10.1186/1742-2094-9-156>.

Howell, O.W. *et al.* (2011) ‘Meningeal inflammation is widespread and linked to cortical pathology in multiple sclerosis’, *Brain*, 134(9), pp. 2755–2771. Available at: <https://doi.org/10.1093/brain/awr182>.

<https://www.atlasofms.org/map/spain/epidemiology/number-of-people-with-ms> (2020) *Atlas of MS*. Available at: <https://www.atlasofms.org/map/spain/epidemiology/number-of-people-with-ms> (Accessed: 6 February 2021).

<https://www.mssociety.org.uk/what-we-do/our-work/our-evidence/ms-in-the-uk> (2018) *MS Society*. Available at: <https://www.mssociety.org.uk/what-we-do/our-work/our-evidence/ms-in-the-uk> (Accessed: 4 April 2022).

- Ingle, G.T. *et al.* (2005) 'Is inflammation important in early PPMS? a longitudinal MRI study', *J Neurol Neurosurg Psychiatry*, 76, pp. 1255–1258. Available at: <https://doi.org/10.1136/jnnp.2004.036590>.
- Jäckle, K. *et al.* (2020) 'Molecular signature of slowly expanding lesions in progressive multiple sclerosis', *Brain*, 143(7), pp. 2073–2088. Available at: <https://doi.org/10.1093/BRAIN/AWAA158>.
- De Jager, P.L. *et al.* (2009) 'Integration of genetic risk factors into a clinical algorithm for multiple sclerosis susceptibility: a weighted genetic risk score', *The Lancet Neurology*, 8(12), pp. 1111–1119. Available at: [https://doi.org/10.1016/S1474-4422\(09\)70275-3](https://doi.org/10.1016/S1474-4422(09)70275-3).
- Jersild, C., Svejgaard, A. and Fog, T. (1972) 'HL-A antigens and multiple sclerosis.', *Lancet (London, England)*, 1(7762), pp. 1240–1. Available at: <https://doi.org/10.1038/nm.3485>.
- Jokubaitis, V.G. *et al.* (2016) 'Predictors of long-term disability accrual in relapse-onset multiple sclerosis', *Annals of Neurology*, 80(1), pp. 89–100. Available at: <https://doi.org/10.1002/ana.24682>.
- Josefowicz, S.Z., Lu, L.F. and Rudensky, A.Y. (2012) 'Regulatory T cells: mechanisms of differentiation and function', *Annu Rev Immunol*, 30, pp. 531–564. Available at: <https://doi.org/10.1146/annurev.immunol.25.022106.141623>.
- Jung, W. *et al.* (2018) 'Whole brain g-ratio mapping using myelin water imaging (MWI) and neurite orientation dispersion and density imaging (NODDI)', *NeuroImage*, pp. 379–388. Available at: <https://doi.org/10.1016/j.neuroimage.2017.09.053>.
- Kallmann, B.A. *et al.* (2006) 'Early abnormalities of evoked potentials and future disability in patients with multiple sclerosis', *Multiple Sclerosis*, 12(1), pp. 58–65. Available at: <https://doi.org/10.1191/135248506ms1244oa>.
- Kapoor, R. *et al.* (2010) 'Lamotrigine for neuroprotection in secondary progressive multiple sclerosis: a randomised, double-blind, placebo-controlled, parallel-group trial', *The Lancet Neurology*, 9(7), pp. 681–688. Available at: [https://doi.org/10.1016/S1474-4422\(10\)70131-9](https://doi.org/10.1016/S1474-4422(10)70131-9).
- Kappos, L. *et al.* (2018) *Siponimod versus placebo in secondary progressive multiple sclerosis (EXPAND): a double-blind, randomised, phase 3 study*, www.thelancet.com. Available at: [https://doi.org/10.1016/S0140-6736\(18\)30475-6](https://doi.org/10.1016/S0140-6736(18)30475-6).
- Kappos, L. *et al.* (2020) 'Contribution of Relapse-Independent Progression vs Relapse-Associated Worsening to Overall Confirmed Disability Accumulation in Typical Relapsing Multiple Sclerosis in a Pooled Analysis of 2 Randomized Clinical Trials', *JAMA Neurology*, 77(9), pp. 1132–1140. Available at: <https://doi.org/10.1001/JAMANEUROL.2020.1568>.
- Kaunzner, U.W. *et al.* (2019) 'Quantitative susceptibility mapping identifies inflammation in a subset of chronic multiple sclerosis lesions', *Brain*, 142(1), pp. 133–145. Available at: <https://doi.org/10.1093/brain/awy296>.
- Khaleeli, Z. *et al.* (2008) 'Predicting progression in primary progressive multiple sclerosis: A 10-year multicenter study', *Annals of Neurology*, 63(6), pp. 790–793. Available at:

<https://doi.org/10.1002/ana.21375>.

Khalil, M. *et al.* (2009) 'Quantitative assessment of brain iron by R(2)* relaxometry in patients with clinically isolated syndrome and relapsing-remitting multiple sclerosis.', *Multiple sclerosis (Houndmills, Basingstoke, England)*, 15(9), pp. 1048–54. Available at: <https://doi.org/10.1177/1352458509106609>.

Khalil, M. *et al.* (2013) 'Quantitative Susceptibility Mapping in Multiple Sclerosis', *Radiology*, 267(2), pp. 551–559. Available at: <https://doi.org/10.1148/radiol.12120707>.

Khatri, B.O. (2016) 'Fingolimod in the treatment of relapsing-remitting multiple sclerosis: long-term experience and an update on the clinical evidence.', *Therapeutic advances in neurological disorders*, 9(2), pp. 130–47. Available at: <https://doi.org/10.1177/1756285616628766>.

Khayati, R. *et al.* (2008) 'A novel method for automatic determination of different stages of multiple sclerosis lesions in brain MR FLAIR images', *Computerized Medical Imaging and Graphics*, 32(2), pp. 124–133. Available at: <https://doi.org/10.1016/j.compmedimag.2007.10.003>.

Kidd, D. *et al.* (1999) 'Cortical lesions in multiple sclerosis', *Brain*, 122(1), pp. 17–26. Available at: <https://doi.org/10.1093/brain/122.1.17>.

Kim, J.H. *et al.* (2006) 'Detecting axon damage in spinal cord from a mouse model of multiple sclerosis', *Neurobiology of Disease*, 21(3), pp. 626–632. Available at: <https://doi.org/10.1016/J.NBD.2005.09.009>.

Kincses, Z.T. *et al.* (2011) 'Lesion probability mapping to explain clinical deficits and cognitive performance in multiple sclerosis', *Multiple Sclerosis Journal*, 17(6), pp. 681–689. Available at: <https://doi.org/10.1177/1352458510391342>.

Klistorner, S. *et al.* (2021) 'Expansion of chronic lesions is linked to disease progression in relapsing–remitting multiple sclerosis patients', *Multiple Sclerosis Journal*, 27(10), pp. 1533–1542. Available at: <https://doi.org/10.1177/1352458520974357>.

Klistorner, S. *et al.* (2022) 'Expansion of chronic MS lesions is associated with an increase of radial diffusivity in periplaque white matter', *Multiple Sclerosis Journal*, 28(5), pp. 697–706. Available at: <https://doi.org/10.1177/13524585211033464>.

Koch-Henriksen, N. and Sørensen, P.S. (2010) 'The changing demographic pattern of multiple sclerosis epidemiology', *The Lancet Neurology*, 9(5), pp. 520–532. Available at: [https://doi.org/10.1016/S1474-4422\(10\)70064-8](https://doi.org/10.1016/S1474-4422(10)70064-8).

Korn, T. *et al.* (2009) 'p-IL-17 and Th17 Cells.', *Annual review of immunology*, 27(1), pp. 485–517. Available at: <https://doi.org/10.1146/annurev.immunol.021908.132710>.

Kornek, B. *et al.* (2000) 'Multiple sclerosis and chronic autoimmune encephalomyelitis: A comparative quantitative study of axonal injury in active, inactive, and remyelinated lesions', *American Journal of Pathology*, 157(1), pp. 267–276. Available at: [https://doi.org/10.1016/S0002-9440\(10\)64537-3](https://doi.org/10.1016/S0002-9440(10)64537-3).

Krishnamoorthy, G. *et al.* (2009) 'Myelin-specific T cells also recognize neuronal autoantigen in a transgenic mouse model of multiple sclerosis', *Nature Medicine* 2009 15:6, 15(6), pp. 626–632. Available at: <https://doi.org/10.1038/nm.1975>.

Krupp, L.B. *et al.* (2013) 'International Pediatric Multiple Sclerosis Study Group criteria for pediatric multiple sclerosis and immune-mediated central nervous system demyelinating disorders: Revisions to the 2007 definitions', *Multiple Sclerosis Journal*, 19(10), pp. 1261–1267. Available at: <https://doi.org/10.1177/1352458513484547>.

Kuhlmann, T. *et al.* (2017) 'An updated histological classification system for multiple sclerosis lesions', *Acta Neuropathologica*, 133, pp. 13–24. Available at: <https://doi.org/10.1007/s00401-016-1653-y>.

Kurtzke, J.F. (1975) 'A reassessment of the distribution of multiple sclerosis.', *Acta neurologica Scandinavica*, 51(2), pp. 137–57.

Kurtzke, J.F. (1983) 'Rating neurologic impairment in multiple sclerosis: An expanded disability status scale (EDSS)', *Neurology*, 33(11), pp. 1444–1444. Available at: <https://doi.org/10.1212/WNL.33.11.1444>.

Kurtzke, J.F. (2013) 'Epidemiology in multiple sclerosis: a pilgrim's progress', *Brain*, 136(9), pp. 2904–2917. Available at: <https://doi.org/10.1093/BRAIN/AWT220>.

Kutzelnigg, A. *et al.* (2005) 'Cortical demyelination and diffuse white matter injury in multiple sclerosis', *Brain*, 128(11), pp. 2705–2712. Available at: <https://doi.org/10.1093/brain/awh641>.

Kwong, K.C.N.K. *et al.* (2021) 'The prevalence of paramagnetic rim lesions in multiple sclerosis: A systematic review and meta-analysis', *PLoS ONE*. Public Library of Science, p. e0256845. Available at: <https://doi.org/10.1371/journal.pone.0256845>.

Langer-Gould, A. *et al.* (2006) 'Clinical and demographic predictors of long-term disability in patients with relapsing-remitting multiple sclerosis: A systematic review', *Archives of Neurology*, 63(12), pp. 1686–1691. Available at: <https://doi.org/10.1001/archneur.63.12.1686>.

Langille, M.M., Rutatangwa, A. and Francisco, C. (2019) 'Pediatric Multiple Sclerosis: A Review', *Advances in Pediatrics*, 66, pp. 209–229. Available at: <https://doi.org/10.1016/J.YAPD.2019.03.003>.

Langkammer, C. *et al.* (2012) 'Quantitative susceptibility mapping (QSM) as a means to measure brain iron? A post mortem validation study', *NeuroImage*, 62(3), pp. 1593–1599. Available at: <https://doi.org/10.1016/j.neuroimage.2012.05.049>.

Langkammer, C. *et al.* (2013) 'Quantitative susceptibility mapping in multiple sclerosis', *Radiology*, 267(2), pp. 551–559. Available at: <https://doi.org/10.1148/radiol.12120707>.

Lassmann, H. *et al.* (1997) 'Remyelination in multiple sclerosis', *Multiple Sclerosis*, 3(2), pp. 133–136. Available at: <https://doi.org/10.1177/135245859700300213>.

Lassmann, H. *et al.* (1998) 'Immunopathology of multiple sclerosis: Report on an international meeting held at the Institute of Neurology of the University of Vienna', *Journal of Neuroimmunology*, 86(2), pp. 213–217. Available at: [https://doi.org/10.1016/S0165-5728\(98\)00031-9](https://doi.org/10.1016/S0165-5728(98)00031-9).

Lassmann, H. (2019) 'Pathogenic Mechanisms Associated With Different Clinical Courses of Multiple Sclerosis', *Frontiers in Immunology*, 9, p. 3116. Available at: <https://doi.org/10.3389/fimmu.2018.03116>.

Lassmann, H., Brück, W. and Lucchinetti, C.F. (2007) 'The Immunopathology of Multiple Sclerosis: An Overview', *Brain Pathology*, 17(2), pp. 210–218. Available at: <https://doi.org/10.1111/j.1750-3639.2007.00064.x>.

Laura, A. *et al.* (2016) 'Effects of particulate matter exposure on multiple sclerosis hospital admission in Lombardy region, Italy', *Environmental Research*, 145, pp. 68–73. Available at: <https://doi.org/10.1016/j.envres.2015.11.017>.

Leng Tan, I. *et al.* (2002) 'Magnetic resonance image registration in multiple sclerosis: Comparison with repositioning error and observer-based variability', *Journal of Magnetic Resonance Imaging*, 15(5), pp. 505–510. Available at: <https://doi.org/10.1002/jmri.10093>.

Leray, E. *et al.* (2010) 'Evidence for a two-stage disability progression in multiple sclerosis', *Brain* [Preprint]. Available at: <https://doi.org/10.1093/brain/awq076>.

LeVine, S.M. and Chakrabarty, A. (2004) 'The role of iron in the pathogenesis of experimental allergic encephalomyelitis and multiple sclerosis', *Annals of the New York Academy of Sciences* [Preprint]. Available at: <https://doi.org/10.1196/annals.1306.021>.

Libbey, J.E., McCoy, L.L. and Fujinami, R.S. (2007) 'Molecular Mimicry in Multiple Sclerosis', *International Review of Neurobiology*, 79, pp. 127–147. Available at: [https://doi.org/10.1016/S0074-7742\(07\)79006-2](https://doi.org/10.1016/S0074-7742(07)79006-2).

Liddelow, S.A. *et al.* (2017) 'Neurotoxic reactive astrocytes are induced by activated microglia', *Nature*, 541(7638), p. 481. Available at: <https://doi.org/10.1038/NATURE21029>.

Liu, Z. *et al.* (2021) 'Disease modifying therapies in relapsing-remitting multiple sclerosis: A systematic review and network meta-analysis', *Autoimmunity Reviews*, 20(6). Available at: <https://doi.org/10.1016/J.AUTREV.2021.102826>.

Lladó, X. *et al.* (2012) 'Automated detection of multiple sclerosis lesions in serial brain MRI', *Neuroradiology*, 54(8), pp. 787–807. Available at: <https://doi.org/10.1007/s00234-011-0992-6>.

Loevner, L.A. *et al.* (1995) 'Microscopic disease in normal-appearing white matter on conventional MR images in patients with multiple sclerosis: assessment with magnetization-transfer measurements.', *Radiology*, 196(2), pp. 511–515. Available at: <https://doi.org/10.1148/radiology.196.2.7617869>.

Lorscheider, J. *et al.* (2016) 'Defining secondary progressive multiple sclerosis', *Brain*, 139(9), pp. 2395–2405. Available at: <https://doi.org/10.1093/brain/aww173>.

Lublin, F. *et al.* (2016) *Oral fingolimod in primary progressive multiple sclerosis (INFORMS): A phase 3, randomised, double-blind, placebo-controlled trial, The Lancet.* Available at: [https://doi.org/10.1016/S0140-6736\(15\)01314-8](https://doi.org/10.1016/S0140-6736(15)01314-8).

Lublin, F.D. *et al.* (2014) 'Defining the clinical course of multiple sclerosis: The 2013 revisions', *Neurology*, 83(3), pp. 278–286. Available at: <https://doi.org/10.1212/WNL.0000000000000560>.

Lublin FD, R.S. (1996) 'Lublin FD, Reingold SC. Defining the clinical course of multiple sclerosis: results of an international survey.', *Neurology*, pp. 907–11.

Lucchinetti, C. *et al.* (2000) 'Heterogeneity of multiple sclerosis lesions: Implications for the pathogenesis of demyelination', *Annals of Neurology*, 47(6), pp. 707–717. Available at: [https://doi.org/10.1002/1531-8249\(200006\)47:6<707::AID-ANA3>3.0.CO;2-Q](https://doi.org/10.1002/1531-8249(200006)47:6<707::AID-ANA3>3.0.CO;2-Q).

Lucchinetti, C.F. *et al.* (1996) 'Distinct patterns of multiple sclerosis pathology indicates heterogeneity in pathogenesis', in *Brain Pathology*, pp. 259–274. Available at: <https://doi.org/10.1111/j.1750-3639.1996.tb00854.x>.

Luchetti, S. *et al.* (2018) 'Progressive multiple sclerosis patients show substantial lesion activity that correlates with clinical disease severity and sex: a retrospective autopsy cohort analysis', *Acta Neuropathologica*, 135(4), pp. 511–528. Available at: <https://doi.org/10.1007/s00401-018-1818-y>.

Lukas, C. *et al.* (2014) 'Cervical spinal cord volume loss is related to clinical disability progression in multiple sclerosis.', *Journal of neurology, neurosurgery, and psychiatry*, 1(4), pp. 410–418. Available at: <https://doi.org/10.1136/jnnp-2014-308021>.

Lunde, H.M.B. *et al.* (2017) 'Survival and cause of death in multiple sclerosis: A 60-year longitudinal population study', *Journal of Neurology, Neurosurgery and Psychiatry*, 88(8), pp. 621–625. Available at: <https://doi.org/10.1136/jnnp-2016-315238>.

Lynch, S.G., Peters, K. and LeVine, S.M. (1996) 'Desferrioxamine in chronic progressive multiple sclerosis: a pilot study.', *Multiple sclerosis (Houndmills, Basingstoke, England)*, 2(3), pp. 157–160. Available at: <https://doi.org/10.1177/135245859600200306>.

Macmillan, E.L. *et al.* (2016) 'Progressive multiple sclerosis exhibits decreasing glutamate and glutamine over two years', *Multiple Sclerosis*, 22(1), pp. 112–116. Available at: <https://doi.org/10.1177/1352458515586086>.

Mader, I. *et al.* (2000) 'Serial proton MR spectroscopy of contrast-enhancing multiple sclerosis plaques: Absolute metabolic values over 2 years during a clinical pharmacological study', *American Journal of Neuroradiology*, 21(7), pp. 1220–1227. Available at: <http://www.ncbi.nlm.nih.gov/pubmed/10954272> (Accessed: 16 August 2019).

Maggi, P. *et al.* (2020) 'Paramagnetic Rim Lesions are Specific to Multiple Sclerosis: An International Multicenter 3T MRI Study', *Annals of Neurology*, p. ana.25877. Available at: <https://doi.org/10.1002/ana.25877>.

Maggi, P. *et al.* (2021) 'Chronic White Matter Inflammation and Serum Neurofilament Levels

in Multiple Sclerosis', *Neurology*, 97(6), pp. e543–e553. Available at: <https://doi.org/10.1212/WNL.0000000000012326>.

Magliozzi, R. *et al.* (2007) 'Meningeal B-cell follicles in secondary progressive multiple sclerosis associate with early onset of disease and severe cortical pathology', *Brain*, 130(4), pp. 1089–1104. Available at: <https://doi.org/10.1093/brain/awm038>.

Magliozzi, R. *et al.* (2010) 'A Gradient of neuronal loss and meningeal inflammation in multiple sclerosis', *Annals of Neurology*, 68(4), pp. 477–493. Available at: <https://doi.org/10.1002/ANA.22230>.

Mahad, D.H., Trapp, B.D. and Lassmann, H. (2015) 'Pathological mechanisms in progressive multiple sclerosis', *The Lancet Neurology*, 14(2), pp. 183–193. Available at: [https://doi.org/10.1016/S1474-4422\(14\)70256-X](https://doi.org/10.1016/S1474-4422(14)70256-X).

Marrie, R.A. *et al.* (2015) 'A systematic review of the incidence and prevalence of comorbidity in multiple sclerosis: Overview', *Multiple Sclerosis Journal*. SAGE Publications Ltd, pp. 263–281. Available at: <https://doi.org/10.1177/1352458514564491>.

McMahon, E.J. *et al.* (2005) 'Epitope spreading initiates in the CNS in two mouse models of multiple sclerosis', *Nature Medicine* 2005 11:3, 11(3), pp. 335–339. Available at: <https://doi.org/10.1038/nm1202>.

Mehta, V. *et al.* (2013) 'Iron Is a Sensitive Biomarker for Inflammation in Multiple Sclerosis Lesions', *PLoS ONE*, 8(3), p. 57573. Available at: <https://doi.org/10.1371/journal.pone.0057573>.

Miller, D.H. *et al.* (2008) 'Differential diagnosis of suspected multiple sclerosis: A consensus approach', *Multiple Sclerosis*, pp. 1157–1174. Available at: <https://doi.org/10.1177/1352458508096878>.

Miller, D.H., Chard, D.T. and Ciccarelli, O. (2012) *Clinically isolated syndromes*, *The Lancet Neurology*. Available at: [https://doi.org/10.1016/S1474-4422\(11\)70274-5](https://doi.org/10.1016/S1474-4422(11)70274-5).

Miller, D.H. and Leary, S.M. (2007) *Primary-progressive multiple sclerosis*. Available at: [https://doi.org/10.1016/S1474-4422\(07\)70243-0](https://doi.org/10.1016/S1474-4422(07)70243-0).

Mitjana, R. *et al.* (2014) 'Diagnostic value of brain chronic black holes on T1-weighted MR images in clinically isolated syndromes', *Multiple Sclerosis Journal*, 20(11), pp. 1471–1477. Available at: <https://doi.org/10.1177/1352458514526083>.

Moccia, M. *et al.* (2019) 'Longitudinal spinal cord atrophy in multiple sclerosis using the generalized boundary shift integral', *Annals of Neurology*, 86(5), pp. 704–713. Available at: <https://doi.org/10.1002/ANA.25571>.

Moccia, M. and Ciccarelli, O. (2017) 'Molecular and Metabolic Imaging in Multiple Sclerosis', *Neuroimaging Clinics of North America*. W.B. Saunders, pp. 343–356. Available at: <https://doi.org/10.1016/j.nic.2016.12.005>.

Molyneux, P.D. *et al.* (2000) ‘The precision of TI hypointense lesion volume quantification in multiple sclerosis treatment trials: A multicenter study’, *Multiple Sclerosis*, 6(4), pp. 237–240. Available at: <https://doi.org/10.1177/13524585000600405>.

Montalban, X. *et al.* (2017) ‘Ocrelizumab versus Placebo in Primary Progressive Multiple Sclerosis’, *New England Journal of Medicine* [Preprint]. Available at: <https://doi.org/10.1056/NEJMoa1606468>.

Montalban, X. *et al.* (2018) ‘ECTRIMS/EAN Guideline on the pharmacological treatment of people with multiple sclerosis.’, *Multiple sclerosis (Houndmills, Basingstoke, England)*, 24(2), pp. 96–120. Available at: <https://doi.org/10.1177/1352458517751049>.

Montalban, X. *et al.* (2019) ‘Placebo-Controlled Trial of an Oral BTK Inhibitor in Multiple Sclerosis’, *New England Journal of Medicine*, 380(25), pp. 2406–2417. Available at: https://doi.org/10.1056/NEJMOA1901981/SUPPL_FILE/NEJMOA1901981_DATA-SHARING.PDF.

Moraal, B. *et al.* (2010) ‘Improved detection of active multiple sclerosis lesions: 3D subtraction imaging.’, *Radiology*, 255(1), pp. 154–163. Available at: <https://doi.org/10.1148/radiol.09090814>.

Morgen, K. *et al.* (1995) *Ring-enhancement in multiple sclerosis: marker of disease severity*. Available at: www.arnoldpublishers.com/journals (Accessed: 21 July 2020).

Mortazavi, D., Kouzani, A.Z. and Soltanian-Zadeh, H. (2012) ‘Segmentation of multiple sclerosis lesions in MR images: A review’, *Neuroradiology*, pp. 299–320. Available at: <https://doi.org/10.1007/s00234-011-0886-7>.

Nakamura, K. *et al.* (2014) ‘Jacobian integration method increases the statistical power to measure gray matter atrophy in multiple sclerosis’, *NeuroImage: Clinical*, 4, pp. 10–17. Available at: <https://doi.org/10.1016/j.nicl.2013.10.015>.

Narayana, P.A. *et al.* (1998) ‘Serial proton magnetic resonance spectroscopic imaging, contrast-enhanced magnetic resonance imaging and quantitative lesion volumetry in multiple sclerosis’, *Annals of Neurology*, 43(1), pp. 56–71. Available at: <https://doi.org/10.1002/ana.410430112>.

Nusbaum, A.O. *et al.* (2000) ‘Quantitative diffusion measurements in focal multiple sclerosis lesions: Correlations with appearance on T1-weighted images’, *American Journal of Roentgenology*, 175(3), pp. 821–825. Available at: <https://doi.org/10.2214/AJR.175.3.1750821>.

Okuda, D.T. *et al.* (2009) ‘Incidental MRI anomalies suggestive of multiple sclerosis’, *Neurology*, 72(9), pp. 800–805. Available at: <https://doi.org/10.1212/01.WNL.0000335764.14513.1A>.

Paling, D. *et al.* (2013) ‘Sodium accumulation is associated with disability and a progressive course in multiple sclerosis’, *Brain*, 136(7), pp. 2305–2317. Available at: <https://doi.org/10.1093/brain/awt149>.

Parmenter, B.A. *et al.* (2007) ‘Screening for cognitive impairment in multiple sclerosis using the Symbol Digit Modalities Test’, *Multiple Sclerosis*, 13(1), pp. 52–57. Available at: <https://doi.org/10.1177/1352458506070750>.

Patriarche, J. and Erickson, B. (2004) ‘A review of the automated detection of change in serial imaging studies of the brain’, *Journal of Digital Imaging*. Springer-Verlag, pp. 158–174. Available at: <https://doi.org/10.1007/s10278-004-1010-x>.

Patrikios, P. *et al.* (2006) ‘Remyelination is extensive in a subset of multiple sclerosis patients’, *Brain* [Preprint]. Available at: <https://doi.org/10.1093/brain/awl217>.

Patsopoulos, N.A. *et al.* (2013) ‘Fine-Mapping the Genetic Association of the Major Histocompatibility Complex in Multiple Sclerosis: HLA and Non-HLA Effects’, *PLoS Genetics*, 9(11), p. 1003926. Available at: <https://doi.org/10.1371/journal.pgen.1003926>.

Patsopoulos, N.A. *et al.* (2019) ‘Multiple sclerosis genomic map implicates peripheral immune cells and microglia in susceptibility’, *Science*, 365(6460). Available at: <https://doi.org/10.1126/SCIENCE.AAV7188>.

Petracca, M. *et al.* (2016) ‘Brain intra- and extracellular sodium concentration in multiple sclerosis: a 7 T MRI study’, *Brain*, 139(3), pp. 795–806. Available at: <https://doi.org/10.1093/BRAIN/AWV386>.

Pitarokouli, K. and Gold, R. (2017) ‘Multiple sclerosis: Progressive multifocal leukoencephalopathy risk stratification’. Available at: <https://doi.org/10.1038/nrneuro.2017.161>.

Polman, C.H. *et al.* (2006) ‘A Randomized, Placebo-Controlled Trial of Natalizumab for Relapsing Multiple Sclerosis’, *New England Journal of Medicine*, 354(9), pp. 899–910. Available at: <https://doi.org/10.1056/NEJMoa044397>.

Polman, C.H. and Rudick, R.A. (2010) ‘The Multiple Sclerosis Functional Composite’, *Neurology*, 74(17 Supplement 3), pp. S8–S15. Available at: <https://doi.org/10.1212/WNL.0B013E3181DBB571>.

Pongratz, V. *et al.* (2019) ‘Prognostic value of white matter lesion shrinking in early multiple sclerosis: An intuitive or naïve notion?’, *Brain and Behavior*, 9(12). Available at: <https://doi.org/10.1002/brb3.1417>.

Popescu, B.F. *et al.* (2017) ‘Pathogenic implications of distinct patterns of iron and zinc in chronic MS lesions’, *Acta Neuropathologica*, 134(1), pp. 45–64. Available at: <https://doi.org/10.1007/s00401-017-1696-8>.

Poursadegh Zonouzi, A. *et al.* (2014) ‘Mitochondrial complex I gene variations; as a potential genetic risk factor in pathogenesis of multiple sclerosis’, *Journal of the Neurological Sciences*, 345(1–2), pp. 220–223. Available at: <https://doi.org/10.1016/J.JNS.2014.07.051>.

Prados, F. *et al.* (2016) ‘A multi-time-point modality-agnostic patch-based method for lesion filling in multiple sclerosis.’, *NeuroImage*, 139, pp. 376–384. Available at: <https://doi.org/10.1016/j.neuroimage.2016.06.053>.

Preziosa, P. *et al.* (2020) ‘Occurrence and microstructural features of slowly expanding lesions on fingolimod or natalizumab treatment in multiple sclerosis’, *Multiple Sclerosis Journal* [Preprint]. Available at: <https://doi.org/10.1177/1352458520969105>.

Preziosa, P. *et al.* (2022) ‘Slowly Expanding Lesions Predict 9-Year Multiple Sclerosis Disease Progression’, *Neurology - Neuroimmunology Neuroinflammation*, 9(2). Available at: <https://doi.org/10.1212/NXI.0000000000001139>.

Prineas, J.W. *et al.* (2001) ‘Immunopathology of secondary-progressive multiple sclerosis’, *Annals of Neurology*, 50(5), pp. 646–657. Available at: <https://doi.org/10.1002/ana.1255>.

Rao, S.M. (1990) ‘A manual for the brief repeatable battery of neuropsychological tests in multiple sclerosis.’, *Ann Neurol Milwaukee*, Wis: Medic.

Rey, D. *et al.* (2002) ‘Automatic detection and segmentation of evolving processes in 3D medical images: Application to multiple sclerosis’, *Medical Image Analysis*, 6(2), pp. 163–179. Available at: [https://doi.org/10.1016/S1361-8415\(02\)00056-7](https://doi.org/10.1016/S1361-8415(02)00056-7).

Rocca, M.A. *et al.* (2005) ‘A Widespread Pattern of Cortical Activations in Patients at Presentation with Clinically Isolated Symptoms Is Associated with Evolution to Definite Multiple Sclerosis’, *AJNR: American Journal of Neuroradiology*, 26(5), p. 1136. Available at: </pmc/articles/PMC8158640/> (Accessed: 10 January 2022).

Rocca, M.A. *et al.* (2021) ‘Association of Gray Matter Atrophy Patterns With Clinical Phenotype and Progression in Multiple Sclerosis’, *Neurology*, 96(11), pp. e1561–e1573. Available at: <https://doi.org/10.1212/WNL.00000000000011494>.

Rocca, M A *et al.* (2015) ‘Clinical and imaging assessment of cognitive dysfunction in multiple sclerosis’, *The Lancet Neurology*, 14(14), pp. 302–317. Available at: [https://doi.org/10.1016/S1474-4422\(14\)70250-9](https://doi.org/10.1016/S1474-4422(14)70250-9).

Roosendaal, S.D. *et al.* (2008) ‘Regional DTI differences in multiple sclerosis patients’. Available at: <https://doi.org/10.1016/j.neuroimage.2008.10.026>.

Roosendaal, S.D. *et al.* (2010) ‘Resting state networks change in clinically isolated syndrome’, *Brain*, 133(6), pp. 1612–1621. Available at: <https://doi.org/10.1093/BRAIN/AWQ058>.

Roura, E. *et al.* (2015) ‘A toolbox for multiple sclerosis lesion segmentation’, *Neuroradiology*, 57(10), pp. 1031–1043. Available at: <https://doi.org/10.1007/s00234-015-1552-2>.

Rovaris, M. (2003) ‘Conventional and magnetization transfer MRI predictors of clinical multiple sclerosis evolution: a medium-term follow-up study’, *Brain*, 126(10), pp. 2323–2332. Available at: <https://doi.org/10.1093/brain/awg232>.

Rudick, R. *et al.* (1997) ‘Recommendations from the national multiple sclerosis society clinical outcomes assessment task force’, *Annals of Neurology*, 42(3), pp. 379–382. Available at: <https://doi.org/10.1002/ANA.410420318>.

Rudick, R.A. *et al.* (2006) ‘Significance of T2 lesions in multiple sclerosis: A 13-year

longitudinal study', *Annals of Neurology*, 60(2), pp. 236–242. Available at: <https://doi.org/10.1002/ana.20883>.

Ruggieri, S., Quartuccio, M.E. and Prosperini, L. (2022) 'Ponesimod in the Treatment of Relapsing Forms of Multiple Sclerosis: An Update on the Emerging Clinical Data', *Degenerative Neurological and Neuromuscular Disease*, 12, p. 61. Available at: <https://doi.org/10.2147/DNND.S313825>.

Sailer, M. *et al.* (2001) 'T1 lesion load and cerebral atrophy as a marker for clinical progression in patients with multiple sclerosis. A prospective 18 months follow-up study', *European Journal of Neurology*, 8(1), pp. 37–42. Available at: <https://doi.org/10.1046/j.1468-1331.2001.00147.x>.

Sastre-Garriga, J. *et al.* (2020) 'MAGNIMS consensus recommendations on the use of brain and spinal cord atrophy measures in clinical practice', *Nature Reviews Neurology*, pp. 171–182. Available at: <https://doi.org/10.1038/s41582-020-0314-x>.

Sawcer, S., Franklin, R.J.M. and Ban, M. (2014) 'Multiple sclerosis genetics Sup.', *Lancet neurology*, 13(7), pp. 700–709. Available at: [https://doi.org/10.1016/S1474-4422\(14\)70041-9](https://doi.org/10.1016/S1474-4422(14)70041-9).

Schiepers, C. *et al.* (1997) 'Positron emission tomography, magnetic resonance imaging and proton NMR spectroscopy of white matter in multiple sclerosis', *Multiple Sclerosis*, 3(1), pp. 8–17. Available at: <https://doi.org/10.1177/135245859700300102>.

Schirmer, L., Srivastava, R. and Hemmer, B. (2014) 'To look for a needle in a haystack: The search for autoantibodies in multiple sclerosis', *Multiple Sclerosis Journal*, pp. 271–279. Available at: <https://doi.org/10.1177/1352458514522104>.

Schmierer, K. *et al.* (2004) 'Magnetization transfer ratio and myelin in postmortem multiple sclerosis brain', *Annals of Neurology*, 56(3), pp. 407–415. Available at: <https://doi.org/10.1002/ana.20202>.

Schreiner, B. *et al.* (2015) 'Astrocyte Depletion Impairs Redox Homeostasis and Triggers Neuronal Loss in the Adult CNS', *Cell Reports*, 12(9), pp. 1377–1384. Available at: <https://doi.org/10.1016/j.celrep.2015.07.051>.

Seewann, A. *et al.* (2012) 'Postmortem verification of MS cortical lesion detection with 3D DIR', *Neurology*, 78(5), pp. 302–308. Available at: <https://doi.org/10.1212/WNL.0B013E31824528A0>.

Selmaj, K., Raine, C.S. and Cross, A.H. (1991) 'Anti—tumor necrosis factor therapy abrogates autoimmune demyelination', *Annals of Neurology*, 30(5), pp. 694–700. Available at: <https://doi.org/10.1002/ANA.410300510>.

Serafini, B. *et al.* (2004) 'Detection of Ectopic B-cell Follicles with Germinal Centers in the Meninges of Patients with Secondary Progressive Multiple Sclerosis', *Brain Pathology*, 14(2), pp. 164–174. Available at: <https://doi.org/10.1111/j.1750-3639.2004.tb00049.x>.

Sethi, V. *et al.* (2016) 'Slowly eroding lesions in multiple sclerosis', *Multiple Sclerosis*

Journal, pp. 464–472. Available at: <https://doi.org/10.1177/1352458516655403>.

Signori, A. *et al.* (2016) ‘Long-term impact of interferon or Glatiramer acetate in multiple sclerosis: A systematic review and meta-analysis’, *Multiple Sclerosis and Related Disorders*, 6, pp. 57–63. Available at: <https://doi.org/10.1016/j.msard.2016.01.007>.

Simmons, S.B. and Ontaneda, D. (2022) ‘Slowly Expanding Lesions: A New Target for Progressive Multiple Sclerosis Trials?’, *Neurology*, 98(17), pp. 699–700. Available at: <https://doi.org/10.1212/WNL.0000000000200230>.

Simpson, A., Mowry, E.M. and Newsome, S.D. (2021) ‘Early Aggressive Treatment Approaches for Multiple Sclerosis’, *Curr Treat Options Neurol*, 23, p. 19. Available at: <https://doi.org/10.1007/s11940-021-00677-1>.

Singh, S. *et al.* (2013) ‘Microglial nodules in early multiple sclerosis white matter are associated with degenerating axons’, *Acta Neuropathologica*, 125(4), pp. 595–608. Available at: <https://doi.org/10.1007/s00401-013-1082-0>.

Sinnecker, T. *et al.* (2016) ‘MRI phase changes in multiple sclerosis vs neuromyelitis optica lesions at 7T’, *Neurology: Neuroimmunology and NeuroInflammation*, 3(4). Available at: <https://doi.org/10.1212/NXI.0000000000000259>.

Smith, K.J. and Lassmann, H. (2002) ‘The role of nitric oxide in multiple sclerosis’, *The Lancet Neurology*, 1(4), pp. 232–241. Available at: [https://doi.org/10.1016/S1474-4422\(02\)00102-3](https://doi.org/10.1016/S1474-4422(02)00102-3).

Smith, S.M. *et al.* (2002) ‘Accurate, robust, and automated longitudinal and cross-sectional brain change analysis’, *NeuroImage*, 17(1), pp. 479–489. Available at: <https://doi.org/10.1006/nimg.2002.1040>.

Sormani, M.P. *et al.* (2009) ‘Magnetic resonance imaging as a potential surrogate for relapses in multiple sclerosis: A meta-analytic approach’, *Annals of Neurology*, 65(3), pp. 268–275. Available at: <https://doi.org/10.1002/ANA.21606>.

Sormani, M.P. and Bruzzi, P. (2013) ‘MRI lesions as a surrogate for relapses in multiple sclerosis: A meta-analysis of randomised trials’, *The Lancet Neurology*, 12(7), pp. 669–676. Available at: [https://doi.org/10.1016/S1474-4422\(13\)70103-0](https://doi.org/10.1016/S1474-4422(13)70103-0).

Sosa, S.M. and Smith, K.J. (2017) ‘Understanding a role for hypoxia in lesion formation and location in the deep and periventricular white matter in small vessel disease and multiple sclerosis’, *Clinical Science*, 131(20), pp. 2503–2524. Available at: <https://doi.org/10.1042/CS20170981>.

Spies, L. *et al.* (2013) ‘Fully automatic detection of deep white matter T1 hypointense lesions in multiple sclerosis’, *Physics in Medicine and Biology*, 58(23), pp. 8323–8337. Available at: <https://doi.org/10.1088/0031-9155/58/23/8323>.

Stankoff, B. *et al.* (2011) ‘Imaging central nervous system myelin by positron emission tomography in multiple sclerosis using [methyl-11C]-2-(4-methylaminophenyl)-6-hydroxybenzothiazole’, *Annals of Neurology*, 69(4), pp. 673–680. Available at:

<https://doi.org/10.1002/ana.22320>.

De Stefano, N. *et al.* (2010) ‘Assessing brain atrophy rates in a large population of untreated multiple sclerosis subtypes’, *Neurology*, 74(23), pp. 1868–1876. Available at: <https://doi.org/10.1212/WNL.0b013e3181e24136>.

Stys, P.K. *et al.* (2012) ‘Will the real multiple sclerosis please stand up?’, *Nature Reviews Neuroscience*, 13(7), pp. 507–514. Available at: <https://doi.org/10.1038/nrn3275>.

Summers, M.M. *et al.* (2008) ‘Cognitive impairment in relapsing - Remitting multiple sclerosis can be predicted by imaging performed several years earlier’, *Multiple Sclerosis*, 14(2), pp. 197–204. Available at: <https://doi.org/10.1177/1352458507082353>.

Tam, R.C. *et al.* (2011) ‘The impact of intensity variations in T1-hypointense lesions on clinical correlations in multiple sclerosis’, *Multiple Sclerosis Journal*, 17(8), pp. 949–957. Available at: <https://doi.org/10.1177/1352458511402113>.

Tan, I.L. *et al.* (2002) ‘Image registration and subtraction to detect active T2 lesions in MS: an interobserver study’, *Journal of Neurology*, 249(6), pp. 767–773. Available at: <https://doi.org/10.1007/s00415-002-0712-6>.

Thirion, J.P. and Calmon, G. (1999) ‘Deformation analysis to detect and quantify active lesions in three-dimensional medical image sequences’, *IEEE Transactions on Medical Imaging*, 18(5), pp. 429–441. Available at: <https://doi.org/10.1109/42.774170>.

Thompson, A.J. *et al.* (1991) ‘Major differences in the dynamics of primary and secondary progressive multiple sclerosis’, *Annals of Neurology*, 29(1), pp. 53–62. Available at: <https://doi.org/10.1002/ANA.410290111>.

Thompson, A.J. *et al.* (2017) ‘Position Paper Diagnosis of multiple sclerosis: 2017 revisions of the McDonald criteria’. Available at: [https://doi.org/10.1016/S1474-4422\(17\)30470-2](https://doi.org/10.1016/S1474-4422(17)30470-2).

Thompson, Alan J. *et al.* (2018) ‘Diagnosis of multiple sclerosis: 2017 revisions of the McDonald criteria’, *The Lancet Neurology*, 17(2), pp. 162–173. Available at: [https://doi.org/10.1016/S1474-4422\(17\)30470-2](https://doi.org/10.1016/S1474-4422(17)30470-2).

Thompson, Alan J *et al.* (2018) ‘Multiple sclerosis’, *The Lancet*. Elsevier, pp. 1622–1636. Available at: [https://doi.org/10.1016/S0140-6736\(18\)30481-1](https://doi.org/10.1016/S0140-6736(18)30481-1).

Thompson, A.J. *et al.* (2022) ‘Charting a global research strategy for progressive MS—An international progressive MS Alliance proposal’, *Multiple Sclerosis Journal*, pp. 16–28. Available at: <https://doi.org/10.1177/13524585211059766>.

Tintore, M. *et al.* (2010) ‘Brainstem lesions in clinically isolated syndromes’, *Neurology*, 75(21), pp. 1933–1938. Available at: <https://doi.org/10.1212/WNL.0b013e3181f26f26>.

Tintore, M. *et al.* (2015) ‘Defining high, medium and low impact prognostic factors for developing multiple sclerosis’, *Brain*, 138(7), pp. 1863–1874. Available at: <https://doi.org/10.1093/brain/awv105>.

Trapp, B.D. *et al.* (1998) 'Axonal Transection in the Lesions of Multiple Sclerosis', *New England Journal of Medicine*, 338(5), pp. 278–285. Available at: <https://doi.org/10.1056/NEJM199801293380502>.

Tremlett, H. *et al.* (2008) 'Monthly ambient sunlight, infections and relapse rates in multiple sclerosis.', *Neuroepidemiology*, 31(4), pp. 271–9. Available at: <https://doi.org/10.1159/000166602>.

Tremlett, H., Zhao, Y. and Devonshire, V. (2009) 'Natural history comparisons of primary and secondary progressive multiple sclerosis reveals differences and similarities', *Journal of Neurology*, 256(3), pp. 374–381. Available at: <https://doi.org/10.1007/s00415-009-0039-7>.

Truyen, L. *et al.* (1996) 'Accumulation of hypointense lesions ('black holes') on T1 spin-echo MRI correlates with disease progression in multiple sclerosis', *Neurology*, 47(6), pp. 1469–1476. Available at: <https://doi.org/10.1212/WNL.47.6.1469>.

Tur, C. *et al.* (2014) 'Spatial variability and changes of metabolite concentrations in the cortico-spinal tract in multiple sclerosis using coronal CSI', *Human Brain Mapping*, 35(3), pp. 993–1003. Available at: <https://doi.org/10.1002/HBM.22229>.

Tur, C. *et al.* (2018) 'Assessing treatment outcomes in multiple sclerosis trials and in the clinical setting', *Nature Reviews Neurology*, pp. 75–93. Available at: <https://doi.org/10.1038/nrneurol.2017.171>.

Tur, C. *et al.* (2022) 'Spatial patterns of brain lesions assessed through covariance estimations of lesional voxels in multiple Sclerosis: The SPACE-MS technique', *NeuroImage: Clinical*, 33, p. 102904. Available at: <https://doi.org/10.1016/J.NICL.2021.102904>.

Uhlenbrock, D. and Sehlen, S. (1989) 'The value of T1-weighted images in the differentiation between MS, white matter lesions, and subcortical arteriosclerotic encephalopathy (SAE)', *Neuroradiology 1989* 31:3, 31(3), pp. 203–212. Available at: <https://doi.org/10.1007/BF00344344>.

Uitdehaag, B. *et al.* (2002) 'Multiple sclerosis functional composite: impact of reference population and interpretation of changes'. Available at: <https://doi.org/10.1191/1352458502ms835oa>.

Vacchi, L. *et al.* (2017) 'Working memory network dysfunction in relapse-onset multiple sclerosis phenotypes: A clinical-imaging evaluation', *Multiple Sclerosis*, 23(4), pp. 577–587. Available at: <https://doi.org/10.1177/1352458516656809>.

Valcarcel, A.M. *et al.* (2018) 'A dual modeling approach to automatic segmentation of cerebral T2 hyperintensities and T1 black holes in multiple sclerosis', *NeuroImage: Clinical*, 20, pp. 1211–1221. Available at: <https://doi.org/10.1016/j.nicl.2018.10.013>.

Van Der Valk, P. and De Groot, C.J.A. (2000) 'Staging of multiple sclerosis (MS) lesions: Pathology of the time frame of MS', *Neuropathology and Applied Neurobiology*. John Wiley & Sons, Ltd (10.1111), pp. 2–10. Available at: <https://doi.org/10.1046/j.1365-2990.2000.00217.x>.

Valverde, S. *et al.* (2017) 'Improving automated multiple sclerosis lesion segmentation with a cascaded 3D convolutional neural network approach', *NeuroImage*, 155, pp. 159–168. Available at: <https://doi.org/10.1016/j.neuroimage.2017.04.034>.

Vos, C.M.P. *et al.* (2005) 'Blood-brain barrier alterations in both focal and diffuse abnormalities on postmortem MRI in multiple sclerosis', *Neurobiology of Disease* [Preprint]. Available at: <https://doi.org/10.1016/j.nbd.2005.06.012>.

Vrenken, H. *et al.* (2013) 'Recommendations to improve imaging and analysis of brain lesion load and atrophy in longitudinal studies of multiple sclerosis', *Journal of Neurology*, 260(10), pp. 2458–2471. Available at: <https://doi.org/10.1007/s00415-012-6762-5>.

van Waesberghe, J.H. *et al.* (1998) 'Patterns of lesion development in multiple sclerosis: longitudinal observations with T1-weighted spin-echo and magnetization transfer MR.', *AJNR. American journal of neuroradiology*, 19(4), pp. 675–83. Available at: <https://doi.org/10.3174/ajnr.a0701>.

Van Waesberghe, J.H.T.M. *et al.* (1998) 'Patterns of lesion development in multiple sclerosis: Longitudinal observations with T1-weighted spin-echo and magnetization transfer MR', in *American Journal of Neuroradiology*. American Journal of Neuroradiology, pp. 675–683. Available at: <http://www.ncbi.nlm.nih.gov/pubmed/9576653> (Accessed: 15 October 2019).

Van Waesberghe, J.H.T.M. *et al.* (1999) 'Axonal loss in multiple sclerosis lesions: Magnetic resonance imaging insights into substrates of disability', *Annals of Neurology*, 46(5), pp. 747–754. Available at: [https://doi.org/10.1002/1531-8249\(199911\)46:5<747::AID-ANA10>3.0.CO;2-4](https://doi.org/10.1002/1531-8249(199911)46:5<747::AID-ANA10>3.0.CO;2-4).

van Walderveen, M.A.A. *et al.* (1998) 'Histopathologic correlate of hypointense lesions on T1-weighted spin-echo MRI in multiple sclerosis', *Neurology*, 50(5), pp. 1282–1288. Available at: <https://doi.org/10.1212/WNL.50.5.1282>.

Van Walderveen, M.A.A. *et al.* (1998) 'Histopathologic correlate of hypointense lesions on T1-weighted spin-echo MRI in multiple sclerosis', *Neurology*, 50(5), pp. 1282–1288. Available at: <https://doi.org/10.1212/WNL.50.5.1282>.

Van Walderveen, M.A.A. *et al.* (2001) 'Hypointense lesions on T1-weighted spin-echo magnetic resonance imaging: Relation to clinical characteristics in subgroups of patients with multiple sclerosis', *Archives of Neurology*, 58(1), pp. 76–81. Available at: <https://doi.org/10.1001/archneur.58.1.76>.

Walton, C. *et al.* (2020) 'Rising prevalence of multiple sclerosis worldwide: Insights from the Atlas of MS, third edition', *Multiple Sclerosis Journal*, 26(14), pp. 1816–1821. Available at: <https://doi.org/10.1177/1352458520970841>.

Waxman, S.G. (2008) 'Mechanisms of Disease: sodium channels and neuroprotection in multiple sclerosis—current status', *Nature Clinical Practice Neurology* 2008 4:3, 4(3), pp. 159–169. Available at: <https://doi.org/10.1038/ncpneuro0735>.

Weber, C.E. *et al.* (2022) 'Long-term dynamics of multiple sclerosis iron rim lesions', *Multiple Sclerosis and Related Disorders*, 57, p. 103340. Available at:

<https://doi.org/10.1016/J.MSARD.2021.103340>.

Wisnieff, C. *et al.* (2015) 'Quantitative susceptibility mapping (QSM) of white matter multiple sclerosis lesions: Interpreting positive susceptibility and the presence of iron', *Magnetic Resonance in Medicine*, 74(2), pp. 564–570. Available at: <https://doi.org/10.1002/mrm.25420>.

Wu, Y. *et al.* (2006) 'Automated segmentation of multiple sclerosis lesion subtypes with multichannel MRI', *NeuroImage*, 32(3), pp. 1205–1215. Available at: <https://doi.org/10.1016/j.neuroimage.2006.04.211>.

Wucherpfennig, K.W. and Strominger, J.L. (1995) 'Molecular mimicry in T cell-mediated autoimmunity: Viral peptides activate human T cell clones specific for myelin basic protein', *Cell*, 80(5), pp. 695–705. Available at: [https://doi.org/10.1016/0092-8674\(95\)90348-8](https://doi.org/10.1016/0092-8674(95)90348-8).

Xu, Z. *et al.* (2015) 'Dimethyl fumarate for multiple sclerosis', *Cochrane Database of Systematic Reviews*, 4(4), p. CD011076. Available at: <https://doi.org/10.1002/14651858.CD011076.pub2>.

Yao, B. *et al.* (2012) 'Chronic Multiple Sclerosis Lesions: Characterization with High-Field-Strength MR Imaging', *Radiology*, 262(1), pp. 206–215. Available at: <https://doi.org/10.1148/radiol.11110601/-/DC1>.

Yao, B. *et al.* (2015) 'Heterogeneity of Multiple Sclerosis White Matter Lesions Detected With T2*-Weighted Imaging at 7.0 Tesla', *Journal of Neuroimaging*, 25(5), pp. 799–806. Available at: <https://doi.org/10.1111/jon.12193>.

Zhang, Y. *et al.* (2016) 'Quantitative Susceptibility Mapping and R2* Measured Changes during White Matter Lesion Development in Multiple Sclerosis: Myelin Breakdown, Myelin Debris Degradation and Removal, and Iron Accumulation', *American Journal of Neuroradiology*, 37(9), pp. 1629–1635. Available at: <https://doi.org/10.3174/AJNR.A4825>.

Zipp, F. and Aktas, O. (2006) 'The brain as a target of inflammation: common pathways link inflammatory and neurodegenerative diseases', *Trends in Neurosciences*, 29(9), pp. 518–527. Available at: <https://doi.org/10.1016/J.TINS.2006.07.006>.